Development of a cell sensing and electrotherapeutic system for a smart stent

Anubhav Bussooa

BSC(Hons), MSc

Submitted in fulfilment of the requirements for the degree of Doctor of Philosophy

Institute of Cardiovascular and Medical Sciences

College of Medical, Veterinary and Life Sciences

University of Glasgow

September 2019

Author's declaration

"I declare that, except where explicit reference is made to the contribution of others, this dissertation is the result of my own work and has not been submitted for any other degree at the University of Glasgow or any other institution."

Signature: _____

Printed name: _____

Acknowledgement

I would like to express my heartfelt gratitude to my PhD supervisors Dr John Mercer and Dr Steven Neale for their unflinching support for the duration of this PhD project. John has been an excellent mentor, constantly encouraging me to improve my skills and techniques and has undoubtedly made me a better researcher. Steve has been an excellent guide for the engineering aspects of the project, always providing me with realistic assessments of my crazy ideas.

I would also like to thank all my colleagues in the British Heart Foundation Glasgow Cardiovascular Research Centre for their help with the project and for creating a very friendly work environment. Special thanks goes to Daniel, for successfully taking over the project and for his help with the final experiments. I also wish to thank all the staff of the James Watt Nanofabrication Centre for their expert advice and colleagues from the engineering department: Yang, for his help with L-edit electrode design and Carlos, for his crucial help with engineering experiments at the start of the project.

I wish to thank my family for their constant support, encouragement and love, despite the distance. All the calls and messages have helped me get through these very challenging 4 years, without feeling disconnected from my beloved family. My holidays back home also provided my with some much-needed breaks.

Last, but not least, I wish to thank the Glasgow Swing Dance community for being like a second family. All the classes and social events provided my with very refreshing breaks after work.

Table of contents

List of figures

List of tables

List of publications

- *Future of smart cardiovascular implants*, **Bussooa, A.**, Neale, S., & Mercer, J. R. (2018). Sensors (Switzerland), 18(7), 1–11. (https://doi.org/10.3390/s18072008).

- *The Future of Cardiovascular Stents: Bioresorbable and Integrated Biosensor Technology,* Hoare, D., **Bussooa, A.**, Neale, S., Mirzai, N., & Mercer, J. (2019). Advanced Science, (https://doi.org/10.1002/advs.201900856).

Definitions / Abbreviations

7-AAD	7-aminoactinomycin D
AC	Alternating Current
ACS	Acute Coronary Syndrome
ADP	Adenosine Diphosphate
AO	Acridine Orange
ANDK	Apoptosis / Necrosis Detection Kit
AUC	Area Under Curve
BMS	Bare Metal Stent
CAD	Coronary Artery Disease
CABG	Coronary Artery Bypass Grafting
CAM	Calcein Acetoxymethyl
CC	Constant Current
CCH	Cell Culture Hood
CE	Circular Electrode
CHD	Coronary Heart Disease
CV	CytoCalcein Violet 450
CVD	Cardiovascular diseases
DAPT	Dual Antiplatelet Therapy
DC	Direct Current
DES	Drug Eluting Stents
DNA	Deoxyribonucleic Acid
EC	Endothelial Cells
EPC	Endothelial Progenitor Cells
ETHD	Ethidium Homodimer
GSDMD	Gasdermin D
HEPES	4-(2-hydroxyethyl)-1-piperazineethanesulfonic acid
HUVEC	Human Umbilical Vein Endothelial Cell
IHD	Ischaemic Heart Disease
ISR	In-stent Restenosis
IVUS	Intravascular ultrasound
JWNC	James Watt Nanofabrication Centre
LC	Inductor - Capacitor
MASMCs	Mouse Aortic Smooth Muscle Cells

MECs	Mouse Endothelial Cells
MEMS	Microelectromechanical Systems
MIA	Multiple Image Alignment
MPA	Multiple Position Acquisition
nIDE	normal Interdigitated Electrodes
NiTi	Nitinol
NO	Nitric Oxide
NRK	Normal Rat Kidney
PBS	Phosphate Buffered Saline
PCI	Percutaneous Coronary Intervention
PE	Pendulum Electrodes
PGE_2	Prostaglandin
PRF	Phenol Red Free
PS	Phosphatidylserine
PTCA	Percutaneous Transluminal Coronary Angioplasty
ROS	Reactive Oxygen Species
rpm	revolutions per minute
SF	Serum Free
sIDE	small Interdigitated Electrode
ssIDE	super small Interdigitated Electrode
ST	Stent thrombosis
TUNEL	Terminal deoxynucleotidyl transferase dUTP nick end labelling
ULMCAD	Unprotected Left Main Coronary Artery Disease
VSMC	Vascular Smooth Muscle Cells
WSS	Wall Shear Stress

Abstract

Cardiovascular diseases (CVD) is one of the main causes of death worldwide. Coronary heart disease (CHD) and strokes are the highest contributors to CVD deaths (46 % and 26 % respectively) in the UK. The condition which leads to CHD is Coronary artery disease (CAD). The main cause of CAD is coronary atherosclerosis, which involves an inflammatory response of the artery wall to chronic multifactorial injury, which then results into formation of atherosclerotic plaques. One of the main treatment strategies for CAD is Percutaneous Coronary Intervention (PCI).

PCI is a procedure during which a balloon mounted catheter with an unexpanded stent is inserted either into the femoral artery or the brachial artery and threaded up to the site of stenosis in the coronary artery. PCI usually involves stenting with a Bare Metal Stent (BMS) or Drug Eluting Stent (DES). BMS are associated with 20 % in-stent restenosis (ISR) rates. DES have decreased ISR rates to 15 % but not eliminated this complication.

In this project, the proof of concept experiments were carried out for the development of a smart stent, as a solution to ISR. The proposed smart stent would have diagnostic and therapeutic capabilities. It was demonstrated that a cell sensing and electrotherapeutic system based on interdigitated electrodes (IDEs) could potentially be used for diagnosing and intervening on ISR.

Preliminary tests showed that IDEs were minimally susceptible to changes in volume and conductivity of culture medium, during baseline impedance measurements. The 2 cell types in this project were Mouse Aortic Smooth Muscle Cells (MASMCs) and Mouse Endothelial Cells (MECs). Cell adherence to the electrodes increased the impedance. The optimal sensing frequency range was 1 kHz to 50 kHz and the optimal sensing frequency was 10 kHz.

IDEs of different dimensions were fabricated. The largest version was referred to as normal IDE (nIDE) and the smallest one as super small IDE (ssIDE). The ssIDE had an effecting electrode surface area 16 times smaller than the nIDE. Experiments with MASMCs showed that the increase in impedance for the same cell density was 4.35 times higher with ssIDE as compared to nIDE, implying that miniaturising the IDE increased detection sensitivity.

For the same cell density, MASMCs caused higher increases in impedance. The IDEs could potentially be used to distinguish the MASMCs and MECs based on the difference in impedance spectra over a broad frequency sweep. The adherence of cells to the IDE could be reliably monitored intermittently (at 24 h intervals) or continuously (at 15 min intervals). Continuous monitoring allowed the gradual changes in impedance as a result of cell adherence to the electrodes, proliferation and death to be correlated with timelapse imaging.

IDEs could be used as both sensors, for detecting adherence of MASMCs or MECs, and therapeutic probes, for inducing apoptosis of MASMCs. Sensing required a small voltage and small current (10 μA). Applying voltages in the 2.0 V to 2.5 V range could induce death of MASMCs. When 2.5 V DC was applied to a cell monolayer using Pendulum Electrodes (PEs), this produced a reproducible "tearing effect". Application of 2.0 V AC to a cell monolayer using nIDE and ssIDE caused a localised and controlled effect. This effect could be monitored using the impedance measurement: the application of the voltage caused an immediate drop in impedance. Using an Apoptosis / Necrosis kit, it was confirmed that the type of cell death cause by the application of an AC sine voltage of 2 $V_{peak\text{-}to\text{-}peak}$ 40 kHz for 1 min was apoptosis.

As the fabricated biosensors were intended to be integrated onto a future smart stent, which would be implanted *in vivo* and would be subjected to blood flow, it was important to test them under flow conditions. The nIDE and ssIDE were incorporated into microfluidic flow devices. Results showed that the IDEs could detect cell adherence under flow conditions. They were also suitable for monitoring the gradual migration and proliferation of an endothelial monolayer within a microfluidic channel (simulating regrowth of endothelium over smart stent struts with biosensors).

CHAPTER 1
INTRODUCTION

1.1 Cardiovascular disease

Cardiovascular diseases (CVD) is one of the main causes of death worldwide (Smolina *et al.*, 2012). In 2013, the number of deaths due to CVD was 17.5 million, representing 30 % of global deaths. Within the UK, mortality from CVD varies widely between the different regions (Bhatnagar *et al.*, 2015). Scotland (347 / 100000) and North of England (320 / 100000) have the highest age-standardised death rates. Coronary heart disease (CHD) and strokes are the highest contributors to CVD deaths (46 % and 26 % respectively) in the UK. Coronary artery disease (CAD) is the condition that leads to CHD.

The number of prescriptions dispensed for CVD in the England in 2013 was more than 300 million, which was 6 times higher than the number issued in 1981 (Bhatnagar *et al.*, 2015). Every year in England, there are more than 38 million prescriptions for antiplatelet drugs. The total number of surgical operations carried out in the UK has been increasing. In 2012 in the UK, just under 17000 coronary artery bypass grafting (CABG) procedures were carried out for the management of CAD. Percutaneous coronary intervention is more commonly used for CAD because it is less invasive. In 2012 in the UK, more than 90000 PCI were carried out, which was 2 times higher than the number carried out in 2002.

Over the last 20 years, the number of prescriptions and surgical operations for CVD in the UK have significantly increased (Bhatnagar *et al.*, 2015). In 2004, CVD cost £ 29.1 billion to the UK economy (Luengo-Fernández *et al.*, 2006). 60 % of this cost was on CVD healthcare and 17 % on informal care related cost. The remaining 23 % was due to productivity losses as a result of mortality and morbidity. In 2012 / 2013, the National Health Service spent £ 6.8 billion on CVD, mostly for secondary care (Bhatnagar *et al.*, 2015).

1.2 Coronary Artery Disease

The myocardium receives its blood supply through the coronary arteries (shown in Figure 1). In patients with right dominant coronary circulation, 84 % of the blood flow to the left ventricle comes from the left main coronary artery (El-Menyar, Al Suwaidi and Holmes, 2007). When atherosclerosis affects the coronary arteries, this leads to Coronary artery disease (CAD).It has several clinical manifestations, including chronic heart disease, angina pectoris, myocardial infarction and sudden cardiac death (Willerson and Holmes, 2015). This involves an inflammatory response of the artery wall to chronic multifactorial injury, which then results into formation of atherosclerotic plaques. Atherosclerosis is considered an inflammatory disease because inflammation plays an important role.

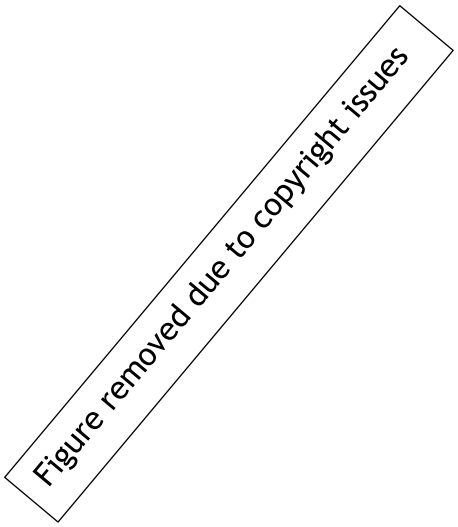

Figure 1: Posterior and anterior views of heart showing the location and distribution of the main coronary vessels (Reproduced from Pappano and Gil Wier (2013))

1.3 Pathophysiology of coronary artery disease

1.3.1 Normal arterial anatomy

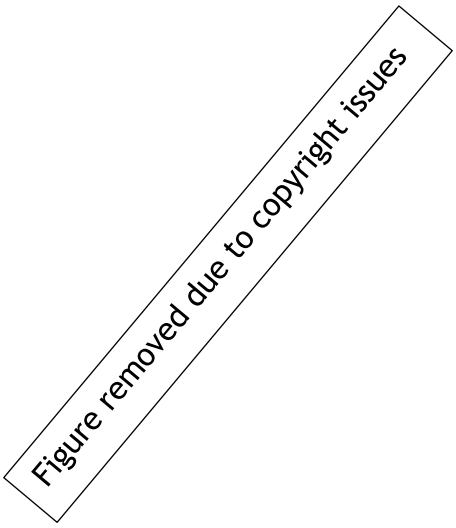

Figure 2: Structure of a normal large artery with the intima, the media and adventitia (Reproduced from Lusis (2000)).

As shown in Figure 2, arteries consist of 3 layers: intima (innermost layer), media (middle layer) and adventitia (outermost layer) (Tousoulis, 2018). The intima consists of the internal elastic lamina, the basement membrane and the endothelial layer. The normal endothelium is made up of a thin monolayer of endothelial cells. These cells can regulate vascular homeostasis by producing vasodilating and antithrombogenic agents.

Nitric oxide (NO) is one of the most important cardiovascular signalling molecules (Mudau *et al.*, 2012). Reduced NO bioavailability leads to endothelial dysfunction, which is the inability of the endothelium to initiate vasodilation in response to vasodilatory stimuli such as shear stress and acetylcholine. In the presence of endothelial dysfunction or damage, the artery goes into a prethrombotic state and proatherosclerotic changes occur (Tousoulis, 2018). The basement membrane contains fibronectin, laminin, collagen and other extracellular matrix molecules. These are produced by smooth muscle cells and supports the endothelial layer. The extracellular matrix helps in regulating smooth muscle cell phenotype (Moiseeva, 2001). Vascular contractile smooth muscle cells are embedded in the extracellular matrix and enclosed by an incomplete basement membrane. Laminin has an important role in differentiation and maintaining smooth muscle cells in the contractile phenotype.

The elastic membrane connects the intima to the medial layer (Tousoulis, 2018). The medial layer consists of concentric layers of smooth muscle cells and layers of extracellular matrix rich in elastin. The adventitia comprises collagen fibrils and a scarce cell population consisting of mast cells and fibroblasts. Vasa vasorum and nerve endings are also present.

1.3.2 Atherosclerosis

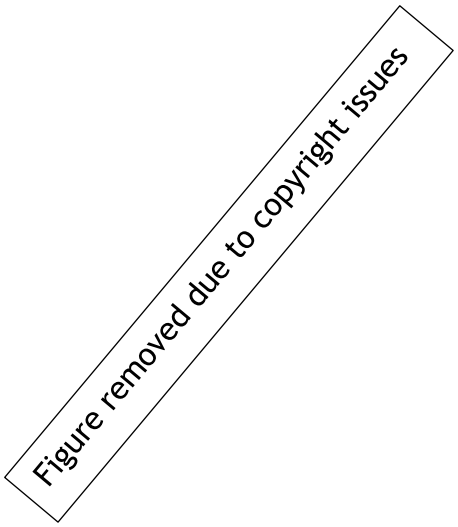

Figure 3: Stages of atheromatic plaque progression (Reproduced from Tousoulis (2018))

For most of the last century, atherosclerosis was considered a cholesterol storage disease, while in the 1960s and 1970s, focus was placed on the formation of atherosclerotic plaque due to smooth muscle cell proliferation (Libby, 2012). Over the last 30 years, research has been focussed on the primordial role of inflammation in atherogenesis. Atherosclerosis is a condition that develops over the course of 50 years, with the onset being in the early teenage years (Insull, 2009). Figure 3 shows the stages of atheromatic plaque progression.

It involves chronic inflammation of vulnerable sites in the arterial walls as a result of lipid oxidation, retention and modification. It first involves fatty streaks which evolve into fibrous plaques. Some of these are susceptible to rupture leading to stenosis or thrombosis. Figure 4 shows a schematic of vulnerable plaques, characterised by a thin fibrous cap, large atheromatous lipid core with high lipid content, outward remodelling, plaque infiltration by lymphocytes and macrophages and thinning of the media accompanied by a decrease in number of smooth muscle cells (Tousoulis, 2018).

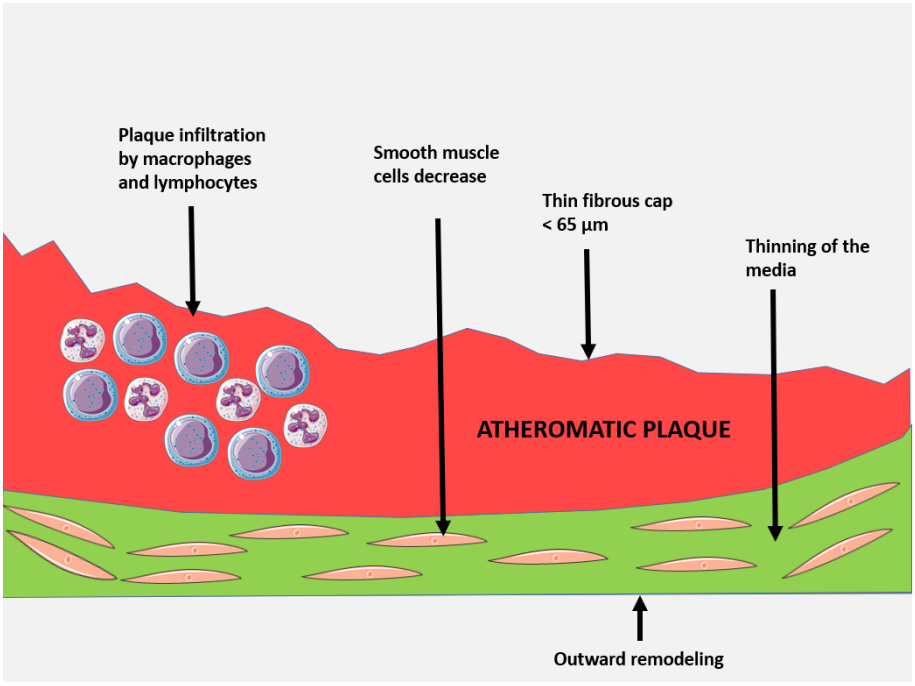

Figure 4: Vulnerable plaque characteristics (Adapted from Tousoulis (2018))

1.3.3 Arterial remodelling

In atherosclerotic disease, arterial geometric remodelling is a crucial factor in luminal narrowing (Pasterkamp and Smits, 2002). Lumen loss by plaque formation is delayed by positive (expansive) remodelling and accelerated by negative (constrictive) remodelling. In positive remodelling, the luminal area remains patent, but the plaque under the surface of the lumen hides a large atheroma with substantial inflammation. Plaque rupture and subsequent myocardial infarction are associated with these features. In most cases, negative remodelling is associated with stable coronary syndromes.

1.3.4 Acute coronary syndrome

Acute coronary syndrome (ACS) usually presents with unstable angina, acute myocardial infarction and sudden cardiac death (Virmani *et al.*, 2006). Most cases of ACS are a result of sudden luminal thrombosis (Burke *et al.*, 1997). There are 3 different pathologies for luminal thrombosis: plaque rupture, plaque erosion and calcified nodule (Virmani *et al.*, 2006). In case of plaque rupture the lesion consists of a necrotic core with an overlying thin ruptured fibrous cap. This rupture allows platelets to get in contact with the thrombogenic necrotic core, leading to luminal thrombosis. Plaque erosion presents with a luminal thrombus with an underlying base rich in smooth muscle cells and proteoglycans with minimal inflammation. Calcified nodule presents with an underlying calcified plate with overlaid bony nodules. This results in a gap in the fibrous cap and is devoid of endothelium, with overlying luminal thrombus.

1.3.5 Unprotected left main coronary artery disease

Coronary angiography became common practice as from the 1960s and allowed risk stratification of patients (Collet *et al.*, 2018). Patients with unprotected left main coronary artery disease (ULMCAD) had increased mortality rates, because this artery provides blood supply to a large proportion of the myocardium (Braunwald, 2016). . In the past, patients with ULMCAD, who received medical therapy only, had a 3-year mortality rate of 50 % (Herrick, 1983). Survival rates greatly improved with the advent of surgical revascularisation, making it the treatment of choice for ULMCAD (Yusuf *et al.*, 1994).

1.3.6 Coronary artery bypass grafting

Coronary artery bypass grafting (CABG) is a surgical procedure during which the coronary arteries that are partially or completely stenosed by atherosclerotic plaque, are bypassed by autologous arterial or venous grafts (Alexander and Smith, 2016). The left internal thoracic artery and the greater saphenous vein are the most commonly used bypass conduits.

After implantation of the saphenous vein graft and return of the circulatory flow, it is immediately subjected to much higher pulsatile blood pressures (100 mm Hg vs 10 mm Hg) of the arterial system (Harskamp *et al.*, 2013). The walls of the vein graft are exposed to higher shear stress, causing the formation of neointima consisting mainly of smooth muscle cells. These cells release pro-inflammatory agents, which create a highly atherogenic environment within the graft and increases the risk of vein graft failure. The main disadvantage of internal thoracic artery grafts is that they are prone to spasms and early occlusion (Sabik *et al.*, 2005). However, internal thoracic grafts rarely develop atherosclerosis and result in higher long term patency rates compared to saphenous vein grafts (Hillis *et al.*, 2011).

As CABG is associated with a significant risk of morbidity and death from the open surgical procedure, cardiologist have explored minimally invasive techniques (Braunwald, 2016). In the last 10 years, several studies have shown the advantages of catheter based revascularisation (Collet *et al.*, 2018). Two randomised clinical trials carried out in 2016, namely NOBLE (Nordic-Baltic-British Left Main Revascularisation Study) (Mäkikallio *et al.*, 2016) and EXCEL (Evaluation of XIENCE versus Coronary Artery Bypass Surgery for Effectiveness of Left Main Revascularization) (Stone *et al.*, 2016) proved the efficacy and safety of Percutaneous Coronary Intervention (PCI) compared to Coronary Artery Bypass Grafting (CABG) in a selected group of patients.

1.4 Percutaneous Coronary Intervention

1.4.1 History of PCI

The first PCI, which involved balloon angioplasty only, was performed by Grunzig in 1977 (Grüntzig, 1978). Since then, balloon angioplasty became common practice for treatment of CAD. However the results were unpredictable as abrupt vessel recoil occurred a few hours to a few days after intervention (Byrne *et al.*, 2017). Another major issue was restenosis, which occurred in 30 % of cases, up to 18 months post procedure, due to a combination of neointimal hyperplasia, constrictive remodelling, elastic recoil and plaque prolapse (Byrne, Joner and Kastrati, 2015).

In order to overcome the issues with balloon angioplasty, Ulrich Sigwart developed the first coronary stent (Sigwart *et al.*, 1987). Its purpose was to act as a mechanical scaffold and prevent arterial recoil, following balloon dilation. It was tested in man for the first time in 1986.

1.4.2 Percutaneous transluminal coronary angioplasty

During percutaneous transluminal coronary angioplasty (PTCA), a balloon mounted catheter is inserted either into the femoral artery or the brachial artery and threaded up to the site of stenosis in the coronary artery (Shedden, Oldroyd and Connolly, 2009). Inflation of the balloon causes the plaque to be compressed against the artery wall and allows blood flow to be restored. The major disadvantage of PTCA is acute elastic recoil, resulting in a need for emergency CABG in 10 % of patients (Slavin, Chhabra and Tobis, 2007). This occurs minutes after balloon deflation and involves mechanical collapse of the vessel wall, which can result in up to 50 % loss of vessel cross sectional area. Another issue with PTCA is post-angioplasty restenosis.

1.4.3 Post-angioplasty Restenosis

The pathogenesis of post-angioplasty restenosis is similar to wound healing and is distinct from atherosclerotic plaque formation (Slavin, Chhabra and Tobis, 2007). This process can be divided into neointimal hyperplasia and negative vascular remodelling. The intravascular pressure increases during balloon inflation (Scott *et al.*, 1996). This often causes rupture of the medial layer at the junction between the atherosclerotic plaque and the normal segment. This in turn causes dissections in the tunica media and exposes the subendothelial components. There is a loss of antithrombotic factors as a result of endothelial denudation, which promotes platelet adhesion and aggregation. Platelets release platelet-derived growth factors (PDGF) which act as chemotactic signals for vascular smooth muscle cells (VSMC) and macrophages. Within the tunica media, VSMC are usually in a contractile, though genotypically quiescent state. Vascular injury causes the VSMC to transdifferentiate into myofibroblasts, which have migratory, proliferative, secretory and synthetic properties (Newby, 2005).

1.4.4 Bare metal stents

Stenting led to more stable results following PCI, as the deployed stent covered plaques and dissection flaps (Colleran and Kastrati, 2018). It also provided mechanical strength radially, thus preventing arterial recoil. By 1998, 70 % of PCI involved bare metal stenting (Laskey, Kimmel and Krone, 2000). However, acute and subacute vessel occlusion rates remained high (Colleran and Kastrati, 2018). This was due to increased rates of early stent thrombosis. In order to minimise this, aggressive anticoagulation therapy was employed, but this increased rates of bleeding and vascular complications. The Intracoronary Stenting and Antithrombotic Regimen (ISAR) trial showed that dual antiplatelet therapy (DAPT - consisting of aspirin and ticlodipine) decreased the rates of ischaemic and haemorrhagic events. To date, this remains part of the medical protocol following PCI. The other major issue with bare metal stent is in-stent restenosis (ISR) as a result of neointimal hyperplasia. Despite advances in procedural techniques, stent design, delivery system design and pharmacologic therapy, restenosis rates with bare metal stents remains significant at about 20 % (Carrozza *et al.*, 1992).

1.4.5 Drug eluting stents

Several clinical trials were carried out to investigate the effects of systemic administration of agents, such as antioxidants, statins, angiotensin-converting enzyme inhibitors, calcium channel blockers, anticoagulants and antiplatelets on rates of in-stent restenosis (Slavin, Chhabra and Tobis, 2007). Results showed that these methods had low efficacy. Moreover, the main disadvantage of systemic pharmacotherapy is that it is unable to deliver a high dose of the agent to the lesion site, without causing systemic side effects. Drug Eluting Stents (DES) are coated with an anti-proliferative agent, which can be delivered locally to the lesion site, without inducing systemic effects (Slavin, Chhabra and Tobis, 2007).

One method of coating a BMS with an anti-proliferative agent is dip it into the agent or spray it with the agent (Heldman *et al.*, 2001). With this type of DES, a large bolus of the agent is delivered instead of a gradual release. Most DES are made up of a BMS and a biodegradable or non-biodegradable biopolymer loaded with an anti-proliferative agent, which allows for a sustained release.

The early generation of DES have significantly decreased 9-month and 12-month revascularisation rates to 4.34 % (compared to 12.32 % with BMS) (McCormick, 2018). The latest generation of DES have caused a modest decrease in revascularisation rates to 2.91 %, given the vast research budget invested in newer stent technologies.

For a comprehensive review of the latest DES development refer to McCormick(2018). Briefly, DES such as BioMatrix (Biosensors International) and Nobori (Terumo) have a biodegradable polymer - drug coating applied to the abluminal side of the stent only, in order to achieve more efficient drug delivery and faster reendothelialisation. Biodegradable polymer-coated DES have shown improved safety and efficacy when compared early-generation durable polymer DES (Stefanini *et al.*, 2012).

Another major innovation is the implementation of polymer-free DES such as Carbostent (Sorin Group) and Yukon stent (Translumina GmbH) (McCormick, 2018). Drug loading and controlled released is achieved by introducing surface porosity at the nano-, micro- and macro-scale. With the Yukon stent, drug type(s) and dose to be selected by the interventional cardiologist, as the drug coating is applied on-site within the catheterization lab at the time of the stent procedure.

1.4.6 Reendothelialisation following stent deployment

In their physiological environments, endothelial cells are in contact with the basement membrane (Wood *et al.*, 2010). This consists of a grid of submicron and nanoscale structures, which are linked with improved gene regulation, cell proliferation and cell adhesion. Endothelial cells are subjected to wall shear stress (WSS) which is the product of velocity gradient near the wall (shear rate) and the viscosity of blood (Serruys and Onuma, 2017). Balloon angioplasty and deployment of the stent damages the endothelial layer and causes loss of endothelial cells (Van der Heiden *et al.*, 2013). Endothelial cells (EC) have an important role in regulating vascular tone and function and in suppression of inflammation and thrombosis (Otsuka *et al.*, 2012). It is an important therapeutic goal to restore a healthy endothelium following stenting as this decreases the chances of ISR and in-stent thrombosis.

Following BMS implantation, low endothelial shear stress promotes ISR through interactions of shear- sensing endothelial cells with SMCs (Koskinas *et al.*, 2012). After DES implantation, by which re-endothelialisation is retarded pharmacologically, endothelial shear stress may act on SMCs directly via endothelium-independent mechanisms. Low endothelial shear stress promotes the activation, proliferation, and migration of SMCs. As shown in Figure 5a, thick stent struts can precipitate stent thrombosis by increasing endothelial-shear-stress induced platelet activation on top of the struts and impeding reendothelialisation. The degree of deendothelialization downstream of struts is proportional to strut thickness, which is due to more intense flow disturbance.

The normal migration of EC towards the injured stented portion of the artery is affected by the presence of the stent struts, which is an artificial surface (Van der Heiden *et al.*, 2013). Moreover, the stent struts perturb the local blood flow pattern (Figure 5): there are regions of disturbed shear stress and flow reversal between the stent struts (Jiménez and Davies, 2009).

DES have decreased rates of ISR as the antiproliferative drugs prevent vascular smooth muscle cell overgrowth (Joner *et al.*, 2006). However, the drugs impair reendothelialisation and can lead to lethal late-stage thrombosis. This has been linked to cessation of dual antiplatelet therapy, which indicates incomplete reendothelialisation of the stent struts (Lüscher *et al.*, 2007). With early-generation DES, the same concentrations of sirolimus and paclitaxel that was required to inhibit human smooth muscle cell proliferation, also inhibited endothelial cell proliferation (Parry *et al.*, 2005).

These limitation have driven the development of newer drugs (e.g. limus analogs) for the latest-generation DES. Moreover, there is an urgent need to develop therapeutic methods to promote rapid reendothelialisation following stenting (Van der Heiden *et al.*, 2013). De Prado *et al.* (2011) investigated reendothelialisation of 2 BMS and 1 DES in non-atherosclerotic arteries of swine models. Results (Figure 6) showed that reendothelialisation was more complete with BMS compared to DES at 7 days.

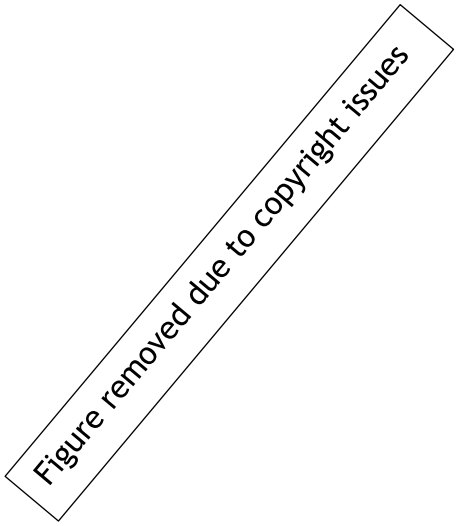

Figure 5: (a) Blood flow over thick non-streamlined stent strut showing high shear rate and platelet activation over strut (b) Blood flow over thin streamlined stent strut showing physiological shear rate and quiescent platelets over strut (Reproduced from Serruys and Onuma (2017))

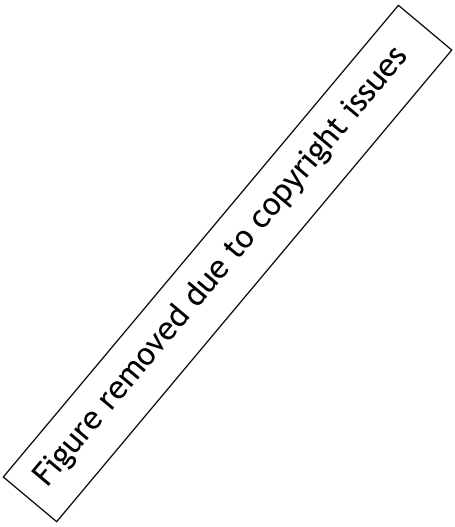

Figure 6: Reendothelialisation of the different stents at 7 days. (a) Stainless steel stents, (b) cobalt-chromium stents, and (c) tacrolimus-eluting stents. The endothelialisation assessment is depicted with black and white areas over the images (white areas: uncovered struts; black areas: struts covered by fibrin/giant cells).
(Adapted from De Prado et al. (2011))

1.4.7 Stent thrombosis and dual antiplatelet therapy

Stent thrombosis (ST) can occur within minutes to hours following PCI, whereas ISR develops over weeks to months (Kim and Dean, 2011). A study carried out by Serruys *et al.* (1991) showed that early vessel closure as a result of ST occurred in 25 % of cases within the first 14 days after implantation. These complications occurred even though the patients were given large doses of heparin of up to 15000 units. Moreover, this resulted in significant mortality and morbidity linked to haemorrhagic complications. Major bleeding occurred in 9 % of patients (Schömig *et al.*, 1994). Dual antiplatelet therapy (DAPT) with aspirin and ADP (Adenosine Diphosphate) receptor inhibitor led to a decrease in ST and bleeding complications, as compared to oral antithrombotic therapy (Leon *et al.*, 1998). Yin et al, (2019) (Yin *et al.*, 2019) carried out a systematic review and network meta-analysis to evaluate efficacy and safety of short term (< 6 months), standard term (12 months) and long term (> 12 months) DAPT. They concluded that patients implanted with DES (including newer-generation DES) and treated with clopidogrel required short term DAPT (< 6 months). Standard term DAPT showed similar efficacy and safety compared with short term DAPT. Long term DAPT resulted in more death and bleeding-related events.

1.4.8 In-stent restenosis

In-stent restenosis (ISR) involves a complex inflammatory and healing response to vascular injury, sustained during PCI (Kim and Dean, 2011). It occurs over a much shorter time period (weeks to months) as compared to atherosclerotic disease (years). ISR can be referred to as an excessive reaction to vascular injury. ISR occurs as a result of both vascular remodelling and neointimal hyperplasia. The restenosis of the treated segment reaches a maximum at 3 months and remains stable after 6 months (Kastrati *et al.*, 1993), but may take as long as 18 months to manifest. The predictive factors for instent restenosis can be classified as procedural predictors, vessel predictors and patient predictors (Kim and Dean, 2011). The factors for bare metal stent restenosis are shown in Table 1 and those for drug eluting stent are shown in Table 2.

As a result of these studies, newer generation of stents incorporate much thinner struts (Kim and Dean, 2011). The length of the implanted stent is also an important procedural predictive factor (Kobayashi *et al.*, 1999). The rates of ISR with stents > 35 mm was twice as high as compared to those with stents < 20 mm. One of the notable procedural predictive factors was the thickness of the stent struts (Pache *et al.*, 2003). Several studies have shown that first generation stents with thicker struts led to a higher rates of clinically significant and angiographic restenosis as compared to second generation stents with thinner struts.

Procedural factors	Vessel factors	Patient factors
Smaller poststent minimal luminal diameter (< 3mm)	Chronic occlusion	Diabetes mellitus
Multiple stents	Lesion located at left anterior descending artery	Restenosis after PTCA
Suboptimal stent apposition and/or stent under-expansion	Lesion located at saphenous vein graft	Chronic renal failure
Stent fracture	Small vessel (diameter < 3 mm)	High serum C-reactive protein
	Long lesion (length > 20 mm)	High serum IL-6
	Bifurcation lesion	Low serum IL-10
	Ostial location	CCS (Canadian Cardiovascular Society) Class IV angina
	Type C lesion	

Table 1: Predictive factors for bare metal stent restenosis (Kim and Dean, 2011)

Procedural factors	Vessel factors	Patient factors
Non-uniform stent expansion	Chronic occlusion	Female gender
Stent fractures	Instent restenosis	Diabetes mellitus
Over-dilation of undersized stent	Bifurcation lesion	Chronic renal failure on haemodialysis
Stent under expansion	Lesion located at left anterior descending artery	Prior myocardial infarction
Smaller poststent minimal luminal diameter	Small vessel (diameter <2.75 mm)	Prior percutaneous coronary intervention
	Long lesion (> 20mm)	Drug resistance or hypersensitivity
	Severe calcification or tortuosity	
	Ostial location	
	Type C lesion	

Table 2: Predictive factors for drug eluting stents restenosis (Kim and Dean, 2011)

1.4.9 Waksman classification for DES-ISR

The patterns of DES-ISR can be classified using Waksman ISR Classification (Shlofmitz, Iantorno and Waksman, 2019). This "differentiates between mechanical (Type I), biologic (Type II), or mixed (Type III) causes, including chronic total occlusions (Type IV) and lesions of DES-ISR previously treated with > 2 stents (Type V)" (Figure 7). This allows personalisation of DES-ISR, so as to ensure higher efficiency.

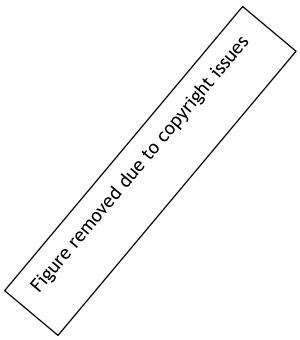

Figure 7: Waksman In-Stent Restenosis Classification (Reproduced from Shlofmitz, Iantorno and Waksman (2019))

1.4.10 Management of in-stent restenosis

Plain old balloon angioplasty (POBA)

This was one of the first treatment strategies implemented for ISR (Macander *et al.*, 1994). It had satisfactory immediate results and very low incidence of complications (Her and Shin, 2018). Non-compliant balloons and high pressure balloon dilatation were usually required for optimal results. One of the issues with this method was that minutes after the last balloon inflation, tissue re-intrusion back into the lumen would occur.

Cutting balloon therapy

Lateral blades are mounted onto a balloon, and these deeply incise neointima tissue. This method had superior efficacy (~ 40.0 %) in terms of rates of target lesion revascularisation as compared to POBA (~ 12.5 %). Moreover, this procedure requires fewer balloons (as compared to POBA) and less additional stenting.

Debulking techniques

Atheroablative techniques were implemented for the treatment of ISR because of the poor long-term outcomes with PTCA only, which has a restenosis rate of 54 % - 85 % (Mehran *et al.*, 2012). Atheroablation with adjunct PTCA has shown a higher reduction of in-stent neointimal tissue. Atheroablative techniques include excimer laser and directional/rotational atherectomy. *In vitro* and *in vivo* animal models

demonstrated that excimer lasers were able to precisely cut through atheroma (including calcium) without any harmful thermal injury.

Vascular brachytherapy

This technique showed the most efficacy at treatment of neointimal hyperplasia associated with BMS-ISR (Her and Shin, 2018). A radioactive isotope was temporarily deposited into the diseased coronary segment. This significantly reduced rate of clinical and angiographic restenosis. Results from randomised clinical trials showed that brachytherapy was more effective at preventing the progression of ISR than POBA or debulking techniques (Leon *et al.*, 2001).

However, brachytherapy was abandoned when DES was implemented (Her and Shin, 2018). Results from 2 large clinical trials showed that DES was more effective at decreasing restenosis rates and the need for revascularisation when compared to brachytherapy (Holmes *et al.*, 2006).

Repeat stenting

In ISR associated with BMS, repeat stenting with another BMS produces a higher acute lumen gain as compared to POBA (Mintz *et al.*, 1998). However, due to late lumen loss, the final angiographic appearance with repeat BMS and POBA are similar at 6-month follow up (Her and Shin, 2018). In ISR associated with BMS, repeat stenting with a DES is a promising solution as it potently inhibits neointimal proliferation (Her and Shin, 2018). The rates of recurrent restenosis were significantly lower when repeat stenting was carried out with sirolimus-DES (14.3 %) and paclitaxel-DES (21.7 %) as compared with POBA alone (44.6 %).

The treatment of ISR associated with DES is more difficult and the outcomes of patients with this complication is usually poorer as compared to patients with BMS associated ISR (Byrne *et al.*, 2013). If the ISR is a result of a mechanical complication such as stent fracture, stent undersizing or edge dissection, placing another DES usually improves the outcome (Her and Shin, 2018). However, 10 – 20 % of patients with DES associated ISR will develop recurrent ISR despite repeat stenting with another DES (Kastrati *et al.*, 2005), and this is often detected late or by chance.

1.4.11 Percutaneous coronary intervention vs Coronary artery bypass grafting

The SYNTAX trial compared the outcomes of patients undergoing PCI and CABG for left main coronary artery disease or three-vessel coronary artery disease (or both) (Serruys *et al.*, 2009). The 12-months rates of adverse cardiovascular events were lower with CABG. The death rates and myocardial infarction rates at 1 year were similar for patients undergoing PCI (with drug eluting stents) and CABG. The rates of stroke were increased for CABG patients while the rates of repeat revascularisation were increased for PCI patients. The conclusion from the trial was that CABG had lower rates of major cardiovascular adverse events at 1 year for patients with left main coronary artery disease or three-vessel coronary disease (or both). However, the 1-year follow-up period of this trial was not sufficient to compare the two treatment strategies.

The more recent FREEDOM (Future Revascularization Evaluation in Patients with Diabetes Mellitus: Optimal Management of Multivessel Disease) trial, carried out for the 2005 to 2010 period, employed the newest CABG and PCI techniques available at the time (Farkouh *et al.*, 2012). The conclusions of the trial were that "CABG was superior to PCI with drug-eluting stents in patients with diabetes and advanced (predominantly three-vessel) coronary artery disease in that CABG significantly reduced rates of death and myocardial infarction, with a higher rate of stroke".

1.5 Innovative stent technologies

1.5.1 Stents with endothelial progenitor cell capture technologies

Endothelial progenitor cells (EPCs) are circulating cells derived from the bone marrow, which can migrate to hypoxic or ischaemic regions, adhere to damaged endothelium and promote regeneration or angiogenesis (Asahara *et al.*, 1997). One possible mechanism by which EPCs promote reendothelialisation is that they incorporate into the vessel wall and differentiate into new endothelial cells (Tomasevic *et al.*, 2019). Another possible mechanism is that, once adhered to the damaged endothelium, the EPCs secrete pro-angiogenic factors which stimulate resident endothelial cells to proliferate and migrate (Haider, Aziz and Al-Reshidi, 2017).

Several research groups have developed stents with EPC capture technologies (Walter *et al.*, 2004; Larsen *et al.*, 2012; Lee *et al.*, 2012; van Beusekom *et al.*, 2012). Lee *et al.* (2012) coated a stent with anti-VE-cadherin antibodies, which targets endothelial progenitor cell markers. The stent was tested in a rabbit model, and showed reduced neointimal formation and accelerated reendothelialisation. Sedaghat *et al.* (2013) tested a similar stent which had anti-CD133 antibodies coating. Results showed that the coating did not affect neointimal thickening or reendothelialisation. Using another approach, Andukuri *et al.* (2013) developed a stent with "bioinspired multifunctional nanomatrix which mimicked endothelial surface characteristics". The stent surface was capable of recruiting endothelial progenitor cells and promoting their differentiation towards an endothelial cell lineage.

1.5.2 BMS with controllable H_2O_2

Park *et al.* (2019) developed a new type of BMS with controllable H_2O_2 generation to inhibit restenosis. H_2O_2 is a type of reactive oxygen species (ROS), which has been shown to suppress smooth muscle cell proliferation, while promoting endothelial cell proliferation (Alexander *et al.*, 2018). Park *et al.* (2015) reported a new method of ROS generation through the galvanic coupling of 2 metals having different chemical potentials.

The stent was made of nitinol (NiTi), which is an alloy made up of nickel and titanium. The stent struts had separated sections which were galvanically coupled with a magnesium zinc alloy (Mg-Zn). A redox reaction with the NiTi working as cathode and Mg-Zn working as anode occurred with the O_2 molecules, producing H_2O_2. *In vitro* analyses showed that the produced H_2O_2 inhibited proliferation of human aortic smooth muscle cells without affected human umbilical vein endothelial cells.

1.5.3 Optimised surface topography and overflowing wall shear stress for potential stent applications

McCracken *et al.* (2013) developed "an array of ensemble nanostructures consisting of RGD-conjugated nanoparticle-nanowells" for enhancing adhesion and retention of human umbilical vein endothelial cells (HUVECs) under low physiological shear stress conditions similar to those in resistance vasculature. At sub-physiological WSS (1.7 dyn / cm^2) HUVECs aligned along the flow while under low physiological wall shear stress (4.7 dyn / cm^2), they aligned along the pattern. This potentially points towards a threshold WSS for cell guidance and related retention.

1.6 AHA guidelines for PCI

The decision to carry out revascularisation is based on the angiographic criteria (Levine *et al.*, 2011). The criteria in favour of revascularization is significant stenosis, which is defined as ≥ 70 % diameter narrowing (≥ 50 % for left main coronary artery disease). The risk of stent thrombosis is significantly increased in patients who prematurely discontinue dual antiplatelet therapy (DAPT), and stent thrombosis is associated with mortality rates of 20 % - 45 %. With BMS, the risk of stent thrombosis is highest during the first 14 to 30 days. Hence, this is the minimum recommended duration of DAPT therapy for these patients (Levine *et al.*, 2011). It is recommended that patients implanted with DES stay on DAPT for at least 12 months to avoid late (after 30 days) stent thrombosis. The interventional cardiologist should discuss with the patient the need for and

duration of DAPT, and the ability of the patient to comply with and tolerate DAPT, before implantation of DES.

Early discontinuation of DAPT is associated with the greatest risk for DES thrombosis (Levine *et al.*, 2011). In patients with high bleeding risk or inability to comply with 12 months of DAPT due to anticipated invasive or surgical procedures within the next 12 months, balloon angioplasty only or BMS should be used. In the United States, the 4 currently approved types of DES are: zotarolimus-eluting stents, sirolimus-eluting stents, paclitaxel-eluting stents, and everolimus-eluting stents.

In-stent restenosis is classified according to these angiographic characteristics: Pattern I includes focal lesions ≤ 10 mm in length; Pattern II is in-stent restenosis > 10 mm within the stent; Pattern III includes in-stent restenosis > 10 mm extending outside the stent; and Pattern IV is totally occluded in-stent restenosis (Levine *et al.*, 2011). Treatment of BMS in-stent restenosis with balloon angioplasty, repeat BMS, or atheroablation devices for Patterns I to IV resulted in 1-year target-lesion revascularization rates of 19 %, 35 %, 50 %, and 83 %, respectively. For clinical restenosis after BMS, repeat stenting with DES is preferred. Studies have demonstrated lower recurrent restenosis rates with DES compared with BMS or vascular brachytherapy.

The predominant angiographic pattern for DES in-stent restenosis is focal (≤ 10 mm in length) (Levine *et al.*, 2011). Several technical, mechanical and biological factors may contribute to DES in-stent restenosis, including stent under-expansion, stent strut fracture, drug resistance, hypersensitivity, non-uniform stent strut coverage, gap in stent coverage and residual uncovered atherosclerotic lesion. Intravascular ultrasound (IVUS) might be considered to determine the cause for in-stent restenosis and help guide treatment strategy.

Interventional cardiologists may treat focal DES restenosis with balloon angioplasty and treat non-focal DES restenosis with BMS, CABG, or repeat DES with the same or an alternative antiproliferative drug (Levine *et al.*, 2011). Small, observational cohort studies have demonstrated angiographic restenosis rates of 25 % to 30 % with repeat DES either involving the same or an alternative drug. The most appropriate treatment of restenosis of DES remains unknown.

1.7 Clinical challenges associated with current stent technologies

The revascularisation rates were 12.32 % with BMS, 4.34 % with early generation DES and 2.91 % with newer generation DES (McCormick, 2018). Based on the significant decrease in revascularisation rates, early generation DES are considered a revolution in stent technology. Despite the huge funds spent to develop newer generation DES, only a modest decrease in revascularisation rates has been achieved. This suggests that DES might have reached a plateau phase in terms of performance. There is thus a need for a new revolution in stent technology in order to make PCI as efficient as possible by attempting to eliminate in-stent restenosis and stent thrombosis.

There is a need to develop strategies that would allow the vascular healing response to be monitored continuously, following stent deployment. Techniques such as intravascular ultrasounds and optical coherence tomography could be used to track the healing response and patency of stented portion. However, these techniques require vascular access and have low resolution, which makes it very difficult to determine whether endothelial cells or smooth muscle cells are covering the stent struts. An alternative technique would be the use of biosensors which can detect and distinguish different cell types.

It would be valuable to determine when the stent struts are completely reendothelialised, in case of a normal healing response. This would indicate that DAPT could be safely stopped without the risk of stent thrombosis. This would lead to a higher quality of life for the patient, as prolonged DAPT is linked to risk of bleeding. In case of an abnormal healing response, it would be useful to be able to monitor the in-stent restenotic process and the percentage occlusion of the vessel. If the occlusion reaches a threshold percentage, intervention could be possible before the patient experiences any complications.

Different patients will respond differently to implantation of a stent. It is therefore important to develop strategies to personalise stents to specific patients rather than developing stents which are efficient in a majority of patients (and leads to complications in a minority of patients).

1.8 Smart stents

1.8.1 Introduction

Due to the persistent issue of ISR, and the high incidence of PCI stent deployments (predicted to increase further), several research groups have investigated the possibility of a stent with sensors to monitor this phenomenon. There are several physical and biological changes occurring during ISR that could make this approach attractive.

1.8.2 Working principles of smart stents

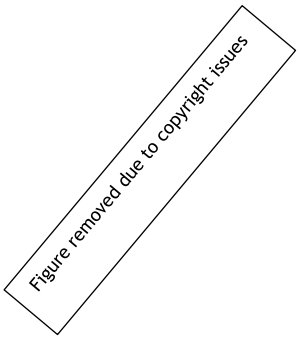

Figure 8: (a) The inductive stent + capacitive pressure sensor is deployed and functions in a similar way to a conventional stent by pushing away plaque and restoring blood flow. (b) Post-deployment, this stent allows wireless monitoring of blood pressure within the stent, as it also functions as an inductor-capacitor tank. (c) ISR changes the blood pressure within the stent and this is detected a shift in resonant frequency. (Reproduced from Chen et al. (2018))

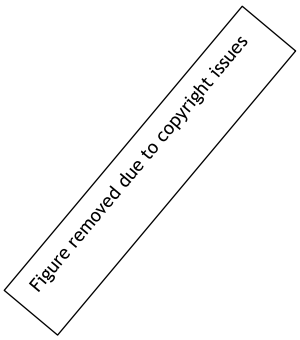

Figure 9: Wireless reading scheme of smart stent integrating a MEMS capacitive pressure sensor (Reproduced from Brox et al. (2015)).

Chen, Brox and Assadsangabi (2014) and Takahata *et al.* (2003) fabricated smart stents (Figure 9) by integrating microelectromechanical systems (MEMS) capacitive pressure sensors onto helical stents. The stent was configured to work as an inductive antenna (Figure 10). Hence, the stent and capacitive sensor worked as an inductor-capacitor (LC) resonant circuit/tank. The blood pressure within the stent could be wirelessly read by using magnetic inductive coupling to an external loop antenna. Preliminary studies showed that the wireless read range was limited to less than 1 cm. With the onset of ISR, there is intimal hyperplasia within the stent, which obstructs the blood flow (Chen *et al.*, 2017). The local blood pressure and haemodynamics around the stent changes, causing the resonant frequency of the inductive stent + capacitive sensor to shift from its original pre-ISR value.

Other research groups have attempted to exploit the electrical properties of biological tissue (restenotic tissue) as a way of monitoring in-stent restenosis. Shedden *et al.* (2010) proposed to use the whole stent as an electrode for the measurement of electrical impedance of restenotic tissue. Their results showed that the ratio of reactive impedance to resistance was higher in the presence of restenotic tissue. Another research group took this approach further and developed a method which could be used to determine the type of cell adhering to an implantable device (Bozsak *et al.*, 2017). The authors of this patent claim that their method allows discriminating different cell types, based on the frequency spectrum of the impedance.

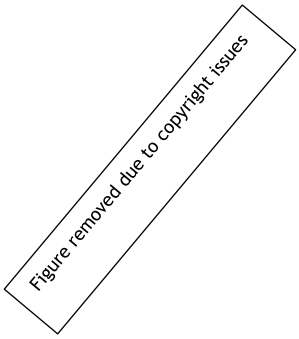

Figure 10: Schematic illustration of bioresorbable stent with bioresorbable flow and temperature sensors, memory modules and bioresorbable / bioinert therapeutic nanoparticles (Reproduced from Son et al. (2015)).

Son *et al.* (2015) developed a bioresorbable electronic stent (Figure 10). Their stent was equipped with sensors for temperature monitoring and flow sensing, data storage, wireless power / data transmission, localised drug delivery and hyperthermia therapy. This stent was successfully tested *ex vivo* using a canine aorta. This innovative technology demonstrated that different types of sensors for detecting a range of physical, chemical and biological conditions within an artery could be integrated onto a stent along with complementary circuitry for communication with external world.

1.9 Our proposed solution to ISR

We hypothesise that a smart stent that could monitor cell adherence and growth (endothelial cells and smooth muscle cells) on the struts and counteract cell overgrowth could help solve the problem of ISR. Monitoring cell numeracy and growth could be achieved using sensors similar to the commercially available Electric Cell-substrate Impedance Sensing (ECIS) system (Wegener, Keese and Giaever, 2000). The same sensors could also be used as therapeutic probes to irreversibly electroporate cells in case of hyperplasia, thereby inducing cell death. The characteristics of the electroporation pulse could be optimised to irreversibly damage cells, leading to apoptosis, which is a controlled form of cell death. Figure 11 shows a section of the proposed smart stent, showing 1 cell biosensor and an integrated circuit. Ideally the smart stent would consist of an array of cell biosensors all connected to and controlled by the integrated circuit. Each biosensor would allow sensing of the cells immediately in between the fingers. In case of smooth muscle cell overgrowth, the integrated circuit could apply a controlled voltage and induce apoptosis of these cells. If the intervention failed, impedance tomography using a combination of 2 or more biosensors would allow (Sun *et al.*, 2010) imaging of the hyperplasia within the stent.

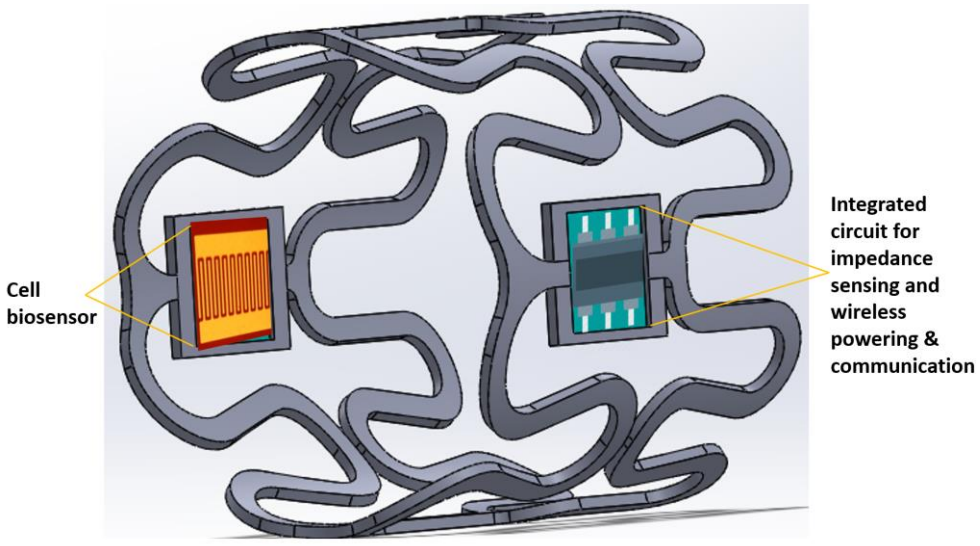

Figure 11: Section of future smart stent showing cell biosensor and integrated circuit for impedance sensing and wireless powering & communication

1.10 Electric Cell-substrate Impedance Sensing

1.10.1 Introduction

Electric Cell-substrate Impedance Sensing (ECIS) was invented over 30 years ago by Ivar Giaever and Charles R. Keese at the General Electric Research Laboratory in New York (USA) (Ablin and Jiang, 2012). The first paper (Giaever and Keese, 1984) about ECIS was published in 1984. The results in this paper proved that fibroblastic WI-38 cells could be detected by measuring changes in the impedance of the gold electrode system before and after cell seeding. ECIS is a non-invasive way of monitoring cell attachment and spreading onto artificial gold surfaces (Siddiquei *et al.*, 2010). The system is commercialised by the company Applied Biophysics.

1.10.2 Working principles

ECIS uses electric fields between electrodes to monitor behaviour of cells (Ablin and Jiang, 2012). With ECIS, the electric field is generated by applying an AC voltage rather than DC voltage, to prevent the build-up of electrochemical products and polarisation of the electrodes. To increase the sensitivity of cell detection, one of the electrodes needs to be made sufficiently small to create an "electrical bottleneck" in the system. In an AC circuit, the reactance is a combination of capacitive components (capacitors) and inductive components (inductors) (Ablin and Jiang, 2012). In an AC circuit including biological cells, the cell membrane behaves as capacitors, but there are no structural components in cells or tissues which exhibit significant inductance.

Hence the reactance is dominated by the capacitive component. Most of the electrode designs commercialised have circular electrodes with 250 µm diameter (Ablin and Jiang, 2012). The surface resistance of the circular electrode is inversely proportional to the area. The solution resistance (constriction resistance) is inversely proportional to the radius. The circular electrode thus has to be made sufficiently small (250 µm diameter), so that the electrode resistance dominates the solution resistance.

When adherent cells are seeded into ECIS devices, the cells gradually settle down, anchor and spread onto the small circular electrodes. A small current of approximately 1 μA is applied through the ECIS electrodes and this results in a small voltage drop of a few millivolts across the cells (Ablin and Jiang, 2012). This small voltage drop has no detectable effects on the cells, making ECIS a non-invasive observation method at low frequencies. The insulating plasma membranes forces the electric current to flow underneath and between the cells, resulting in large changes in impedances. The size of the circular electrodes restricts the number of cells that can adhere to about 100 cells, depending on cell type (Ablin and Jiang, 2012). It is not possible to increase the number of cells that can be monitored by increasing the surface area of the circular electrode, as this causes the solution resistance to dominate. More cells can be monitored by having more circular electrodes in parallel.

1.10.3 Cell monitoring using ECIS

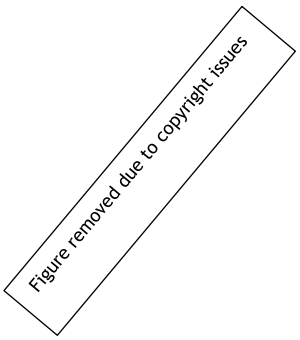

Figure 12: Frequency sweep without and with cells (WI-38 VA13) 24 h after cell seeding (Reproduced from Giaever and Keese, (1991)).

There are several modes of operation for ECIS. The impedance can be measured at a specific frequency at regular time intervals. This allows monitoring of cell attachment, spreading, proliferation, migration and death. Another method for cell monitoring is to carry out frequency sweeps at larger time intervals. Giaever and Keese (1991) carried out an experiment using 0.1 mm^2 electrodes with an initial frequency sweep (22 Hz, 44 Hz, 88 Hz, 176 Hz, 352 Hz, 704 Hz, 1408 Hz, 2816 Hz, 5632 Hz, 11264 Hz, 22528 Hz, 45056 Hz & 90112 Hz) in the absence of cells. WI-38 VA13 cells (fibroblast) were then seeded at a density of 1 x 10^5 cells / cm^2 into the devices and allowed to adhere and spread for at least 24 h. Then, another frequency sweep was carried out. The two sweeps were plotted in a logarithmic (log_{10}) scale (Figure 12). The cells increased the resistance of the system at all frequencies. The electrodes were sensitive to the cells in the 100 Hz to 100 kHz range. Based on the graph in Figure 12, at a frequency of 10 kHz, the impedance without cells was approximately 1000 Ω, while the impedance with cells was approximately 6000 Ω. This implied that adherence of the cells to the 0.1 mm^2 electrodes caused an increase of approximately 5000 Ω.

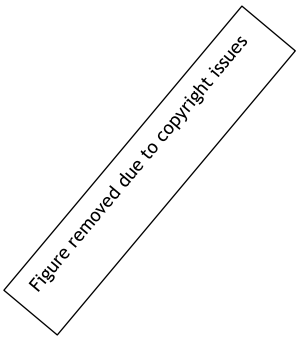

Figure 13: Impedance increases detected by working electrode with radius 150 µm and 100 µm, due to 10000 and 20000 cells / cm^2 (n = 3). (Reproduced from Zhang et al. (2017))

Zhang *et al*. (2017) studied the effects of changes in electrode dimensions on the impedance increase detected. They seeded bovine aortic endothelial cells at densities of 10000 and 20000 cells / cm^2 on working electrodes with radius 150 µm and 100 µm, in separate experiments. For the same cell density, the smaller electrode provided larger impedance increases. This implied that smaller electrodes could detect finer changes in cell density. The ratio of large electrode size to small electrode size was 1.5 : 1.0. The ratio of impedance increase of large electrode to small electrode was 1.0 : 1.7 at 10000 cells / cm^2 and 1.0 : 1.5 at 20000 cells / cm^2.

In another experiment, a multi-well ECIS device was used Figure 14 (Ablin and Jiang, 2012). Three wells were used, one without any cells (culture medium only), one with Normal Rat Kidney (NRK) epithelial cells and one with BSC-1 cells (African green monkey kidney cells). The experiment was carried out at a single frequency of 4000 Hz, and the results are shown in Figure 15.

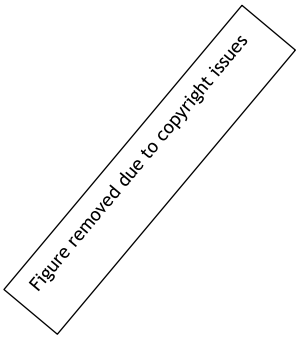

Figure 14: (a) Multi-well ECIS device (b) One well showing counter electrode (rectangular band at the top of the image) and working electrode (small circle in the middle of the image) (c) Microscopic image showing cells on and around circular working electrode. (Reproduced from Ablin and Jiang (2012))

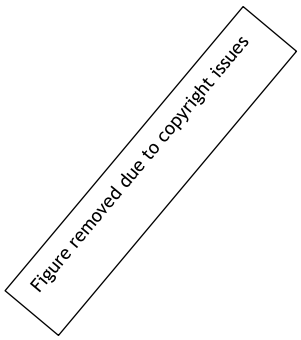

Figure 15: ECIS experiment carried out with 3 wells. No cells were seeded in well 3. BSC-1 cells were seeded in well 4 while NRK cells were seeded in well 5. Impedance was measured at regular time intervals at a single frequency of 4000 Hz. The wells with BSC-1 and NRK cells both showed increases in impedances with time, while the well without cells showed constant impedance with time (Adapted from Ablin and Jiang (2012)).

1.10.4 ECIS model

The ECIS system does not allow direct quantification of number of cells on the electrodes (Ablin and Jiang, 2012). However, it allows the change in surface coverage of the electrode, as a function of time to be monitored. ECIS can be used in the spectroscopic mode, where the complex impedance is measured over a wide frequency range, for example, 10 Hz to 100 kHz. This complex impedance can be broken down into the real component, which is the resistance and the imaginary component, which is the reactance. The capacitance can be calculated from the reactance using the following equation:

$$\boldsymbol{capacitance} = \frac{\mathbf{1}}{\boldsymbol{2\pi} \times \boldsymbol{frequency} \times \boldsymbol{reactance}}$$

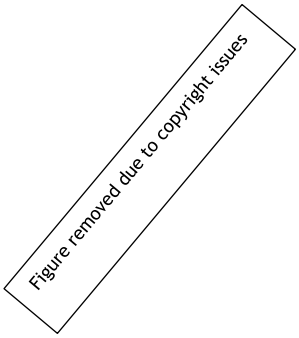

Figure 16: (A) Red arrows shows the electric current flowing from ECIS electrode and through the narrow spaces beneath and between the cells. Green arrows show the electric current capacitively coupling through the plasma membranes. The relative amounts of current flowing through those 2 routes varies with the AC frequency. (B) Measuring the complex impedance of electrodes covered with cells at different AC frequencies allows the impedance to be modelled using 3 parameters: α, which is related to the size and extent of passages beneath the cells, C_m, which is the combined series capacitances of the apical and basal membranes and R_b, which is the barrier function of the cell monolayer. (Adapted from Ablin and Jiang (2012))

The frequency which is used to measure the impedance, determines the pathway (Figure 16) of the electrical current, which can be through the cells or around the cells (Ablin and Jiang, 2012). At 400 Hz, the electrodes are insensitive to electrode coverage. The sensitivity is improved at 4 kHz, but the correlation between electrode coverage and impedance is non-linear. At 40 kHz, this correlation had a more pronounced non-linearity. The impedance readings of cells growing on ECIS electrodes allow cell proliferation and electrode coverage to be monitored. However, a complicated calibration would be required in order to extract cell proliferation and doubling times from these readings. The impedance magnitude and resistance (real component of impedance) can be used to track growth of cells on ECIS electrodes, as long as the results are compared only for one particular cell line, under constant experimental conditions (Ablin and Jiang, 2012). Capacitance measured at high frequencies (40 kHz) has a linear correlation and high sensitivity with electrode coverage. It is also insensitive to the electrical properties of the cells on the surface.

1.10.5 Cell sensing using Interdigitated Electrodes

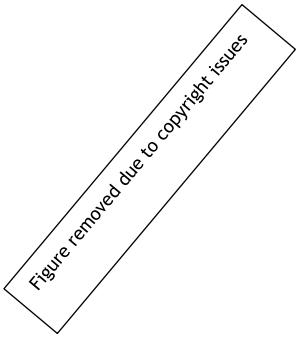

Figure 17: The schematic principles of electrical impedance spectroscopic measurement when cells are absent and present on the electrodes, along with their equivalent circuits, and the respective Bode impedance spectra and fitting spectra. In the equivalent circuits, R_{sol} and C_{dl} refer to the solution resistance and the double layer capacitance of the electrodes, respectively; R_{cell} and C_{cell} refer to the resistance and capacitance induced by the cell attachment on the IDE surface (Reproduced from Mamouni and Yang (2011))

Mamouni and Yang (2011) carried cell sensing experiments using Interdigitated Electrodes (IDE). The IDE consisted of 50 pairs of fingers, with 5 mm finger length, 15 μm finger width and 15 μm finger separation. The total electrode area was 7.5 mm^2. The different experimental conditions, equivalent circuit diagrams and impedance & phase spectra are shown in Figure 17. In the absence of cells, and with culture medium only, the impedance of the system comes from two components, which are the resistance of the solution (R_{sol}) and the double layer capacitance of the electrodes (C_{dl}). In the presence of cells on the electrode surface, the equivalent circuit contains the impedance contributions from the cells in addition to the R_{sol} and C_{dl}. The cell types used were oral cancer (CAL 27)

and non-cancer (Het-1A) oral epithelial cells. The electrodes were sensitive to the cells in the 1 kHz to 100 kHz. Based on the graphs in Figure 17, at a frequency of 10 kHz, the impedance without cells was approximately 80 Ω, while the impedance with cells was approximately 100 Ω. This implied that the 7.5 mm^2 electrodes detected an increase of approximately 20 Ω due to cell adherence. The impedance change due to cell attachment in the frequency range of 10 kHz to 100 kHz was linearly correlated to the cell number on the electrode surface and thus can be used as the basis for enumeration of cancer cells in a sample. At equal cell number, non-cancer oral epithelial cells generated a much smaller magnitude of impedance than oral cancer cells did. Therefore, the impedance measurement using IDEs could be used to detect oral cancer cells and distinguish them from non-cancer cells.

1.10.6 Monitoring cell proliferation using ECIS

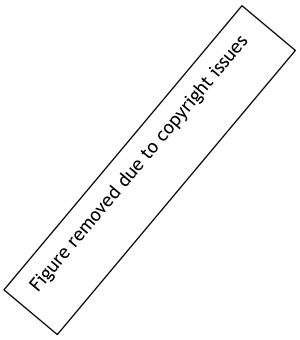

Figure 18: Two different types of ECIS electrodes commercialised by Applied Biophysics (a) 8W1E electrode with circular working electrode of 250 µm diameter (b) 8WCP electrode with a total electrode area of 3.985 mm^2. (Reproduced from (Applied Biophysics, 2014))

There are several types of ECIS electrodes, each suitable for different applications (Ablin and Jiang, 2012). When carrying out cell proliferation monitoring using ECIS, it is important to consider the size of the electrode as compared to the total growth area. The 8W1E (Figure 18a) electrode provides the highest sensitivity as it allows detection of a single cell. However, the electrode occupies only 0.1 % of the total surface area of the well. Hence this small sensing area is not

representative the situation in the well after cell adhesion, as cells might settle all around the sensing area and not directly on it. For cell proliferation experiments, ECIS electrodes (such as 8WCP electrodes) occupying a higher percentage of the well are more suitable. However, the major disadvantage of using larger electrodes is that this decreases sensitivity. Stolwijk, Michaelis and Wegener (2012) carried out a cell proliferation experiment using Normal Rat Kidney (NRK) cells at different cell densities. All measurement were taken at a frequency of 16 kHz. Figure 19a shows the normalised impedance as a function of time while Figure 19b shows the normalised capacitance as a function of time. The black curve represents the wells with the highest cell density of 3.40×10^5 cells / cm^2. The red, green and blue curves represent wells with 1.10×10^5, 0.45×10^5 and 0.08×10^5 cells / cm^2, respectively. On Figure 19a, all the curves show an increase in normalised impedance with time, with the black curve showing the highest and fastest increase. On Figure 19b, all the curves show a decrease in normalised capacitance with time, with the black curve showing the fastest decrease.

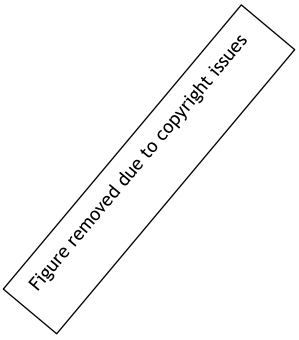

Figure 19: Cell proliferation experiments carried out with Normal Rat Kidney (NRK) cells at different cell densities (a) Normalised impedance (b) Normalised capacitance. (Adapted from Stolwijk, Michaelis and Wegener (2012))

Holland, McCormick and Connolly (2018), attempted to distinguish between pulmonary artery porcine endothelial cells, human umbilical vein endothelial cells and coronary artery porcine smooth muscle cells using ECIS-based electrodes. By using a 3D representation of impedance with both time and frequency, they were able to show that each cell type had a characteristic 3D impedance-frequency-time spectrum.

1.10.7 Detection of response of cells to external agents using ECIS system

When mammalian cells are challenged by external agents such as drugs, DNA, ligands, changes in temperature or changes in pH, they respond through morphological changes and other mechanisms (Ablin and Jiang, 2012). Changes in cell morphology causes variations in impedance, which can be detected by the ECIS system.

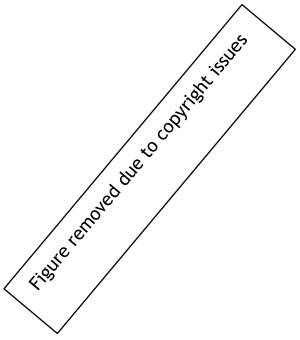

Figure 20: Responses of fibroblastic V79 cells measured as Impedance per cell against time per hour for 3 cytotoxic drugs: (A) cadmium chloride at 2.9, 4.6, 6.2 & 8.1 µM (a, b, c & d), (B) benzalkonium chloride at 15.2, 18.3, 21.3 & 30.4 µM (a, b, c & d) and (C) sodium arsenate at 45, 60, 140 & 200 µM (a, b, c & d) (Reproduced from Xiao et al. (2002)).

The changes in impedance with time could be used to assess the effects of different drugs on cells (Xiao *et al.*, 2002). If the drug was effective, it caused a decrease in proliferation, which slowed down the change in impedance or capacitance. Xiao *et al.* (2002) carried out an ECIS cell proliferation assay to assess the effects of varying concentrations of 3 different cytotoxic drugs, cadmium chloride, benzalkonium chloride and sodium arsenate, on fibroblastic V79 cells. The results are shown on Figure 20. In all 3 graphs, the control represented a well where no treatment was applied. The impedance per cell gradually increased and reached a maximum of approximately 150 Ω / cell (A), 100 Ω / cell (B) and 100 Ω / cell (C). As the concentrations of the respective drugs increased, the impedance per cell decreased and reached the cell free impedance per cell value at the highest drug concentration.

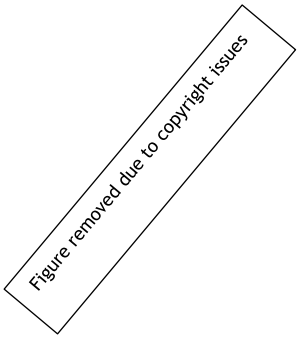

Figure 21: Effects of different titres of IHNV (infectious hematopoietic necrosis virus) on carp EPC (*Epithelioma papulosum cyprini*) cells monitored using ECIS electrodes. (Reproduced from Campbell et al. (2007)).

Campbell *et al.* (2007) studied the effects of different titres of IHNV (infectious hematopoietic necrosis virus) on carp EPC (*Epithelioma papulosum cyprini*) cells, using ECIS electrodes. The cells were seeded into ECIS wells and allowed to grow. Viability and growth of cells was monitored by measuring the resistance at 4000 Hz (Figure 21). At 70 h post-seeding, the different wells were infected with serial dilutions of the virus. For the highest titre, there was a latent period of approximately 40 h, after which the resistance started to drop until it reached the cell free resistance value. The lower the concentration of the virus, the more time it took the resistance to drop. With the control well, the resistance did not drop and gradually increased.

1.10.8 Using ECIS electrodes to induce electromediated apoptosis and necrosis

As discussed in Section 1.10, cell death can occur through apoptosis or necrosis or a mixture of the 2 processes. Apoptosis and necrosis have very specific morphological signatures (Stolwijk, Michaelis and Wegener, 2012). Cells undergoing apoptosis, shrink but do not lose the plasma membrane integrity. These cells also lose contact with neighbouring cells, exhibit nuclear membrane and plasma membrane blebbing, form cytoplasmic vacuoles with condensation and DNA fragmentation.

Cells undergoing necrosis swell and there is rupture of the plasma membrane, releasing cytoplasmic molecules into the extracellular space. When the whole cell population within a culture well is affected by apoptosis or necrosis, the electric current injected by the electrodes is not impeded by dielectric cell bodies because of cell permeabilisation or cell rounding (Stolwijk, Michaelis and Wegener, 2012). When cells on ECIS electrodes are exposed to several volts for tens of seconds, there is irreversible dielectric breakdown of the plasma membrane (electroporation), leading to irreversible membrane permeabilisation and ultimately to cell death. This is an example of fast and irreversible necrosis.

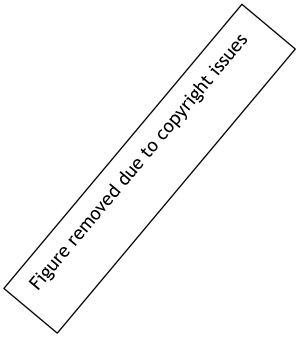

Figure 22: Fluorescent micrographs of Normal Rat Kidney (NRK) cells grown on ECIS 8W1E electrodes after staining with Ethidium Homodimer (ETHD) and Calcein AM (CAM) (a) Control well where no invasive electric was applied (b) Treatment well where a sinusoidal voltage pulse of 5 V and 40 kHz was applied for 30 s. (Reproduced from Stolwijk, Michaelis and Wegener (2012))

Figure 22 shows 2 culture wells containing ECIS 8W1E electrodes with Normal Rat Kidney (NRK) cells. The cells in both wells were stained with Calcein Acetoxymethyl (CAM) and Ethidium Homodimer (ETHD) (Anthea Stolwijk, 2011). CAM is the non-fluorescent membrane-permeable precursor of Calcein, which is fluorescent and membrane impermeable. CAM is converted to Calcein in the cytoplasm of living cells by unspecific esterases. ETHD is a non-fluorescent membrane-impermeable dye. When the cell membrane is damaged, ETHD diffuses into cells and the nucleoplasm and incorporates into the DNA and shows a bright red fluorescence.

The well in Figure 22a was the control well where no voltage was applied. All the cells appeared green due to the Calcein dye. In Figure 22b a sinusoidal voltage pulse of 5 V and 40 kHz was applied for 30 s. The image was captured after the application of this voltage. The cells around the circular electrodes all appeared green. The cells directly on the electrode all showed bright red fluorescence because the voltage damaged the cell membrane and allowed ETHD to integrate into the DNA.

1.11 Cell death and its mechanisms

1.11.1 Introduction

Cell death can occur as a result of passive disruption of plasma membrane by external environmental factors or as a result of activation of intrinsic cell death programs (Zhang *et al.*, 2018). Apoptosis is the most characterised type of cell death which occurs with an intact cell membrane. Necrosis involves rupture of plasma membrane. Dying cells can undergo silent removal (without inflammation) or noisy removal (with inflammation) (Kung, Konstantinidis and Kitsis, 2011). Figure 23 shows scanning electron micrographs of cells undergoing apoptosis, necroptosis and pyroptosis.

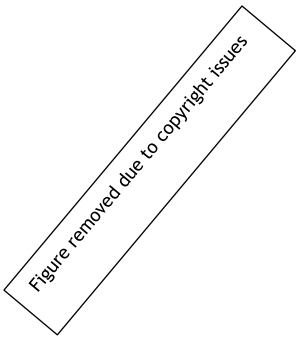

Figure 23: Scanning electron micrographs of RAW264.7 cells undergoing apoptosis, necroptosis and pyroptosis (Reproduced from Zhang et al. (2018)).

1.11.2 Apoptosis

Apoptosis involves of DNA fragmentation, nuclear condensation, caspase activation and phosphatidylserine flipping (Kurokawa and Kornbluth, 2009). Other morphological changes involved are cytoplasmic condensation, chromatin condensation, cell shrinkage, breakage of cells and formation of membrane bound apoptotic bodies (Zhang *et al.*, 2018). The plasma membrane first undergoes blebbing and then bleb separation, leading to formation of apoptotic bodies. Membrane blebbing is driven by an increase in hydrostatic pressure due to cell shrinkage and loss of interaction with the cytoskeleton. The flipping of phosphatidylserines (PS) is enriched in apoptotic blebs (Coleman *et al.*, 2001). PS flipping aids in apoptotic cell recognition and clearance by phagocytes (Poon *et al.*, 2014). PS flipping is inducible and reversible. When a cell is undergoing apoptosis, intact organelles, fragmented organelles, fragments of nucleus and DNA are trapped inside apoptotic bodies, which are non-uniform sub-cellular fragments. Not all cells undergoing apoptosis fragment into apoptotic bodies. Apoptotic cells are not required to disassemble into sub-particles to be efficiently cleared as professional phagocytes engulf their targets in their entirety (Parnaik, Raff and Scholes, 2000). It is still not clear whether apoptotic bodies form in order to facilitate cell clearance.

1.11.3 Necrosis

Necrosis involves dysfunction of lysosomal membranes (resulting in protease release), endoplasmic reticulum membrane (resulting in release on intracellular Ca^{2+}) and plasma membrane (resulting in loss of cell homeostasis and cell swelling) (Kung, Konstantinidis and Kitsis, 2011). Necrotic cells can be removed without inflammation if they exhibit PS on their surface (Krysko, de Ridder and Cornelissen, 2004). However, if the necrotic cells are already affected by membrane permeabilisation, they release nucleic acid and protein factors that mediate an inflammatory response (Kung, Konstantinidis and Kitsis, 2011).

1.11.4 Other types of cell death

Recent studies have shown that necrotic cell death can be caused by intrinsic programs (Nagata and Tanaka, 2017). Rogers *et al.* (2017) showed that the rupture of the plasma membrane in apoptotic cells progressing to secondary necrosis is intrinsically programmed. This involves plasma membrane pore formation. It is the gradual loss of plasma membrane integrity of apoptotic cells (Berghe *et al.*, 2010). It can be observed *in vivo*, in tumour cells subjected to chemotherapy or radiotherapy, when apoptotic cells are not effectively cleared by scavenging cells (Rogers *et al.*, 2017). The morphological changes occurring during necroptosis are swelling of organelles and rupture of plasma membrane (Zhang *et al.*, 2018). The intracellular osmolality increases due to influx of Na^+ and other cations through MLKL channels, leading to an explosion-like membrane rupture. Pyroptosis also involves plasma membrane rupture (Zhang *et al.*, 2018). During pyroptosis, plasma membrane rupture is mediated by the GSDMD (Gasdermin D) pore (Chen *et al.*, 2016). It involves pyroptotic body formation and cell flattening. Pyroptotic cells can be observed *in vitro* as cells with flattened cytoplasm, which remain tightly attached to the culture slides. Unlike MLKL channels, GSDMD pores have no selectivity for cations or anions. This is why pyroptotic cells show minimal swelling and flattened cytoplasm.

1.11.5 Distinguishing the different types of cell death

Apoptosis can be identified using stains such as Annexin, which bind to PS exposed on cell surface of apoptotic cells. Terminal deoxynucleotidyl transferase dUTP nick end labelling. Terminal deoxynucleotidyl transferase dUTP nick end labelling (TUNEL) allows detection of apoptotic DNA fragmentation (Kung, Konstantinidis and Kitsis, 2011). Necrosis can be identified morphologically through cell swelling and organelle swelling. Distinguishing these 2 types of cell death is difficult because they employ some common molecular pathways (Kung, Konstantinidis and Kitsis, 2011). Moreover, TUNEL may not be specific to any of these 2 types of cell death. *In vitro*, phagocytes are not usually present in the cell cultures to clear apoptotic cells. These cells usually transition to secondary necrosis. Hence, cell death has to be analysed early in the process.

1.12 Cell culturing under flow conditions

Li *et al.* (2013) cultured bovine pulmonary artery endothelial cells within compliance chambers under culture medium flow conditions. The flow was generated using a pulsatile blood pump, which could generate low pulsatility and high pulsatility. The mean flow rate was kept constant for both conditions leading to a mean shear stress of 12 dyn / cm^2. For both low and high pulsatility, the length of the endothelial cells after flow exposure for 24 h was higher compared to static conditions. Moreover, the elongation was higher with high pulsatility than with low pulsatility. However, high pulsatility flow was associated with a high percentage of cell loss.

1.13 Migration of endothelial cells against flow

Under certain conditions, endothelial cells migrate against the blood flow. One of these conditions is the regression of blood vessel segments, which is a process required for functional vascular branching patterns (Franco *et al.*, 2015). Endothelial cells orientate and migrate against the blood flow because of local differences in blood flow. Polarised migration of endothelial cells leads to the regression of segments subjected to low flow and the stabilization of segments subjected to high flow. In another study, Rochon, Menon and Roman (2016) demonstrated that activin receptor-like kinase 1 (Alk1) played an important role "in preventing development of shunts through proximal pre-capillary segments by preventing arterial endothelial cell migration into these vessels, in the direction of blood flow".

1.14 Literature review rationale and aims of the project

Despite years of innovation in stent technologies, the newer generation DES are associated with 2.91 % revascularisation rates. This indicates that DES have reached a plateau phase and that there is a need for a new revolution if stent technologies. Several research groups have attempted to develop smart stents. In some approaches, the whole stent was used as an electrode, providing average impedance measurement of the whole stent. Other approaches coupled capacitive sensors to inductive stents as a way of measuring intra-stent blood pressure to monitor progression of in-stent restenosis. Other research groups have developed impedimetric sensors in view of integrating this onto smart stents. This is a very promising approach, as it had the potential of distinguishing different cell types.

The aims of the project are as follows:

- Design and fabricate different types of electrodes for use as biosensors for cell detection.
- Use a high cell density to identify optimum sensing frequency range and optimum sensing frequency.
- Determine electrode type which is less susceptible to external factors such as volume and conductivity changes, and thus more suitable for cell sensing.
- Vary dimensions of the chosen electrode to optimise sensitivity.
- Determine sensitivity of the electrodes.
- Continuously monitor adherence, growth and death of cells.
- Test cell sensing with different cell types (smooth muscle cells and endothelial cells).
- Distinguish smooth muscle cells and endothelial cells.
- Determine voltage characteristics which induce death of smooth muscle cells.
- Determine type of cell death (apoptosis or necrosis) triggered by applied voltage.
- Determine if electrodes can detect gradual cell migration and proliferation under flow conditions.

CHAPTER 2

MATERIALS AND METHODS

2.1 Introduction

The project involved both biological and engineering aspects. Thus, work had to be carried out in several laboratories of the University of Glasgow. These included the British Heart Foundation Level 4 (cell culturing, cell seeding, device assembly, preliminary testing, impedance measurements, live cell microscopy, timelapse imaging and image analyses), James Watt Nanofabrication Centre (substrate cleaning, resist spinning, photolithographic patterning, plasma ashing and e-beam metal deposition) and Ranking Building Level 8 Biomedical Engineering (reflected microscopy and preliminary testing).

2.2 Cell culture

2.2.1 Cell types

Two cell types were used for the project. The first one was Mouse Aortic Smooth Muscle Cells (MASMCs). These cells were isolated from whole mouse aorta C57BLK6/J mice (Envigo - UK). The aorta was cut into 1 mm^2 sections and placed inside a 6-well plate with a sterile glass cover slips. 2 mL of pre-warmed DMEM culture media (Dulbecco's Modified Eagle's Medium - high glucose - D5671 – Sigma Aldrich - UK) was pipetted into each chamber and incubated for 2 - 4 weeks. Then the explanted cells were trypsinised and confirmed as smooth muscle actin positive as per Mercer *et al.* (2005). The lowest passage number for MASMCs was 3 and the highest passage number was 20. The second cell type was murine endothelial cell line sEND1, which had been previously characterised by Leiper *et al.* (2002). This cell type was referred to as Mouse Endothelial Cells (MECs) throughout the whole thesis. The lowest passage number for MECs was 15 and highest passage number was 30.

2.2.2 Cell culturing, counting and seeding

Most of the cell culturing was carried out using HEPES DMEM (DMEM HEPES - 12430054 - ThermoFisher Scientific - UK) while some experiments were carried out using normal DMEM (DMEM - 11965092 - ThermoFisher Scientific - UK). HEPES (4-(2-hydroxyethyl)-1-piperazineethanesulfonic acid) DMEM was used as it allowed the pH to be buffered (for a maximum of 24 h) when the cell culture chambers were taken out of the incubator for impedance measurements. Normal DMEM was used for long term timelapse imaging inside the CO_2 buffered microscope enclosure. MASMCs and MECs were grown in T75 and T150 culture flasks (Corning™ Cell Culture Treated Flasks – 430825 – Fisher scientific - UK). Excess cells were frozen down at a cell suspension density of 1 x 10^6 cells / mL with 10 % DMSO (Dimethyl Sulfoxide - Fisher Chemical D/4120/PB08 – Fisher scientific - UK). This ensured a stock of both cell types throughout the project.

In order to seed cells into fabricated devices, MASMCs or MECs were detached from the bottom of the culture flasks. This was carried by pipetting out the culture medium, washing with phosphate-buffered saline (DPBS – 14190250 - ThermoFisher Scientific - UK), washing with TrypLE™ Select Enzyme (A1217701 – ThermoFisher Scientific - UK) and detaching using TrypLE™ Select Enzyme for 5 min. TrypLE was quenched by adding an equal volume of culture medium. Cell counting was carried out using a haemocytometer. The cell suspension was spun down in a centrifuge at 2000 rpm (revolutions per minute) for 5 min. Most of the supernatant was removed, ensuring that most of the TrypLE was removed. The cell pellet was resuspended in 1 mL. The required volume of cell suspension (containing the required number of cells) was pipetted out and seeded into the fabricated devices. Fresh HEPES DMEM was then pipetted into the devices.

All experiments were carried out using either a cell chamber (length 24 mm, width 20 mm and height 10 mm) and a microfluidic chamber (length 50 mm, width 5 mm and height 0.8 mm). Preliminary experiments allowed the minimum cell number required for formation of a cell monolayer within 18 h to be identified as 200,000 cells for the cell chamber. This was particularly important for experiments where the electrodes were used to monitor adherence, plateau phase and death phase. In experiments where proliferation was studied lower cell numbers such as 100,000 were used. This lower cell number was also important when effects of

higher voltages were studied on individual cells, rather than on the whole monolayer. In experiments where the highest possible impedance increase was required 400,000 cell were seeded. The microfluidic chamber required seeding at a cell density of 500000 cells / mL to establish a monolayer.

2.2.3 Cell seeding of flow device

For experiments involving cell culturing with flow of culture medium, flow chambers were acquired from Ibidi (sticky-Slide I Luer 0.8 mm – 80198 - ibidi GmbH – Germany). These were assembled on top of electrode-patterned slides (Section 2.5.2). The device was sterilised (Section 2.7.1). The microfluidic channel was coated with collagen (Collagen Type I solution from rat tail - C3867 – Sigma Aldrich – UK). 200 µL of 10 µg /cm^2 collagen solution was made up from the stock solution and this was pipetted into the microfluidic channel. The solution was removed after 5 h and the channel was allowed to dry for 5 h. The instructions (Ibidi, 2015) provided with the flow chamber were used for seeding cells into the channel. Previous attempts showed that the optimum MASMCs or MECs density for the channel was 500000 cells / mL. The cell suspension was prepared in a universal flask. The flow channel had a volume of 200 µL. This volume of cell suspension was pipetted into the channel using a 200 µL pipette. The tip of the pipette was placed at the edge of the channel (Figure 24) and the suspension was slowly pipetted down, avoiding any air bubbles.

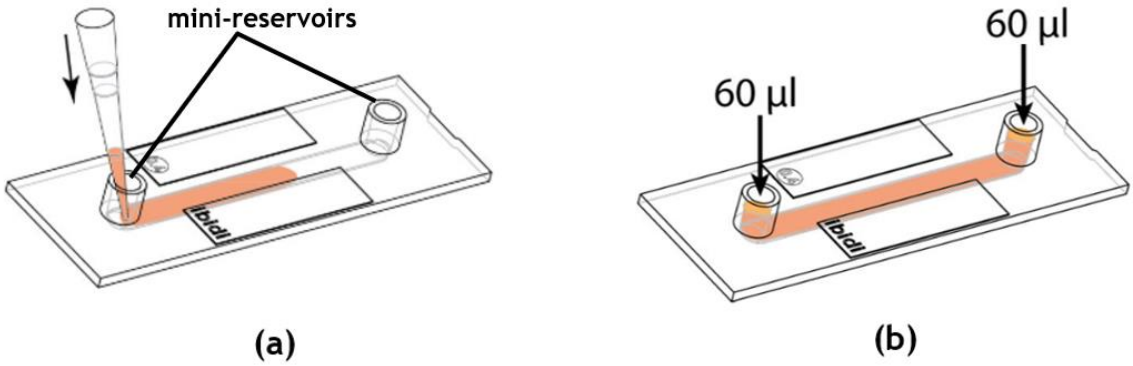

Figure 24: (a) Technique for seeding cells into flow channel & (b) Mini-reservoirs filled with 60 µL of culture medium. (Adapted from Ibidi (2019))

The mini-reservoirs at both ends were then filled with 60 µL of culture medium each. The cells where then allowed to settle down in an incubator (37 ^{0}C with CO_2 supply) for 3 - 5 h until the cells had adhered to the bottom of the channel. Then, the flow circuit was connected and culture medium flow started (Section 2.8). For some experiments, cells were only required in a fraction of the channel. Hence the cell suspension was only pipetted into that fraction of the channel. The flow device was then left inside an incubator for 3 - 5 h, until the cells had settled down. Then, fresh culture medium was pipetted into the channel (until it was completely filled) and into the mini-reservoirs. Then the flow circuit was connected (Section 2.8).

2.2.4 Cell staining

Acridine Orange (AO)

AO is a metachromatic intercalator which is sensitive to DNA (Deoxyribonucleic acid) conformation (Parng *et al.*, 2004). It is widely used for detecting apoptosis. This dye diffuses easily through the cell membrane (Vermes and Haanen, 1994). It accumulates in lysosomes due to its weak basic property. AO can still accumulate inside lysosomes during the early stages of apoptosis but not during necrosis. When cellular DNA forms a monomeric bond with AO, this results in green fluorescence. In this case, the excitation maximum is 502 nm and the emission maximum is 525 nm (green) (AAT, 2019). When RNA forms a polymeric bond with AO, this results in red fluorescence. In this case, the excitation maximum shifts to 460 nm (blue) and the emission maximum shifts to 650 nm (red).

A working solution of 3 µg / mL was prepared from a stock solution (Acridine Orange - A3568 - ThermoFisher Scientific - UK). In order to stain the cells (adherent), the culture medium was first pipetted out of the devices. Then the cells were washed with 1 mL of PBS. Then, 1 ml of the AO working solution was pipetted onto the cells. The dye was allowed to incubate for 5 min. Then, the dye was removed and the cells were washed with 1 mL PBS. Fresh culture medium (2 mL) was then pipetted onto the cells. The device was covered with aluminium foil to prevent the dye from bleaching, and then transported to the live cell microscope for imaging.

Apoptosis / Necrosis Detection Kit

This kit (Apoptosis/Necrosis Detection Kit - ab176749 – abcam - UK) (Abcam, 2016) allowed simultaneous monitoring of apoptotic, necrotic and live cells. It is a mixture of Apopxin Green Phosphatidylserine (PS), 7-AAD (7-aminoactinomycin D) and CytoCalcein Violet 450 (CV). PS and 7-AAD were ready to be used. CV had to be prepared from a powder. 100 µL of DMSO was added to make up a 200X solution. In order to stain cells, the DMEM media was first pipetted out of the device. The cells were washed with PBS. The working dye solution was prepared using Phenol Red Free (PRF) - Serum Free (SF) - HEPES media. Culture media without Phenol Red was used, as the Phenol Red would interfere with the fluorescent dyes. 5 µL of each of PS, 7-AAD and CV were pipetted into 500 µL of PRF - SF - HEPES media.

The staining solution was pipetted onto the cells, and the dyes were allowed to incubate for 1 h. Then the staining solution was pipetted out, the cells were washed with PBS and fresh PRF - HEPES (with serum) was pipetted onto the cells. The device was covered with an aluminium foil and transported to the live cell microscope for imaging.

	Channel/ color	Apoptotic cell	Necrotic cell	Viable cell
Apopxin Green	Green	Yes	No	No
7-AAD	Red	Yes (at late stage)	Yes	No
Cytocalcein violet 450	Blue	No	No	Yes

Table 3: Fluorescent channel and type of cell stained by Apopxin green, Cytocalcein violet and 7-AAD. (Reproduced from Abcam (2016)

2.3 Microscopy

2.3.1 Hardware components

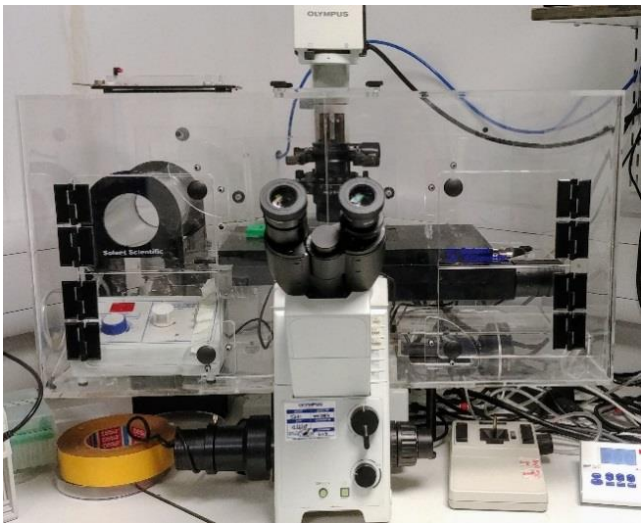

Figure 25: Live cell microscope (Olympus IX71) with warmed (37 ^{0}C) and CO_2 buffered enclosure (Solent Scientific).

A live cell microscope (IX71 - Olympus - Japan) with warmed enclosure (Solent Scientific Ltd - UK) was used for acquiring microscopic images throughout the project. The enclosure also included a CO_2 supply with regulator, which allowed long experiments (> 24h) to be carried out using normal DMEM media. This inverted microscope allowed for transmitted microscopy only because the bright field light source was at the top and the camera at the bottom. It also included a fluorescent light source, thus allowing for fluorescence imaging. The setup included a motorised stage which could be controlled using the cellSens software (Olympus - Japan) and allowed features such as multiple positions acquisition (MPA) and Multiple Image Alignment (MIA).

2.3.2 Software components

The microscope was interfaced using cellSens software (Figure 26). Microscopic images at 2x, 10x and 40x could be viewed live using the camera. The images could be acquired at single timepoints or at multiple timepoints (resulting in a timelapse series). By using the motorised stage, several positions could be

selected and timelapse series created for each position. The MIA feature allowed for several frames to be stitched together in order to view the whole sample.

For this project, it was useful to acquire images of the whole electrode area. This was not always possible at 2x magnification, as the some of the electrodes were larger than the field of view. Hence, MIA allowed two or more frames to be stitched together, resulting in an image of the whole electrode (or area of interest). Under bright field light, the phase ring was adjusted so that it casted a shadow on the cells resulting in a pseudo 3D relief. This made it easier to distinguish the cell outlines.

For fluorescence imaging, FITC, DAPI and Texas Red channels were used. For Acridine Orange (AO) stain, images were acquired on FITC channel only with an exposure time of 500 ms. For Apoptosis / Necrosis Detection Kit (ANDK), FITC, DAPI and Texas Red were used at the following exposure times respectively: 3 s, 5 s and 3 s.

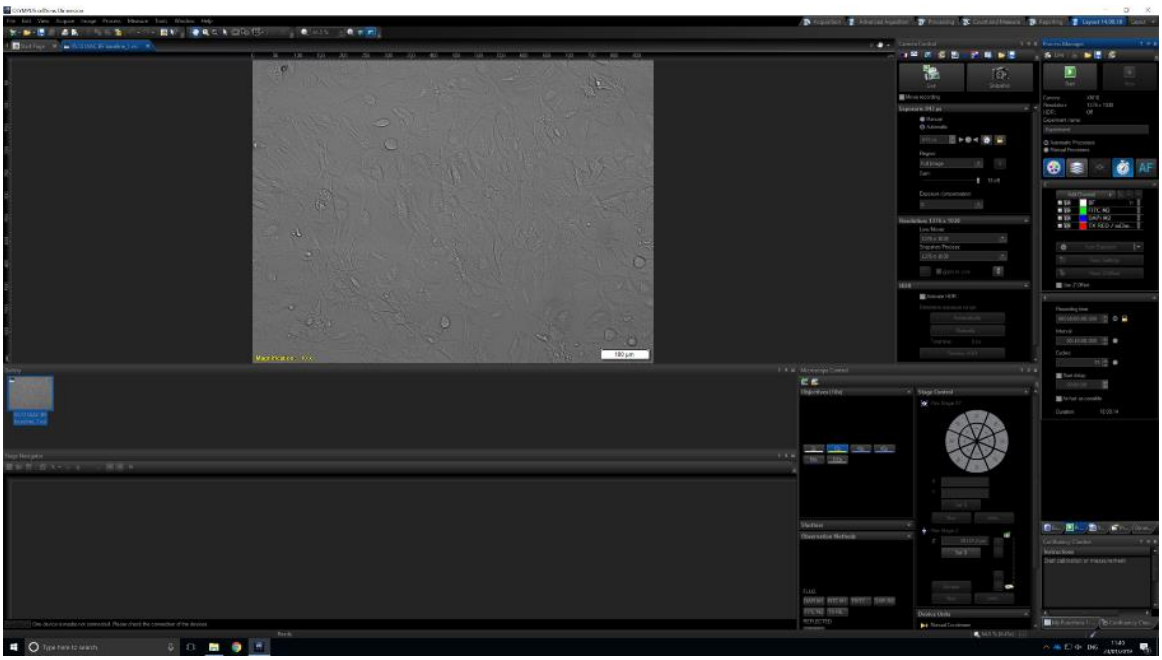

Figure 26: cellSens interface.

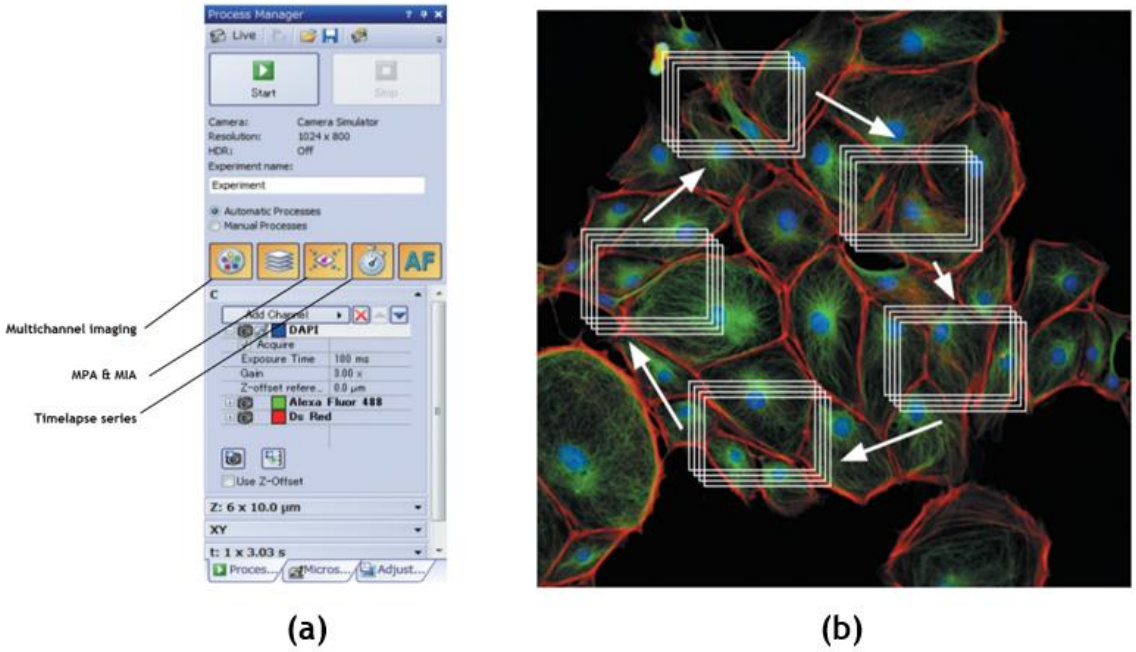

Figure 27: (a) Process manager window of cellSens software allowing multichannel imaging, MPA, MIA and timelapse series (b) Example of large observation field acquired at 10x and 5 observation positions acquired at 40x (Reproduced from Olympus (2013)).

2.3.3 Timelapse imaging

The cellSens dimensions software allowed timelapse series to be generated by acquiring images at regular time intervals. For most of the experiments, 15 min intervals were chosen, while for some 10 min or 1 s intervals were chosen. The total duration of the timelapse also had to be set. This varied from a few minutes to 96 h for the experiments.

2.3.4 Multiple Position Acquisition and Multiple Image Acquisition

MPA allowed for several positions to be selected in a large observation field (Olympus, 2013). This large field was generated under 2x or 10x magnifications. Then single observation positions (2x or 10x magnification) were selected. This was a useful way of generating replicates, for example, 3 experimental positions and 3 control positions.

2.3.5 Multichannel imaging

This feature allowed images to be acquired under fluorescent light. In the experiments, red (Texas Red), blue (DAPI) and green (FITC) channels were used. The cellSens software allowed each channel to be acquired individually. A combined multichannel image was then created using 2 or 3 channels. Additionally, the fluorescent image could be overlaid onto the bright field image.

2.3.6 Combined image acquisition

Any of the above acquisition modes could be combined. The following combinations were used in the experiments:

- MPA and timelapse series
- MIA and timelapse series
- MPA, timelapse series and multichannel
- MIA and multichannel

2.4 Electrode design and mask fabrication

The software L-edit (Mentor Graphics Corporation - USA) was used to design the electrodes. The 2 electrode designs used were Interdigitated Electrodes (IDE), Pendulum Electrodes (PE). The number of fingers, finger width, finger length and finger separation were changed to create different types of IDEs.

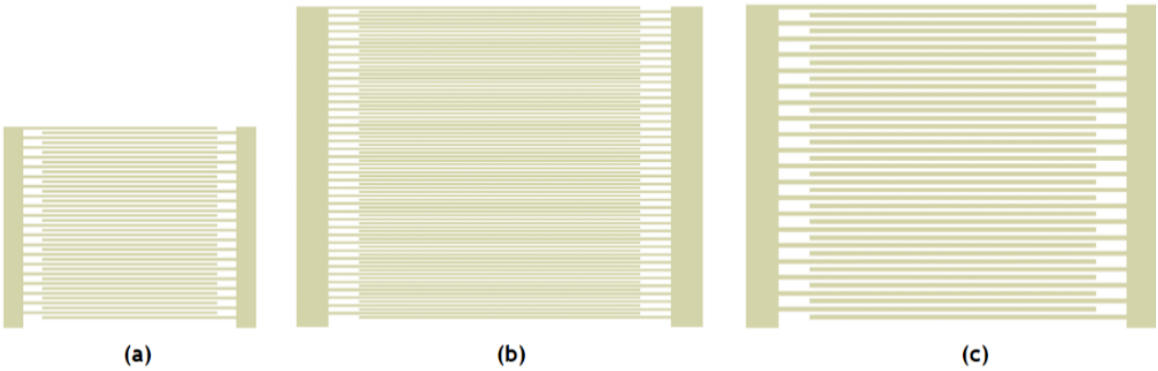

Figure 28: L-Edit designs of different electrodes: (a) super small Interdigitated Electrode (ssIDE), (b) small Interdigitated Electrode (sIDE) and (c) normal Interdigitated Electrode nIDE (drawings not to scale)

The IDE used in most experiments was referred to as the normal IDE (nIDE) (Figure 28c) and had the following dimensions and features:

- 20 sets of fingers on each side.
- Each finger had a length of 8 mm and width of 100 µm.
- The separation between each finger was 100 µm.
- Effective electrode surface area of 28.8 mm^2.

The small IDE (sIDE) (Figure 28b) had the following dimensions and features:

- 40 sets of fingers on each side.
- Each finger had a length of 8 mm and width of 50 µm.
- The separation between each finger was 50 µm.
- Effective electrode surface area of 28.8 mm^2.

The super small IDE (ssIDE) (Figure 28a) had the following dimensions and features:

- 20 sets of fingers on each side.
- Each finger had a length of 2 mm and width of 50 µm.
- The separation between each finger was 50 µm.
- Effective electrode surface area of 1.8 mm^2 (16 times smaller than nIDE and sIDE).

The pendulum electrodes (PEs) (Figure 29):

- Consisted of 4 circular electrodes and a large counter-electrode.
- Each CE had a surface area of 0.2 mm^2 while the counter-electrode had a surface area of 162.6 mm^2 (approximately 813 times larger than CE).
- The minimum separation between the CE and counter-electrode was 2.8 mm.

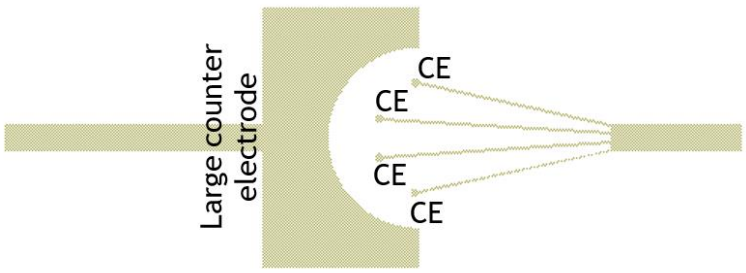

Figure 29: L-Edit design of Pendulum Electrode (PE)

Microfabrication

Microfabrication of the IDEs and PEs was carried out in the James Watt Nanofabrication Centre (JWNC) of the University of Glasgow. The substrate used was glass microscope slides. Gold was deposited onto the glass with a titanium adhesion layer.

2.4.1 Substrate cleaning

Fabrication was carried out using microscope glass slides (Sigma Aldrich - UK) as substrate. The substrate was cleaned to the microscopic level, in order to promote metal adhesion during the deposition process. The cleaning process was carried out as follows inside a Laminar Flow Cabinet:

- The slides were placed inside a slide holder, which was then filled with absolute acetone.
- The holder was placed onto an ultrasonic water bath and ultrasonic cleaning was carried out for 5 min.
- The acetone was then decanted.
- Immediately after, the holder was filled with isopropanol, ultrasonic cleaning carried out for 5 min, and the isopropanol was then decanted.
- Immediately after, the holder was filled with methanol, ultrasonic cleaning carried out for 5 min, and the methanol was then decanted.
- The slides and holder were thoroughly rinsed under Reverse Osmosis water for 2 min.
- Each slide was then carefully removed from the holder using tweezers and air-dried.

2.4.2 Spin coating of primer & resist and baking

In order to pattern the metal, a positive photoresist was required. 80/20 Primer was first spin-coated at 4000 rpm for 30 s onto the slides. Then, S1818 photoresist was spin-coated at 4000 rpm for 30 s. The slides with primer and resist were then baked on a hotplate at 115 ^{0}C for 5 min.

2.4.3 Photolithography and resist development

The photomask fabricated by Compugraphics was used for this step. A copy of the required design was then transferred into a ferrite mask copy. This copy was used in a Mask Aligner (MA6 – SUSS MicroTec - USA) to expose the spin-coated photoresist to Ultraviolet light. The exposure time was 8 s and the alignment gap was 50 μm. The photoresist then had to be developed. This carried out by immersing the slide into MF319 Developer (MicroChem Corp – USA) and squirting this solution onto the slides for 75 s by using a pipette. The development was then stopped by immersing the slide into Reverse Osmosis water. The slides were then air-dried.

2.4.4 Plasma ashing, e-beam metal deposition and lift off

Plasma ashing was the final cleaning step required just before metal deposition. This was carried out at 100 W for 2 min. This step activates the substrate and improves metal adhesion. Metal deposition was carried out using Plassys MEB 400S Electron Beam Evaporator (PLASSYS Bestek – France). The 2 recipes used were ***Titanium 5 nm / Gold 30 nm*** and ***Titanium 10 nm / Gold 100 nm***. Hence, an adhesion layer of titanium was first deposited onto the slides. Then gold was deposited. The slides were then left in warm acetone (50 ^{0}C) for 18 h to lift off the excess metals.

2.4.5 Final electrodes

The first batch of fabricated electrodes (Figure 30) had missing parts. These missing parts were generally at the ends of the slides. The middle parts were unaffected. Thorough examination under the microscope showed that the photoresist was still present in the missing regions, and this prevented the metals from adhering to the glass. The photoresists formed “arcs” at the ends of the slides. This was attributable to the spin-coating steps. As the slides were rectangular, photoresist would tend to accumulate at the ends. In order to minimise this effect, spin-coating of both primer and resist were carried out at 6000 rpm as opposed to 4000 rpm. This improved the final result (Figure 31).

Figure 30: First batch of electrodes (spin coating carried out at 4000 rpm) showing gaps in the patterns

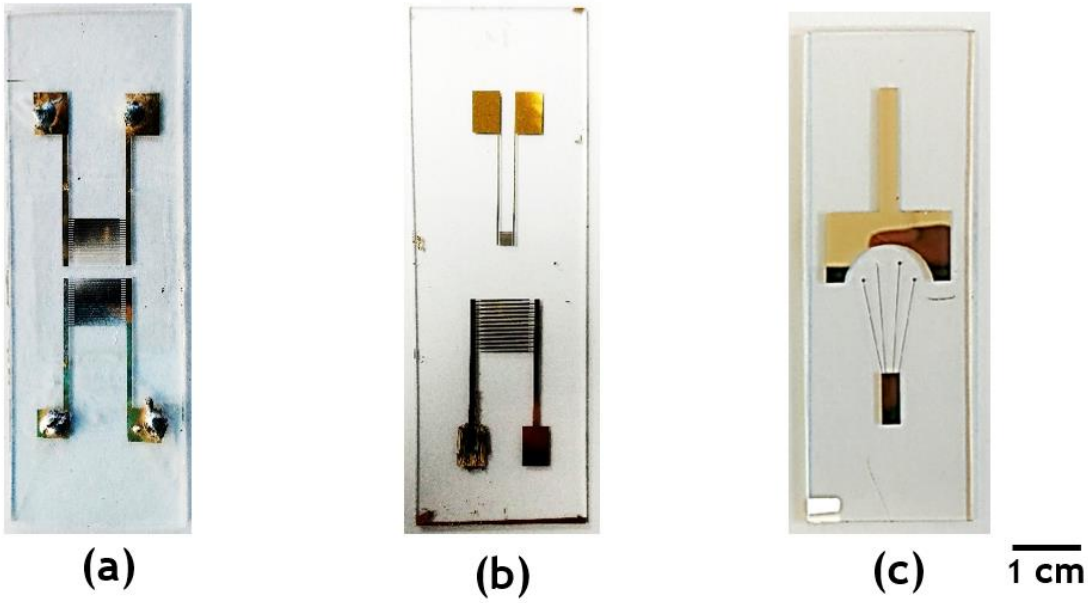

Figure 31: Second batch of electrodes where spin coating was carried out at 6000 rpm. (a) nIDE + nIDE, (b) nIDE + ssIDE and (c) PE

2.5 Assembly of impedance, apoptosis and flow devices

2.5.1 Materials

The materials required for assembling the devices were as follows:

- Electrode-patterned slides
- 2-well slide chambers (Sigma Aldrich - UK)
- Electric wires (RS components - UK)
- Solder (RS components - UK)
- UV curable glue (Loctite – UK)
- Sticky-Slide I Luer 0.8 mm (Ibidi – Germany)

2.5.2 Assembly of devices

The plastic component of a 2-well slide chamber was first removed. The chamber was then cut resulting in a one-well chamber (Figure 32c). UV curable glue was then spread along the bottom edges of the chamber. This was then carefully mounted on top of the electrode-patterned glass, while ensuring that the electrode was at the middle of the well. The glue was then cured using UV light. Wires were then soldered to the contact pads.

The flow device was first assembled by using the double-sided tape already present at the bottom of sticky-Slide (Ibidi, 2019). However, preliminary tests with the flow circuit connected led to culture medium leakage from the assembled device. The double-sided tape was not adhering strongly enough to the electrode-patterned glass.

Hence, the sticky-Slide was glued onto the glass using UV curable glue. The glue was spread around the channel and inlet/outlet. The glue was cured using UV light. As the glue was initially liquid, it settled down irregularly leading to an irregular channel, once cured. Wires were then soldered to the contact pads.

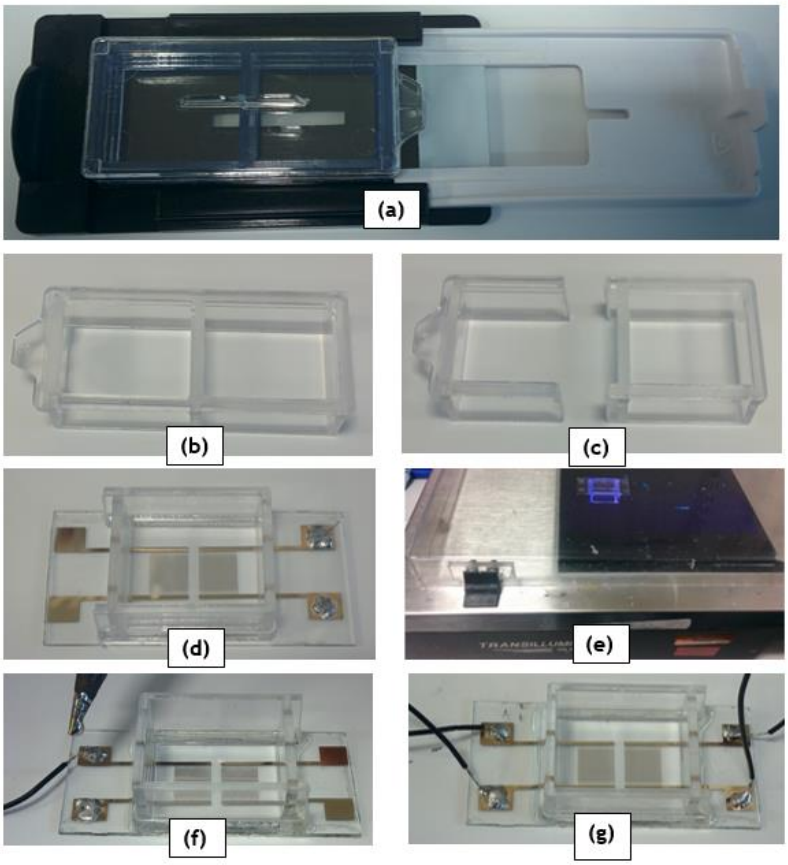

Figure 32: (a)(b) Plastic chamber was dismounted from glass slide, (c) Chamber was cut resulting in one-well chamber, (d) UV curable glue was used to mount chamber onto electrode-patterned glass, (e) Glue was cured using UV light, (f)(g) Wires were soldered to contact pads.

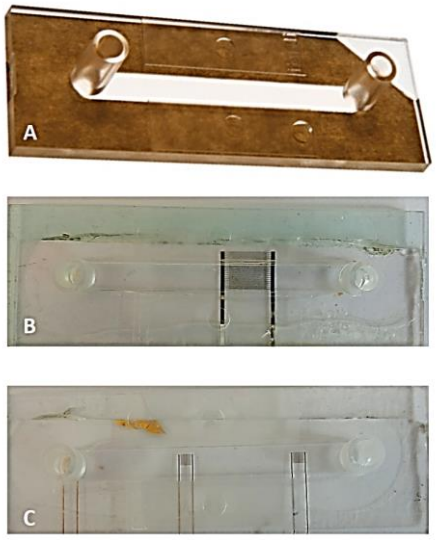

Figure 33: (A) Commercial sticky-Slide I Luer (0.8 mm depth) with double-sided tape at the bottom (Ibidi, 2019), (B) Sticky slide was mounted, using UV curable glue, onto a slide containing 1 nIDE and (C) Sticky slide was mounted, using UV curable glue, onto a slide containing 3 ssIDEs.

2.5.3 Continuity testing

To ensure that soldering was correctly done, continuity tests were performed from one of the wires to the end of the electrode conducting arm. If the resistance was > 500 Ω, the soldering was done again. Continuity tests were also performed from one electrode to the other to check for short circuits. If resistance was too low, this indicated a short circuit. This could be caused a piece of gold stuck between the fingers after the metal lift-off during microfabrication. Hence, cleaning of the electrode using a cotton bud removed the short circuit. Another cause of the short circuit could be a defect during the fabrication process leading to a "metallised" short circuit. In this case, it was very difficult to remove the short circuit and the device had to be discarded.

2.6 Device sterilisation

2.6.1 Pre-seeding cleaning

As device fabrication was carried out under non-sterile conditions, sterilisation was required before each biological experiment. The Interdigitated Electrode devices (IDE) and Pendulum Electrode (PE) devices were first rinsed under tap water for 30 s. Then 70 % ethanol was sprayed into the device. They were then transferred into the cell culture hood (CCH).

The devices were then rinsed using deionised water into and out of them. These devices were allowed to dry and were then ready for cell seeding. The flow devices were sterilised by first flowing 70 % ethanol through the channels using 5 mL syringes. The channels were then rinsed using deionised water. The flow devices were transferred into the CCH and were ready for cell seeding.

2.6.2 Post-experiment cleaning

After each experiment, the devices needed to be cleaned to remove cells and cell debris. The IDE and PE devices were thoroughly rinsed under tap water. Cotton buds were used to clean the electrodes and substrate of cells and cell debris. Cleaning of the flow devices was more difficult as the electrodes were enclosed within the channel. The channels and mini-reservoirs were filled with 2x TrypLE. Syringes with 2 mL of TrypLE were then attached to the mini-reservoirs. TrypLE was flowed from one syringe to the other for a few times. This was then left for 18 h. Then the TrypLE was flowed across the channel again, ensuring all cells and cell debris were detached. The TrypLE was then removed and the channel was rinsed with deionised water. The devices were then ready for sterilisation and further experiments.

2.7 Flow circuit

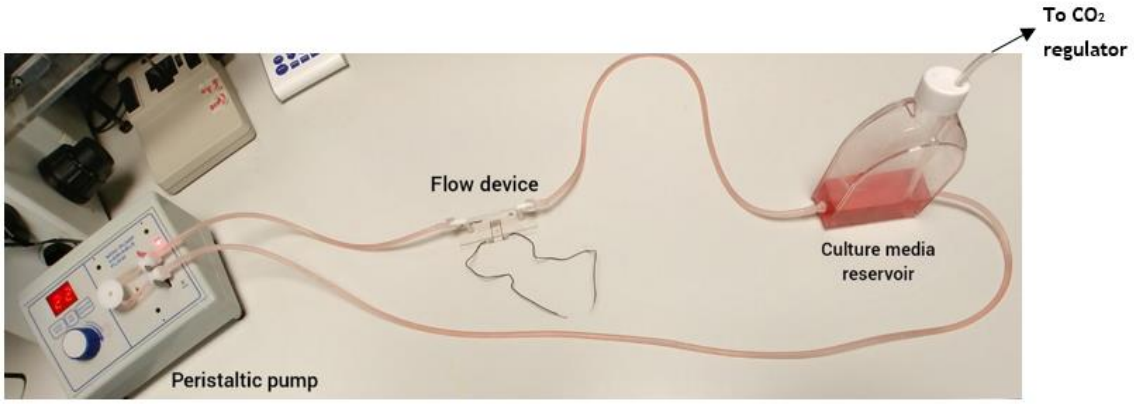

Figure 34: Flow circuit consisting of flow device, connecting tubes, culture media reservoir and peristaltic pump.

The flow circuit consisted of a flow device, connecting tubes, a culture media reservoir and an adjustable peristaltic pump (Cole-Parmer Peristaltic Pump - OU-73160-32 - Cole-Parmer - UK). The reservoir was made from a T75 culture flask. Two holes were drilled on the side walls and tubing were connected using connectors. The cap from a Universal Container (Sterilin™ Quickstart Universal Polystyrene 30 mL Containers - 128A - ThermoFisher Scientific - UK) was used to replace vented cap. A hole was made in the cap for a tubing, to allow carbogen to be bubbled through the media.

Another small hole (0.5 mm radius) was made to allow the carbogen to escape from the flow circuit, thus preventing a pressure build up. The reservoir was not filled to the top and this allowed it to work as a "air bubble trap". The flow circuit was set up as follows:

- The reservoir and tubing were sterilised by rinsing with 70 % ethanol, then deionised water. These were then transferred to a CCH together with the flow device seeded with cells.
- The reservoir and tubing were filled with enough normal DMEM to cover the reservoir inlet/outlet and fill the tubing, up to the connectors (these were held higher than the reservoir to prevent culture media from flowing out of the system).
- The caps closing the mini-reservoirs of the flow device were removed and a 200 µL pipette was used to fill the mini-reservoirs to the top. This prevented air bubbles from forming inside the channel.
- The connectors were then connected to the mini-reservoirs completing the flow circuit.
- The tubing was set onto the peristaltic pump. Any bubbles trapped within the circuit could be removed by turning on the peristaltic pump at maximum speed for 30 s.
- The whole flow circuit was kept within the warmed enclosure so that the culture medium and cells were kept at 37 ^{0}C.
- Carbogen gas mixture (95 % O_2 and 5 % CO_2) was bubbled directly through the culture medium to ensure that it remained at the optimum pH.

The flow rate was set at 5 mL / min, which was the minimum setting which allowed the rotor assembly to compress the tubing at regular time intervals. Based on the conversion table available from Ibidi GmbH (2016), the shear stress generated by this flow rate is approximately 1.2 dyn / cm^2. The shear stress experienced by endothelial cells *in vivo* within rat arteries is in the range 0.5 to 10 dyn / cm^2 (Morin *et al.*, 2003). The electrodes within the microfluidic channel have a thickness of 130 nm, and thus they could potentially interfere with the laminar flow profile within the channel. This could affect cell growth around the electrodes.

2.8 Electrical impedance setup

An LCR meter (IM3536 - Hioki - Japan) was used to measure impedance of the devices under different experimental conditions. The LCR meter was connected to the devices using a 4-terminal probe (4-Terminal Probe L2000 - Hioki - Japan). The LCR meter had several operation modes. The settings that were used in the experiments were Constant Current (CC) set at 10 µA. The LCR meter was supplied with a software which allowed it to be controlled from a computer. This allowed impedance measurements to be taken over a long frequency range and also at regular time intervals.

Figure 35: (A) LCR meter Hioki IM3536 and (B) 4-terminal probe L2000 (Hioki (2019)).

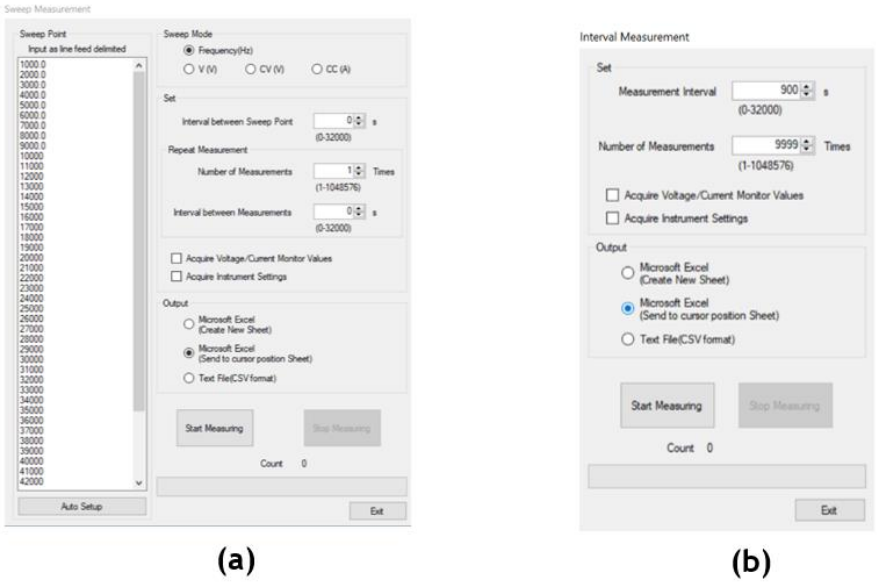

Figure 36: (a) LCR software interface allowing measurements to be taken over a frequency range (b) LCR software interface allowing impedances for a specific frequency to be measured for a specified time interval.

2.9 Power pack setup

A function generator (Aim-TTi TG5011 Function Generator 50MHz - 707-2841 - TG5011 – RS component Ltd - UK) was used to apply controlled voltages to the electrodes. The amplitude, waveform, frequency and offset of the AC voltages could be set as required. To ensure that the required voltage was applied to a set of electrodes, the impedance of the electrodes (at the required applied frequency) had to be determined so that the function generator could be set accordingly. Hence, impedance (at the required frequency) of electrodes had to be measured using LCR meter prior to application of voltage.

It was not possible to apply a pure DC voltage with the function generator. This type of voltage was applied by setting the waveform to sine wave and the amplitude to the smallest possible (10 mV). The offset was then set to the required DC voltage. For example, if a DC voltage of 1000 mV was required, the offset was set at 1000 mV. Thus, the output was a sine wave oscillating about 1000 mV (from 990 mV to 1010 mV).

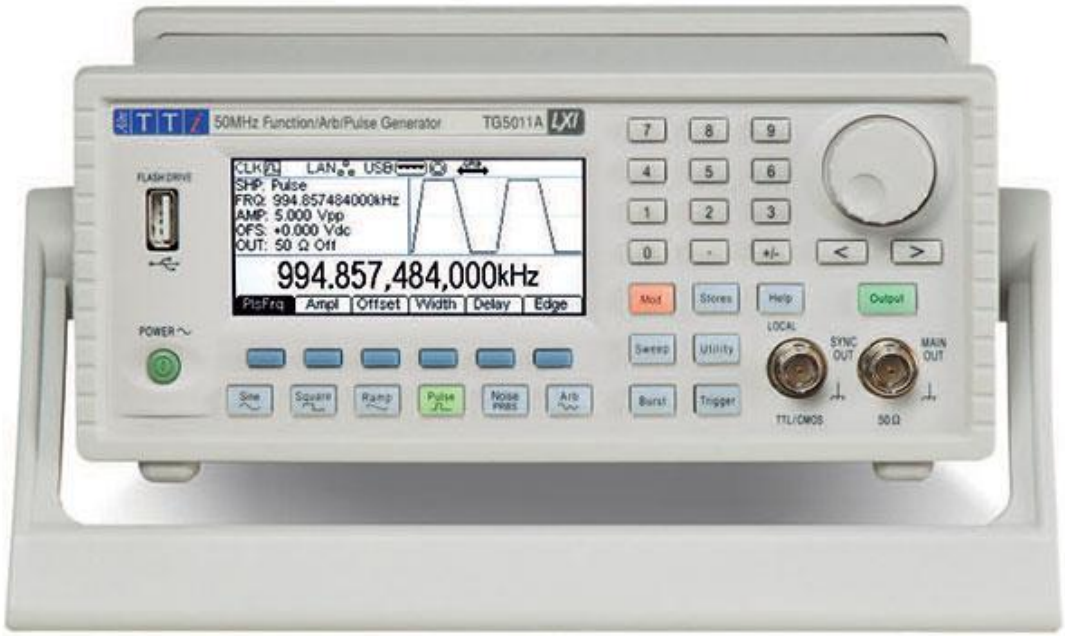

Figure 37: Aim-TTi TG5011 Function Generator 50MHz. (AimTTI (2019))

2.10 Conductivity meter

A conductivity meter (LAQUAtwin EC-22 - Horiba - Japan) was used, according to the manufacturer's instructions to measure conductivity of culture medium.

Figure 38: Horiba EC-22 Twin Conductivity/Salinity Pocket Tester (Horiba (2019))

2.11 Statistical Analysis

All analysis was performed and plotted using Graph pad Prism (v 5). Data involving technical replicates were presented as mean ± standard deviation. Student's paired t-tests (two-tailed distribution) was used for comparing two groups. One way analysis of variance (ANOVA) was used to determine significant difference between two or more independent groups, with a Tukey post-test for large sample sizes. Statistical significance was displayed as $P < 0.05$ (* - one star), $P < 0.01$ (** - two stars) or $P < 0.001$ (*** - three stars).

CHAPTER 3

PRELIMINARY TESTING OF FABRICATED DEVICES

3.1 Rationale

In order to ensure that the fabricated electrodes could be used for cell sensing and cell apoptosing experiments, preliminary tests were carried out. Several other research groups have used electrodes for cell sensing at specific frequencies. However, as the electrodes in this project were custom-designed and materials and dimensions were different, parameters such as optimum sensing frequency ranges and sensitivities to changes in volume and conductivity of culture medium had to be determined.

3.2 Introduction

The first devices fabricated were the normal Interdigitated Electrode (nIDE) and the Pendulum Electrode (PE) devices. These were intended to be used for cell impedance sensing, cell monolayer wounding or both. These required an excitation voltage to be applied to the electrodes. The excitation voltage for impedance sensing was lower than for cell monolayer wounding. The aims of this chapter were:

- To determine the optimum sensing frequency range for the different electrodes.
- To determine effects of changes in volume and conductivity of media on impedance.
- To determine direct contribution of cells adherence to changes in impedance
- To determine the effects of changing the dimensions of the IDE on the increase in impedance detected.

3.3 Optimum sensing frequency range of nIDE devices

3.3.1 Introduction

Applied Biophysics commercialise an interdigitated electrode design (Section 1.9.5) very similar to the nIDE. The optimum cell sensing frequency for this design is 4000 Hz. The nIDE fabricated for this project had a higher number of fingers (40 compared to 10) and thus a higher cell sensing surface area. Hence, a preliminary experiment with cells was carried out to determine the optimum sensing frequency range and a single optimum sensing frequency.

3.3.2 Experimental procedure

The experiment was carried out as follows:

- 4 nIDE devices were sterilised (Section 2.7.1).
- Fresh HEPES culture medium was pipetted into each of the devices inside a cell culture hood (CCH).
- The devices were each connected in turn to the LCR meter.
- A large frequency sweep (10 Hz to 1 MHz) was measured for each device. This was referred to as the baseline (cell-free) impedance spectra.
- The devices were then transferred back to the CCH.
- The devices were seeded with mouse aortic smooth muscle cells (MASMC) (Section 2.2.2) at a very high cell density (400000 cells per device).
- The cells were allowed to settle down for 18 h in an incubator kept at 37 ^{0}C with 5 % CO_2.
- After 18 h, the cells were observed under the microscope to ensure that they had settled down and spread on the bottom of the devices.
- Experimental impedance sweeps were then measured for each device.

3.3.3 Results and discussion

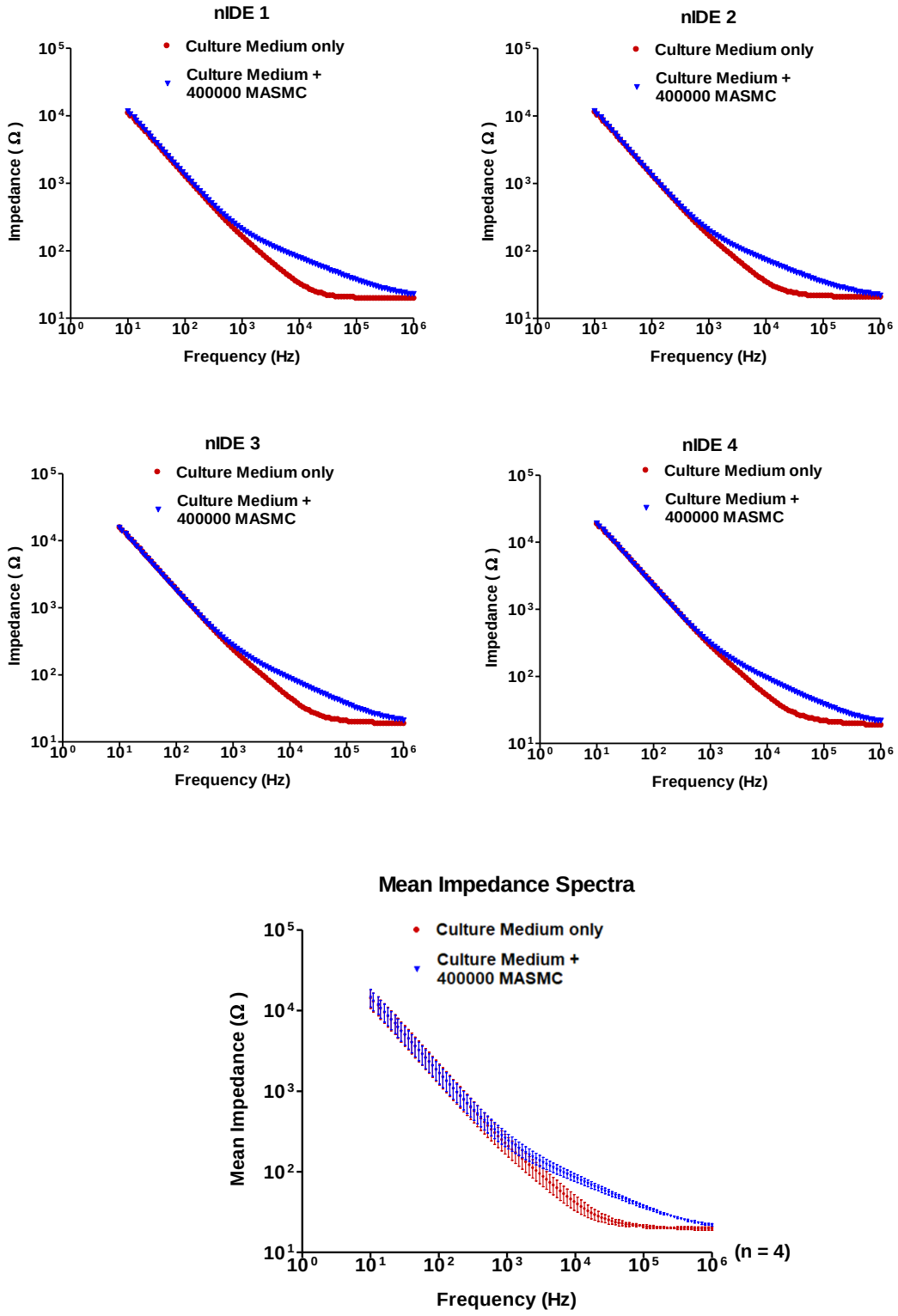

Figure 39: Individual and mean impedance spectra for nIDE devices showing culture medium only sweep in red and culture medium + cells sweep in blue

.

Figure 39 shows the impedance sweeps carried out for each device. The red curves represent the baseline impedance (culture medium only and cell free). The blue curves represent the impedance of culture medium + 400000 MASMCs. As the frequency range was broad, the curves were plotted using a logarithmic scale. The red and blue curves coincide from 10 Hz to 1 kHz. The curves then split apart as from 1 kHz reaching a maximum separation between 10 kHz and 100 kHz. The curves converge again towards 1 MHz. The results were analysed by measuring the area under the curves for the baseline sweeps (red curves) and the experimental sweeps (blue curves). A student's t-test was carried out to test the difference between the 2 different sets of area under the curves.

There was a statistically significant ($p < 0.001$) difference between the baseline and experimental sweeps. These results showed that the nIDE were sensitive to MASMCs in the 1 kHz to 50 kHz frequency range. Hence, the optimum sensing frequency range was chosen as 1 kHz to 50 kHz. In order to carry out further preliminary tests, a single sensing frequency also had to be chosen, and this was 10 kHz.

Even though the nIDE detected an increase in impedance within the optimum sensing frequency range, the actual cause of this increase was not clear. It could be due to the cells adhering to the electrodes (as MASMCs are adherent cells) or to changes in volume and conductivity of culture medium. Further experiments had to be carried out to determine the cause of this increase.

3.4 Effect of changes in culture medium volume on impedance measurements

3.4.1 Rationale

The previous section allowed an optimum sensing frequency range of 1 kHz to 50 kHz and optimum sensing frequency of 10 kHz to be identified for the nIDE. The seeding of the cells into the chambers containing the electrodes appeared to have caused an increase in impedance. It was not clear whether the increase was due to the direct adherence of the cells to the electrodes or due to indirect effects such as changes in volume (due to leakage or evaporation) or conductivity (due to cells taking up or releasing ions) of culture medium. In this section, effects of changes in volume of culture medium (in absence of cells) on the impedance were investigated for nIDE and PE devices.

3.4.2 Experimental procedure

The experiment was carried out as follows:

- 6 nIDE devices were sterilised (Section 2.7.1).
- 1 mL of HEPES culture medium was pipetted into each of the devices
- The devices were each connected in turn to the LCR meter and the impedances at 10 kHz were measured.
- Another 1 mL of media was pipetted into the devices (hence a total of 2 mL media) and impedances were recorded again.
- This was repeated until the total volume reached 4 mL, which was the maximum capacity of each chamber.
- The mean impedances at 1 mL, 2 mL, 3 mL and 4 mL were calculated for all the nIDE devices together.
- The experiment was repeated using 4 PE devices.

3.4.3 Result and discussion

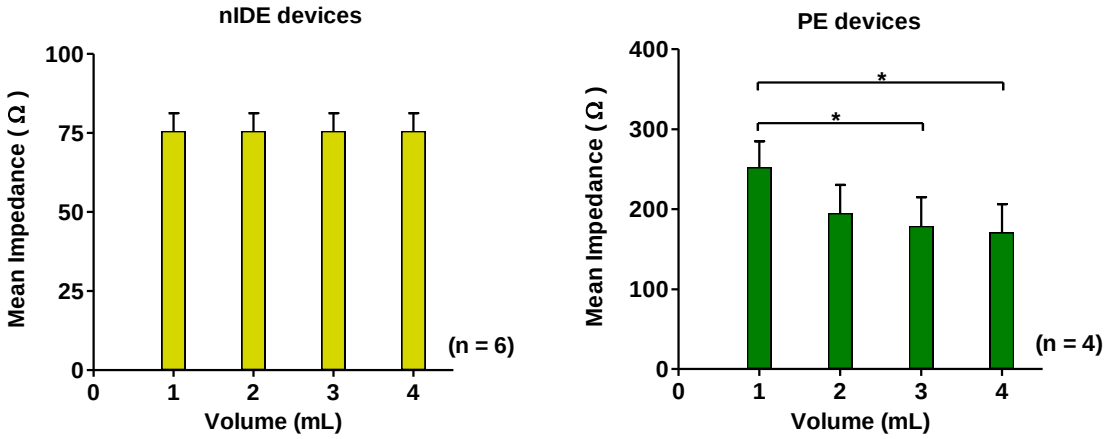

Figure 40: Effect of changes in volume of culture medium on impedance of nIDE and PE (n = 4 & 6).

The results with nIDE showed that the impedance remained constant at 75.5 Ω as the volume was increased from 1 mL to 4 mL. This implied the impedance measurements would not be affected by leakage or evaporation when the volume of culture medium varied between 1 mL to 4 mL. This is an advantage as any changes in impedance could be attributable to cells and other changes such as change in conductivity of culture medium. It is hypothesised that the mean impedance with the nIDE does not change when culture medium volume is increased from 1 mL to 4 mL because most of the electric field lines between the fingers of the nIDE travel within the lower 1 mL of culture medium. Decreasing the volume below 1 mL could cause a change in impedance. However, 1 ml of culture medium was the minimum volume required to cover the bottom (glass + nIDE) of the devices. A smaller volume would lead to a dry area in the middle of the device, which would not allow cells to survive. Hence, all experiments involving the nIDE devices were carried in at least 1 mL of culture medium.

The results with PE showed a decreasing trend in the impedance, as the volume increased. One-way ANOVA with Tukey's multiple comparison post-test was used to determine whether the mean impedances were statistically different at the different volumes. The difference in mean impedances between 1 mL and 2 mL was not statistically different. The differences between 1 mL & 3 mL and 1 mL & 4 mL were statistically different ($p < 0.05$).

This implied that a change in volume (due to leakage or evaporation) of more than 2 mL caused a significant change in impedance. The results suggested the PE were less suitable for sensing adherence of cells as compared to nIDE. This could be illustrated using the following example: if the device was seeded with cells in 3 mL of media and an increase in impedance was recorded, this increase could be attributable to cell adherence only, to culture medium change only, to change in media conductivity or to a combination of the two or more factors.

3.5 Effects of change in conductivity of culture medium on impedance measurements

3.5.1 Rationale

The conductivity of the culture medium was another factor that was likely to change during the course of an experiment. This could be due to evaporation, changes in pH and due to cells taking up and / or releasing ions. Hence the effects of changes in conductivity had to be investigated for the nIDE and PE.

3.5.2 Experimental procedure

The experiment was carried out as follows:

- 3 nIDE and 3 PE devices were sterilised (Section 2.7.1).
- The volume was kept constant at 1 mL throughout the experiment.
- The first impedance measurements (at 10 kHz) for each device were taken was with 1 mL of HEPES culture medium which had a conductivity of 11.3 mS/cm (as measured by the conductivity meter).
- In order to decrease the conductivity of the solution, different volumes of deionised water were added to the stock culture medium solution yielding solutions with conductivities of 9.3, 7.9 and 6.7 mS/cm.
- In order to increase the conductivity of the solution, different volumes of Phosphate Buffered Saline (PBS) were added to the stock culture medium solution yielding solutions with conductivities of 12.4 and 12.9 mS/cm.
- A maximum conductivity of 15.1 mS/cm was achieved by pipetting 1 mL of PBS directly into the devices.

3.5.3 Results and discussion

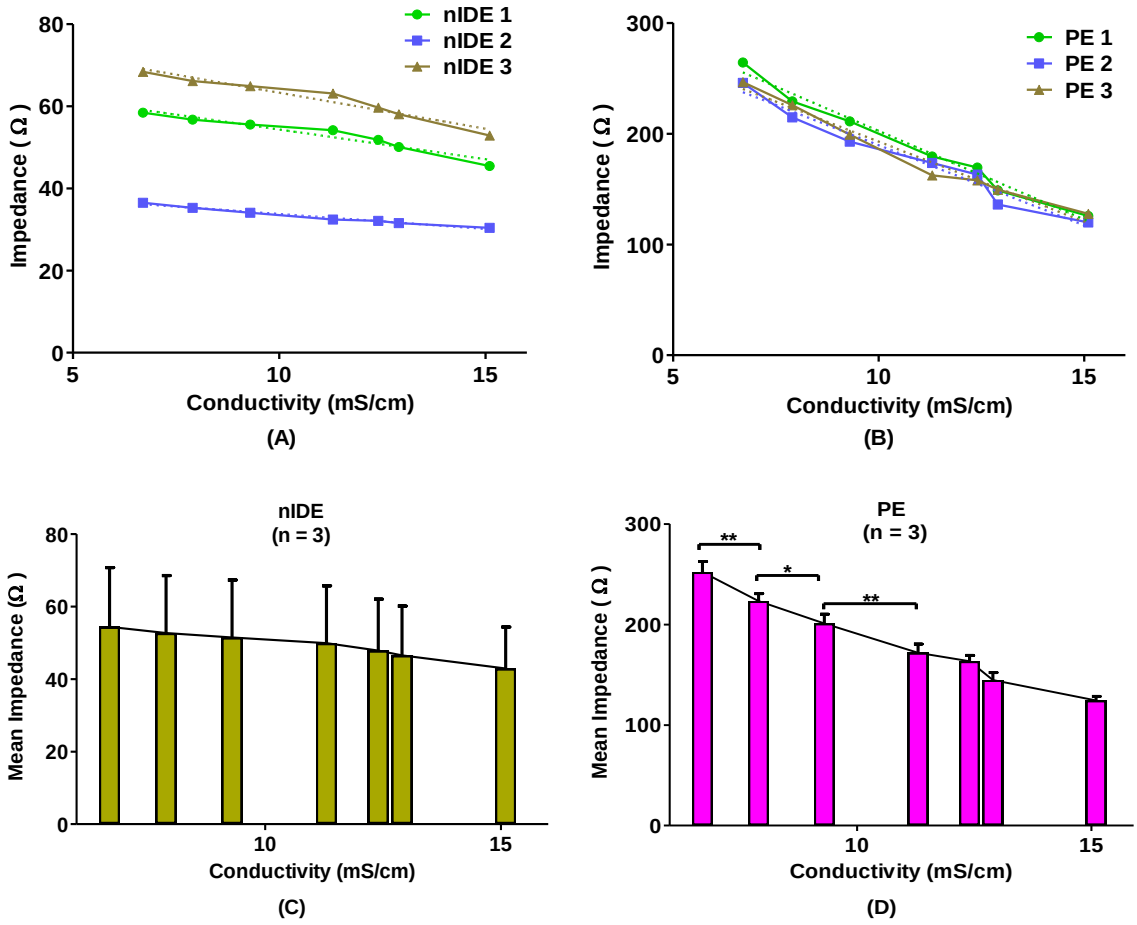

Figure 41: Effects of changes in conductivity of culture medium on impedance measurements. (A) nIDE 1, 2 and 3. (B) PE 1, 2 and 3. (C) Mean impedances for nIDE. (D) Mean impedances for PE (n = 3).

Figure 41C show the mean impedance for 3 nIDE devices plotted against the conductivity of the medium. One-way ANOVA showed that the mean impedances were not different between any of the conductivities. However, there was a decreasing trend in the mean impedance as the conductivity increases.

In order to determine whether the decrease in impedance was statistically significant, the impedances were individually plotted for each device (Figure 41A). nIDE 1, 2 and 3 showed a decreasing trend in impedance as the conductivity increased. A linear regression analysis was carried out to determine the line of best fit (dashed line). The slopes were calculated for each regression line. One sample t-tests showed the magnitudes of the linear regression line slopes were not significantly ($p > 0.05$) different from 0.

This implies that the change in impedance over the 6.7 mS/cm to 15.1 mS/cm conductivity range was not significant. Hence, the nIDE were not be significantly influenced by changes in conductivity of media, and would mainly detect changes due to cells.

For the devices with PE, when the conductivity was 11.3 mS/cm the mean impedance was 171 Ω. Decreasing the conductivity to 9.3, 7.9 and 6.7 mS/cm increased the impedance to 201 Ω, 223 Ω and 252 Ω respectively. Increasing the conductivity to 12.4, 12.9 and 15.1 mS/cm decreased the mean impedance to 163 Ω, 144 Ω and 124 Ω respectively.

One-way ANOVA with Tukey's multiple comparison post-test was carried out to determine whether the differences in impedances were significant. The difference between the impedances at 6.7 mS/cm and 7.9 mS/cm was statistically significant ($p < 0.01$). The difference between the impedances at 7.9 mS/cm and 9.3 mS/cm was statistically significant ($p < 0.05$). The difference between the impedances at 9.3 mS/cm and 11.3 mS/cm was statistically significant with a ($p < 0.01$). The differences between the impedance at higher conductivities (12.4, 12.9 and 15.1 mS/cm) were not statistically significant.

There was a decreasing trend in the mean impedance as the conductivity increased. In order to determine whether the decrease in impedance was statistically significant, the impedances were plotted for each device and linear regression analyses carried out. Student's t-tests was carried out for the values of the slopes. The values were statistically different ($p < 0.01$) from 0. This implied that there was a decreasing trend in the impedance as the conductivity increased.

The results show that PE were more susceptible to changes in conductivity of culture medium than nIDE. Section 3.4 also showed that the PE were more susceptible to changes in volume of culture medium. Hence these 2 sets of experiments show strong evidence that the nIDE could act as better cell adherence sensors than PE. All forthcoming experiments involving cell sensing were carried out using interdigitated electrodes (nIDE, sIDE and ssIDE). PE were not used for cell sensing and were considered more suitable for electromediated cell death experiments.

3.6 "Scratching off test" to determine direct contribution of cell adherence to impedance changes

3.6.1 Rationale

In Sections 3.4 and 3.5, it was shown that the nIDE were not affected by changes in volume and conductivity of culture medium. The following experiment was carried out to ensure that cells adhering to the electrode surface were the direct cause of the increase in impedance detected in Section 3.3.

3.6.2 Introduction

To determine whether cell adherence to the electrodes were the direct cause of the increase in impedance, cells were seeded into a nIDE device. Instead of allowing the cells to settle down inside an incubator, they were allowed to settle down inside the microscope enclosure kept at 37 ^{0}C with 5 % CO_2, with the LCR meter connected for continuous impedance measurements (at 10 kHz). The impedance measurements allowed changes occurring to the cells to be tracked in real time.

3.6.3 Hypothesis

Adherence of cells to the nIDE surface directly increases the impedance.

3.6.4 Experimental procedure

The experiment was carried out as follows:

- One nIDE device was sterilised (Section 2.7.1).
- 2 mL of HEPES culture medium was pipetted into the device.
- The device was connected to the LCR meter and impedance (at 10 kHz) was recorded at 1 min intervals.
- The control for this experiment was carried out by making scratches on the electrodes, using a thin flexible plastic filament, at regular time intervals during the first 58 min of the experiment.

- The culture medium was then pipetted out and the device was sterilised again.
- The device was seeded with 200000 MASMCs and 2 mL of HEPES media was added.
- The device was transferred to the live cell microscope with warmed enclosure, and the LCR meter was connected.
- Impedance measurements were acquired at 1 min intervals.
- The cells were allowed to settle down up to the 179 min timepoint. Microscopic observations were used to ensure that the cells had adhered and spread on the electrodes.
- The nIDE device was transferred to the cell culture hood.
- The HEPES media was pipetted out of the device and Acridine Orange was pipetted in and allowed to incubate for 5 min.
- The Acridine Orange was then pipetted out, and the device was washed with 1 mL of HEPES media to remove residual Acridine Orange.
- 2 mL of HEPES media was pipetted into the device.
- The device was transferred back to the microscope enclosure.
- The impedance was allowed to reach a plateau again (254 min).
- At 254 min a fluorescent micrograph (FITC channel) of the cells in the electrode area was acquired.
- A scratch was made to the cell monolayer using the thin plastic filament and another micrograph of the cells was acquired.
- Scratches and image acquisitions were repeated until the whole electrode was cleared of cells.

3.6.5 Results and discussion

During the first 58 min of the experiment, when the control scratches were performed, the impedance was fairly constant at approximately 27 Ω. This implies that the thin plastic filament used for the scratches did not damage the electrodes. Damage to the electrode would have led to an increase in impedance, due to a decrease in surface area for electric current conduction. The cells were seeded at 59 min. The impedance gradually increased from approximately 27 Ω to 60 Ω at 125 min. A plateau was reached at that point as most of the cells had settled down (Figure 42).

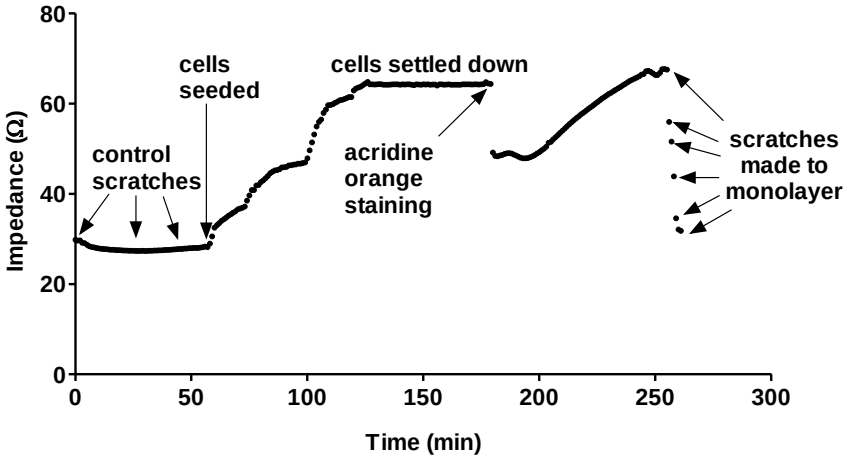

Figure 42: Impedance measurements recorded during the scratching off experiment.

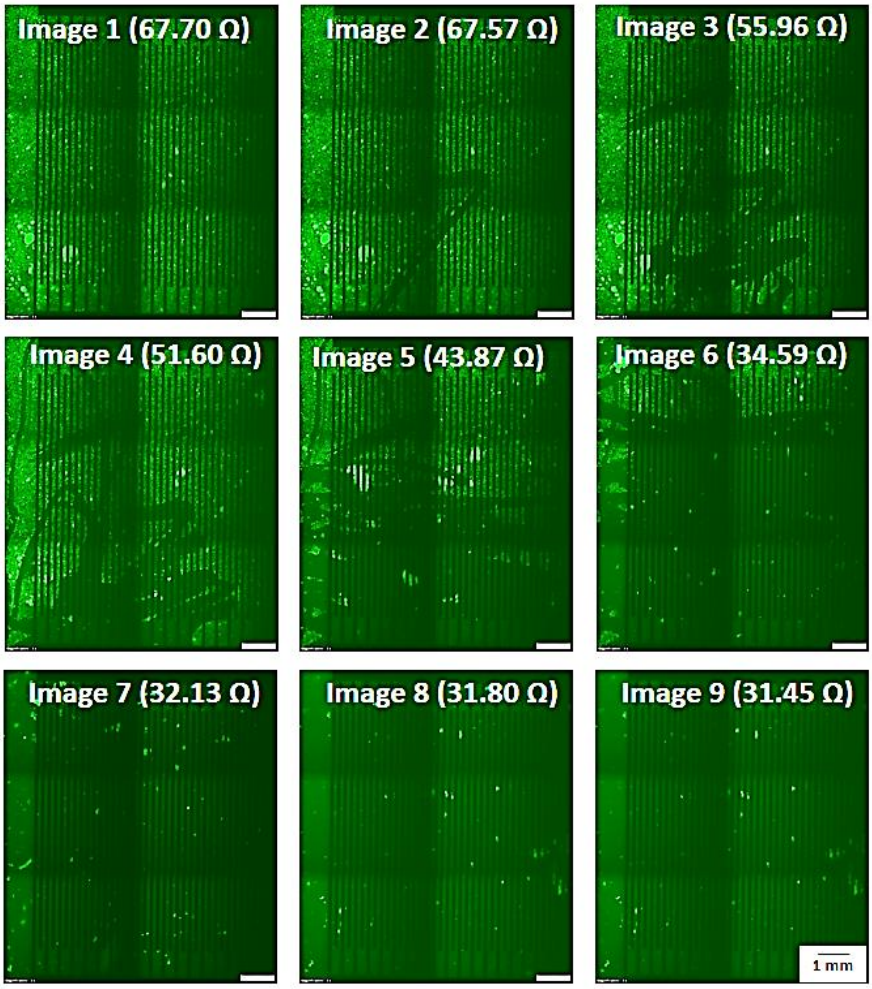

Figure 43: Fluorescent micrographs in FITC channel showing intact cell monolayer stained with Acridine Orange (Image 1), monolayer with scratches (Images 2 - 6) and completely cleared from electrodes (Images 7 - 9).

The impedance dropped to approximately 49 Ω following Acridine Orange staining. The cells recovered gradually and the impedance reached approximately 67 Ω. The scratches to the cell monolayer were made as from 254 min. Image 1 shows an intact monolayer. All the live cells were stained green. The impedance at this point was 67.70 Ω. The first scratch was made on image 2, and the impedance slightly dropped and reached 67.57 Ω. Further scratches were made and the impedance dropped to 55.96 Ω (image 3) and 51.60 Ω (image 4). On image 5, around half of the monolayer was scratched off the electrode and the impedance reached 43.87 Ω.

One third of the monolayer was cleared on image 6, and the impedance reached 34.59 Ω. On images 7, 8 and 9, the whole monolayer has been scratched off the electrode, and the impedance dropped back to baseline impedance (approximately 30 Ω). This experiment showed that the increase in impedance detected by the nIDE was mostly due to the direct adherence of cells onto the electrodes. The scratches caused the cells to be physically detached from the electrode and this led to a decrease in impedance. Other factors such as change in volume, conductivity and pH of culture medium might slightly change the impedance, but the adherence of cells to the electrode had a larger contribution to the changes in impedance.

3.7 Effect of changing dimensions of IDE on impedance increase detected

3.7.1 Change in widths of fingers and separation with constant effective surface area

Introduction and experimental procedure:

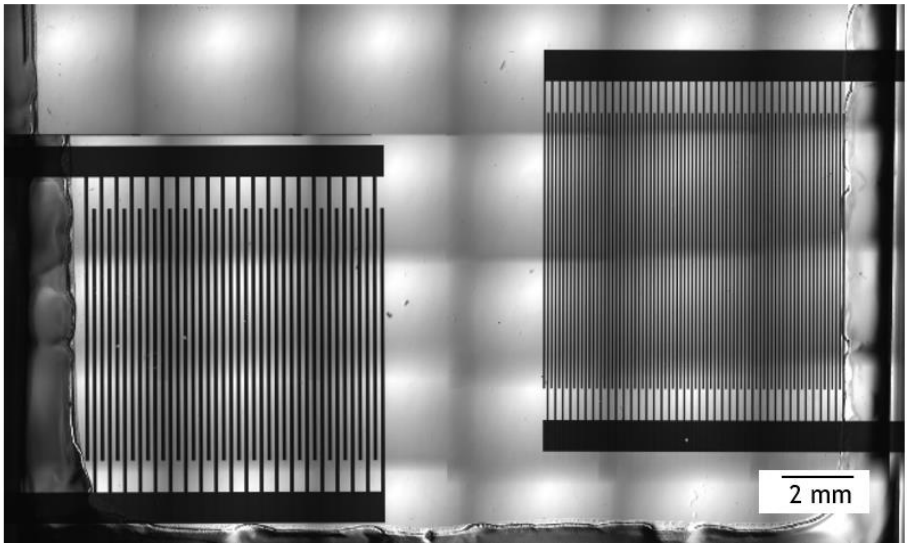

Figure 44: MIA showing nIDE on the left and sIDE on the right.

In this experiment, the effects of changes in dimensions of the IDE on the increase in impedance was investigated. The first IDE fabricated was referred to as normal IDE (nIDE), which consisted of 40 fingers with 100 µm width and 100 µm separation. The small IDE (sIDE) consisted of 80 fingers with 50 µm width and 50 µm separation. The effective electrode surface area were the same for nIDE and sIDE.

In order to determine whether the finger width and separation were the main factors influencing the magnitude of the change in impedance, a device consisting of normal IDE (nIDE) and small IDE (sIDE) was fabricated. Both electrodes were patterned on the same microscope slide and a chamber enclosing both within the same well was mounted on top. Figure 44 shows the MIA of the 2 electrodes within the same well. The 2 electrode types were fabricated within the same chamber so that the same monolayer would cover both of them, minimising differences due to biological and chemical conditions.

The nIDE had an optimum sensing frequency of 10 kHz. The optimum frequency for the sIDE could be different. Hence the experiment was carried out at several frequencies (10, 20, 30, 40 & 50 kHz). Baseline impedance readings were taken at the different frequencies with culture medium only. 200000 MASMCs were then seeded uniformly into the chambers and allowed to settle down for 18 h inside an incubator kept at 37 ^{0}C with $C0_2$ supply. After 18 h, experimental impedance readings for cells + culture medium were taken. The mean increases in impedance due to cells were calculated for each frequency.

Results and discussion:

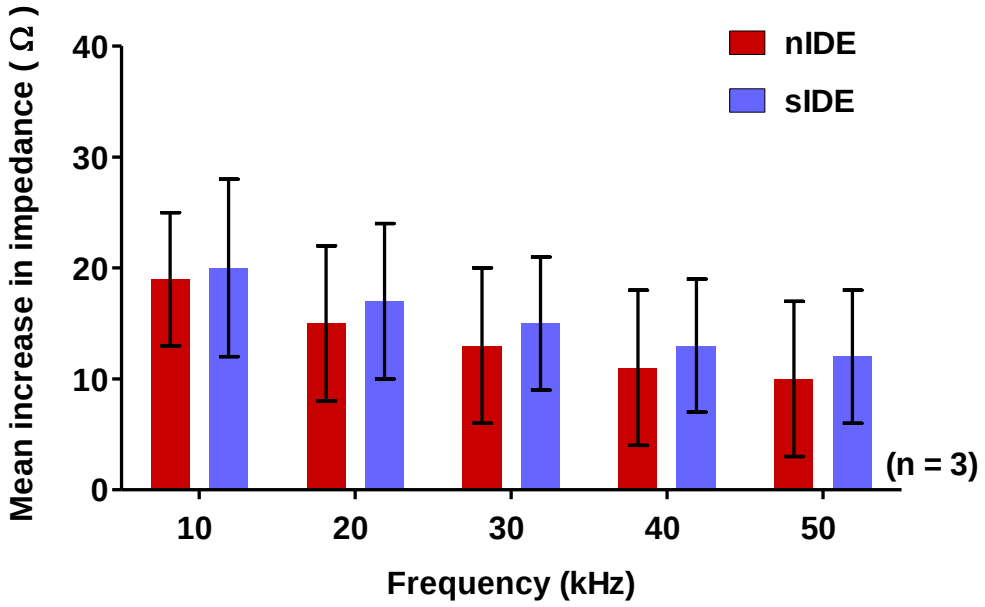

Figure 45: Mean increases in impedance at different frequencies due to 200000 MASMCs detected by nIDE vs sIDE (n = 3).

The nIDE detected a mean increase in impedance of 19 Ω at 10 kHz while the sIDE detected a 20 Ω increase at the same frequency. Two-way ANOVA was carried out to determine whether the mean increase in impedance detected by nIDE and sIDE at the different frequencies were statistically significant. The analyses showed that the differences were not significant at any of the frequencies. Hence both nIDE and sIDE detected the same increase in impedance when 200000 MASMCs were seeded into the chambers. This implied that the changes made to the finger width and separation, while conserving the effective electrode surface area, did not influence the detection capability of the IDE.

3.7.2 Change is effective electrode surface area

Introduction and experimental procedure:

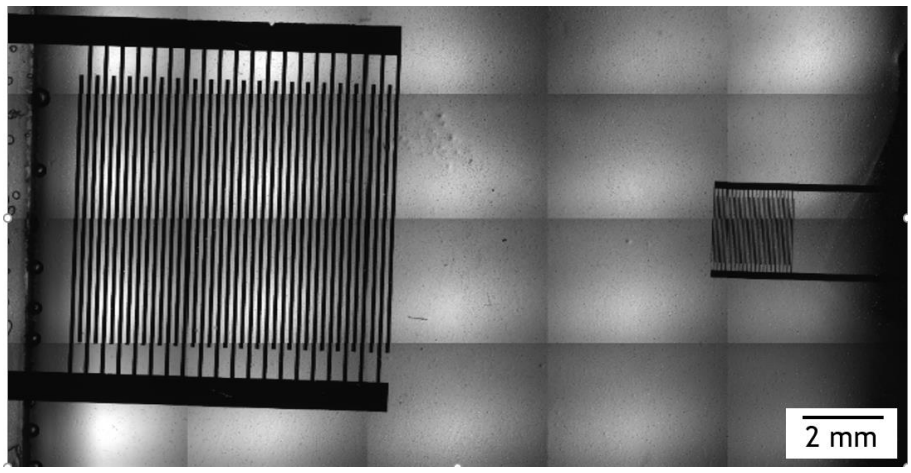

Figure 46: MIA showing nIDE on the left and ssIDE on the right.

In this experiment, the effect of changing the effective electrode surface area on the detection capability was investigated. The nIDE was linearly scaled down by a factor of 4. This electrode was referred to as super small IDE (ssIDE). The effective electrode length was decreased from 8 mm to 2 mm. The finger width was decreased from 100 µm to 25 µm. The effective electrode surface area decreased by a factor of 16. Both the nIDE and ssIDE were fabricated on the same slide Figure 46. The experiment was carried out in the same way as in Section 3.7.1.

Results and discussion:

The results are shown in Figure 47. Two-way ANOVA was carried out to determine whether the mean increases in impedances detected by nIDE and ssIDE at the different frequencies were statistically significant. The analyses showed that the differences were statistically significant ($p < 0.001$) at all the frequencies. Table 4 shows the mean increase in impedance with ssIDE was on average 4.35 times higher than the mean increase detected by nIDE. Hence, decreasing the effective electrode surface area by a factor of 16 resulted in an increase in detection capability by a factor of approximately 4.

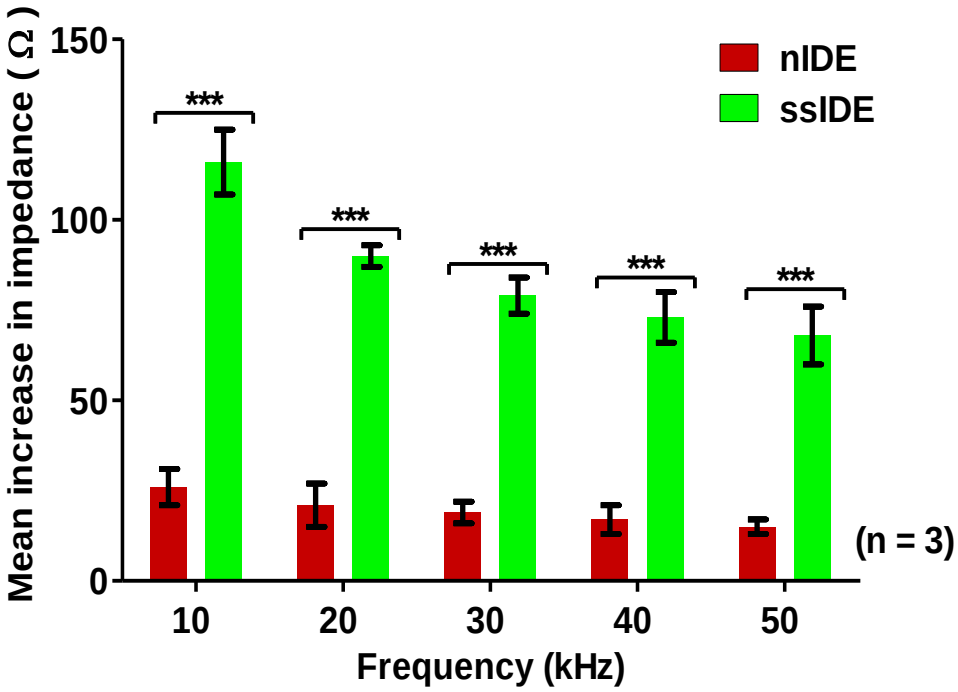

Figure 47: Mean increase in impedance at different frequencies due to 200000 MASMCs detected by nIDE vs ssIDE (n = 3).

Frequency (kHz)	[A] Impedance increase with nIDE (Ω)	[B] Impedance increase with ssIDE (Ω)	$\frac{B}{A}$
10	26	116	4.46
20	21	90	4.29
30	19	79	4.16
40	17	73	4.29
50	15	68	4.53
		Mean	**4.35**

Table 4: Comparison of increases in impedance at the different frequencies for nIDE and ssIDE.

3.8 Summary and discussion

The optimum sensing frequency range for the nIDE was determined by measuring the impedance spectra over a large frequency range, before and after seeding + adherence of a high cell density of MASMCs. Results from Figure 39 showed that the nIDE (electrode area 28.8 mm^2) were sensitive to MASMCs in the 1 kHz to 1 MHz range. Giaever and Keese (1991) used 0.1 mm^2 electrodes to sense fibroblasts. These cells were detected in the 100 Hz to 100 kHz range. Mamouni and Yang(2011) used 7.5 mm^2 electrodes to sense epithelial cells. These cells were detected in the 1 kHz to 100 kHz range. The differences between our optimum sensing frequency range compared to these two studies could be due to the differences in electrode surface area. However, the differences could also be due to the different cell types used, implying that different cell might have different signature impedance spectra. If this was the case, then the impedance spectra differences could be used to distinguish between different cells types, for example, smooth muscle cells and endothelial cells. Within the optimum sensing frequency range for nIDE, a single frequency of 10 kHz was chosen for other preliminary tests and for continuous measurements.

Experiments at a single frequency of 10 kHz with culture medium only (absence of cells) showed that the nIDEs were less susceptible to changes in volume (Figure 40) and conductivity (Figure 41) of culture medium. This made the nIDE the most suitable electrode for cell sensing. To ensure that the impedance increase detected after cell seeding and plating were due to the direct contribution of cell adherence to the electrodes, a “scratching off” test was carried out. Cells were seeded and allowed to adhere onto the nIDE, with continuous impedance measurements (at 10 kHz). When scratches were made to the monolayer, the impedance decreased, indicating that cell adhesion was the major contributor to this increase. Changing the width of the fingers and the separation of the fingers of the IDE, while conserving the effective electrode area did not change the impedance increase detected, for the same cell density. However, decreasing the finger length, width and separation by a factor of 4 (decreasing effective electrode area by a factor of 16), caused the impedance increase to increase by a factor of 4.35. This is in line with results (Figure 13) obtained by Zhang *et al.* (2017), which showed an inverse relation between electrode size and impedance increase detected with cells.

CHAPTER 4

ELECTRICAL IMPEDANCE SENSING WITH CELLS

4.1 Introduction

One of the aims of the project is to find a way of detecting regrowth of cells over a stent. Several research groups have used different designs of gold electrodes, acting as biosensors, to detect adherence of biological cells. A stent consists of metal struts which have a thickness of less than 100 μm (Savage *et al.*, 2004). To integrate biosensors onto a stent, these would have to be smaller than the thickness of the stent struts. In order to initially test whether it was possible to develop a cell sensing system, the electrodes were fabricated onto microscope glass slides. Interdigitated Electrodes (IDE) were one of the electrode designs used for by other research groups, and this was the first electrode type used for cell sensing in the experiments in this project.

4.2 Impedance sensing of MASMCs

4.2.1 Rationale

The experiment in Section 3.3.3 allowed the optimum sensing frequency range of these nIDEs to be determined. The experiment involved a large frequency sweep from 10 Hz to 1 MHz. Results showed that the nIDE were able to sense the MASMCs (region where blue curve separates from red curve in Figure 39) from 1 kHz to 1 MHz. The aim of the following experiment was to determine whether a difference in impedance due to cell adherence could be detected for shorter impedance sweep (1 kHz to 50 kHz).

4.2.2 Hypothesis

Adherence of 200000 MASMCs onto the nIDE can be detected using impedance sweeps in the 1 kHz to 50 kHz frequency range.

4.2.3 Experimental procedure

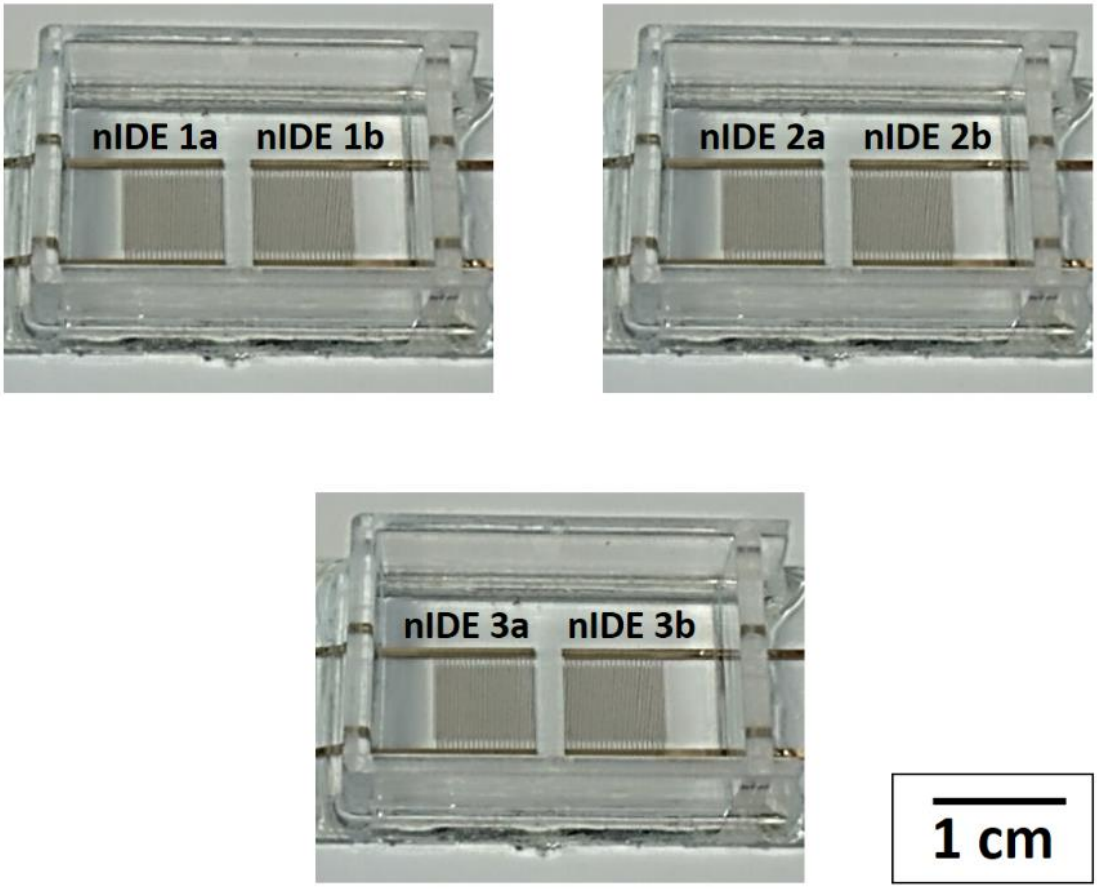

Figure 48: The 3 devices with 2 sets of independent nIDEs.

The experiment was carried out as follows:

- 3 devices each containing 2 sets of independent nIDE were sterilised (Section 2.7.1).
- Baseline impedance sweeps from 1 kHz to 50 kHz were carried out with culture medium only.
- MASMCs were detached from a sub-confluent flask (Section 2.2.2).
- 200000 MASMCs were seeded into each of the devices, and the cells were allowed to settle down for 18 h.
- After 18 h, experimental impedance sweeps were carried out.

4.2.4 Results and discussion

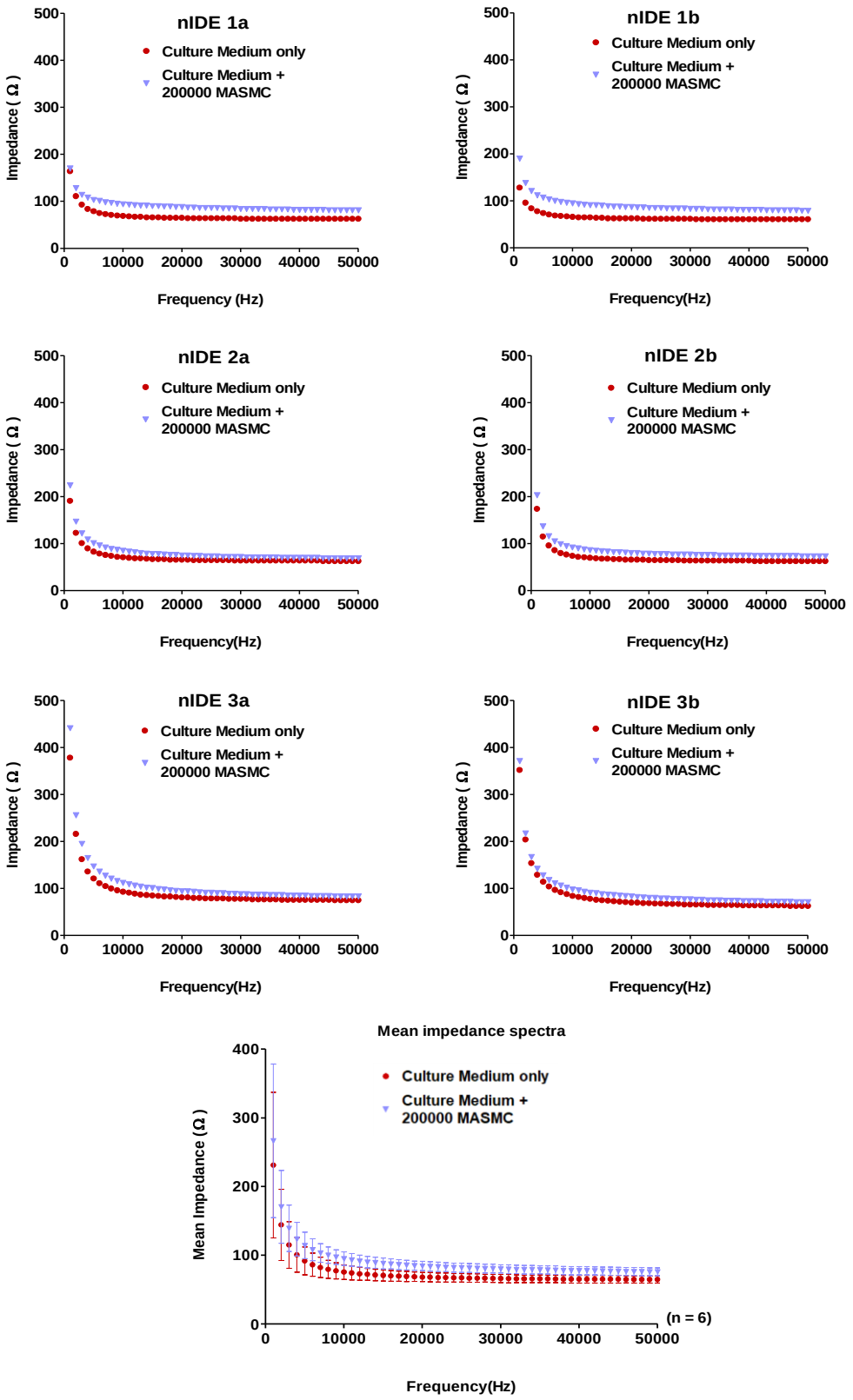

Figure 49: Individual and mean impedance spectra from 1 kHz to 50 kHz carried out without cells and with 200000 MASMCs using 3 devices containing 2 sets of independent nIDEs.

The results show that the blue curves (culture medium + cells) were always higher than the red curves (culture medium only). This implied that within the 1 kHz to 50 kHz range, the MASMCs increase the impedance of the nIDE. At 10 kHz, nIDE 1a detected 25 Ω increase in impedance, nIDE 1b detected 29 Ω increase, nIDE 2a detected 19 Ω increase, nIDE 2b detected 14 Ω increase, nIDE 3a detected 14 Ω increase and nIDE 3b detected 16 Ω increase.

There were innate differences in the baseline impedances because the devices were fabricated using a semi-manual process. There were differences in the metal deposition of the electrodes and also further differences were created during wire soldering. However, the same number of cells (200000 cells) were seeded into each of the devices.

Cells exhibit natural biological variation and thus settle down differently in the different devices. These could also be due to differences in the surface chemistry across the different devices. However, each chamber contained 2 independent sets of electrodes and it was assumed that the cells settled down uniformly in each device, covering both electrodes in a similar way. The impedance increases detected by nIDEs within the same chambers were similar: 25 Ω & 29 Ω (1a & 1b), 19 Ω & 14 Ω (2a & 2b) and 14 Ω & 16 Ω (3a & 3b).

The area under the curves (AUC) with culture medium only (red curves) and with culture medium + cells (blue curves) were calculated for each nIDE. A paired student's t-test was carried out and the results showed that there was a statistically significant difference ($p < 0.01$) between AUC with culture medium only and AUC with culture medium + cells. Hence, these results are evidence towards the fact that adherence of 200000 MASMCs onto the nIDE can be detected using impedance sweeps in the 1 kHz to 50 kHz frequency range.

4.3 Impedance sensing of MECs

4.3.1 Rationale

In sections 3.3 and 4.2, Mouse Aortic Smooth Muscle Cells (MASMCs) were seeded on nIDEs. Results showed that these electrodes were able to detect adherence of MASMCs. This is the culprit cell type which leads to an abnormal healing response and ultimately to instent restenosis. The following experiment investigated whether the nIDE were capable of detecting another cell type, the Mouse Endothelial Cells (MECs). These cells would reendothelialise the stent struts during a normal healing response.

4.3.2 Hypothesis

Adherence of 200000 MECs onto the nIDE can be detected using impedance sweeps in the 1 kHz to 50 kHz frequency range.

4.3.3 Experimental procedure

The experiment was carried out as follows:

- 2 impedance devices each with 2 sets of independent nIDE were sterilised (Section 2.7.1).
- Baseline impedance sweeps from 1 kHz to 50 kHz were carried out with culture medium only.
- MECs were detached from a sub-confluent flask (Section 2.2.2).
- 200000 MECs were seeded into each of the devices, and the cells are allowed to settle down for 18 h.
- After 18 h, experimental impedance sweeps were carried out.

4.3.4 Results and discussion

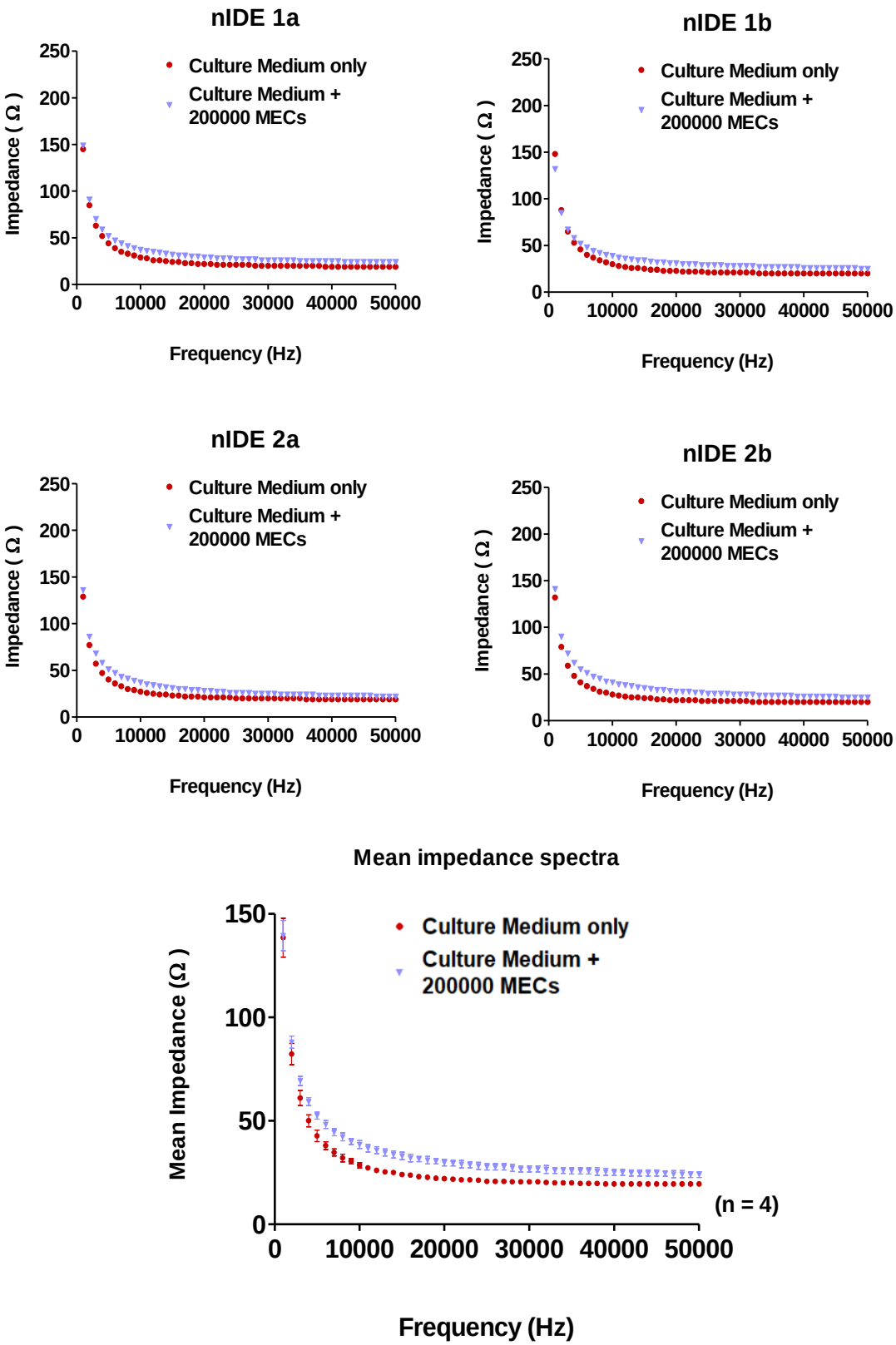

Figure 50: Individual and mean impedance spectra from 1 kHz to 50 kHz carried out without cells and with 200000 MECs on nIDEs.

The blue impedance spectra were consistently higher than the red impedance spectra, implying that the impedances with cells were always higher than the impedances without cells. In a similar way to the experiments with MASMCs, the presence of MECs was detected as an increase in impedance over the 1 kHz to 50 kHz range. At 10 kHz, nIDE 1a detected an increase of 8 Ω, nIDE 1b detected 9 Ω, nIDE 2a detected 10 Ω and nIDE 2b detected 13 Ω. The area under the curves were calculated and a paired student t-test was carried out. Results showed that the curves with culture medium + cells were statistically different ($p < 0.01$) from the curves with culture medium only. This implied that the nIDE were also capable of detecting MECs.

This can be regarded as an advantage as the 2 cell types involved in vascular healing process (reendothelialisation or smooth muscle cell hyperplasia) could be detected. However, this could also be a disadvantage. Over the 1 kHz to 50 kHz, the impedance curves due to cells + medium for both MASMCs and MECs do look very similar. The nIDE do not seem to distinguish the 2 cell types over this frequency range. Further investigations are required to determine whether differentiating the 2 cell types could be possible at a different frequency range.

4.4 Impedance increase detection by nIDE due to MASMCs as compared to MECs for the same cell densities.

4.4.1 Rationale

In this experiment, the detection capability of the nIDE for MASMCs as compared to MECs was investigated. The previous experiments in Section 4.2.4 and 4.3.4 seemed to show that the impedance increase due to MASMCs was higher than the impedance increase due to MECs, when the same number of cells was used. However, cells may behave differently at different times due to external factors such as temperature, CO_2 levels and pH of medium. Hence, in this experiment 3 nIDE devices were used, each with 2 independent sets of electrodes. The 3 devices were simultaneously seeded with 3 different cell numbers, while maintaining identical environmental conditions.

4.4.2 Hypothesis

For the same cell density, the increase in impedance detected by nIDE is higher with MASMCs than with MECs at all frequencies.

4.4.3 Experimental procedure

The experiment was carried out as follows:

- 3 impedance devices each with 2 sets of independent nIDE were sterilised (Section 2.7.1).
- A baseline impedance measurement at 10 kHz was carried out with culture medium only.
- MASMCs were detached from a confluent flask (Section 2.2.2).
- 200000 MASMCs were seeded into the 1st device, 100000 MASMCs were seeded into the 2nd device, 50000 MASMCs were seeded into the 3rd device and the cells were allowed to settle down for 18 h.
- After 18 h, experimental impedance measurements were carried out.
- The impedance increases for each of the electrodes were calculated.

- The cell density of each device was calculated by dividing the number of cells seeded by the surface area (480 mm^2) of each device.
- The experiment was repeated with MASMCs at a later time point.
- The experiment was repeated 2 times with MECs, at different time points.

4.4.4 Results and discussion

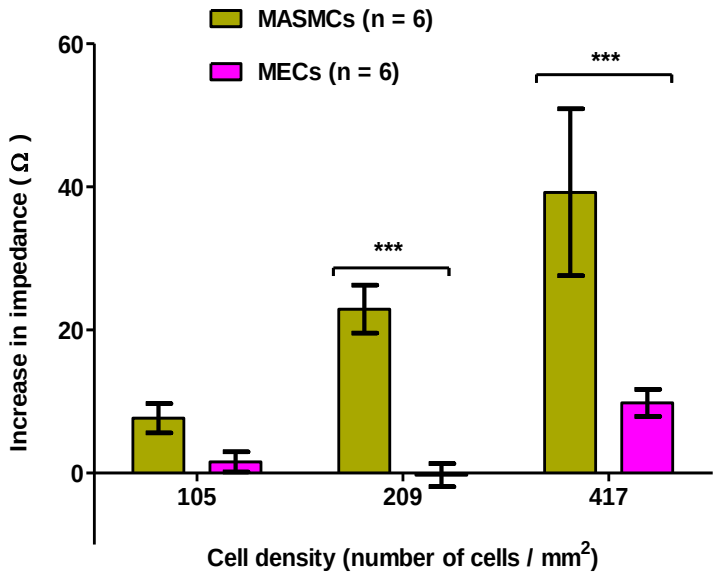

Figure 51: Increase in impedance plotted against cell density for MASMCs and MECs. Two-way ANOVA showed that the mean increases in impedance were statistically different ($p < 0.001$) at 209 cells / mm^2 and 417 cells / mm^2, but not at 105 cells / mm^2 (n = 6).

Figure 51 shows that at a cell density of 105 cells / mm^2, there was a mean increase in impedance of 7.6 Ω with MASMCs compared to 1.5 Ω with MECs. At a cell density of 209 cells / mm^2 MASMCs caused a mean impedance increase of 22.9 Ω while MECs caused a - 0.2 increase. At 417 cells / mm^2, a mean increase of 39.2 Ω was detected with MASMCs compared to 11.6 Ω with MECs. Two-way ANOVA showed that the mean increases in impedance were statistically different ($p < 0.001$) at 209 cells / mm^2 and 417 cells / mm^2, but not at 105 cells / mm^2. The results imply that the same number of MASMCs (compared to the same number of MECs) caused larger increases in impedance. This could be because the 2 different cell types had different physical and electrical properties. The 10 kHz frequency was within the optimum sensing frequency range of MASMCs. The optimum sensing frequency range of MECs could be different from MASMCs, implying that further experiments using broad impedance sweeps were required.

4.5 Distinguishing MASMCs and MECs using broad impedance and phase sweeps on nIDE

4.5.1 Rationale

The graphs in Figure 49 and Figure 50 showed that the impedance spectra of MASMCs and MECs had similar shapes in the 1 kHz to 50 kHz range. The magnitudes of the increases were different when comparing similar cell densities of MASMCs and MECs. However, if this sensor was integrated onto a stent to monitor cell regrowth onto the stent, a mixture of both cell types could grow onto the sensors. The magnitude of the impedance increase would not give any indication of the cell type. The possibility of distinguishing the 2 cell types based on differently shaped impedance spectra could be useful. Another electrical property that could allow the 2 cell types to be distinguished is the phase. This could be acquired at the same time as the impedance, using the LCR meter. The aim of the following experiment was to distinguish MASMCs and MECs based on the impedance and phase spectra acquired over a broad frequency range.

4.5.2 Hypothesis

MASMCs and MECs can be distinguished using broad impedance and phase sweeps on the nIDE.

4.5.3 Experimental procedure

The experiment was carried out as follows:

- 3 impedance devices each with 1 set of nIDE and 1 set of ssIDE were sterilised (Section 2.7.1). Only readings from nIDEs were used in Section 4.5. Readings from the ssIDE were used in Section 4.6.
- Baseline impedance and phase sweeps from 10 Hz to 10 MHz were carried out with culture medium only.
- MASMCs were detached from a confluent flask (Section 2.2.2).
- 400000 MASMCs were seeded into each device and the cells were allowed to settle down for 18 h.

- After 18 h, experimental impedance and phase sweeps were carried out.
- The experiment was repeated with 400000 MECs.

4.5.4 Results and discussion

The results were plotted in Figure 52. For both experiments, 400000 cells were used. The increase in impedance (as shown by the distance of separation between red curves and blue curves) was higher with MASMCs than MECs. The geometrical shapes of the impedance spectra for both MASMCs and MECs looked very similar over the 10 Hz to 1 MHz range. It was not possible to distinguish the 2 cell types using the shapes of the impedance spectra. The phase spectra were also recorded in this experiment. The phase spectra looked similar in all the graphs, except for nIDE3 with MECs. This could be due to a loose electrical connection.

An interesting feature in all the graphs was that the impedance spectra (baseline and with cells) started to diverge at around 1 kHz. The exact frequency at which this occurred was pinpointed by the dashed black arrow. For the 3 devices with MASMCs, the curves started to separate at a frequency lower than 1 kHz. For the 3 devices with MECs, the curves separated at a frequency higher than 1 kHz. This observation suggested that the nIDE could be used to distinguish the 2 cell types. However, these results were obtained using 3 devices only. Further replicates are required to ensure that this result is reproducible.

MASMCs

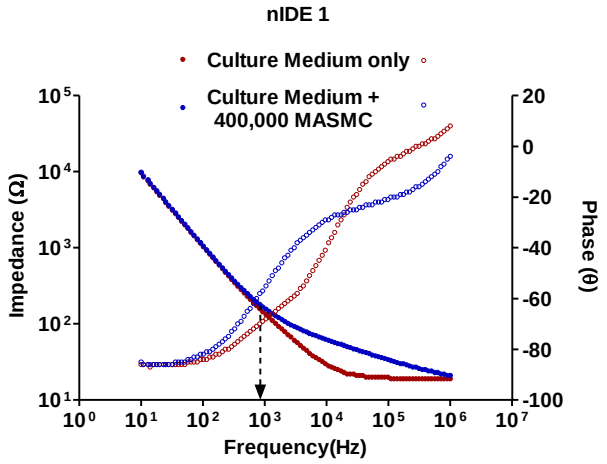
nIDE 1
Culture Medium only
Culture Medium +
400,000 MASMC
Impedance (Ω)
Phase (θ)
Frequency(Hz)

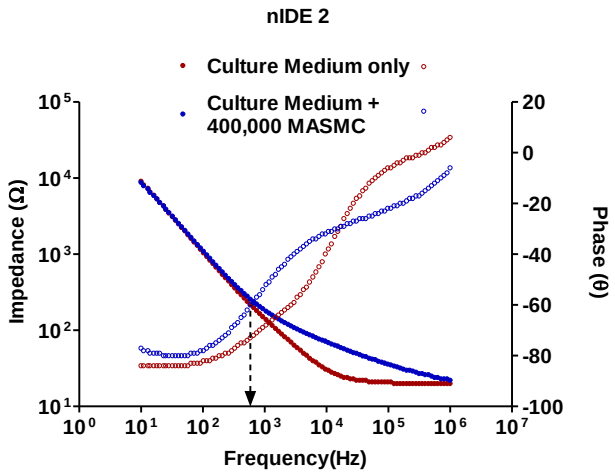
nIDE 2
Culture Medium only
Culture Medium +
400,000 MASMC
Impedance (Ω)
Phase (θ)
Frequency(Hz)

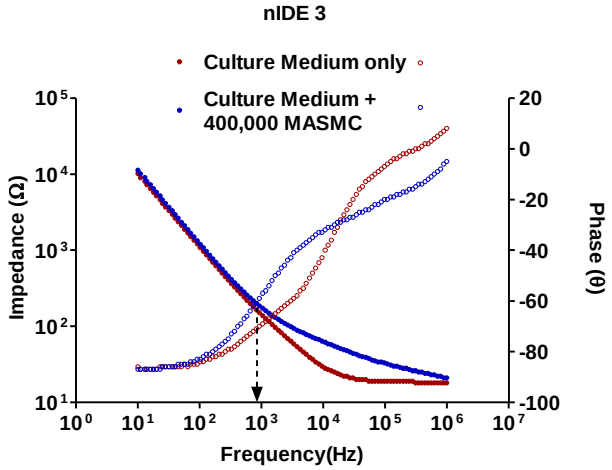
nIDE 3
Culture Medium only
Culture Medium +
400,000 MASMC
Impedance (Ω)
Phase (θ)
Frequency(Hz)

MECs

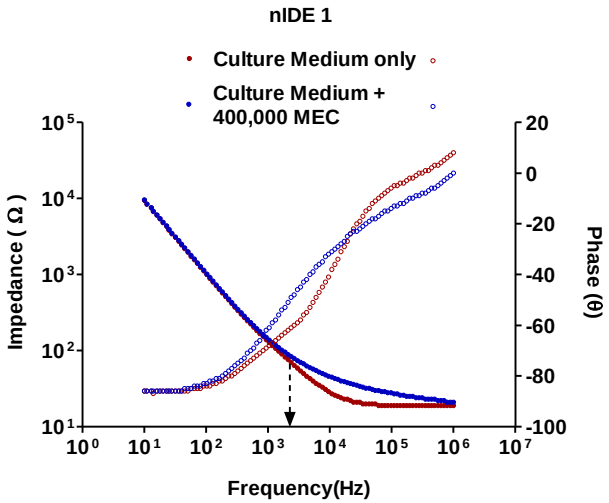
nIDE 1
Culture Medium only
Culture Medium +
400,000 MEC
Impedance (Ω)
Phase (θ)
Frequency(Hz)

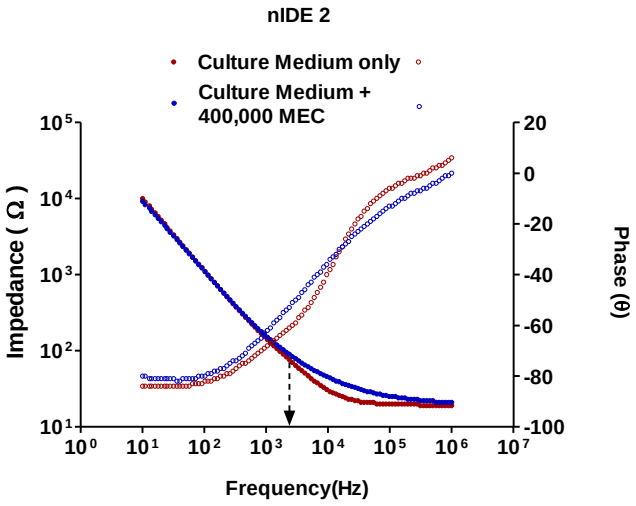
nIDE 2
Culture Medium only
Culture Medium +
400,000 MEC
Impedance (Ω)
Phase (θ)
Frequency(Hz)

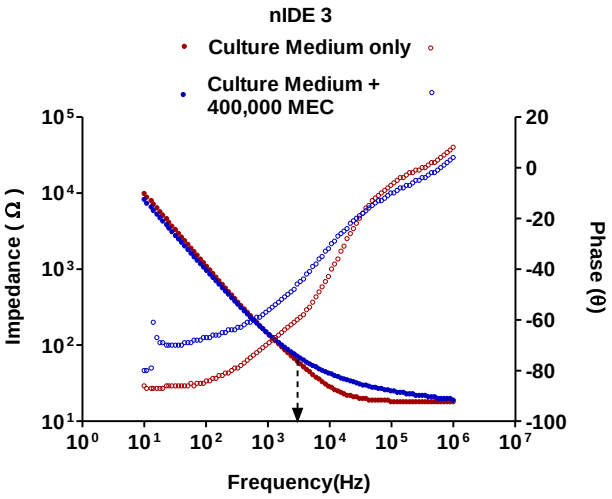
nIDE 3
Culture Medium only
Culture Medium +
400,000 MEC
Impedance (Ω)
Phase (θ)
Frequency(Hz)

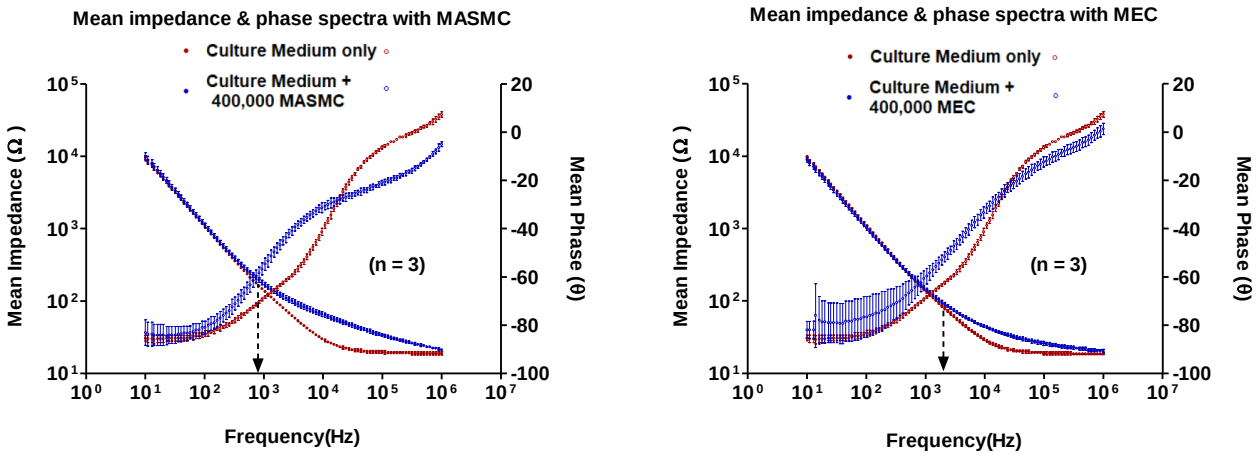

Figure 52: Individual and mean impedance and phase spectra for 400000 MASMCs and 400000 MECs using nIDE devices.

4.6 Distinguishing MASMCs and MECs using broad impedance and phase sweeps on ssIDE

4.6.1 Introduction

In Section 4.5, it seemed that the nIDE were capable of distinguishing MASMCs and MECs. The previous experiment in Section 4.5 was carried out using impedance devices containing both nIDE and ssIDE. Readings were acquired from both electrode types, but only readings from nIDE were used for analysis in Section 4.5. In the current section the readings from ssIDE are analysed. The ssIDE has an effective electrode surface area 16 times smaller than the nIDE.

4.6.2 Results and discussion

The impedance spectra had very similar geometric shapes in all 6 graphs. The same number of cells were used in all devices. In general, the increase in impedance with MASMCs was higher than with MECs. This is indicated by a greater separation between the red and blue impedance curves. The phase spectra also looked similar in all 6 graphs.

MASMCs

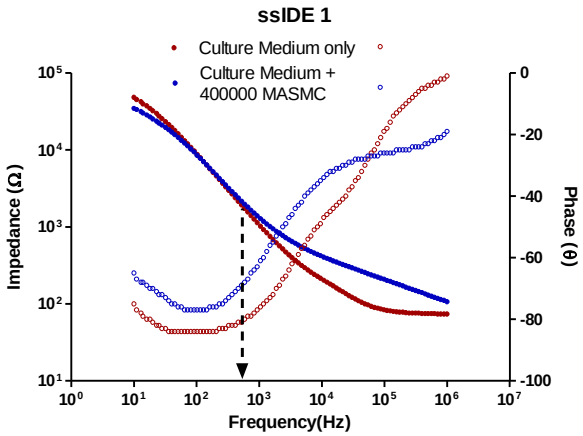
ssIDE 1
Culture Medium only
Culture Medium + 400000 MASMC
Impedance (Ω)
Phase (θ)
Frequency(Hz)

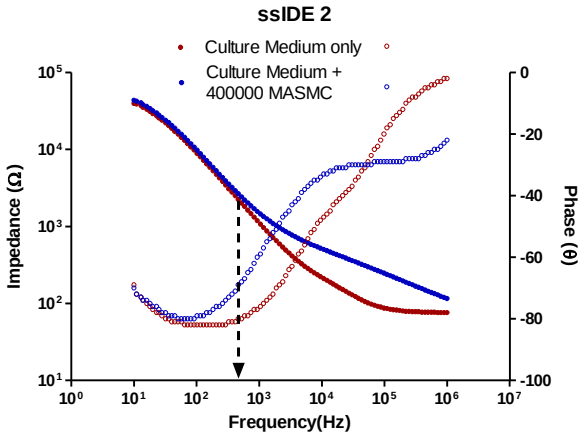
ssIDE 2
Culture Medium only
Culture Medium + 400000 MASMC
Impedance (Ω)
Phase (θ)
Frequency(Hz)

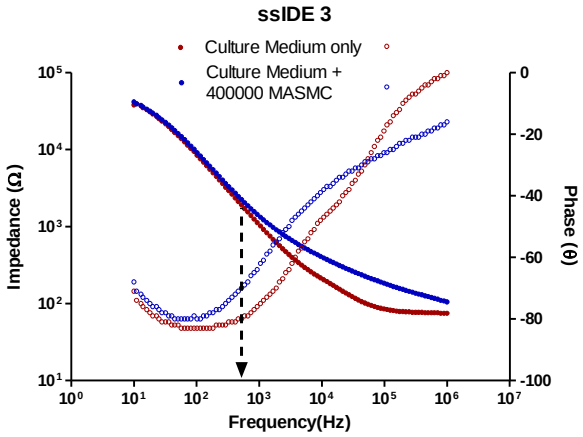
ssIDE 3
Culture Medium only
Culture Medium + 400000 MASMC
Impedance (Ω)
Phase (θ)
Frequency(Hz)

MECs

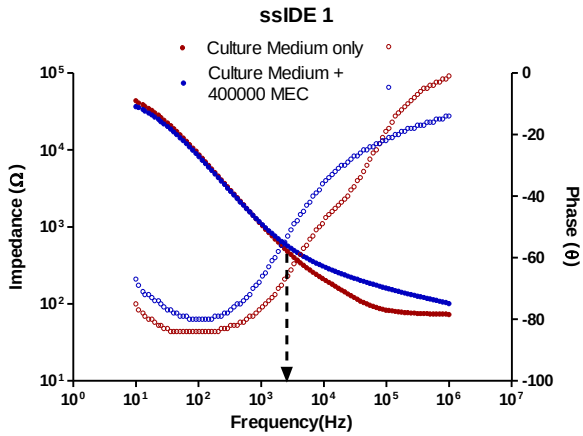
ssIDE 1
Culture Medium only
Culture Medium + 400000 MEC
Impedance (Ω)
Phase (θ)
Frequency(Hz)

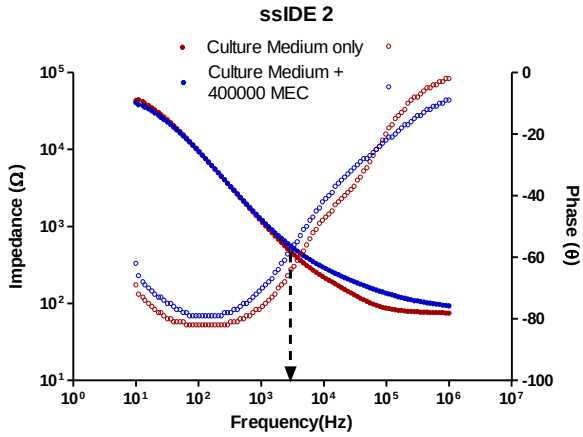
ssIDE 2
Culture Medium only
Culture Medium + 400000 MEC
Impedance (Ω)
Phase (θ)
Frequency(Hz)

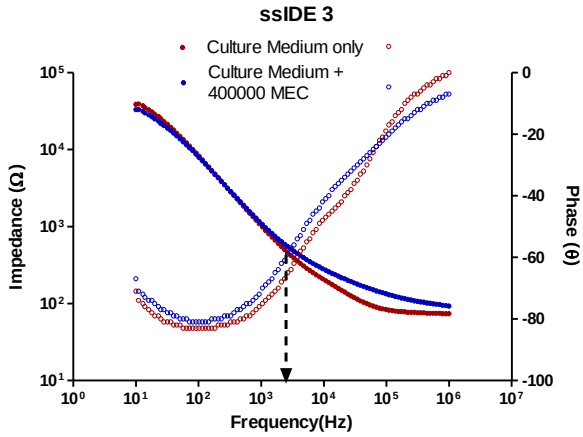
ssIDE 3
Culture Medium only
Culture Medium + 400000 MEC
Impedance (Ω)
Phase (θ)
Frequency(Hz)

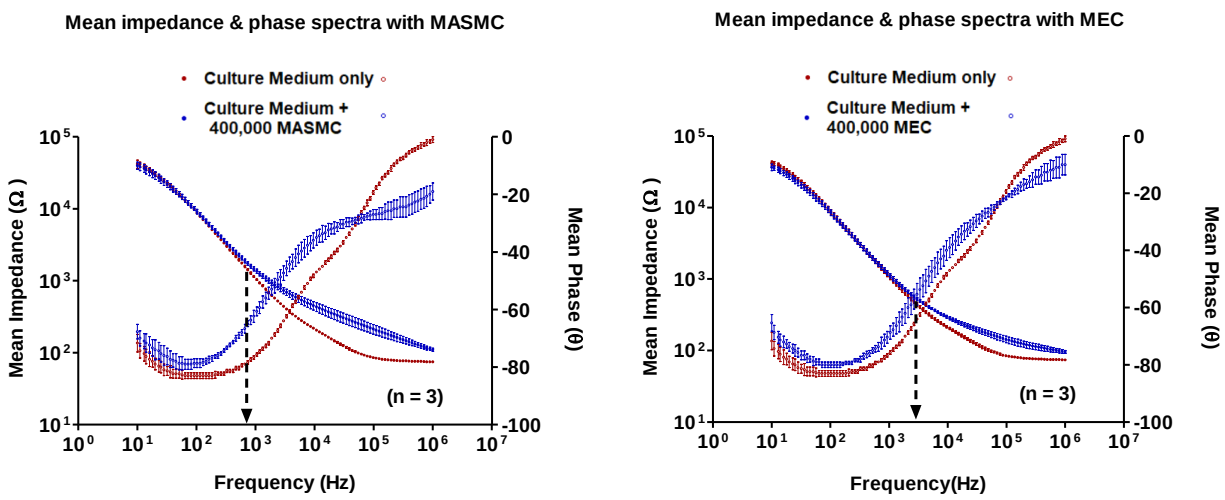

Figure 53: Individual and mean impedance and phase spectra for ssIDE with 400000 MASMCs and MECs.

4.6.3 Comparison between results with ssIDE and nIDE

With nIDE, the red (without cells) and blue (with cells) impedance curves separate out at about 1 kHz and coincide again at about 1 MHz. With ssIDE, the curves separate out at about 1 kHz but stay separate at 1 MHz. This implies that the optimum sensing frequency range for nIDE and ssIDE were slightly different.

When ssIDEs were used, the impedance curves separated out at a frequency of less than 1 kHz for MASMCs while the separation occurred at frequency higher than 1 kHz for MECs. A similar observation was made in Section 4.5.2. Hence, this observation is reproducible but further investigations with a mixed cell population (both MASMCs and MECs within the same cell suspension) were required.

4.7 Broad impedance and phase sweeps using nIDE and ssIDE on a mixed cell sample

4.7.1 Rationale

The experiments in Sections 4.5 and 4.6 suggests that nIDE and ssIDE were able to distinguish MASMCs and MECs. If this type of sensor was integrated onto a stent and deployed inside an artery, it is very likely that a mixture of both endothelial cells and smooth muscle cells would grow on the sensors. It was thus valuable to investigate how the sensors would work in an *in vitro* experiment involving a mixture of MASMCs and MECs.

4.7.2 Hypothesis

A mixed cell population would alter the shapes of the impedance and / or phase spectra.

4.7.3 Experimental procedure

The experiment was carried out as follows:

- 3 impedance devices each with 1 set of nIDE and 1 set of ssIDE were sterilised (Section 2.7.1). Readings from both nIDEs and ssIDEs were used in this experiment.
- Baseline impedance and phase sweeps from 10 Hz to 10 MHz were carried out with culture medium only.
- MASMCs and MECs were detached from separate confluent flasks (Section 2.2.2).
- 200000 MASMCs and 200000 MECs were seeded into each device
- The cell suspension was pipetted up and down a few times to ensure that the 2 cell types formed a uniform cell suspension.
- The cells were allowed to settle down for 18 h.
- After 18 h, experimental impedance and phase sweeps were carried out.

4.7.4 Results and discussion

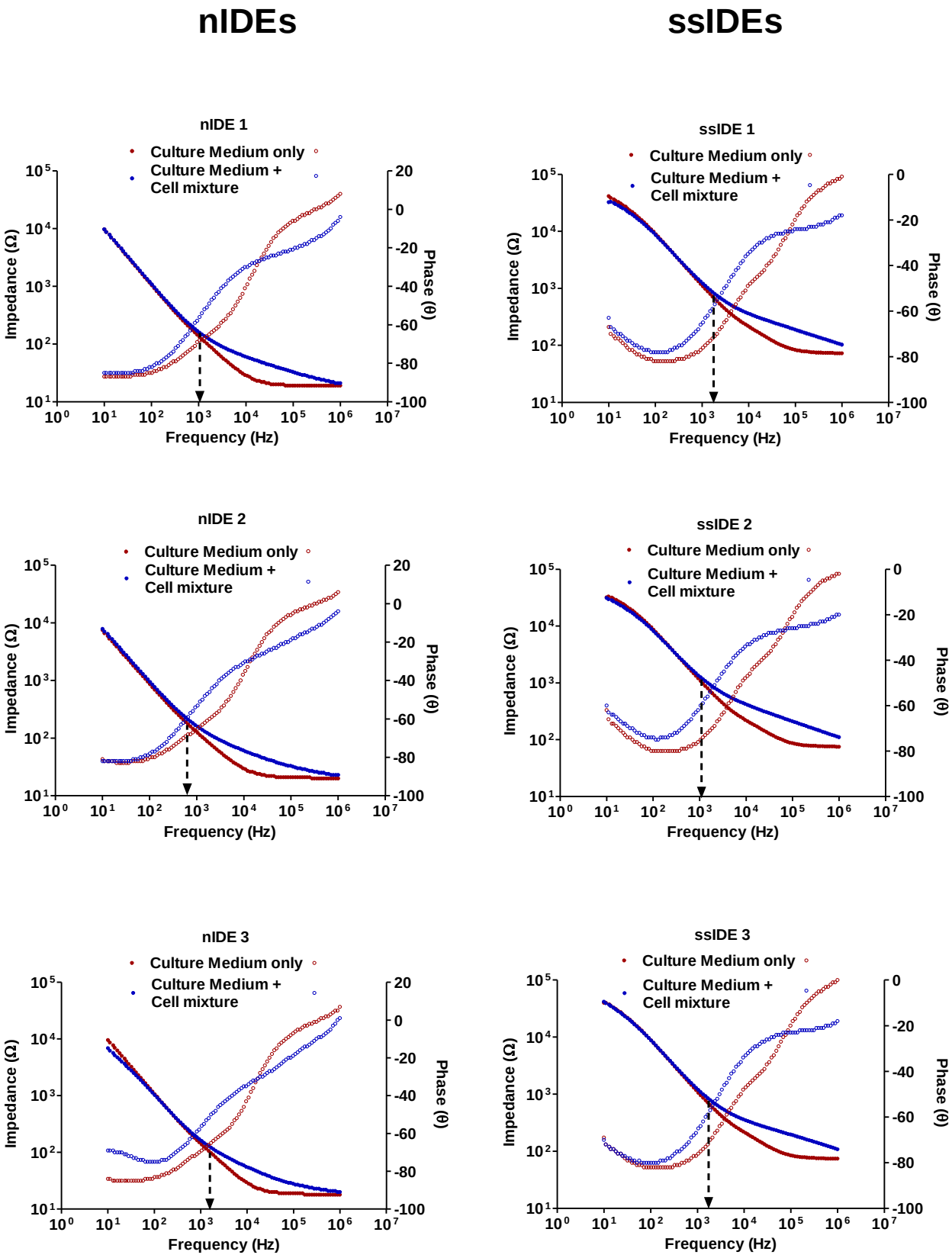

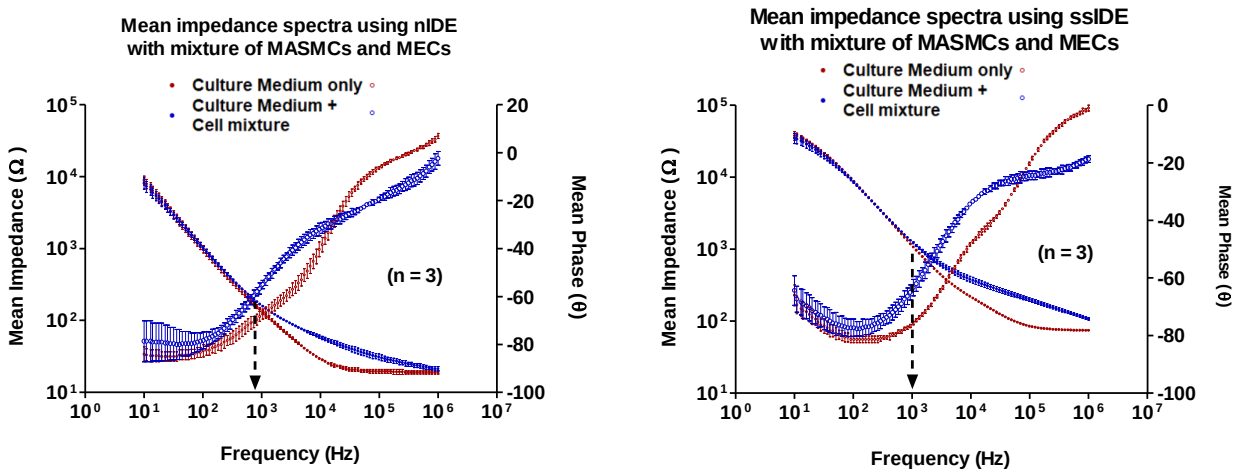

Figure 54: Individual and mean impedance and phase spectra using nIDE and ssIDE with 1:1 ratio of MASMC and MEC.

The impedance and phase sweeps for nIDE and ssIDE were plotted in Figure 54. The impedance and phase spectra of the cell mixture look very similar to ones obtained with a pure MASMCs or MECs sample. For nIDE 1, 2 and 3, the impedances curves separated at frequencies above 1 kHz, below 1 kHz and above 1 kHz respectively. The sample size was too small in order to determine whether the nIDE could be useful for sensing a mixed cell population of MASMCs and MECs.

For ssIDE 1, 2 and 3, the impedance curves all separated at frequencies above 1 kHz. The sample size was too small to determine whether ssIDE could be useful for sensing a mixed cell population. However, there was a trend indicating that 50 % of MECs in the cell population caused the "separating frequency" to be above 1 kHz. Hence a "separating frequency" above 1 kHz on ssIDE could be indicative of a pure MECs population or a mixed cell population made up of 50 % MEC and 50 % MASMCs.

4.8 Continuous impedance monitoring

4.8.1 Introduction

The LCR meter allowed the impedance to be measured at regular time intervals over a long time period. For this purpose, the LCR meter needed to be set at a single frequency. This was chosen as 10 kHz, which was the optimum sensing frequency. The time intervals were set at 15 min for most experiments, and were changed to fit the needs of different experiments.

4.8.2 Control measurements

Introduction

In order to determine whether continuous impedance monitoring was reproducible, control measurements had to be carried out. It was important to determine whether the baseline impedance without cells would change with time as a result of pH changes in the media. Another factor that could influence impedance was the excitation voltage of the LCR meter. During continuous measurement, the LCR meter probes remain connected to the impedance devices. The LCR meter probes were always conducting a small current of 10 μA, even between measurement intervals. Hence, it was essential to determine whether this constant excitation would cause changes in the impedance.

Experimental procedure

The control experiment was carried out as follows:

- An impedance device containing a nIDE was sterilised (Section 2.7.1).
- 2 mL of DMEM culture medium was pipetted into the device.
- The device was transferred to the Olympus microscope enclosure (37 ^{0}C and 5 % CO_2).
- The device was connected to the LCR meter.
- Impedance measurements at 10 kHz were acquired every 15 min for 72 h.

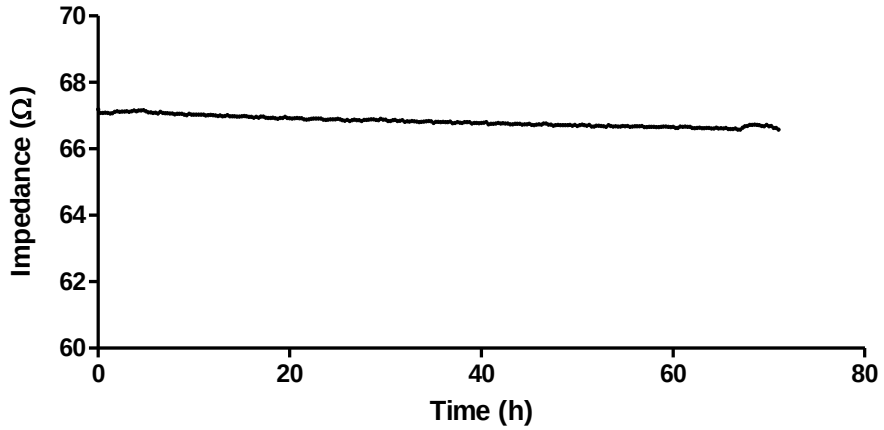

Figure 55: Continuous impedance tracking of DMEM culture medium without cells at 10 kHz for 72 h.

The impedance varies from 67.1 Ω to 66.5 Ω over the 72 h period. There was a 0.6 Ω decrease in impedance. The 5 % CO_2 supply inside the enclosure ensured that the pH of the culture media remained mostly stable. The small change in impedance meant that the constant excitation current from the LCR meter did not significantly affect the impedance of the device, in the absence of cells. This made this setup suitable for long term impedance monitoring.

4.8.3 Continuous impedance measurement with cells

Introduction and experimental procedure

The control experiment in Section 4.8.2 showed that the baseline impedance of the DMEM culture medium did not change significantly over 72 h, when continuously monitored every 15 min by the LCR meter. Hence, in this section, continuous monitoring with cells was attempted. Any changes in impedance could be attributed to the cell adherence, proliferation or death.

The experiment was carried out as follows:

- An impedance device containing a nIDE was sterilised (Section 2.7.1).
- MASMCs were detached from a sub-confluent flask (Section 2.2.2).
- 200000 MASMCs were seeded into the nIDE device.
- The device was transferred to the pre-warmed microscope enclosure, and set on the microscope stage.
- Continuous impedance measurements at 10 kHz (at 15 min intervals) and timelapse imaging (at 15 min intervals) were simultaneously started.
- The experiment was carried out for 20 h.

Results and discussion

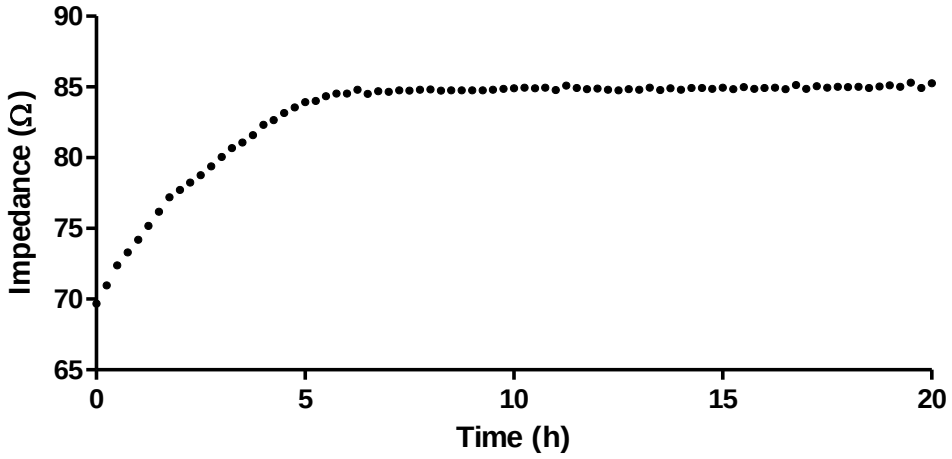

Figure 56: Continuous impedance monitoring at 10 kHz with 15 min intervals for 20 h of 200000 MASMCs settling down onto nIDE.

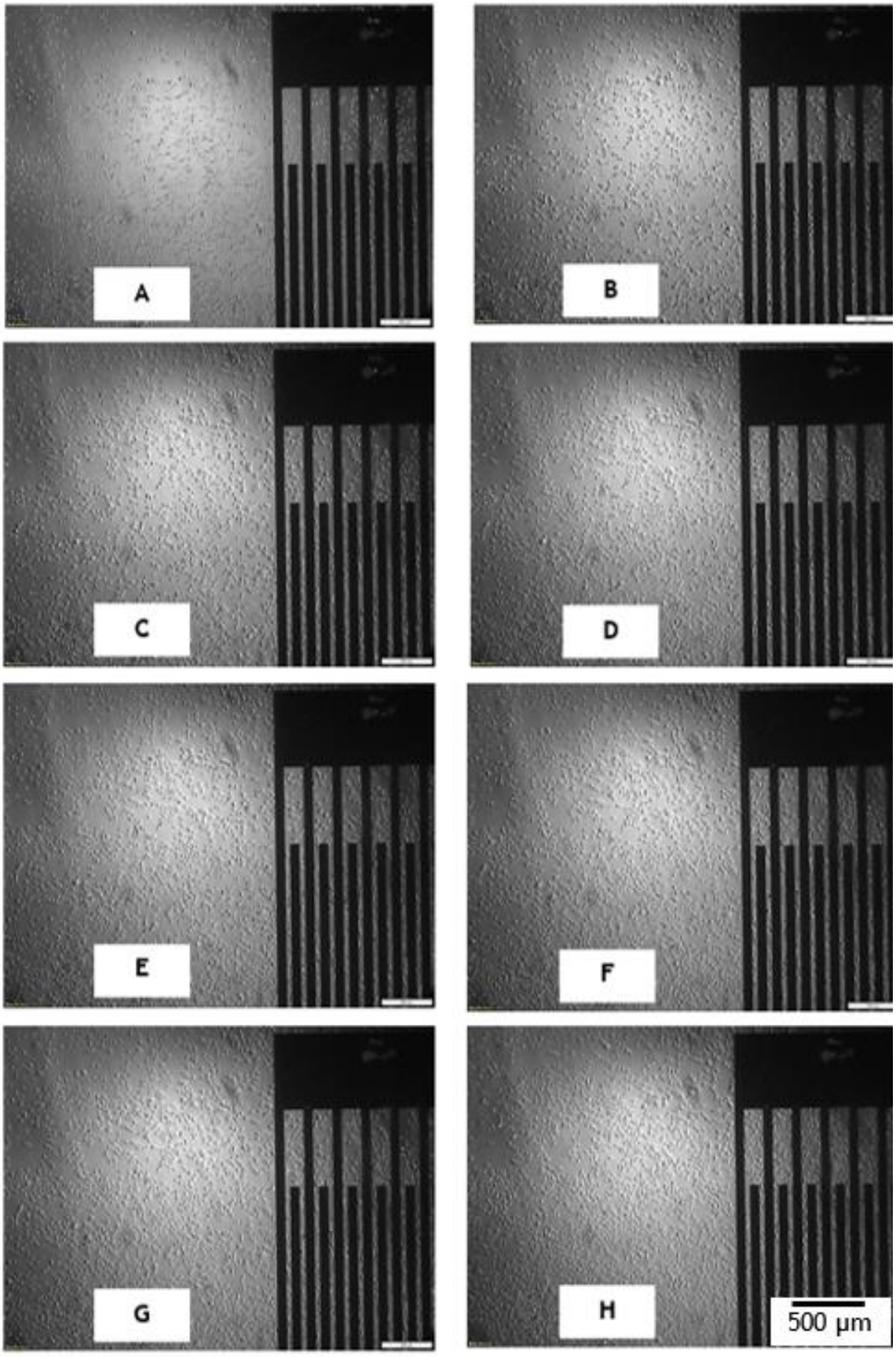

Figure 57: Microscopic images (2x) showing MASMCs in suspension (A), gradually settling down (B - G) and completely settled down (H).

The impedance measurement over 20 h are shown in Figure 56. Immediately after seeding, the impedance was 69 Ω. The cells were in suspension at that point. They gradually settled down, as shown by the images (Figure 57) and the gradual increase in impedance. The impedance reached a plateau of approximately 84 Ω at 6 h. The impedance remained roughly constant until 20 h.

Image A (time 0 h) of Figure 57, was acquired just after cell seeding. At that point, all the cells were in suspension and had a spherical shape. The nIDE was on the right of the image and appeared dark. The cells above the electrode could not be observed. The microscope was focussed onto the electrodes which were at the bottom of the device. Due to this, some of the cells appeared out of focus as they were suspended at a height from the bottom of the device.

On image B (time 1 h), all the cells were in focus as they have settled down to the bottom of the device. However, most of them still had a spherical shape as they had not fully adhered to the bottom surface. On images C, D & E (time 2, 3 & 4 h), spindle shaped cells could be observed. This was the characteristic shape of smooth muscle cells. This implies that these cells were healthy and had adhered to the bottom surface.

It was assumed that cells that were above the electrode had also started to adhere to the electrodes. This was indicated by the gradual increase in impedance. On images F & G (time 5 & 6 h), a higher proportion of cells had a spindle shape rather than spherical shape. This implied that most of the cells had adhered to the bottom of the device, consisting of both glass and electrode. The impedance reached a plateau at that point. On image H (time 7 h), an even higher proportion of cells had the characteristic spindle shape of smooth muscle cells.

It was not possible to observe the cells on the electrodes, as the microscope uses transmitted light. The metal electrodes had a thickness of 130 nm and blocked most of the light, preventing cells on their surface to be observed. Observing those cells would have been possible using reflected light microscopy, as the metal electrodes had a shiny surface. This was unfortunately not possible with the microscope setup.

However, microscopic images (showing cells around electrodes) correlated with impedance measurements were evidence towards the fact that nIDE could be used for continuous monitoring of cell adherence. This experiment was an attempt to simulate the restenotic response over the sensors embedded onto a stent. It was not the best model for this response, as this involves smooth muscle cells migrating from the medial layer of the artery rather than smooth muscle moving from a cell suspension onto a hard surface. However, the nIDE were more sensitive to cells when they were adhering to the electrodes, and were less sensitive to them when suspended. It was promising that the nIDE were more influenced by cells directly adhering rather than cells in suspension. Hence, if this type of sensor was integrated onto a stent, it would give information about cells directly adhering to it, rather than surrounding cells such as red blood cells and white blood cells.

4.9 Sensitivity of Interdigitated Electrodes

4.9.1 Introduction

The following experiment was carried out to determine the number of cells that could be detected by the electrodes. This could be defined as the sensitivity of the electrodes, in terms of number of cells / Ω. This could allow the deduction of the number of cells adhering on the electrodes based on the increase in impedance. The cells were stained using Acridine Orange to allow the nuclei to be distinguished, facilitating cell counting.

4.9.2 Experimental procedure

The experiment was carried out as follows:

- 3 devices each with 1 nIDE and 1 ssIDE were sterilised (Section 2.7.1).
- Baseline impedance measurements at 10 kHz were carried out with culture medium only.
- MASMCs were detached from a sub-confluent flask (Section 2.2.2).
- 400000 MASMCs were seeded into each device and the cells were allowed to settle down for 18 h.
- After 18 h, experimental impedance measurements were carried out.
- The impedance increase for each of the electrodes was calculated.
- The cells were then stained using Acridine Orange (Section 2.2.4).
- MIA of the nIDE and ssIDE were then acquired in the FITC (green) channel.
- The experiment was repeated using 200000 and 100000 MASMCs.

4.9.3 Post-experiment image processing

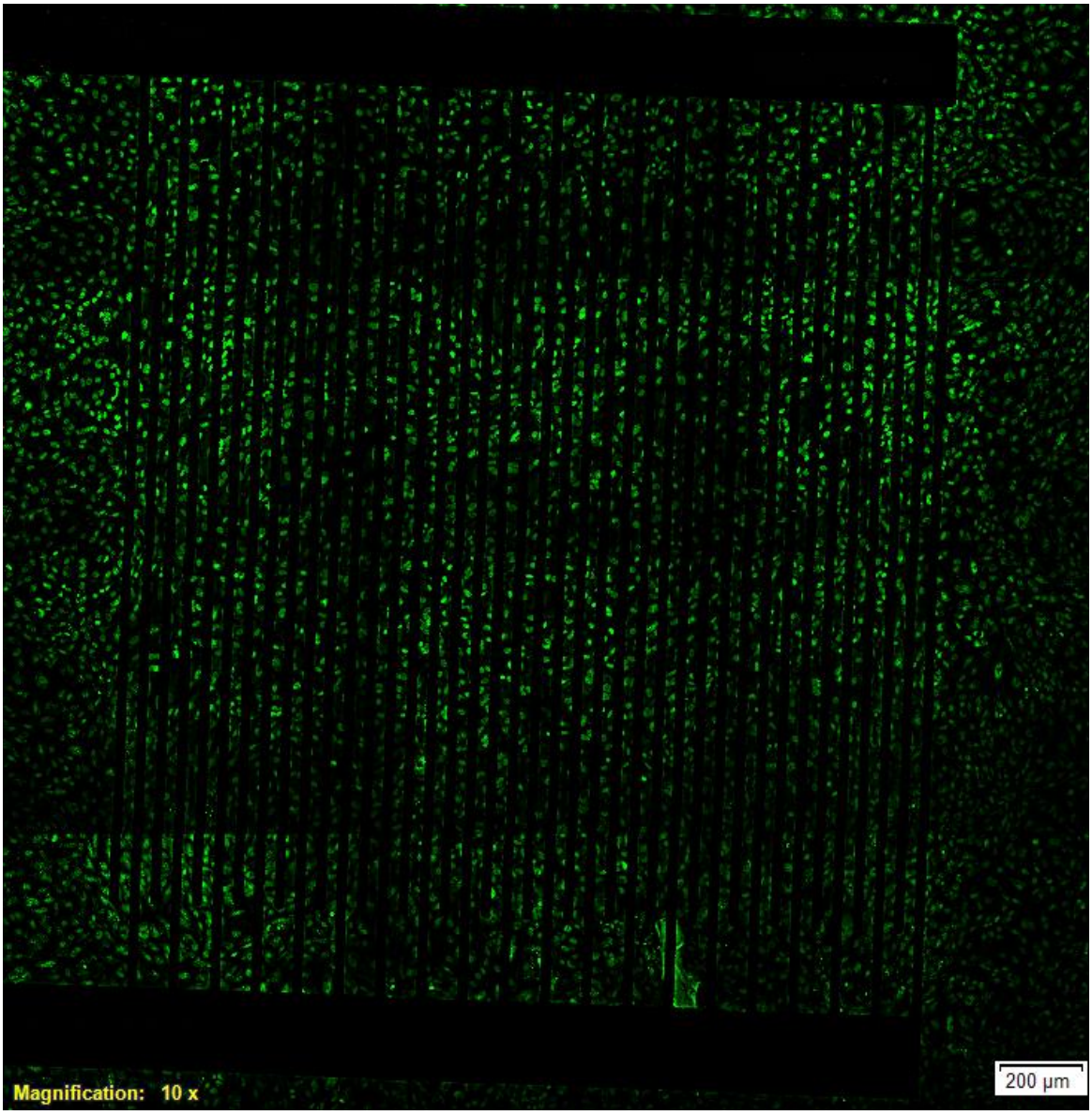

Figure 58: Fluorescent (green) MIA of ssIDE showing MASMCs within and outside electrode area.

The MIA acquired showed the nuclei (stained with Acridine Orange) of the live cells against a dark background. One the MIA is shown in Figure 58. ImageJ was used to process the image in order to obtain an approximate cell count. This was carried out as follows:

- The image was loaded into ImageJ.
- The image type was set at 8-bit.
- The image was thresholded until only the nuclei were visible.
- A region of interest comprising only the effective electrode area was selected.

- The Analyse Particles tool of ImageJ was selected. The Size was set at 200 - 3600 μm^2. The Circularity was set at 0.00 – 1.00. The tool was set so that it showed the outlines of object being counted.
- The cell count was obtained from the Results table generated by the Analyse Particle tool.

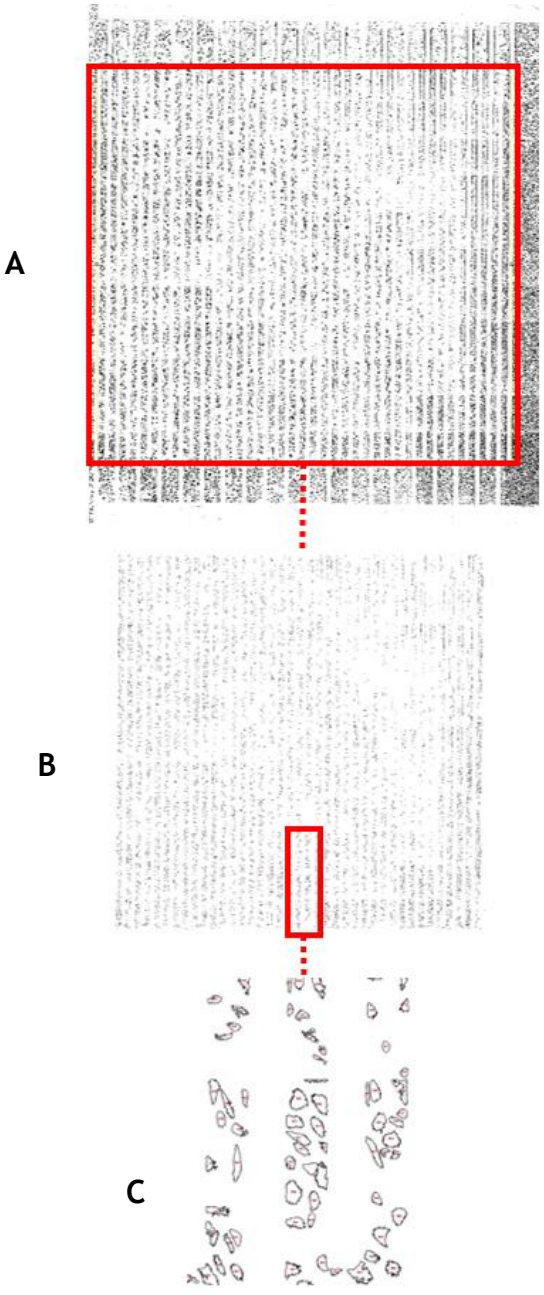

Figure 59: (A) Black and white image of cells on electrode after thresholding, (B) Image after use of "Analyse Particles" tool, showing outline of counted objects (cell nuclei) & (C) Magnified image after use of "Analyse Particles" tool.

4.9.4 Results and discussion

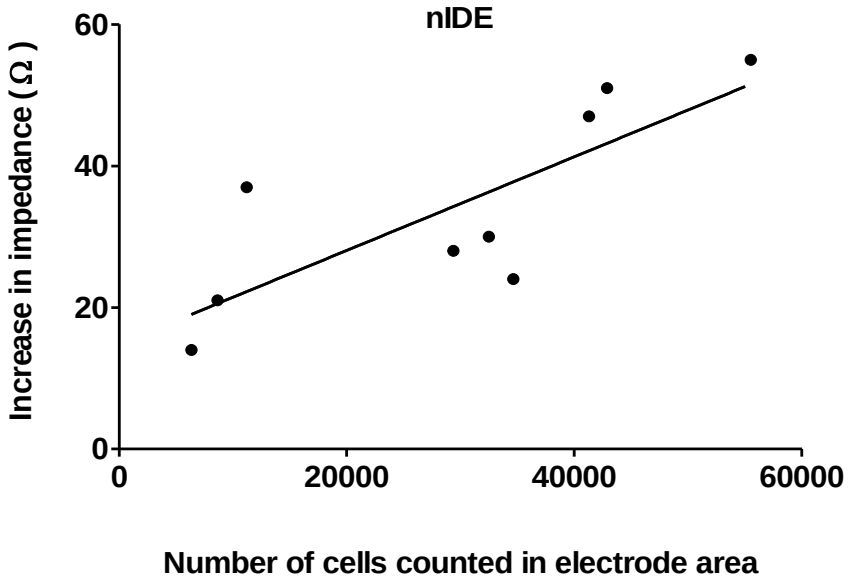

$$\boldsymbol{Impedance\ increase} = \mathbf{15} + (\boldsymbol{Number\ of\ cells\ in\ electrode\ area}\ \times \mathbf{10^{-4}} \times (\mathbf{7}\ \pm \mathbf{2}))$$

Figure 60: Scatter plot of number of cells counted in electrode area of nIDE v/s increase in impedance and equation of linear regression.

Figure 60 shows the scatter plot of increase in impedance against number of cells counted on electrode area, with the linear regression line for nIDE. The equation of the linear regression line with the confidence interval is also shown. The r^2 (goodness of fit) value was 0.6270. From this equation, the increase in impedance detected by the nIDE could be used to predict the number of cells in the electrode area.

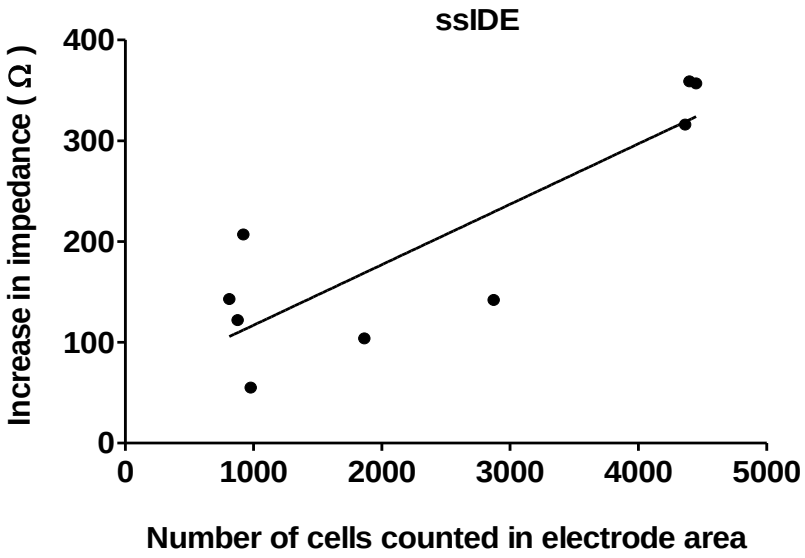

$$\boldsymbol{Impedance\ increase\ = 57 + (number\ of\ cells\ in\ electrode\ area\ \times\ 10^{-2}\ \times (6 \pm 1))}$$

Figure 61: Scatter plot of number of cells counted in electrode area of ssIDE v/s increase in impedance and equation of linear regression.

Figure 61 shows the scatter plot of increase in impedance against number of cells counted on electrode area, with the linear regression line for ssIDE. The equation of the linear regression line with the confidence interval is also shown. The r^2 (goodness of fit) value was 0.7314. From this equation, the increase in impedance detected by the ssIDE could be used to predict the number of cells in the electrode area.

4.10 Summary and discussion

Results from Figure 50 show that the nIDE can also detect another cell type, the MEC. The ECIS system is used by many different research groups around the world with different cell types. For example, Ablin and Jiang (2012) used ECIS electrodes to monitor adherence and proliferation of BSC-1 and NRK cells, within the same experiment (Figure 15). Even, though the nIDE have only been used to detect MASMCs and MECs, it can be assumed that the electrodes could also detect other cell types.

Moreover, Ablin and Jiang (2012) used the ECIS system to continuously monitor adherence and proliferation of the cells. Continuous monitoring could also be achieved using the nIDE (Section 4.8). However, the magnitude of the impedances detected in their experiments were much higher compared to our results (maximum resistance of 15000 Ω v/s maximum impedance of 85 Ω). The difference in magnitudes is explained by the fact that they used much smaller electrodes (0.05 mm^2) compared to ours (28.8 mm^2). The advantage of using smaller electrodes is that increases sensitivity, to the point that cell micromotions can be detected. However, the sensing area only occupies a small percentage of the culture well, and thus, the impedance trace is not always representative of the cell population. The use of larger electrodes occupying a larger area of the well (due to interdigitated design) leads to decreased sensitivity, but the results are more representative of the cell population.

Ablin and Jiang (2012) also hypothesised that they could differentiate cell types based on the continuous impedance trace. The results in Figure 15 show that BSC-1 reached the maximum resistance faster than NRK cells. However, these results are based on a single biological and single technical replicate, and might not be the "signature" impedance trace. Differences in the age of the cells, culture medium and surface properties of the electrode could affect the impedance trace. Hence, differentiating cells based on the continuous impedance trace would not be reliable.

Figure 51 showed that at equal cell densities, MASMC caused a higher increase in impedance compared to MEC. This is similar to finding by Mamouni and Yang (2011), which showed that at equal cell number, non-cancer oral epithelial cells generated a much smaller magnitude of impedance than oral cancer cells did. This

is a potential method of distinguishing between different cell types. However, this relies on knowing the cell densities covering the electrodes. This can be assessed in an *in vitro* situation but would not be possible in an *in vivo* situation (sensors on a stent inside a blood vessel).

We hypothesised that MASMCs and MECs could be distinguished based on clear differences in the geometric shapes of the impedance spectra and phase spectra over a large frequency range. The impedance and phase spectra of MASMC and MEC were compared using nIDE in Figure 52. The mean phase spectra showed large standard deviation as compared to mean impedance spectra. Thus, the impedance spectra was chosen as the most suitable electrical property to help distinguish the 2 cell types. Both MASMC and MEC produced impedance decay curves, and thus the shapes of the curves could not be used to distinguish the cell types. However, the mean experimental and baseline spectra started to diverge < 1 kHz for MASMC and > 1 kHz for MEC. It was possible that MASMC and MEC had a signature "impedance diverging frequency".

MASMC and MEC impedance and phase spectra were compared using ssIDE in Figure 53. Again, the mean phase spectra showed large standard deviation. More importantly, the experimental and baseline spectra started to diverge < 1 kHz for MASMC and > 1 kHz for MEC, as was the case with nIDE. This is further evidence that MASMC and MEC could have a signature "impedance diverging frequency", which would allow the two cell types to be distinguished using Interdigitated Electrodes. These strategies would be useful *in vitro* for distinguishing a pure MASMC population from a pure MEC population. However, *in vivo*, a mixture of smooth muscle cells and endothelial cells are likely to grow on the implanted stent. Experiments with MASMC and MEC in a 1:1 ratio caused the "impedance diverging frequency" vary randomly about 1 kHz. Thus more reliable ways of distinguishing smooth muscle cells, endothelial cells and other cells involved in instent restenosis are required.

CHAPTER 5

ELECTRO-MEDIATED CELL DEATH

5.1 Rationale

If the hypothetical smart stent with cell sensors detected an overgrowth of smooth muscle cells, therapeutic intervention would be the next logical step. Previous experiments with ECIS devices (Section 1.8.8) showed that a higher voltage (1 V - 5 V compared to 1 mV - 10 mV used for measuring) could induce cell death. Hence, the cell sensors could also act a therapeutic probes. This chapter investigated the phenomenon of electro-mediated apoptotic cell death.

5.2 Hypothesis

Application of a higher voltage to IDEs and PEs can induce apoptosis of MASMCs.

5.3 Introduction

In the previous chapters, it was shown that Interdigitated Electrodes (nIDE and ssIDE) were capable of detecting adherence, proliferation and death of smooth muscle cells and endothelial cells, either intermittently or continuously. The measurements were carried out using an LCR meter which used low voltage and low current (10 μA) settings. If this type of sensor (combined with an impedance measuring circuit and a wireless power / data transfer module) was further miniaturised and integrated onto a smart stent, it would allow monitoring of proliferation of cells (smooth muscle cells and / or endothelial cells) over the stent. In this chapter, experiments were carried out to determine whether application of higher voltages to the sensors could induce a controlled form of cell death, which could potentially be used as therapeutic intervention. Attempts were also made to determine the type of cell death occurring. Experiments were carried out with PEs, nIDEs and ssIDEs. The main advantage of the PE was that the effects of the voltage on cells could be more easily observed microscopically. The voltage types used were DC voltage (in the 1.0 V to 2.5 V range) and AC voltage (in the 1.0 V – 5.0 V range). The maximum DC voltage was 2.5 V because higher voltages causes electrolysis of culture medium and damage to the electrodes. AC voltages higher than 5.0 V also caused damage to the electrodes.

5.4 Using interdigitated electrodes with intermittent impedance measurements to monitor death of MASMCs

5.4.1 Rationale

In the previous chapter, it was shown that interdigitated electrodes (nIDE and ssIDE) could be used to monitor adhesion of MASMCs after cell seeding. Immediately after seeding, the cells were spherical and floating in the culture medium. Due to gravity, the cells gradually sank to the bottom (glass + electrodes) the wells. The cells gradually adhered and spread. This could be detected as a gradual increase in the impedance with time. When most of the cells had settled down and covered most the effective electrode area, the impedance reached a plateau. This plateau phase was thus useful for monitoring the health of the monolayer. The following experiment investigated whether the electrodes could also monitor gradual death of the monolayer.

5.4.2 Hypothesis

Intermittent impedance measurement with nIDE can be used to monitor death of MASMCs.

5.4.3 Experimental procedure

The experiment was carried out as follows:

- 5 devices containing nIDE were sterilised (Section 2.7.1).
- A baseline impedance measurement at 10 kHz was carried out with culture medium only.
- MASMCs were detached from a sub-confluent flask (Section 2.2.2).
- 200000 MASMCs were seeded into each device.
- The cells were allowed to settle down for 24 h in an incubator (37 ^{0}C and 5 % CO_2).
- After 24 h, microscopy was used to ensure that the cells had settled down into a monolayer and impedance measurements were carried out again.
- The devices were then put back into the incubator.

- Every 24 h, the cells were checked under the microscope and impedance readings were acquired.
- The endpoint of the experiment was when most of the cells had lost their spindle shape and looked spherical.
- The culture medium was not changed in this experiment.
- The experiment was repeated using 3 devices and the culture medium was replaced with fresh culture medium at 24 h.

5.4.4 Results and discussion

Repeat 1:

Figure 62B shows that there was an increase in mean impedance from 71 Ω to 101 Ω, at 0 h and 24 h, respectively. One-way ANOVA with Tukey's Multiple Comparison Test showed that the mean impedance at 24 h was statistically different from that at 0 h ($p < 0.001$). The increase in impedance was due to cell adherence to the electrodes. There was a decrease in mean impedance from 101 Ω to 80 Ω, at 24 h and 48 h, respectively. One-way ANOVA with Tukey's Multiple Comparison Test showed that the mean impedance at 48 h was statistically different from that at 24 h ($p < 0.01$). The decrease in impedance was due to cell death and detachment from the electrodes. One-way ANOVA with Tukey's Multiple Comparison Test also showed that the mean impedance at 48 h was not statistically different from that at 0 h. This is consistent with the fact that the impedance goes back to the initial cell-free baseline impedance, as the cells die.

Repeat 2:

Figure 62D showed that there was an increase in mean impedance from 101 Ω to 145 Ω, at 0 h and 24 h, respectively. One-way ANOVA with Tukey's Multiple Comparison Test showed that the mean impedance at 24 h was statistically different from that at 0 h ($p < 0.05$). From 24 h to 48 h, the impedance increased from 145 Ω to 150 Ω, but this was not statistically significant. However, this indicated that the monolayer was able to survive longer due to the change in media at 24 h. In Repeat 1, there was no change of media, and the impedance decreased from 24 h to 48 h.

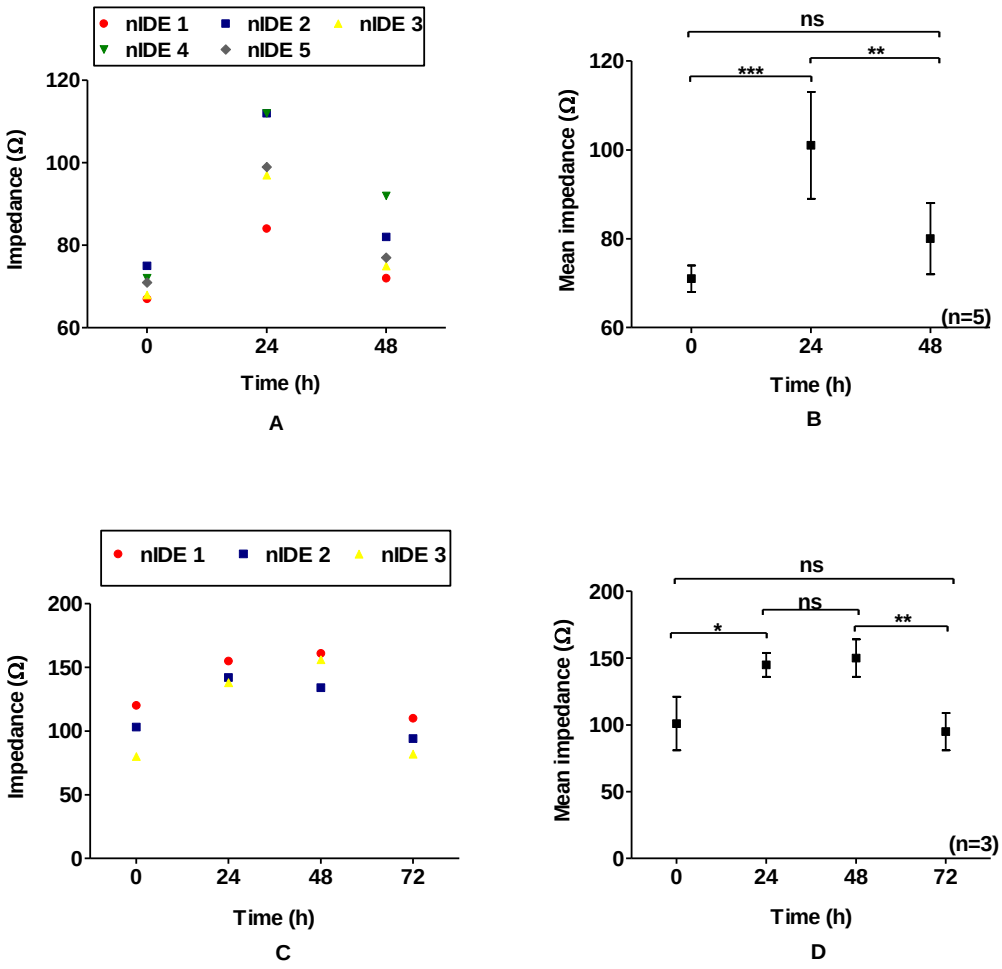

Figure 62: Intermittent impedance measurements -

(A) Repeat 1: Impedances of nIDE 1, 2, 3, 4 and 5 at 0 h (baseline cell-free), 24 h (culture medium + cells) and 48 h (culture medium + dead cells) (n = 5).

(B) Repeat 1: Mean impedances for nIDEs together at the different timepoints. One-way ANOVA with Tukey's Multiple Comparison Test showed that the mean impedance at 24 h was statistically different from that at 0 h ($p < 0.001$) and that the mean impedance at 48 h was statistically different from that at 24 h ($p < 0.01$). The mean impedance at 0 h and 48 h were not statistically different (n = 5).

(C) Repeat 2: Impedances of nIDE 1, 2 and 3 at 0 h (baseline cell-free), 24 h (culture medium + cells), 48 h (culture medium + more cells) and 72 h (culture medium + dead cells) (n = 3).

(D) Repeat 2: Mean impedances of nIDE 1, 2 and 3 together at the different timepoints. One-way ANOVA with Tukey's Multiple Comparison Test showed that the mean impedances at 0 h & 24 h and 48 h & 72 h were statistically different ($p < 0.05$ and $p < 0.01$ respectively). The mean impedances at 0 h & 72 h and 24 h & 48 h were not statistically different (n = 3).

There was a decrease in mean impedance from 150 Ω to 95 Ω, at 48 h and 72 h, respectively. One-way ANOVA with Tukey's Multiple Comparison Test showed that the mean impedance at 48 h was statistically different from that at 72 h ($p < 0.01$) but not statistically different from the impedance at 0 h (baseline without cells). This indicates that the monolayer underwent cell death during the 48 – 72 h period. This could be due to the cells running out of nutrients. The results show that intermittent impedance measurements using nIDE could allow death of a MASMCs monolayer to be monitored. However, it is not clear whether the cell death occurs gradually or at a fast rate.

5.5 Monitoring death of MASMCs using nIDE with continuous impedance measurements

5.5.1 Rationale

In the previous experiment, the death of a MASMCs monolayer was tracked using intermittent impedance measurements on nIDE. The cell death within the monolayer due to shortage of nutrients would occur gradually. It was not clear from the previous experiment whether the nIDE detected a gradual or sudden decrease in impedance as the cell started to die. Hence, in this section, the experiment was carried out with a higher time resolution of 15 min (compared to 24 h for previous experiment). This type of impedance measurement was referred to as continuous measurement (rather than intermittent measurement).

5.5.2 Hypothesis

Gradual death (due to shortage of nutrients) of a MASMCs monolayer can be monitored using nIDE with continuous impedance measurements.

5.5.3 Experimental procedure

The experiment was carried out as follows:

- A device containing nIDE was sterilised (Section 2.7.1).
- MASMCs were detached from a sub-confluent flask (Section 2.2.2).
- 200000 MASMCs were seeded into the device.
- The seeded device was transferred to the microscope enclosure and connected to the LCR meter.
- Impedance readings (at 10 kHz) was acquired at 15 min intervals.
- The experiment was continued until the impedance went back to the baseline impedance (impedance at 0 h).

5.5.4 Results and discussion

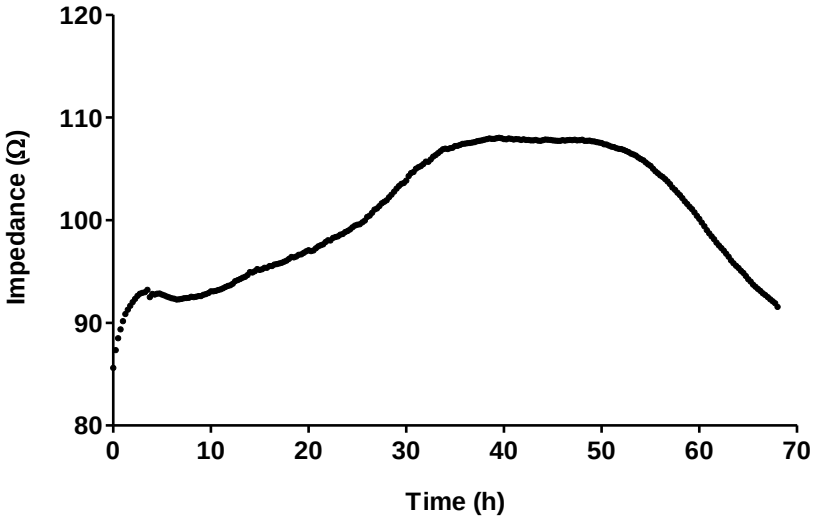

Figure 63: Continuous impedance measurement of nIDE showing increase after MASMCs were seeded, maximum when all the cells had settled down and decrease as the cells started to die (n = 1).

The baseline impedance was 86 Ω at 0 h. This indicated the impedance with very low cell adhesion. The impedance gradually increased during the 0 h to 39 h period. At 39 h, the impedance reached a plateau of approximately 108 Ω. Then, the impedance gradually decreased as from 50 h and reached 92 Ω at 68 h. These results show that the nIDE could track gradual increases in impedance as the cells adhered to the electrodes.

The plateau phase indicated that most of the cells had adhered to the electrodes and settled down into a healthy monolayer. As the cells started to run out of nutrients at approximately 50 h, the impedance gradually decreased. Hence the nIDE could be used to monitor gradual death (due to shortage of nutrients) of a MASMC monolayer.

5.7 Applying DC voltage to a MASMCs monolayer through PE

5.7.1 Introduction

When DC voltage was applied using Pendulum Electrode (PE) devices, there were 2 possible configurations depending on the polarity: the 4 pendulum electrodes were positive while the large counter was negative or the pendulum electrodes were negative while the large counter electrode was positive. Preliminary experiments showed that a more significant effect could be induced on the cells with the pendulum electrodes negative and the large counter electrode positive. These experiments also showed that a DC voltage of 3.0 V caused electrolysis if the culture medium. Hence, in all experiments with DC voltages, a maximum of 2.5 V was applied.

Figure 64 shows the electric field lines between a large positive counter electrode (+q) and a small negative electrode (-q). The electric field density was much higher around the small electrode compared to the large counter electrode. In order to induce such an electric field inside the PE devices, a DC voltage had to be applied to the electrodes with the large counter electrode positive and the 4 small pendulum electrodes negative. Hence a high electric field density was induced around each PE.

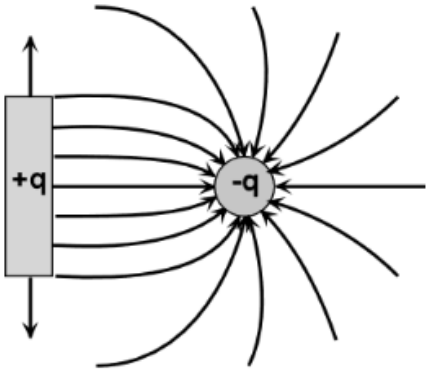

Figure 64: Electric field between a large positive counter electrode +q and a small negative electrode -q. The electric field density is much higher around the small electrode compared to the large counter electrode (Physics Drawings (2019)).

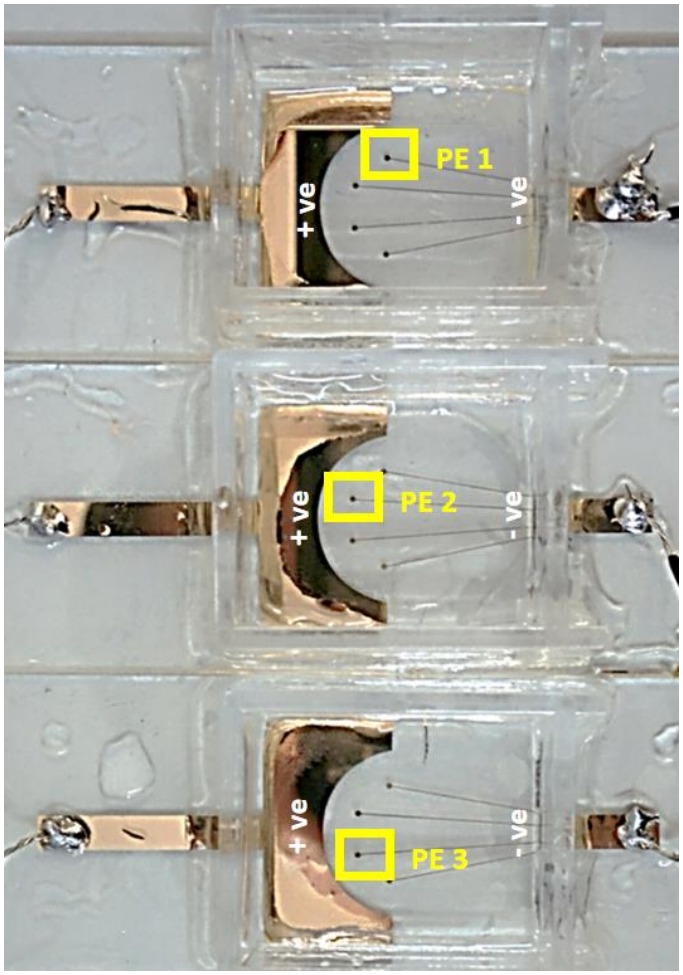

Figure 65: Three devices each containing 4 PEs. Only one PE (1, 2 and 3) in each device was used for imaging.

5.7.2 Hypothesis

Death of MASMCs can be induced by applying a DC voltage using PE.

5.7.3 Experimental procedure

The experiment was carried out as follows:

- 3 devices, each containing 4 PEs were sterilised (Section 2.7.1). Only 1 PE in each device was used for imaging and image analysis.
- MASMCs were detached from a sub-confluent flask (Section 2.2.2) and 200000 MASMCs were seeded into each device.
- 2 mL of HEPES DMEM media was added to each device.
- The seeded devices were kept in an incubator (37 ^{0}C & 5 % CO_2) for 18 h, to allow the cells to settle down.

- After 18 h, the cells were observed under the microscope to ensure that they had adhered to the bottom and had the characteristic spindle shape.
- The device containing PE 1 was set up on the live cell microscope stage.
- The large counter electrode was connected to the positive terminal while the PEs were connected to the negative terminal of the function generator (Figure 65)
- Timelapse imaging was started and images were captured at 30 s interval up to the 150 s timepoint.
- No voltage was applied for the first 25 s.
- From 25 s to 150 s, a DC voltage of 2.5 V was applied to the electrodes using the function generator (Section 2.9).
- This experimental procedure was repeated with the devices containing PE 2 and 3.
- The whole experiment was repeated at a later time.

5.7.4 Image analysis

ImageJ was used to measure the surface area devoid of live cells (Referred to as Live-cell-free area) around each pendulum electrode at 0 s, 30 s, 60 s, 90 s, 120 s and 150 s. The cumulative increase in the Live-cell-free area for each timepoint was calculated for each pendulum electrode and a mean for each timepoint was calculated. This was repeated for the second repeat of the experiment.

5.7.5 Results

The images of PE 1, 2 and 3 with a MASMCs monolayer are shown in Figure 66. The monolayer covered the whole field of view including the PE. It was not possible to observe the cells on the electrodes (thickness 100 nm) because the light transmission through the electrode was too low. No voltage was applied for the first 25 s. From 25 s to 150 s, 2.5 V DC was applied. The MASMC monolayer was clearly disrupted by the application of 2.5 V DC for a short period of time.

Time & Voltage	Repeat 1			Repeat 2		
	Pendulum Electrode			Pendulum Electrode		
	1	2	3	1	2	3
0 s 0.0 V	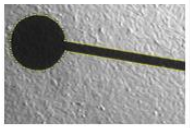	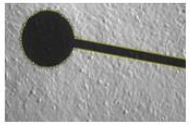	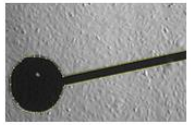		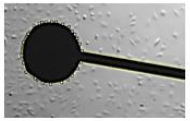	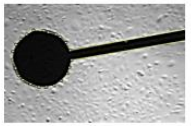
30 s 2.5 V	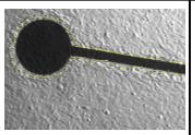	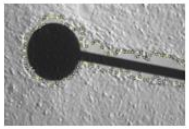	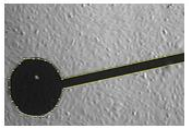		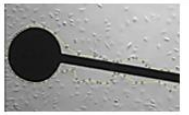	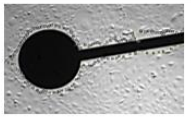
60 s 2.5 V	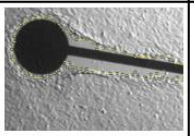	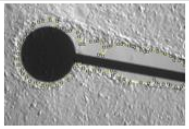	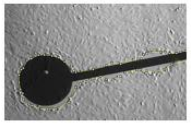	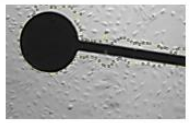	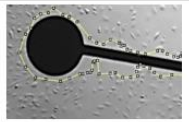	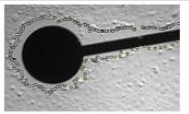
90 s 2.5 V	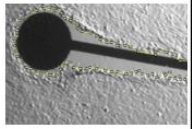	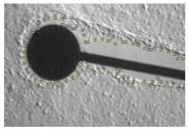		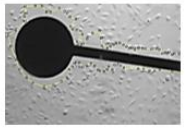		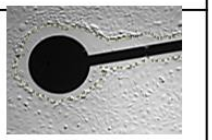
120 s 2.5 V	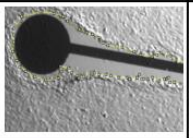	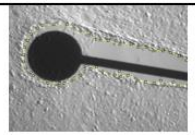	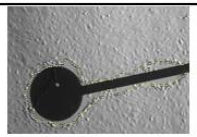		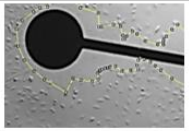	
150 s 2.5 V	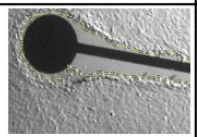	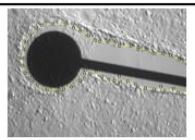	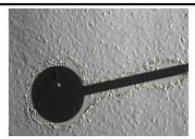	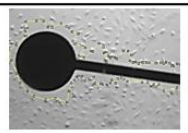	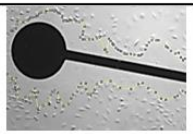	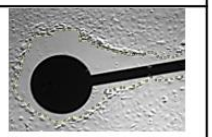

Figure 66: Effects of 2.5 V DC on MASMCs monolayer when applied through PE 1, 2 and 3 for repeats 1 and 2

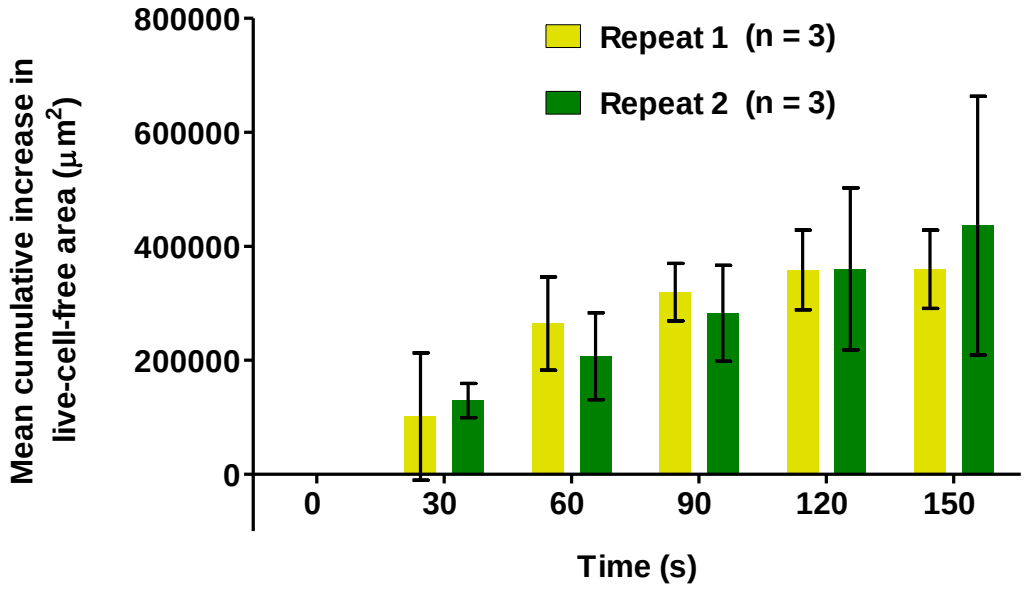

Figure 67: Mean cumulative increase (of PE 1, 2 and 3 together) in live-cell-free area with time for repeats 1 and 2. Two-way ANOVA with Bonferroni post test showed that the differences between the means of the 2 repeats at the different timepoints were not statistically significant.

5.7.6 Discussion

The results show that the mean cumulative increase in live-cell-free area for Repeat 1 and Repeat 2 were statistically similar. This implied that the effects induced by a DC voltage of 2.5 V was reproducible on 2 different biological replicates.

The mean cumulative increase in live-cell-free area increases with time, indicated that a longer duration of the DC voltage caused more significant effects on the cell monolayer. The aim of this chapter was to find ways of intervening at the early onset of instent restenosis.

Applying a DC voltage to the cell sensors (acting as therapeutic probes) is a possibility. However, this would require the smart stent to be equipped with batteries or capacitors and radiofrequency antennas for recharging . The effects induced on the monolayer using both PE were very disruptive, even at a low voltage of 2.5 V DC. If applied in an *in vivo* situation, this type of voltage could adversely affect the healthy layers of the stented artery.

Moreover, if the smart stent was implanted in a coronary artery, this voltage could interfere with the normal electrical activity of the heart. DC voltage could also lead to electrolysis of blood, due to its ionic nature. This would adversely affect the local ionic balance of blood, blood cells and even the metal of the cell sensors / therapeutic probes. Thus, DC voltage might not be suitable for intervening on the early smooth muscle regrowth.

5.8 Recovery of MASMCs monolayer following application of DC voltage on PE

5.8.1 Rationale

The experiment in Section 5.6 showed that 2.5 V DC caused a reproducible "tearing" effect on a MASMCs monolayer when applied through PEs. This "tearing" effect was only the short term observable effect (during the 150 s of voltage application) of the DC voltage. In this section, the long term effect of the application of DC voltage on 1 PE was investigated.

5.8.2 Experimental procedure

The experiment was carried out as follows:

- A device containing PE was sterilised (Section 2.7.1).
- MASMCs were detached from a sub-confluent flask (Section 2.2.2) and 100000 MASMCs were seeded into the device.
- 2 mL of HEPES DMEM media was added to the device.
- The seeded devices were kept in an incubator (37 ^{o}C & 5 % CO_2) for 18 h, to allow the cells to settle down.
- After 18 h, the cells were observed under the microscope to ensure that they had adhered to the bottom and had the characteristic spindle shape.
- The device was then set up on the live cell microscope stage.
- 4 observation positions were selected. 2 positions contained the electrodes and acted as "treatment position". 2 positions did not contain the electrodes and acted as "control positions".
- Images of the 4 positions were acquired at 0 min. For positions 3 and 4, images were also acquired at a higher light intensity, allowing cells adhering directly to the electrodes (which were translucent due to thin 30 nm thickness of gold) to be observed.
- At 4 min, the device was connected to the function generator, with the large counter electrode as the positive terminal and the PE as the negative terminal (Figure 65) and DC voltage of 2.5 V was applied for 1 min.

- Images of the 4 positions were acquired just after application of voltage (5 min).
- The cells were allowed to recover, and further images were acquired at 2000 min and 4000 min.

5.8.3 Results and discussion

Time	Position 1	Position 2	Position 3 (low contrast)	Position 3 (high contrast)	Position 4 (low contrast)	Position 4 (high contrast)
0 min ***Number of live cells***	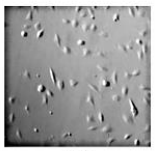 73	 129	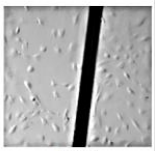 110	 11	 123	 22
5 min ***Number of live cells***	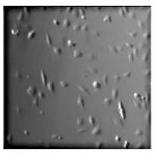 81	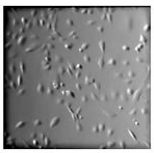 130	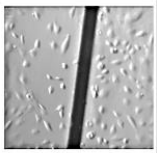 90	 0	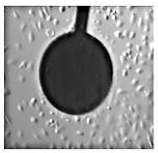 87	 1
2000 min ***Number of live cells***	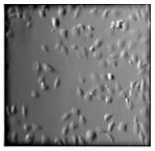 118	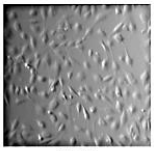 157	 132	 17	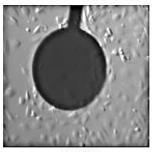 108	 15
4000 min ***Number of live cells***	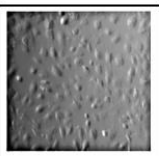 278	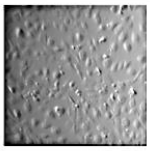 257	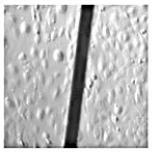 194	 29	 188	 59

Table 5: Microscopic images and number of live cells at the different timepoints for each position.

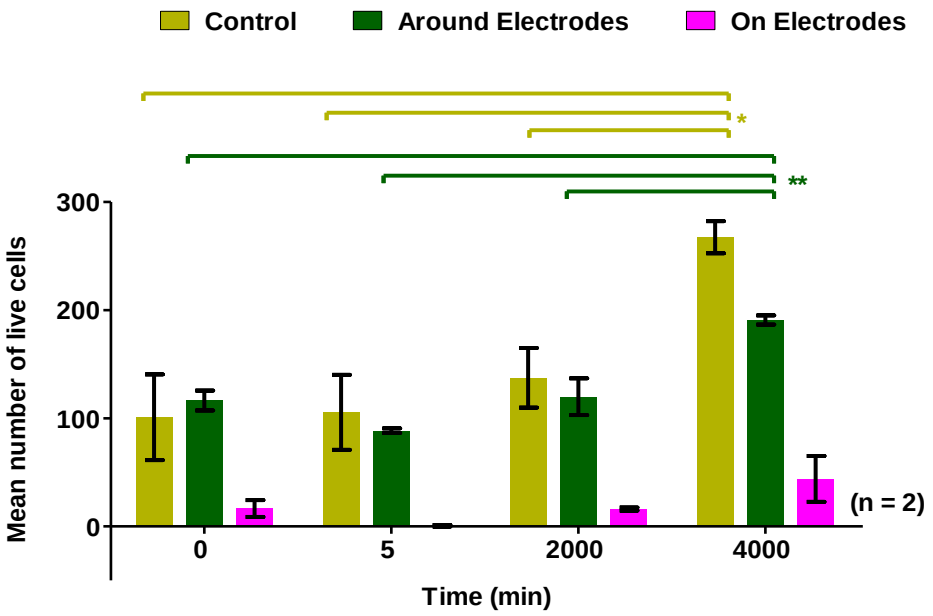

Figure 68: Mean number of live cells at control positions, around the electrodes and on the electrodes.

The number of live cells at each position was manually counted. The mean number of live cell at the control positions were 101, 105, 137 and 267 at 0, 5, 2000 and 4000 min respectively. This appeared to indicate gradual increase in number of live cells. The increase from 0 min to 5 min and 5 min to 2000 min were not statistically significant. The increase from 2000 min to 4000 min was statistically significant ($p < 0.05$).

This was due to a high rate of cell proliferation during this time period, as indicated by images in Table 5 for positions 1 and 2. The mean number of live cell at the positions around the electrodes were 116, 88, 120 and 191 at 0, 5, 2000 and 4000 min respectively. There was a decrease in live cell number from 0 min to 5 min, due to the application of voltage to the electrodes. This implies that cells in close proximity to the electrodes could be affected by the voltage applied. However, the decrease was not statistically significant, due to the low number of technical replicates (n = 2).

There was a statistically significant ($p < 0.01$) increase from 2000 min to 4000 min. The DC voltage applied only had a short term effect on the cells around the electrodes, leading to a decrease in number of live cells from 0 min to 5 min. From 5 min to 2000 min and to 4000 min, the number of live cells increased in a similar way to the control positions.

The mean number of live cell at the positions on the electrodes were 16, 1, 16 and 44 at 0, 5, 2000 and 4000 min respectively. There was a decrease in number of live cells from 16 cells at 0 min to 0 cells at 5 min. This was due to cell death of cells adhering to the electrodes upon application of the DC voltage. The cells went from spindle shaped to flattened. The mean number of cells went back to 16 at 2000 min and then to 44 at 4000 min.

These increases were due to cells migrating from around the electrodes onto the electrodes. However, none of the changes in live cell numbers were statistically significant due to the low number of technical replicates ($n = 2$). These results seem to indicate that a DC voltage of 2.5 V for 1 min causes the highest proportion of cell death directly on the electrodes, a lower proportion of cell death adjacent to the electrodes and no cell death further away from the electrodes. However, the monolayer mostly remained unaffected and unaffected cells proliferate and migrate within 4000 min to replace the dead cells.

Hence, DC voltage seemed to have a very localised and temporary effect on the monolayer. It might not be the suitable voltage type that would allow the sensors (acting as therapeutic probes) to intervene on the early smooth muscle cell proliferation at the onset of in-stent restenosis.

5.9 Application of AC voltage to MASMCs monolayers using nIDE with intermittent impedance measurements.

5.9.1 Rationale

The previous sections investigated the effects of DC voltages on MASMCs. This was the simplest type of voltage that could be applied. In this section the effect of AC voltage, which is another type of voltage was investigated. At high enough frequencies, the issue of electrolysis (which occurs with DC voltages) is avoided. Stolwijk, Michaelis and Wegener (2012) applied AC sinusoidal voltages of 5 V and 40 kHz for 30 s to ECIS electrodes in order to induce cell death. Similar parameters were used in the experiments in this section. All impedance sensing was carried out at 10 kHz. Application of invasive voltages was carried out at a frequency of 40 kHz.

5.9.2 Experimental procedure

The experiment was carried out as follows:

- 3 devices containing nIDE (1, 2 and 3) were sterilised (Section 2.7.1).
- 2 mL of media was pipetted into each device, and a baseline impedance reading (culture medium only – **Day 0**) was measured for each device.
- MASMCs were detached from a sub-confluent flask (Section 2.2.2) and 200000 MASMCs were seeded into each device.
- 2 mL of HEPES DMEM media was added to each device.
- The seeded devices were kept in an incubator (37 ^{0}C & 5 % CO_2) for 24 h, to allow the cells to settle down.
- After 24 h, the cells were observed under the microscope to ensure that they had adhered to the bottom and had the characteristic spindle shape.
- Then, another impedance measurement was taken (medium + cells - **Day 1**) for each device.
- After another 24 h, another impedance measurement was taken (medium + proliferated cells - **Day 2**) for each device.
- Immediately after this measurement, the device containing nIDE 1, was connected to the function generator.

- The output impedance was set to the same value as the impedance measurement (medium + proliferated cells). The waveform was set at sine wave, the amplitude at 2 $V_{peak\ to\ peak}$ and the frequency at 40 kHz.
- The AC voltage was applied for 1 min.
- The device was then disconnected from the function generator and the impedance was measured again.
- This was repeated for nIDE 2 and 3.

5.9.3 Results and discussion

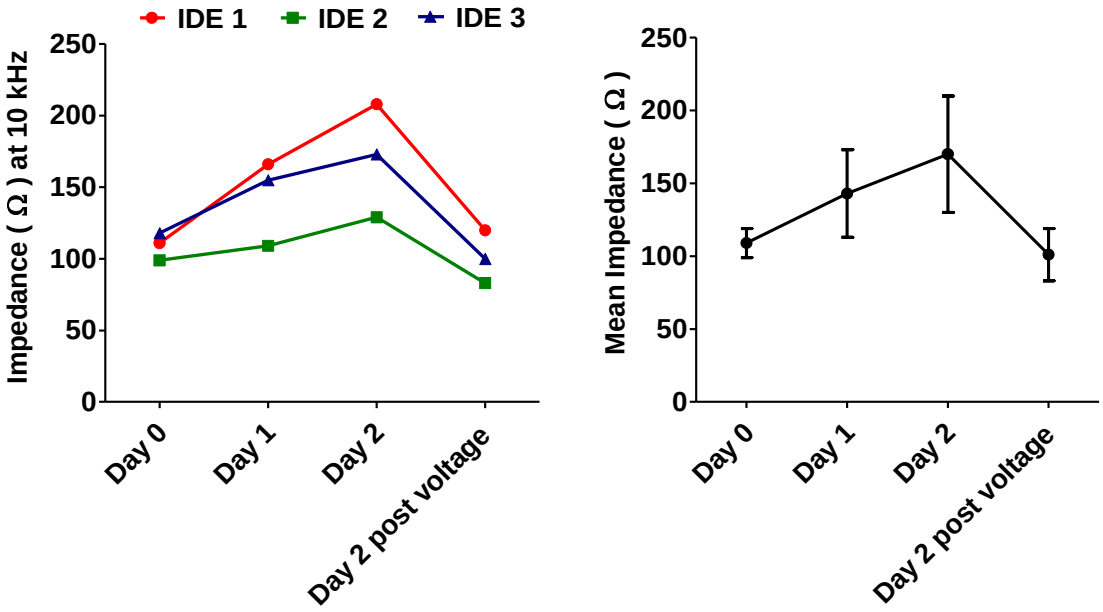

Figure 69: Left panel shows the impedance measurement at 10 kHz for IDE 1, 2 and 3 at the different timepoints. Right panel shows the mean impedance of the 3 device together.

The mean impedance (cell free baseline impedance) at Day 0 was 109 Ω. After cells were seeded and allowed to settle down for 24 h, the mean impedance increased to 143 Ω. The cells were allowed to proliferate for another 24 h and the mean impedance increased to 170 Ω. Immediately after these measurements, the voltage was applied using a function generator. Then impedance measurements were carried out again. The mean impedance dropped by 69 Ω and reached 101 Ω. This was close to the cell free baseline impedance.

These results show that application of an AC voltage of 2 V for 1 min could affect MASMCs. However, it was not clear whether there was only a transient or permanent decrease in impedance. Further measurements after the application of the voltage were required to investigate this effect.

5.10 Application of AC voltage to MASMCs monolayers using nIDE with continuous impedance measurements.

5.10.1 Rationale

In Section 5.5, it was shown that application of an AC voltage of 2 V for 1 min caused a drop in the impedance. However, it was not clear whether this was a transient or permanent drop. If this was a transient effect, it implied that the cells were affected and then recovered. If this was a permanent effect, it would imply that the cells were affected and did not recover.

5.10.2 Hypothesis

The effect of an AC voltage on a MASMC monolayer can be tracked using continuous impedance measurement with nIDE.

5.10.3 Experimental procedure

The experiment was carried out as follows:

- A device containing nIDE was sterilised (Section 2.7.1).
- MASMCs were detached from a sub-confluent flask (Section 2.2.2) and 200000 MASMCs were seeded into the device.
- 2 mL of HEPES DMEM media was added to the device.
- The device was transferred to the live cell microscope stage with warmed enclosure.
- The impedance at 10 kHz was acquired at 15 min intervals.
- At the 20 h timepoint, the device was disconnected from the LCR meter and connected to the function generator.
- A sine voltage of 2 V and 40 kHz was applied for 1 min.
- The LCR meter was then connected again and impedance measurements continued.
- Impedance measurements were acquired up to the 45 h timepoint.

5.10.4 Results and discussion

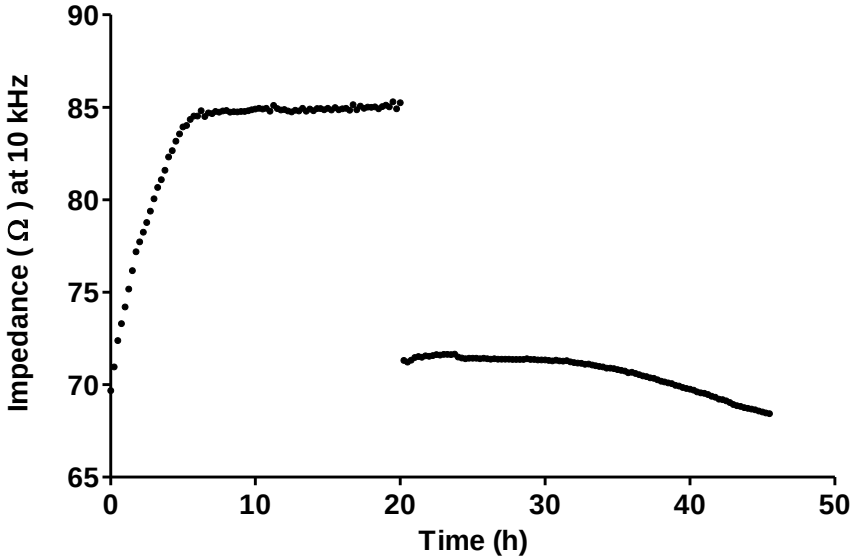

Figure 70: Continuous impedance measurement of 200000 MASMCs settling down for 20 h. At the 20 h timepoint, impedance measurements were paused and an AC sine voltage (2 V and 40 kHz) was applied for 1 min using a function generator (output impedance matched to impedance at 40 kHz at 20 h). Impedance measurement resumed after treatment and acquired up to 45 h.

At 0 h, the impedance (cell free baseline impedance) was 70 Ω. The impedance gradually increased up to the 6 h timepoint and reached a plateau of approximately 85 Ω. This indicated that most of the cells had settled down and adhered to the electrode at that point. At 20 h, the AC voltage was applied, and this caused a sharp drop in the impedance, which reached 71 Ω (which is close to the cell free impedance). The impedance decreased down to 68 Ω at 46 h. This shows that the drop in impedance was permanent, implying that the cells were affected by the voltage and were not able to recover. However, microscopic observations would be required to investigate the morphological effects on the cells.

5.11 Application of AC voltage to MASMCs monolayer using ssIDE with bright field observations only.

5.11.1 Introduction

In this section, the effects of AC voltages on MASMCs monolayers were investigated. Application of an AC voltage to the cell sensors / therapeutic probes might be possible without batteries or capacitors on the proposed smart stent. The cells sensors / therapeutic probes could be powered wirelessly through electromagnetic induction. At high frequencies (kHz to MHz), the AC voltage would not cause electrolysis of blood and would also not cause any damage to the metal electrodes.

5.11.2 Rationale

Planar metal electrodes have been used in previous studies to electroporate cells so that these take up agents such as DNA and drugs. The desired mechanism is reversible electroporation, so that the nanopores created in the membrane seal and cell viability is maintained. However, a side-effect of this mechanism is irreversible electroporation which leads to permanent nanopores in the membrane. Cell viability is thus compromised, leading to cell death. In this experiment this side-effect of electroporation is exploited in order to induce death of MASMCs.

5.11.3 Experimental procedure

The experiment was carried out as follows:

- A device containing ssIDE was sterilised (Section 2.7.1).
- MASMCs were detached from a sub-confluent flask (Section 2.2.2) and 200000 MASMCs were seeded into the device.
- 2 mL of HEPES DMEM media was added to the device.
- The device was transferred to the live cell microscope stage with warmed enclosure.

- MIA timelapse of the ssIDE was acquired at 15 min intervals.
- The impedance at 10 kHz was simultaneously acquired at 15 min intervals.
- At the 20 h timepoint, the device was disconnected from the LCR meter and connected to the function generator.
- A sine voltage of 2 $V_{peak\ to\ peak}$ and 40 kHz was applied for 1 min.
- The LCR meter was then connected again and impedance measurements continued.
- Timelapse images and impedance measurements were acquired up to the 70 h timepoint.

5.11.4 Results and discussion

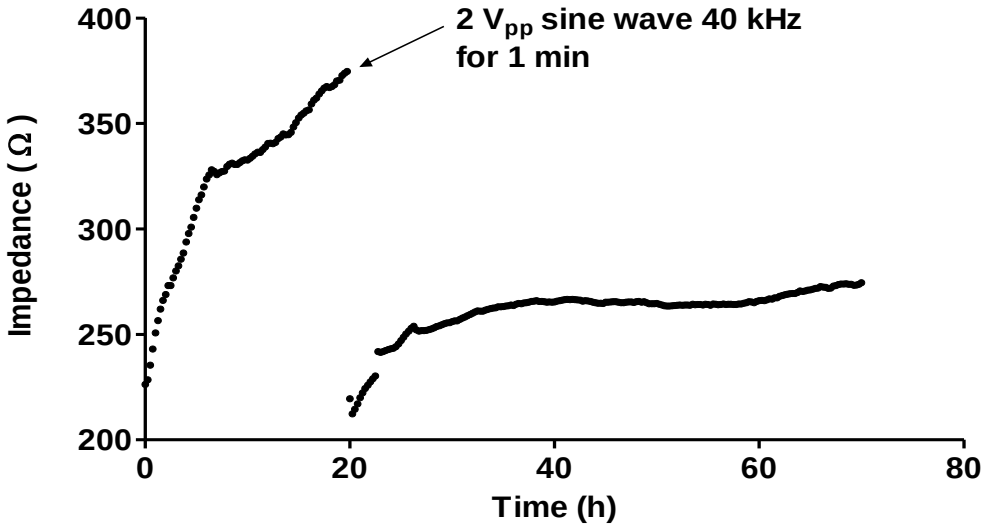

Figure 71: Impedance measurements of ssIDE with MASMCs carried out for 70 h with voltage applied at 20 h to induce cell death.

MASMCs are adherent cells, with a characteristic spindle shape, but they are spherical, following trypsinisation. On the MIA (Multiple Image Acquisition), at time 0 h (just after cell seeding), the MASMCs were spherical and distributed inside and around the electrode area. At that point, all the cells were in suspension and the cell free (baseline) impedance was 226 Ω. At 10 h, most of the cells had adhered to the bottom (glass + electrodes) and the impedance increased to 332 Ω (as a result of cell adherence to the electrodes).

At 20 h, most of the cells had fully adhered and the impedance further increased to 374 Ω. Immediately after this impedance reading, the LCR meter was disconnected and function generator connected in order to apply a sine voltage of 2 $V_{peak\ to\ peak}$ and 40 kHz for 1 min. The LCR meter was then reconnected and the post-voltage impedance was measured. The impedance dropped by 154 Ω and reached 220 Ω.

Time (h) **Impedance (Ω)** **Condition**	**Image**
0 h 226 Ω MASMCs suspended within and around ssIDE	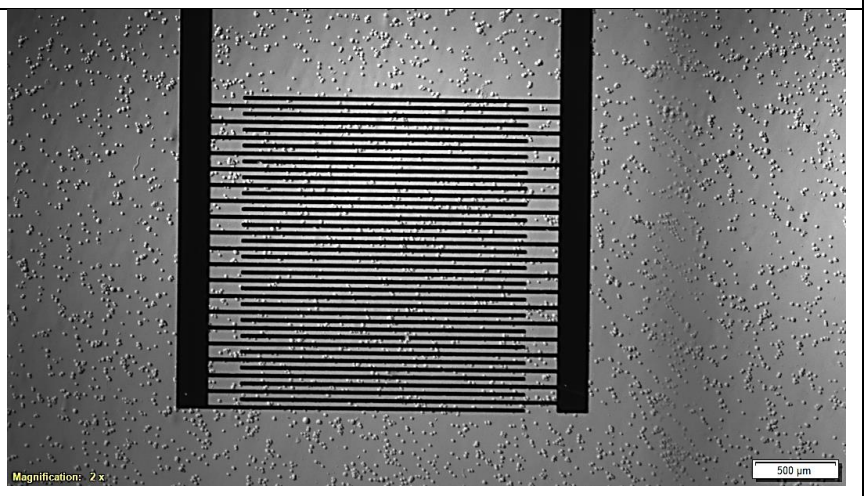
10 h 332 Ω MASMCs settled down and adhered onto and around ssIDE	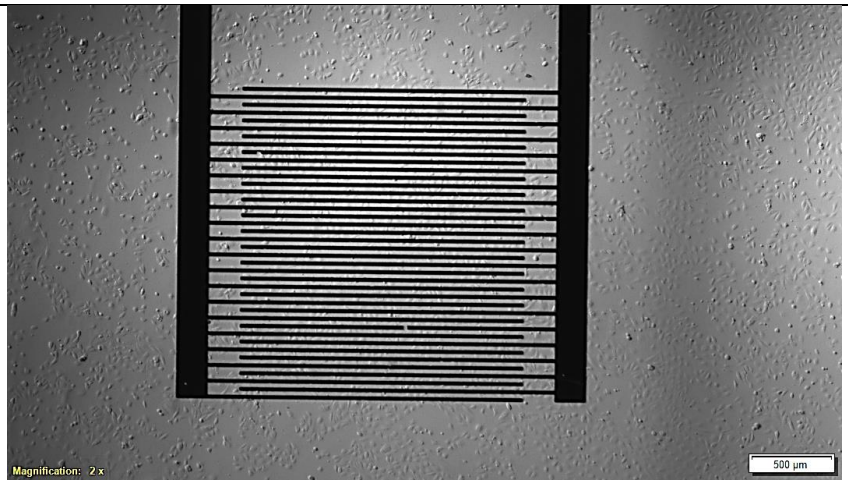

20 h **(pre-voltage application)** 374 Ω	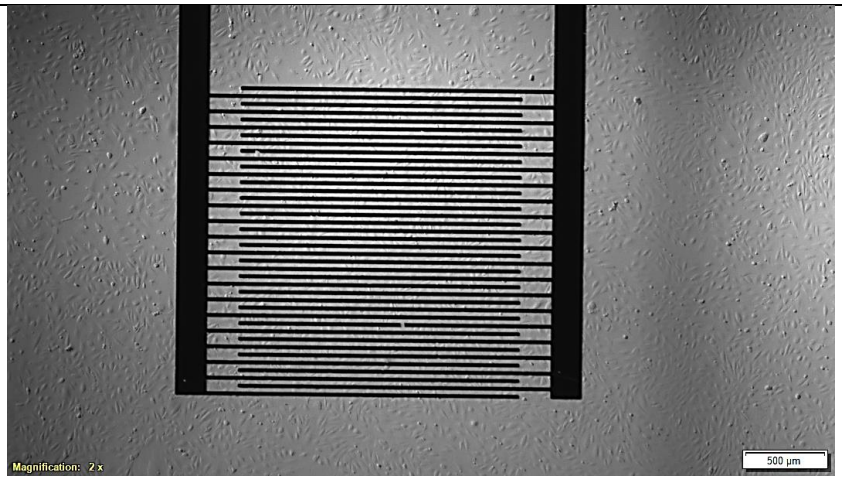
20 h **(post-voltage application)** 220 Ω	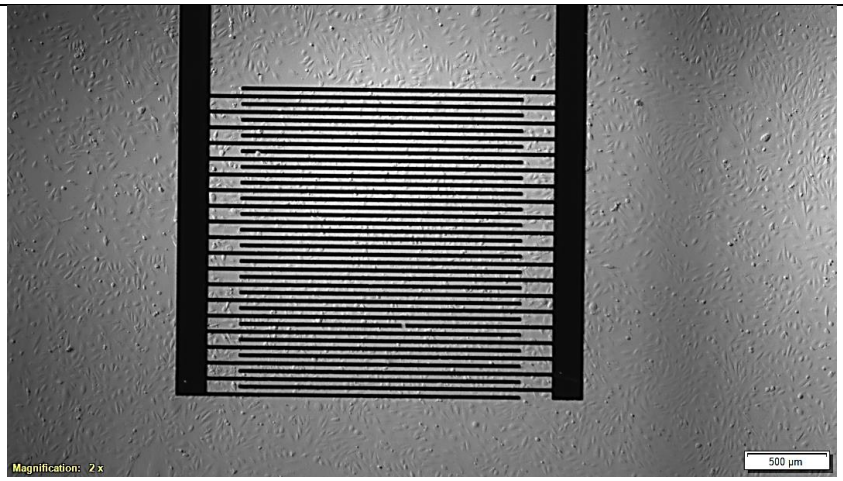
35 h 263 Ω Cell monolayer 15 h after application of voltage	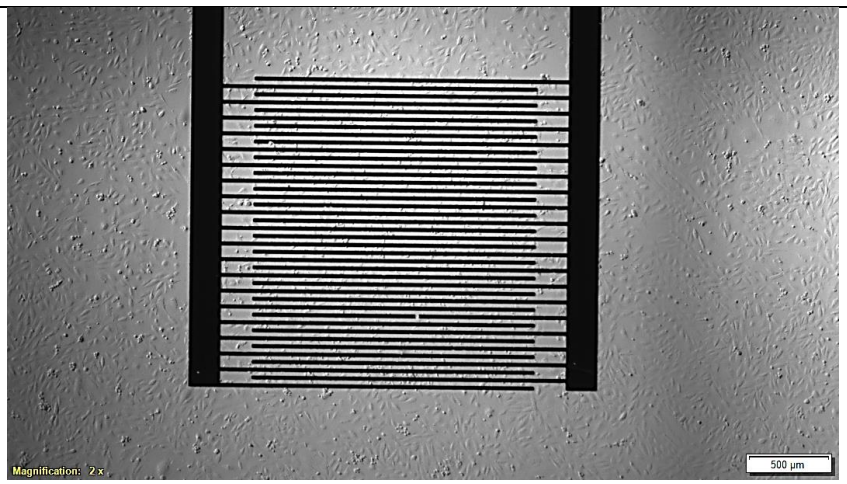

70 h 274 Ω Cell monolayer 50 h after application of voltage	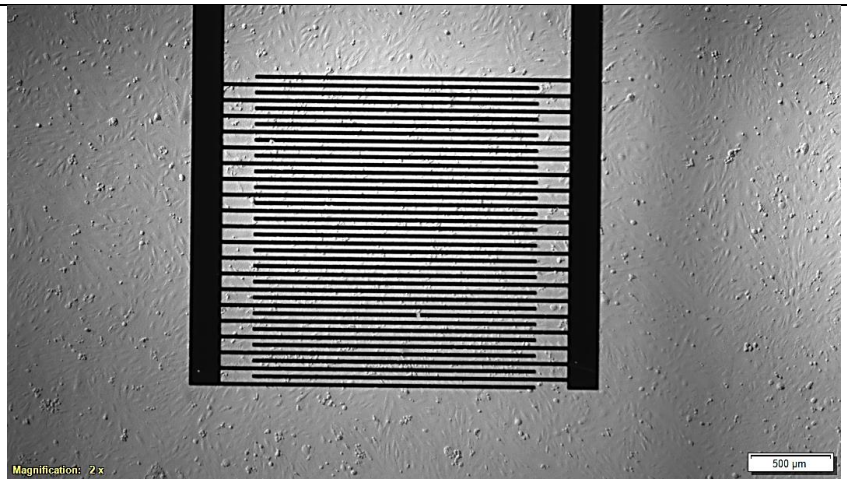

Table 6: MIA showing cells within and around ssIDE at different timepoints with corresponding impedance readings and conditions.

There were no observable microscopic changes between the pre-voltage MIA and the post voltage MIA. This was partly because the magnification was low (2x). 15 h and 50 h (35 h and 70 h timepoints) after the application of voltage, the impedance increased to 263 Ω and 274 Ω respectively. This indicated that some of the cells affected by the voltage were able to recover. Another possibility was that cells around the electrodes that were not affected by the voltage proliferated and covered parts of the electrodes again. Even though the impedance increased from 219 Ω to 274 Ω post-voltage, it did not reach the pre-voltage maximum impedance of 332 Ω even 50 h post-voltage.

This implied that the voltage applied permanently affected the monolayer within the electrode area, even though this could not be confirmed microscopically. The monolayer around the electrode area was healthy at 50 h as most of the cells had the characteristic spindle shape of MASMCs. Hence, in a similar way to application of DC voltage through PEs, an AC voltage on the ssIDE had a very localised effect on a MASMCs monolayer. With the ssIDE, the effect was restricted to the electrode area, that is to the area between the ssIDE fingers.

5.12 Apoptosis detection using Apoptosis / Necrosis Assay Kit

5.12.1 Rationale

The purpose of this section was to test an Apoptosis/ Necrosis Assay Kit (ab176749) commercialised by Abcam (UK) for detection of live, apoptotic and necrotic MASMCs. Once tested, the kit would then be used to determine the type of cell death triggered by applying AC voltages to MASMCs through the ssIDE.

5.12.2 Introduction

The kit used in the following experiments was a mixture of 3 dyes: Apopxin Green, which fluoresces green for apoptosis detection, 7-AAD, which fluoresces red for necrosis detection and CytoCalcein Violet, which fluoresces blue for live cell detection.

5.12.3 Experimental procedure

The experiment was carried out as follows:

- MASMCs were detached from a sub-confluent flask (Section 2.2.2) and 100000 MASMCs were seeded into each well of a 2-well slide chamber (Nunc® Lab-Tek® II Chamber Slide – Sigma Aldrich – UK).
- 2 mL of Phenol-red-free HEPES DMEM media was pipetted into each well.
- The cells were allowed to settle down and adhere to the bottom of the chamber for 18 h, in an incubator kept at 37 ^{0}C.
- Once settled down, the cells were washed twice with Serum-free Phenol-red-free HEPES DMEM media.
- The Apoptosis / Necrosis Assay Kit was prepared according to the manufacturer's instructions.
- A working concentration staining solution was prepared by pipetting 10 µL of each of the 3 dyes into 1 mL of Serum-free Phenol-red-free HEPES DMEM media.

- 500 µL of the working solution was pipetted into each well and the dyes were allowed to incubate for 1 h.
- Then, the cells were washed twice with Phenol-red-free HEPES DMEM media.
- 2 mL of Phenol-red-free HEPES DMEM media was pipetted into each well.
- The slide chamber was transferred to the microscope stage with heated enclosure.
- A multiposition timelapse imaging including bright field, DAPI, FITC and Texas Red channels was started and images were acquired at 10 min intervals.
- There was an observation period of 1 h.
- At the 1 h timepoint, 50 µM etoposide was added to the treatment well, while DMSO was added to the control well.
- Timelapse images were acquired up to the 28 h timepoint.

5.12.4 Results and discussion

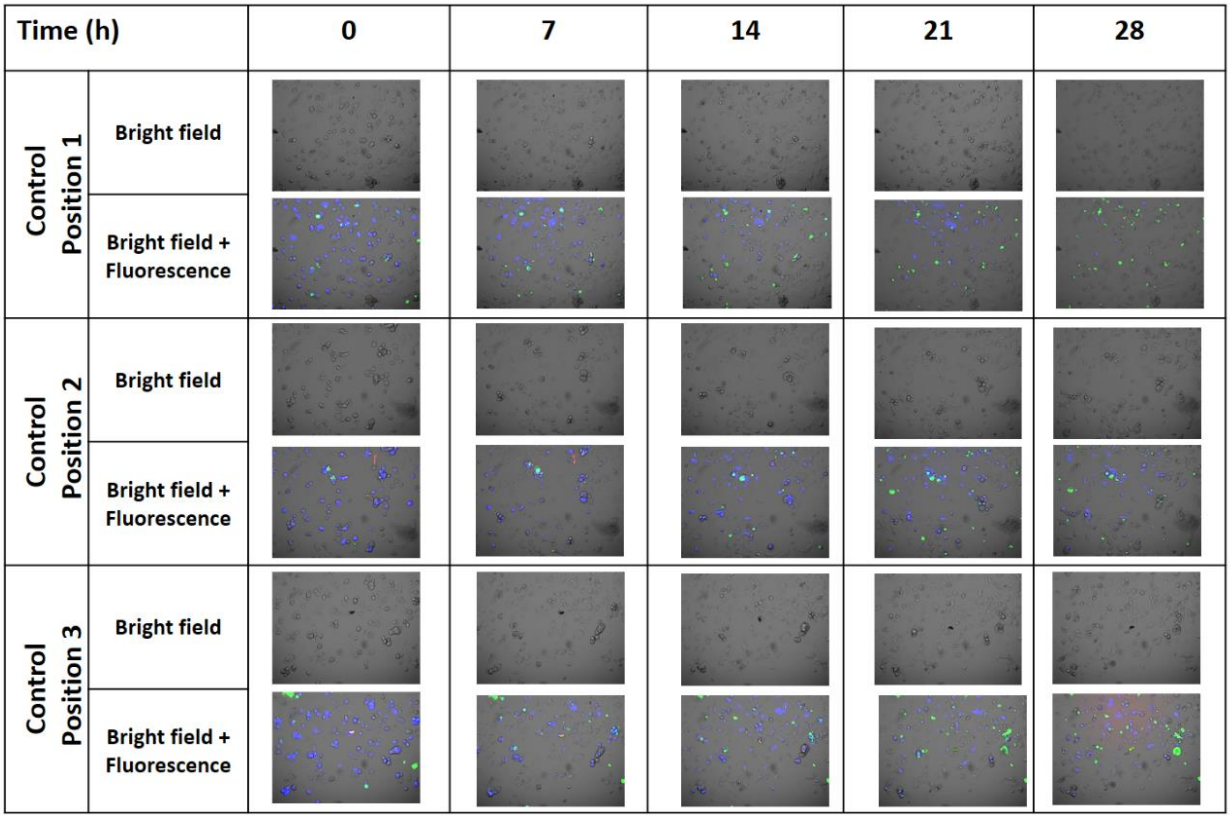

Table 7: Bright only and Bright field + fluorescent images of MASMCs without treatment. Staining was carried out using Apoptosis / Necrosis Assay Kit.

Time (h)		0	7	14	21	28
Treatment Position 1	Bright field	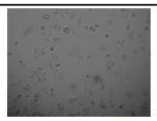	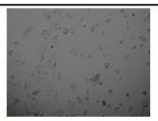	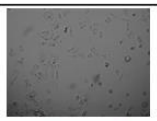	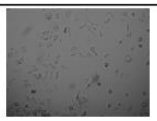	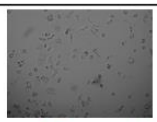
	Bright field + Fluorescence	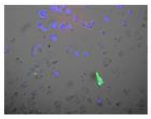	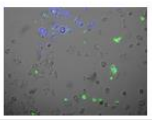	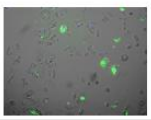	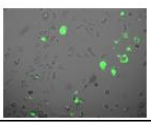	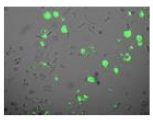
Treatment Position 2	Bright field	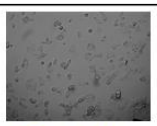	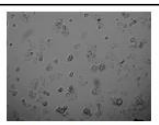	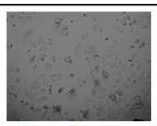	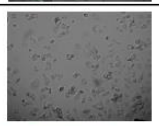	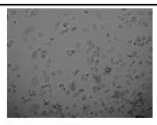
	Bright field + Fluorescence	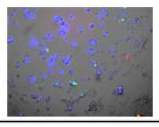	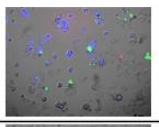	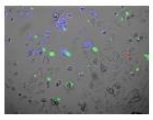	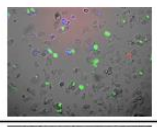	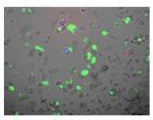
Treatment Position 3	Bright field		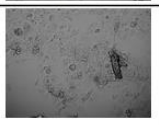	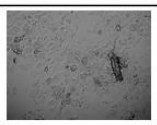	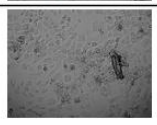	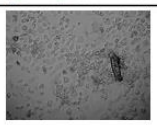
	Bright field + Fluorescence	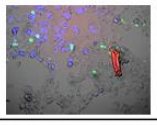	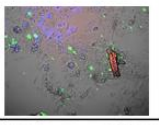	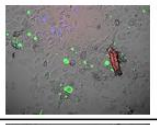	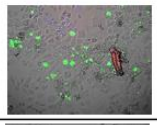	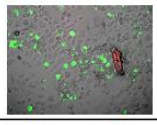
Treatment position 4	Bright field	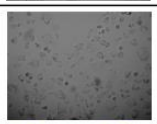	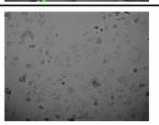	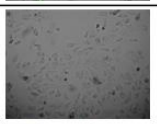	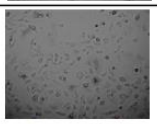	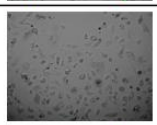
	Bright field + Fluorescence	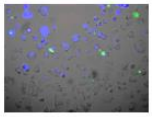	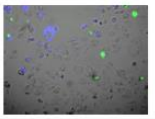	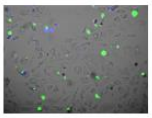	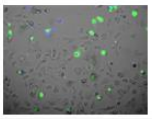	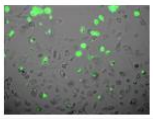

Table 8: Bright only and Bright field + fluorescent images of MASMCs treated with 50 µM etoposide. Staining was carried out using Apoptosis/ Necrosis Assay Kit.

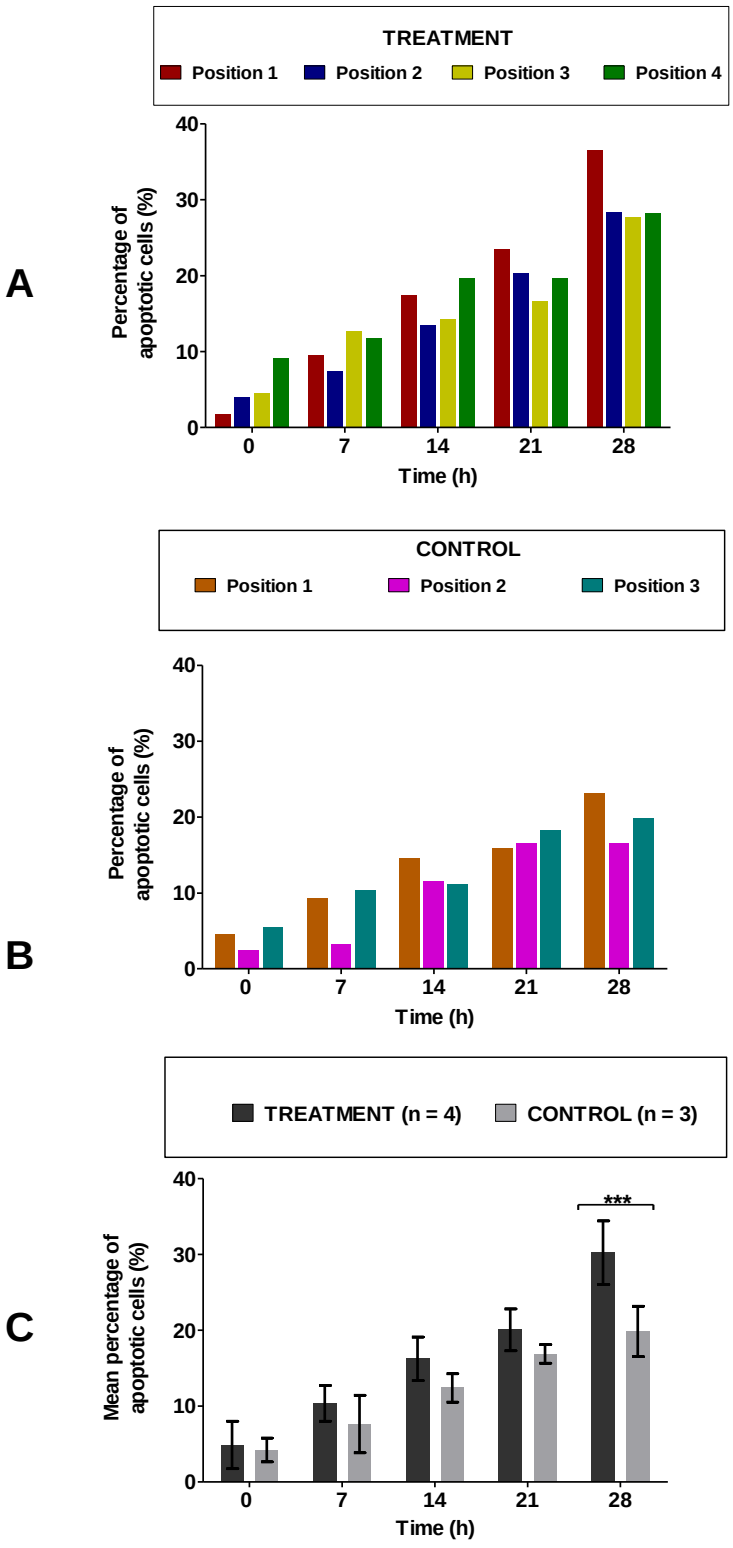

Figure 72: (A) Percentage of apoptotic cells at the different positions at different timepoints for the treatment well. (B) Percentage of apoptotic cells at the different timepoints for the control well. (C) Mean percentage of apoptotic cells at the different timepoints for treatment and control wells. Two-way ANOVA with Bonferroni post-test showed the mean percentage of apoptotic cells for the treatment well and control well were not statistically different at 0 h, 7 h, 14 h and 21 h. However, at 28 h the difference was statistically significant ($p < 0.001$).

Figure 72C shows that the mean percentages of apoptotic cells were always higher at the treatment positions compared to the control positions. However, two-way ANOVA showed that the percentages were not statistically different from the 0 h to 21 h timepoints. At 28 h, the percentages were statistically different ($p < 0.001$). Etoposide is an antineoplastic drug which causes DNA damage, leading to apoptosis (Mizumoto, Rothman and Farber, 1994). It is associated with delayed onset of apoptosis. Hence, the results were consistent with the fact that etoposide caused a delayed onset of apoptosis, which was manifested as a statistically significant increase in percentage of apoptotic cells at 28 h.

The aim of this experiment was to ensure that the Apoptosis / Necrosis kit was staining the cells undergoing apoptosis green (Apopxin Green) and the cells undergoing necrosis red (7-AAD). Due to a missing Bright Field shutter on the live cell microscope, the Bright Field illumination had to be kept on throughout the experiment. 7-AAD stained the nucleus only, and had a weak fluorescence. Due to the strong Bright Field background on the images, it was not possible to distinguish red fluorescence. Apopxin green is a plasma membrane stain, with a strong fluorescent signal. It was thus possible to distinguish the green fluorescence despite the strong Bright Field background.

Etoposide causes a delayed increase in apoptosis. In the experiment, higher percentages of green cells were observed in the treatment etoposide well (Table 8) compared to the control DMSO well (Table 7). Hence, the results suggested that the Apoptosis / Necrosis kit was reliable at staining cells undergoing apoptosis. It was not clear whether, cells undergoing necrosis were stained red.

5.13 Application of AC voltage to MASMCs monolayer using ssIDE with bright field and fluorescent observations.

5.13.1 Rationale

The aim of the following experiment was to induce cell death using ssIDE and also to determine whether cell death was occurring due to necrosis or apoptosis. It was hypothesised that the same electrodes used for cell sensing on the future smart stent could be used for inducing death of cells. Ideally, death of smooth muscle cells only would be induced, allowing endothelial cells to cover the stent struts and sensors. It would be preferable to induce death by apoptosis, as this is a more controlled form of cell death, without any inflammatory reactions. Necrosis, on the other hand, is accompanied by inflammatory reactions. In the following experiment, a specific voltage was used to induce death of MASMCs and the type of cell death induced was investigated.

5.13.2 Experimental procedure

The experiment was carried out as follows:

- A device containing ssIDE was sterilised (Section 2.7.1).
- MASMCs were detached from a sub-confluent flask (Section 2.2.2) and 200000 MASMCs were seeded into the device.
- 2 mL of HEPES DMEM media was added to the device.
- The device was transferred to the live cell microscope stage with warmed enclosure.
- The impedance at 10 kHz was acquired at 15 min intervals.
- At the 22 h timepoint, impedance measurements were stopped.
- The device was transferred to a cell culture hood.
- A positive control was carried out by using a hypodermic needle to make round scratches at 3 positions outside the electrode area.
- The culture media was pipetted out, the monolayer was then washed twice with phenol-red-free serum-free HEPES DMEM.
- 500 µL of the staining solution was prepared according to the manufacturer's instruction using phenol-red-free serum-free HEPES DMEM.

- This was then pipetted onto the monolayer and the dyes were allowed to incubate for 1 h.
- After this, the staining solution was pipetted out, and the monolayer was washed with phenol-red-free DMEM.
- 2 mL of phenol-red-free DMEM was then pipetted into the device.
- The device was transferred to the live cell microscope.
- Fluorescent timelapse imaging and impedance measurements were acquired simultaneously at 10 min intervals and acquired up to the 49 h timepoint.
- The cells were observed for 8 h (from 24 h timepoint to 32 h timepoint) to ensure that the dyes were not causing cell death.
- At 32 h, sine voltage of 2 $V_{peak\ to\ peak}$ and 40 kHz was applied for 1 min.
- At 49 h, the device was transferred to a cell culture hood.
- The media was pipetted out and the monolayer was washed twice with phenol-red-free serum-free HEPES DMEM.
- 500 µL of freshly made staining solution was then pipetted onto the cells and this was allowed to incubate for 1 h.
- A final bright field image and fluorescent image for each position was then acquired.

5.13.3 Results and discussion

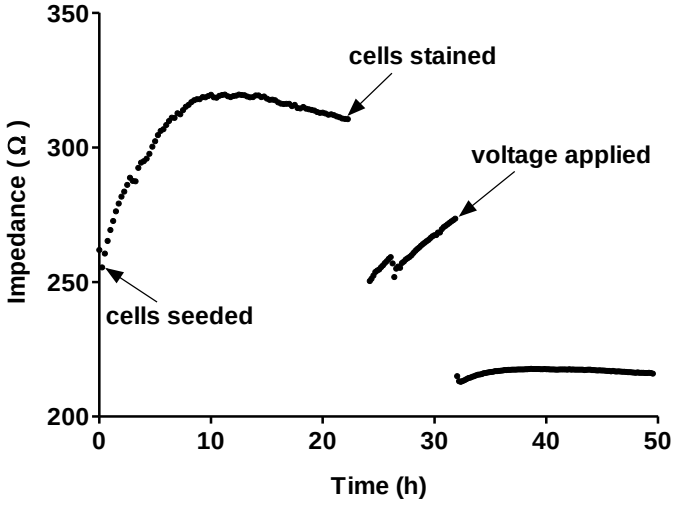

Figure 73: Impedance measurement for the whole experiment showing an initial impedance immediately post-seeding, during cell adherence, post-staining and post-voltage

Figure 73 shows the impedance readings up to the 49 h timepoint. The readings were started just after cells were seeded into the device (0 h). The impedance was 261 Ω at that point. The cells were not adherent at the start, as they had just been detached from a sub-confluent flask. As the cells started to attach, the impedance gradually increased and reached a maximum of 319 Ω at 10 h. The impedance slightly decreased to 310 Ω at 22 h. This could be attributable to a depletion of nutrients from the media, causing the cells to detach slightly from the electrodes.

At 22 h, the impedance measurements were stopped and the staining step was carried out. The impedance measurements were resumed at 24 h and acquired at 10 min intervals (instead of 15 min) to increase the time resolution of the measurements. The staining solution caused the cells to detach slightly from the electrodes, as indicated by a drop in impedance to 250 Ω at 24 h. The cells were allowed to reattach to the electrodes until 32 h, where an impedance of 273 Ω was reached. The voltage was applied at that point, causing an immediate drop in impedance to 215 Ω. The impedance stayed relatively constant from this point and was 215 at 49 h. The application of the voltage could have caused ions from the cells to be released into the culture medium. This could have caused a decrease in impedance, which went lower than the initial cell free baseline.

Figure 74 shows the bright field and fluorescent images acquired at different timepoints of the experiment. The negative control images were acquired at positions outside the electrode area. These positions were not affected by the voltage applied at any point of this experiment. The positive control images were acquired at a position outside the electrode area, where a round scratch had been made. The treatment images were acquired at positions within the electrode area. The initial total number of cells visible were counted for the 1st fluorescent image at (T = 24 h FLUO) for each position. The number of live cells (stained blue), apoptotic cells (stained **green only** or **green + red**) and necrotic cells (stained **red only**) were also counted. The percentages of live, apoptotic and necrotic cells were expressed as a percentage of total number of cells. The number of live, apoptotic and necrotic cells were counted at 32 h (pre-voltage), 32 h (post-voltage), 49 h and 50 h. The live, apoptotic and necrotic cell counts were then expressed as a percentage of the initial total number of cells (Figure 75).

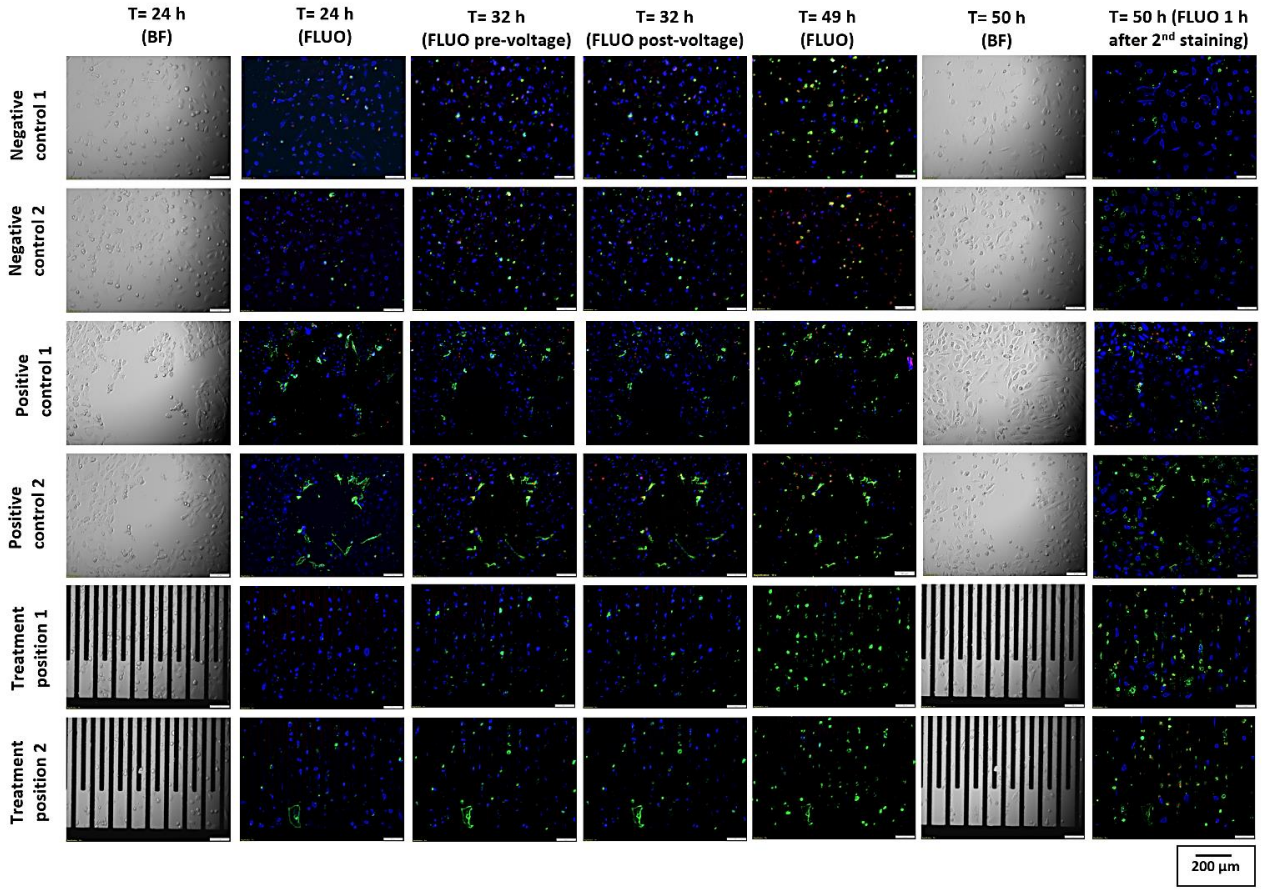

Figure 74: MASMCs under bright field and fluorescent imaging at timepoints 24 h, 32 h (pre-voltage), 32 h (post-voltage), 49 h and 50 h. Cells imaged for negative controls were outside the electrode area and were thus not affected by application of voltage. Cells imaged for the positive control were also outside electrode area and thus not affected by voltage. The physical treatment applied to these cells was a round scratch. Cells imaged for the treatment positions were within the electrode area and were thus affected by the application of voltage.

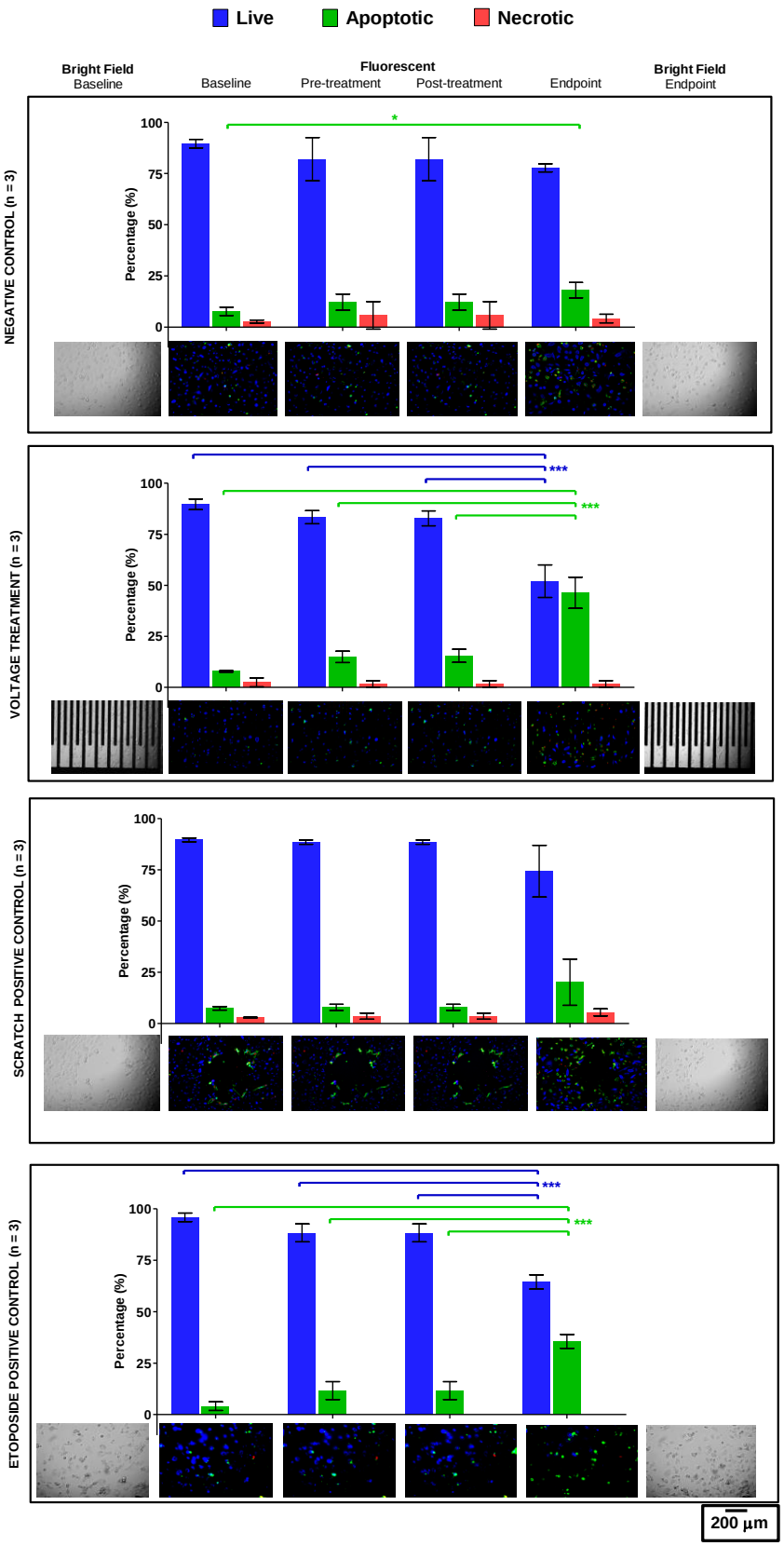

Figure 75: Mean percentage live, apoptotic and necrotic cells for negative control, treatment and positive control with corresponding micrographs. Also included for comparison is the one etoposide positive control from Section 5.11.

Figure 75 shows the mean percentages of live, apoptotic and necrotic cells for the negative control, voltage treatment, scratch positive control and etoposide positive control (from Section 5.11 for comparison). The negative control, voltage treatment and scratch positive control were carried out as part of the same experiment, while the etoposide positive control was carried out as part of a separate experiment. For the etoposide positive control, the live cell percentage was based on the **Bright Field & blue** fluorescence while the apoptotic cell percentage was based on the **green** fluorescence. For the negative control, voltage treatment and scratch positive control, the live cell percentage was based on the **blue** fluorescence, apoptotic percentage was based on the **green** fluorescence and necrotic percentage was based on the **red** fluorescence.

The percentages were compared using One-way ANOVA with Tukey's Multiple Comparison Test. For the negative control, the percentage of apoptotic cells at the endpoint was statistically different ($p < 0.05$) from the baseline, implying that there was a small "physiological" increase in apoptosis from 8 % to 18 %. For the voltage treatment and the etoposide positive control, the percentages of live cells and apoptotic cells at endpoint were statistically different ($p < 0.001$ and $p < 0.001$, respectively) from the percentages at baseline, pre-treatment and post-treatment. This implies that the induction of apoptosis using 2 V sine wave for 1 min had similar effects to 50 μM for 24 h. The percentage of apoptosis induced by the voltage was higher (46 % vs 36 %) compared to etoposide. Hence, a short pulse of voltage could induce a higher percentage apoptosis in a MASMC monolayer compared to a prolonged exposure to etoposide.

5.14 Summary and discussion

Interdigitated electrodes (IDE) can be used to monitor adherence, growth and death of cells both intermittently (e.g. at 24 h intervals) (Figure 62) or continuously (e.g. 15 min intervals) (Figure 63). This implied that IDE could be used to monitor the general health of cells adhering to the electrodes and could thus be used to assess the effects of different treatment in a similar way to Campbell *et al.* (2007) (Figure 21). They tested the effects of different titres of IHNV (infectious hematopoietic necrosis virus) on carp EPC (*Epithelioma papulosum cyprini).* The control well showed a gradual increase in impedance over a 500 h period, indicating cell proliferation. In the control wells, the impedance increased (indicating initial cell proliferation), reached a peak then decreased back to the baseline value (indicating gradual cell death). The higher the concentration of the virus, the faster cell death occurred. Thus, the impedance readings allowed the efficiency of the treatments to be investigated.

We hypothesised that the fabricated electrodes could be used to both monitor health of a MASMC monolayer and induce cell death. The LCR meter would be used to measure impedance using a low current (approximately 10 μA) and low voltage (mV range) and a function generator would be used to apply invasive voltages to induce cell death.

Stolwijk, Michaelis and Wegener (2012) used ECIS 8W1E electrodes (Figure 18a) to apply invasive voltages to Normal Rat Kidney (NRK) cells and induce cell death (Figure 22). They applied an AC sinusoidal voltage of 5 V and 40 kHz for 30 s. We first attempted to apply invasive voltages to MASMC monolayer using the Pendulum Electrodes (PE) as these had a similar large-counter-electrode v/s small-working-electrode configuration (even though our electrodes had larger surface area). A DC voltage of 2.5 V was used rather than an AC voltage of 5.0 V. This produced a reproducible tearing effect on the cell monolayer. Initial experiments with DC voltages on IDE showed that the electrode could be damaged due to electrolysis. Hence only AC voltages were used with the IDE.

Application of an AC voltage of 2 V and 40 kHz for 1 min caused a sharp drop in impedance, back to the baseline (Figure 70 & 71). Moreover, the impedance stayed close to the baseline for at least 25 h after application of voltage. This implied that the effect induced was permanent rather than transient.

Stolwijk, Michaelis and Wegener (2012) studied the effect of applying sinusoidal voltage 5 V and 40 kHz for 30 s on Normal Rat Kidney (NRK) cells using Ethidium Homodimer and Calcein AM. They concluded that the applied voltage induced necrosis of the cells on the electrodes. In order to optimise the Interdigitated Electrodes (IDE) as therapeutic probes, it was important that they induced apoptosis (controlled cell death) rather than necrosis (associated with inflammation). We used a commercial Apoptosis / Necrosis assay kit to determine the type of cell death induced by application of 2 V 40 kHz for 1 min using the IDE. Results in Figure 75 (Second panel) showed that the applied induced a higher percentage of apoptosis compared to necrosis. This is a promising result showing that the IDE could potentially be used *in vivo* to induce apoptosis of smooth muscle cells at an early stage before they lead to in-stent restenosis.

CHAPTER 6

TESTING INTERDIGITATED ELECTRODES UNDER MORE PHYSIOLOGICAL CONDITIONS

6.1 Rationale

In the previous chapters, continuous impedance measurements were used to track adherence of MASMCs and endothelial cells onto the nIDE and ssIDE. Both cells types are adherent and thus needed to be trypsinised before seeding into the devices. When in suspension, these cells were spherical. Once seeded, the cells gradually sank towards the bottom of the well due to gravity and when they reached the bottom (made up of glass and gold electrodes), they adhered, flattened and spread. This could be detected as a gradual increase in the impedance, as the cells started to adhere to the electrodes. When most of the cells had adhered, the impedance reached a plateau phase. This model was thus appropriate for simulating cells moving from blood and attaching onto the stent.

In order to simulate regrowth of vascular cells over the cell sensors under more physiological conditions, a cell chamber allowing flow of culture medium had to be fabricated. This was referred to as a flow device and incorporated a microfluidic channel with a volume of 200 µL (Figure 76).

A flow circuit also had to be fabricated (Section 2.8), and this consisted of silicone tubing, a culture medium reservoir (with carbogen supply for buffering the culture medium) and a peristaltic pump. The pump generated a pulsatile flow, mimicking the pulsatile flow in arteries. Due to the flow, the cells were subjected to shear stress similar to physiological conditions inside blood vessels. The flow rate was set at a minimum value of 5 mL / min, and based on the conversion table from Ibidi GmbH (2016), this generated a shear stress of approximately 1.2 dyn / cm^2. This is within the shear stress range (0.5 to 10 dyn / cm^2) experienced by rat endothelial cells within arteries (Morin *et al.*, 2003). Moreover, studies using human umbilical vein endothelial cells showed that at the cells aligned to flow for shear stresses in the range 1.7 to 4.7 dyn /cm^2 (McCracken *et al.*, 2013).

6.2 Flow devices

There were 2 types flow devices fabricated, one enclosing a nIDE and one enclosing a set of 3 ssIDEs. For the nIDE flow device, the width of the nIDE was larger than the width of the channel, and thus only part of the fingers were exposed to culture medium and cells within the channel.

For the ssIDE flow device, preliminary electrical testing showed that only the middle ssIDE was functioning properly, and thus the other 2 ssIDEs could not be used.

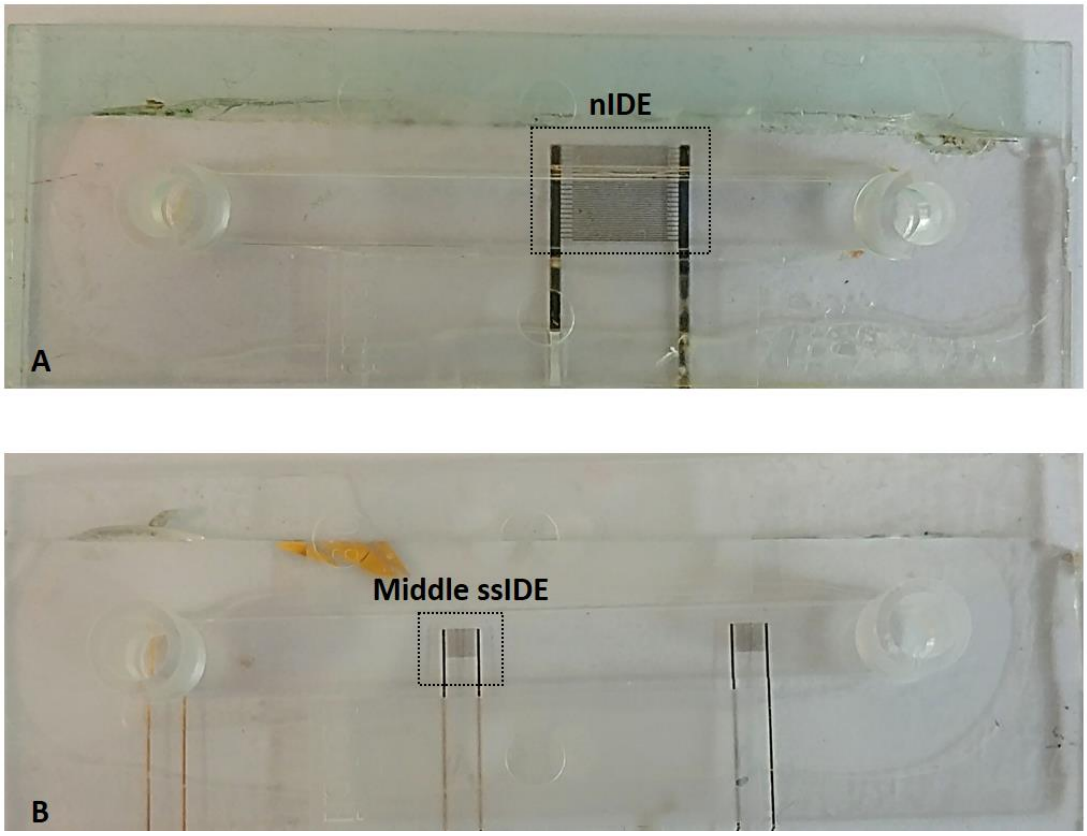

Figure 76: (A) Flow device with nIDE. Only part of the nIDE was exposed inside the microfluidic channel. (B) Flow device with 3 sets of ssIDE. Only the middle ssIDE was functioning properly.

During the PCI stent deployment procedure in humans, the expansion of the stent damages the endothelium, leading to an area void of endothelial cells. As a healing response, endothelial cells migrate from the undamaged portion of the artery towards the damaged portion of the artery. The purpose of the cell sensing system of the smart stent is to monitor regrowth of endothelial cells (normal healing response) or smooth muscle cells (restenotic response) onto the stent.

To simulate the condition of the artery following stent implantation, endothelial cells were seeded into only a fraction of the channel: the portion with the cells simulated the undamaged endothelium and the portion without cells simulated the damaged endothelium.

The seeding was carried out so that the electrode was in the cell free portion of the channel. The flow could also be potentially used to enhance migration of the endothelial cells, thus simulating conditions inside a blood vessel.

6.3 Replicates

For most of this chapter, the experiments presented are drawn from a single biological replicate. Several technical replicates were attempted and required to ensure that the endothelial cells adhered and proliferated inside the microfluidic channel. Once the experiment model worked, the experimental emphasis was to improve the design of the flow device model rather than repeat with additional biological replicates.

6.4 Culture medium flow

In some of the experiments, the microfluidic channel was only partially seeded with cells. There were thus 2 possible scenarios for the circulation of culture medium within the channel. The first scenario was when the culture medium travelled from the *cell monolayer* towards the *electrodes + cell-free portion* of the channel (Figure 77 Top panel). This was referred to as FLOW. The second scenario was when the culture medium travelled from the *electrodes + cell-free portion* of the channel towards the *cell monolayer* (Figure 77 Bottom panel). This was referred to as COUNTERFLOW.

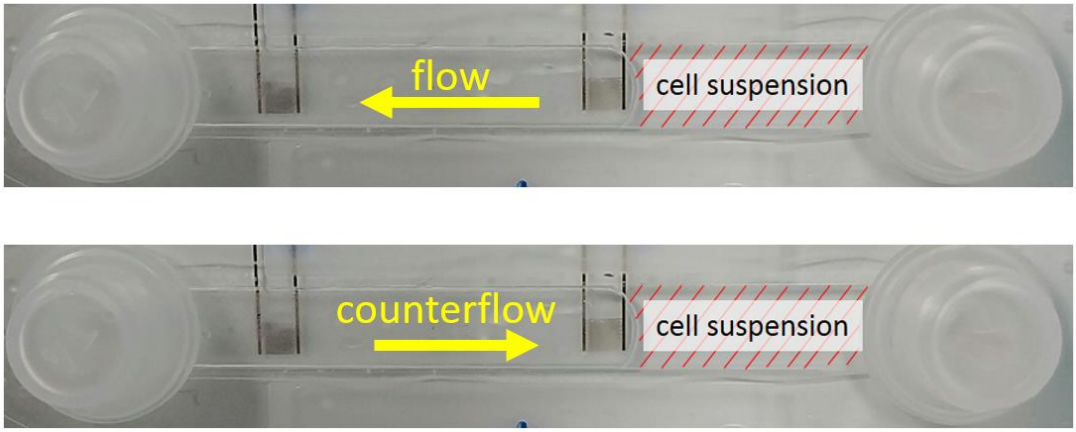

Figure 77: Flow and counterflow of culture medium when the channel was partially seeded with cells.

6.5 Effects of culture medium flow, temperature changes and pH changes on impedance of IDE under flow conditions

6.5.1 Rationale

As a new setup was required for the forthcoming experiments, the effects of pH changes, temperature changes and culture medium flow needed to be investigated to ensure that they have a minimal effect on the impedance.

6.5.2 Hypothesis

Culture medium flow, temperature changes and pH changes do not change the baseline impedance of the flow device.

6.5.3 Experimental setup

The experiment was carried out as follows:

- The flow device (microfluidic channel + 2 reservoirs) was filled with DMEM.

- The flow circuit was also set up using DMEM (Section 2.8) and connected to the flow device.
- The flow circuit and device were placed inside the microscope enclosure. The tubing was set up on the peristaltic pump.
- The electrodes of the flow device were connected to the LCR meter.
- The conditions at the start of the experiment were as follows:
  - Enclosure warming OFF (Temperature 22 ^{0}C)
  - Carbogen supply OFF
  - Peristaltic pump OFF (Flow rate = 0 mL / min)
- The impedance measurement (at 10 kHz) were started and acquired at 15 min intervals.
- At 18 h, the enclosure warming was turned on and set at 37 ^{0}C.
- At 21 h, the peristaltic pump was started and flow rate set at 5 mL / min).
- At 42 h, the carbogen supply was turned on.

6.5.4 Results and discussion

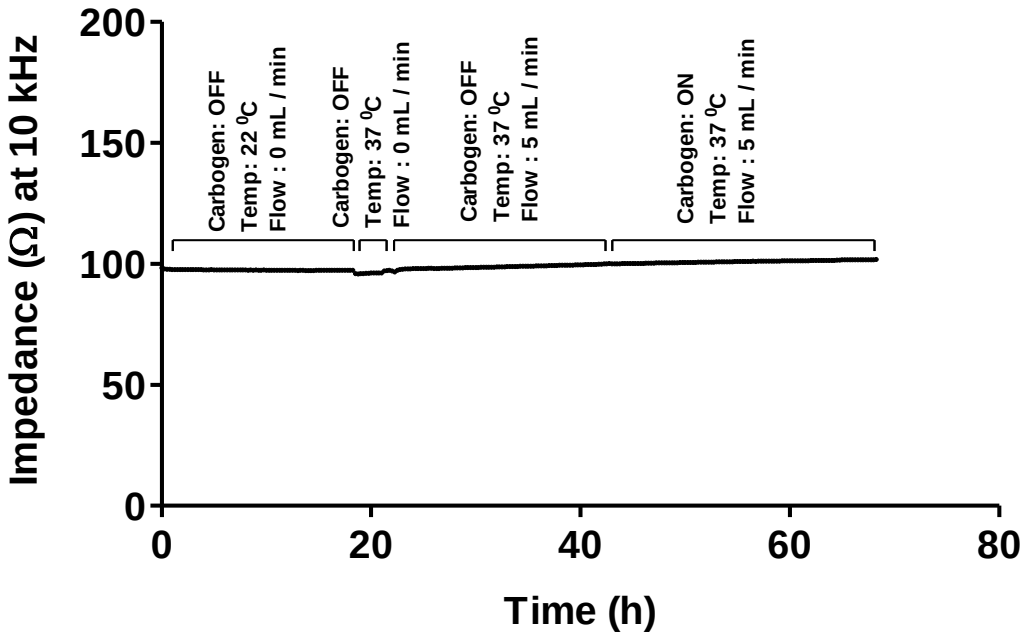

Figure 78: Impedance measurements of nIDE with microfluidic channel (at 10 kHz) under different conditions

The minimum impedance measured was 95 Ω and the maximum was 101 Ω. This represented a maximum impedance change of 6 Ω (6 % change) over 68 h. It was clear from these results that temperature changes (from 22 ^{0}C to 37 ^{0}C), pH changes and flow of culture medium had a minimal effect on the impedance. These effects could be further minimised by maintaining the temperature and pH (through carbogen bubbling into the culture medium). Changing the flow rate from 0 to 5 mL / min also had a minimal effect on the impedance. Hence the sensors could be regarded as suitable for cell sensing under culture medium flow conditions, but further experiments with cells would be required to confirm this.

6.6 Endothelial cell sensing using nIDE inside microfluidic channel under static culture medium condition

6.6.1 Rationale

Initial tests with MASMCs showed they had very poor adhesion to the bottom of the microfluidic channel despite coating with collagen. Hence, all the flow experiments were carried out with mouse endothelial cells, which had better adhesion with the collagen coating. The suitability of nIDE for detecting endothelial cells was shown in Section 4.3. This was carried out within a chamber made up of a well from a slide chamber, under static culture medium conditions. In this section, the ability of nIDE to detect endothelial cells when enclosed inside a microfluidic channel was tested.

6.6.2 Hypothesis

nIDE, enclosed inside a microfluidic channel, can detect adherence of endothelial cells under static culture medium conditions.

6.6.3 Experimental procedure

The experiment was carried out as follows:

- A flow device containing nIDE was sterilised (Section 2.7.1).
- 200 µL of DMEM culture medium was pipetted into the microfluidic channel.
- A baseline impedance sweep from 1 kHz to 50 kHz was carried out for each device.
- MECs were detached from a sub-confluent flask (Section 2.2.2).
- The cells were seeded into the flow device (Section 2.2.3).
- The cells were allowed to settle down in an incubator (37 ^{0}C) for 3 h.
- Then, experimental impedance sweeps were carried out for each device.

6.6.4 Results and discussion

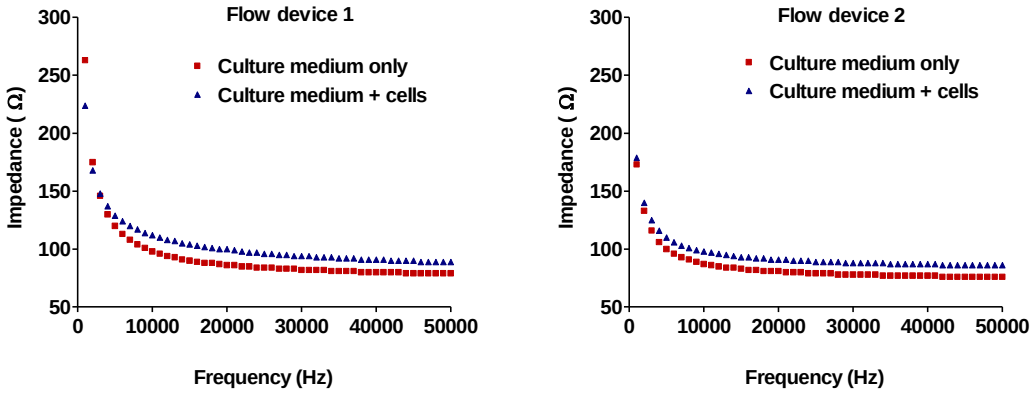

Figure 79: Impedance spectra of nIDE within flow devices 1 and 2 without cells (red curves) and with endothelial cells (blue curves) in absence of culture medium flow (n = 2).

In the all the previous experiments in the previous chapters, the cells were allowed to settle down for 18 h. In the current experiment, the cells were allowed to settle down for 3 h because the channel had a small volume of 200 µL, implying that the cells would quickly run out of nutrients.

The results show that the blue curves (culture medium + cells) were higher than the red curve (culture medium only). At 10 kHz, flow device 1 detected an increase in impedance of 14 Ω and flow device 2 detected an increase of 11 Ω.

These increases were similar to the ones detected in Section 4.3 when endothelial cells were seeded onto nIDE inside slide chambers. Hence, it could be concluded that nIDE detected endothelial cells both when enclosed within slide chambers

and microfluidic channels. Hence this sensor, can detect cells irrespective of the volume of culture medium above it.

6.7 Effect of culture medium flow on mouse endothelial cells morphology

6.7.1 Rationale

In this experiment, the effect of culture medium flow on the morphology of endothelial cells was investigated. These cells respond to flow and shear stress by changing their shapes.

6.7.2 Hypothesis

Mouse endothelial cells elongate in response to flow of culture medium.

6.7.3 Experimental procedure

The experiment was carried out as follows:

- A flow device incorporating nIDE and the flow circuit were sterilised (Section 2.7).
- MECs were detached from a sub-confluent flask (Section 2.2.2) and seeded into the flow device (Section 2.2.3).
- The cells were allowed to settle down in an incubator (37 ^{0}C) for 3 h.
- Once the cells started to adhere to the bottom, as observed under the microscope, the flow circuit (with DMEM) was connected to the flow device.
- The flow device and circuit were kept in an incubator for 12 h to allow the cells to adhere further and spread. After the 12 h, the flow device and circuit were set up on the live cell microscope with warmed enclosure.
- The reservoir was connected to the carbogen supply to keep the media buffered. The tubing was set up on the peristaltic pump and a flow rate of 5 mL / min was selected.
- Culture medium flow was started after the first timelapse image.
- An image was acquired at the start (0 h) of the experiment (Figure 80 Top panel) and after 18 h with 5 mL / min culture medium flow (Figure 80 Bottom panel).

6.7.4 Image analysis

10 random cells were selected from the image at 0 h and the maximum lengths of each cell was measured. A mean was calculated. This was repeated with another set of 10 random cells on the image at 18 h.

6.7.5 Results and discussion

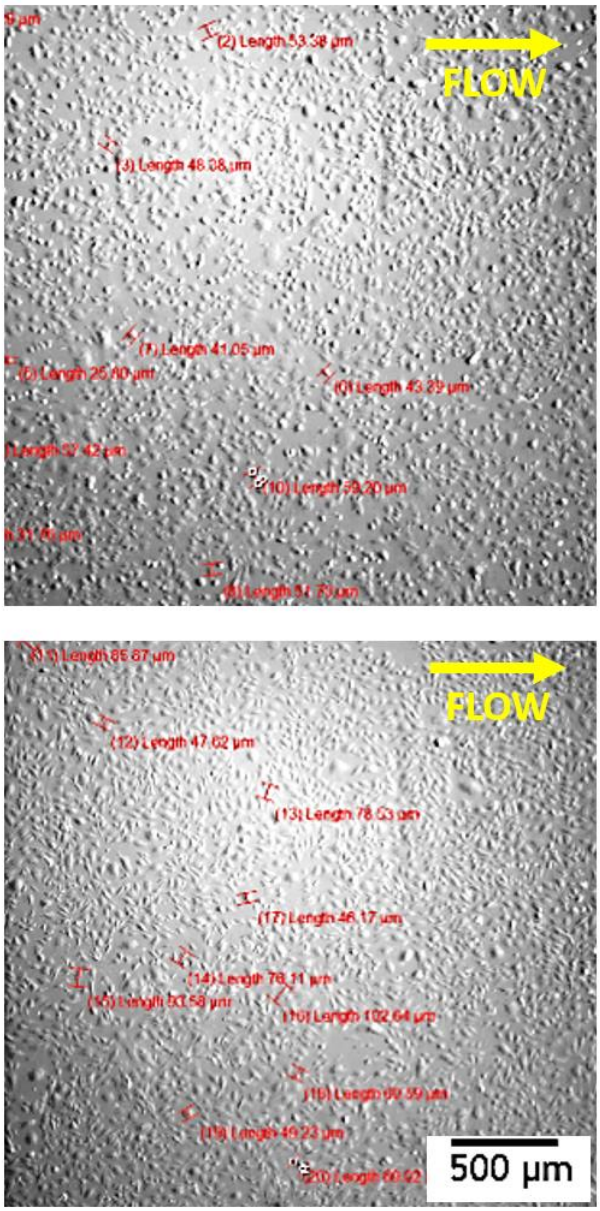

Figure 80: Top panel shows mouse endothelial cells at the start of culture medium flow. Bottom panel shows cells after 18 h of culture medium flow at 5 mL / min. The individual cell length are shown in red.

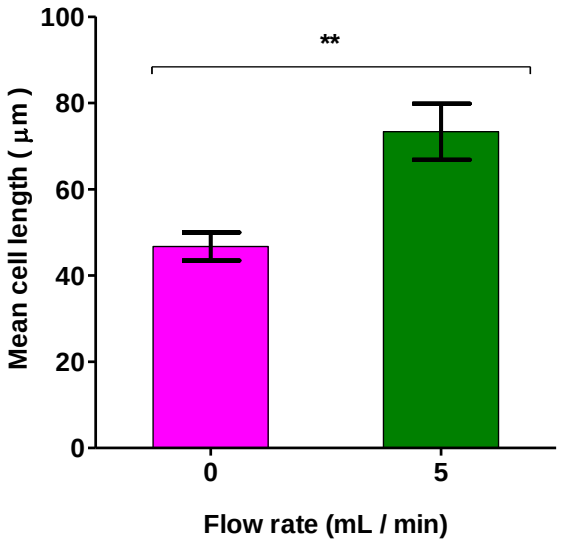

Figure 81: Mean cell length with 0 mL / min flow rate and after 18 h with 5 mL / min flow rate.

The mean cell length in absence of flow was 46 µm while the mean cell length after 18 h at 5 mL/min culture medium flow was 73 µm. A student's t-test was carried out and showed that the mean lengths were statistically different ($p < 0.01$). Hence, it was likely that a 5 mL / min flow rate caused MEC to elongate. The flow rate of 5 mL / min was the minimum that could be generated by the peristaltic pump. With lower settings, the peristaltic pump was unable to compress the tubing at regular time intervals. This flow rate seemed to be sufficient for maintaining a supply of nutrients to sustain the cells for at least 18 h. Moreover, it did not cause the cells to detach. Hence, the forthcoming experiments were carried out with flow rate of 5 mL / min. These results show that the MEC respond to flow of culture medium by changing their shapes and becoming more elongated. This change in shape could possibly be detected by the Interdigitated Electrodes.

6.8 Effect of direction of flow on proliferation and migration of an endothelial cell monolayer

6.8.1 Rationale

In this experiment, the effect of flow and counterflow (Section 6.4) on proliferation and migration of an endothelial cell monolayer was investigated. This would help guide the forthcoming experiments, where the changes in electrode coverage changes with time were investigated.

6.8.2 Hypothesis

The endothelial monolayer migrates and proliferates faster with flow compared to counterflow.

6.8.3 Experimental procedure

The experiment was carried out as follows:

- A flow device containing nIDE was sterilised (Section 2.7.1).
- An endothelial cell suspension (density 500000 cells / mL) was prepared in DMEM and pipetted (Section 2.2.3) into approximately one third of the channel (Figure 84).
- The cells were allowed to settle down and adhere to the bottom of the channel for 3 h in an incubator.
- Then, the channel and the 2 mini-reservoirs were filled with fresh DMEM and the cells were allowed to adhere further for 6 h.
- Then, the flow circuit was connected (Section 2.7).
- The flow device + circuit were transferred to the live cell microscope with warmed enclosure.
- MIA timelapse was acquired at 15 min interval for 62.5 h.
- The flow rate was set at 5 mL / min for Experiment 1.
- The experiment was repeated using another flow device. The counterflow rate was set at 5 mL / min for Experiment 2.

6.8.4 Results and discussion

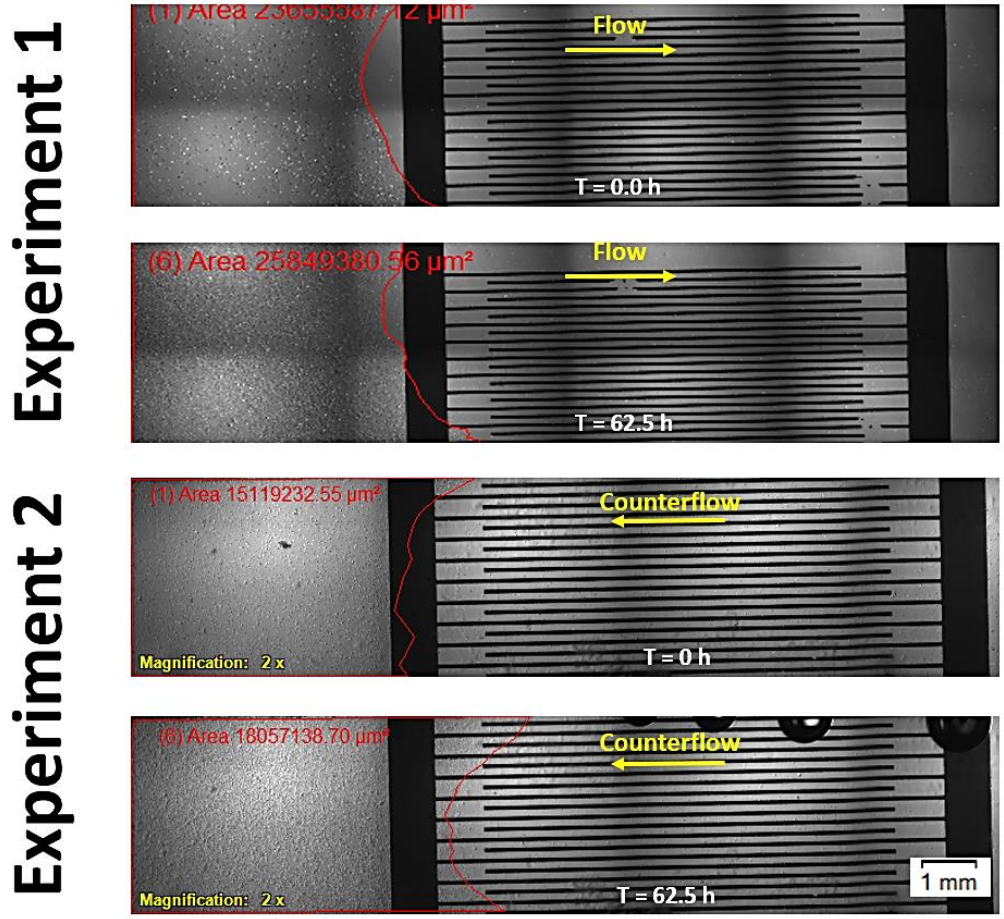

Figure 82: Experiment 1 with flow for 62.5 h and experiment 2 with counterflow for 62.5 h.

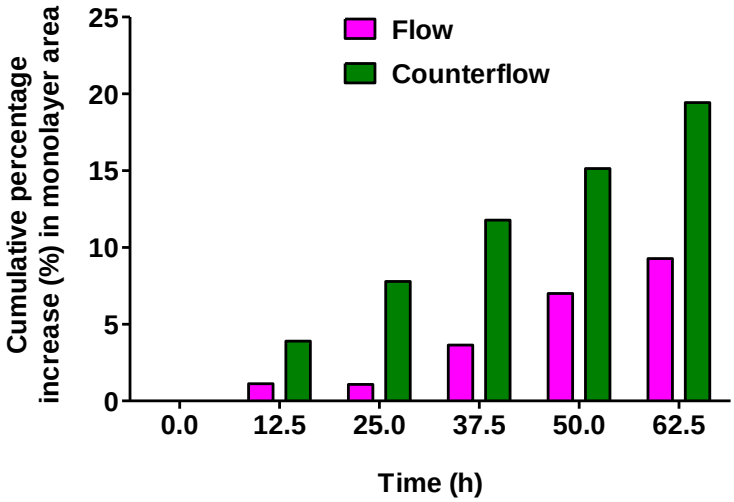

Figure 83: Cumulative increase in area occupied by monolayer with flow and counterflow at different timepoints.

The cumulative percentage increase in monolayer area was higher with counterflow, as compared to flow, at all the timepoints. The experiment was carried out with one technical replicate for the flow and one technical replicate for the counterflow. These results seem to suggest that the endothelial cell monolayer migrated faster with counterflow (against the flow) compared to flow (with the flow). Further experiments tracking the migrations of individual MECs were required to confirm this effect.

6.9 Effect of direction of flow on migration of individual endothelial cells

6.9.1 Rationale

This experiment was carried out to confirm whether the individual endothelial cells migrated with the flow or against the flow. This would help to guide the forthcoming experiments, which attempted to simulate regrowth (migration and proliferation) of endothelial cells from the undamaged part of the endothelium (portion of microfluidic channel seeded with cells) to the damaged de-endothelialised part of the artery (portion of channel which is cell free and contains the cell sensor).

6.9.2 Experimental procedure

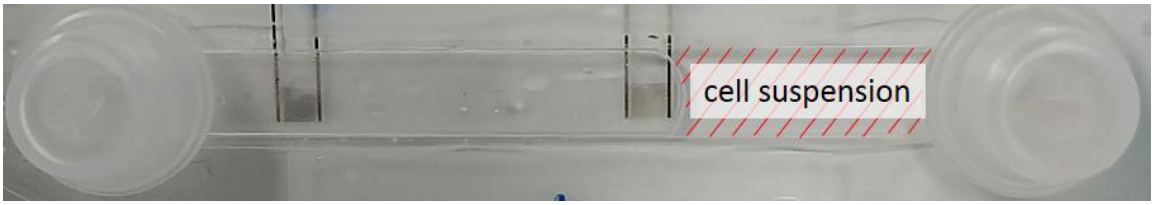

Figure 84: Endothelial cell seeding into the right third of the microfluidic channel.

The experiment was carried out as follows:

- A flow device containing nIDE was sterilised (Section 2.7.1).
  An endothelial cell suspension (density 500000 cells / mL) was prepared in DMEM and pipetted (Section 2.2.3) into approximately one third of the channel (Figure 84).
- The cells were allowed to settle down and adhere to the bottom of the channel for 3 h in an incubator.
- Then, the channel and the 2 mini-reservoirs were filled with fresh DMEM and the cells were allowed to adhere further for 6 h.
- The flow circuit was connected (Section 2.8).
- The flow device + circuit was transferred to the live cell microscope with warmed enclosure.
- Timelapse was acquired at 15 min interval for 48 h.

- The flow rate was set at 5 mL / min.
- The direction of flow for the first 24 h was from the cell monolayer towards the electrode (right to left).
- The direction of flow for the last 24 h was from the electrode towards the cell monolayer (left to right).

6.9.3 Image analysis, results and discussion

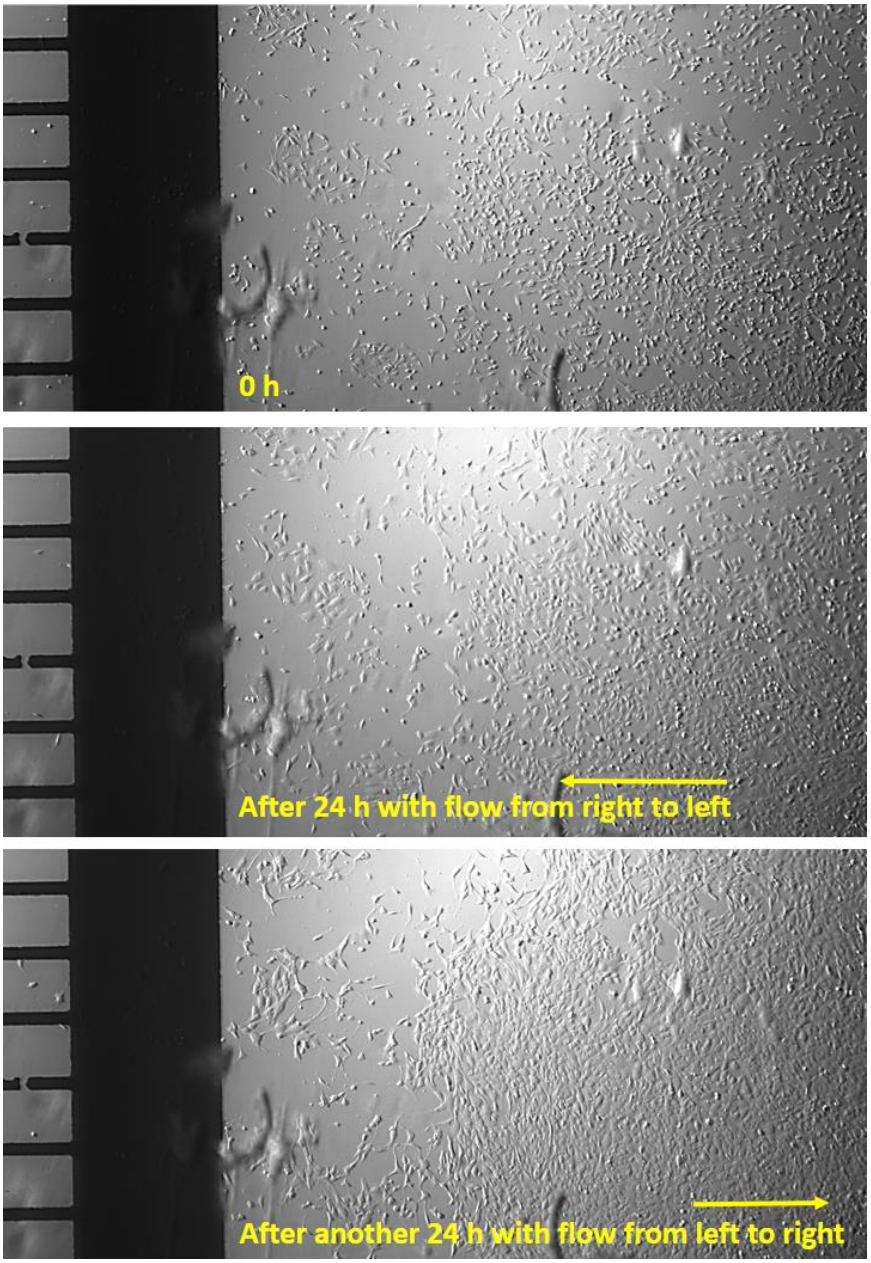

Figure 85: Micrographs of endothelial cells inside microfluidic channel. The top panel is the image just before flow was started. The middle panel is the image after 24 h of flow from right to left. Bottom panel is the image after another 24 h with flow from left to right.

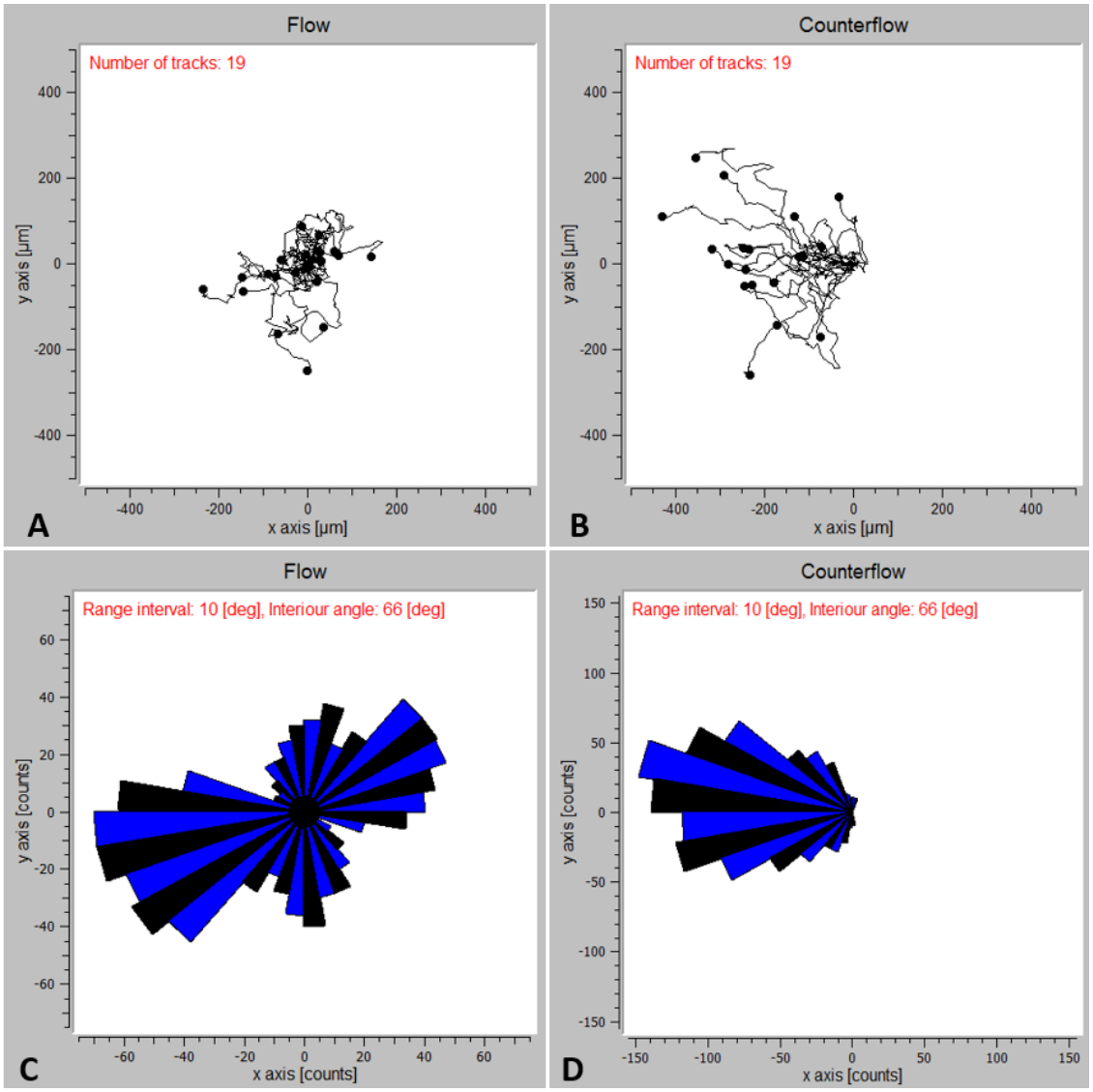

Figure 86: (A)(B) Spider diagrams showing final positions of 19 cells relative to their starting position, under flow and counterflow conditions. (C)(D) Rose diagrams of cumulative number of cells located at different angles relative to the starting positions.

Figure 85 shows the micrographs of the endothelial cells at the different timepoints. The top panel represents the baseline starting imaging before the flow of culture medium was started. The middle panel shows the cells after 24 h of FLOW (culture medium flowing from monolayer towards the electrodes). The bottom panel shows the cells after further 24 h of COUNTERFLOW (culture medium flowing from electrodes towards the monolayer). From the images, it was clear that the cells migrated and proliferated further towards the electrode during COUNTERFLOW.

The timelapse movie was analysed by using the MTrackJ plugin (Meijering, Dzyubachyk and Smal, 2012) in ImageJ. The results were then post-processed using the Chemotaxis and Migration Tool V2.0 (Ibidi). For the FLOW phase (first 24 h), 19 random cells were selected and their displacements tracked for the whole 24 h. For the COUNTERFLOW phase (second 24 h), 19 random cells were selected and their displacements tracked for the whole 24 h. Spider diagrams (Figure 86A & 84B) and Rose diagrams (Figure 86C & 84D) were then generated.

The graphs for the FLOW show that the displacement and angle of displacement were mostly random from the initial starting positions of the cells. However, the Rose diagram shows that the angular displacements of the cells were slightly more towards the negative x-axis (towards the electrodes).

The graphs for the COUNTERFLOW show that the displacement and angle of displacement were more towards the negative x-axis (towards the electrodes) from the initial starting positions of the cells. It was clear that COUNTERFLOW caused the individual cells to displace towards the electrodes, against the flow of culture medium.

All these results show that Mouse Endothelial Cells migrate against the flow of culture medium.

6.10 Endothelial cell migration and sensing using nIDE under culture media flow conditions

6.10.1 Rationale

This experiment investigated whether it was possible to use the nIDE within the microfluidic channel to monitor migration and proliferation of the endothelial cell monolayer. The nIDE was thus mimicking one cell sensor on the hypothetical smart stent. The cells were seeded in only one portion of the channel, mimicking the undamaged portion of the endothelium. The nIDE was kept in the cell free portion of the channel (mimicking the damaged endothelium).

6.10.2 Hypothesis

The normal Interdigitated Electrode (nIDE) within the microfluidic channel can monitor migration and proliferation of an endothelial cell monolayer.

6.10.3 Experimental procedure

The experiment was carried out as follows:

- A flow device containing nIDE was sterilised (Section 2.7.1).
- An endothelial cell suspension (density 500000 cells / mL) was prepared in DMEM and pipetted (Section 2.2.3) into approximately one third of the channel (Figure 84).
- The cells were allowed to settle down and adhere to the bottom of the channel for 3 h in an incubator.
- Then, the channel and the 2 mini-reservoirs were filled with fresh DMEM and the cells were allowed to adhere further for 6 h.
- The flow circuit was connected (Section 2.8).
- The flow device + circuit were transferred to the live cell microscope with warmed enclosure.
- The nIDE was connected to the LCR meter.
- The peristaltic pump was switched on and set at a flow rate of 5 mL / min.
- MIA timelapse imaging and impedance measurements were started simultaneously and acquired at 15 min intervals up to the 208 h timepoint.

6.10.4 Image analysis

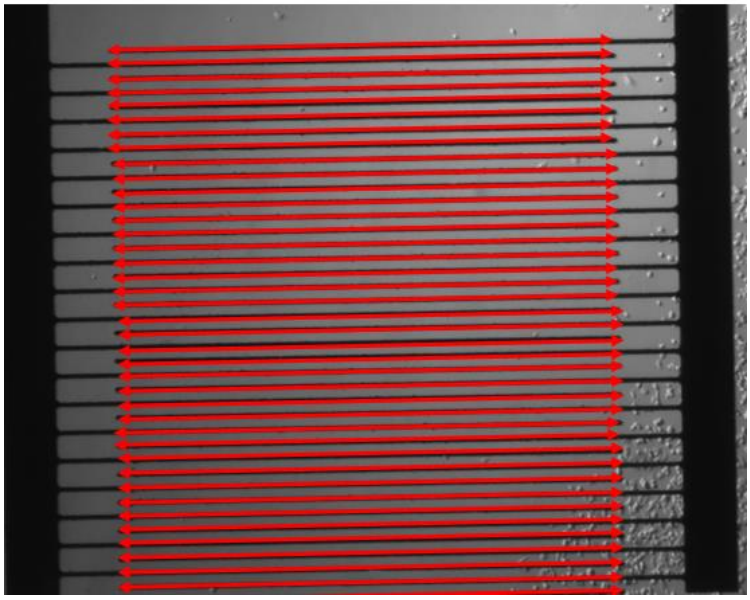

Figure 87: Red arrows represent effective sensing length of each finger of the nIDE. The total effective length is the total length of all the 40 arrows together.

Coverage of the nIDE by cells was assessed using the percentage length coverage. The total effective length of the nIDE was calculated. This was the total of the length of the middle part of 40 fingers. It was assumed that only cells directly adhering to the fingers contribute to the impedance increase. Hence the lengths of the portions of the fingers covered by cells were measured. The total length covered by the cell monolayer was calculated and expressed as a percentage of the total effective length of the nIDE.

6.10.5 Results and discussion

Time (h)	Image
0	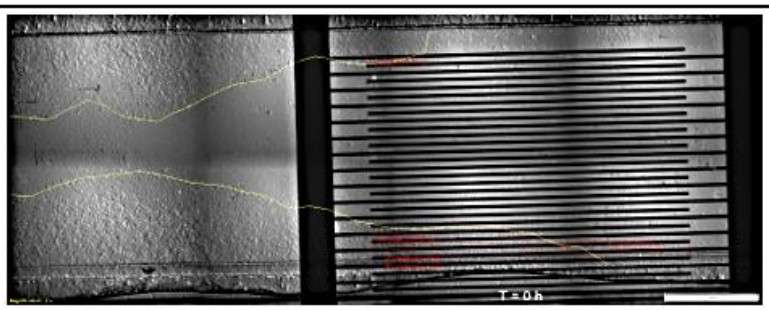
70	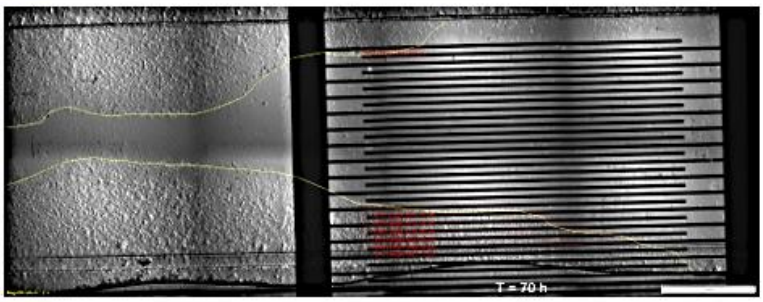
116	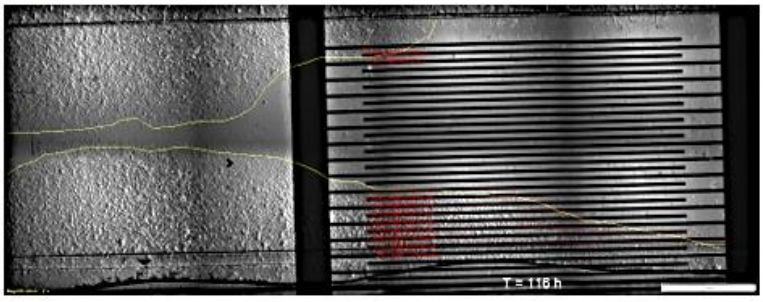
142	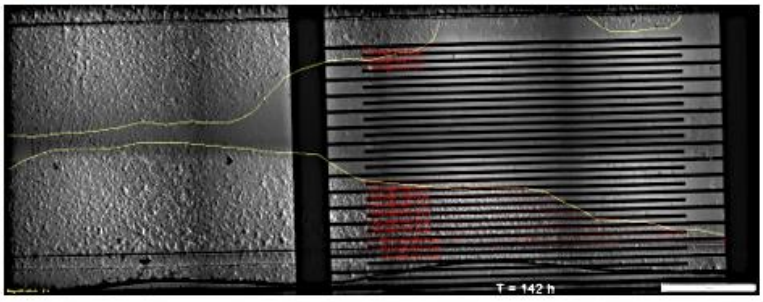
208	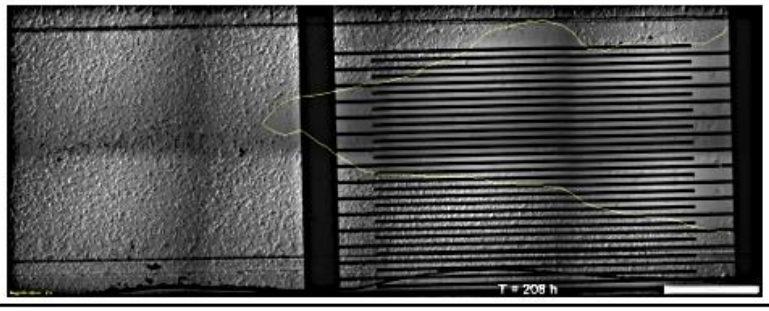

Table 9: MIA at 0 h, 70 h, 116 h, 142 h and 208 h showing migration and proliferation of mouse endothelial cell monolayer within microfluidic channel under flow conditions.

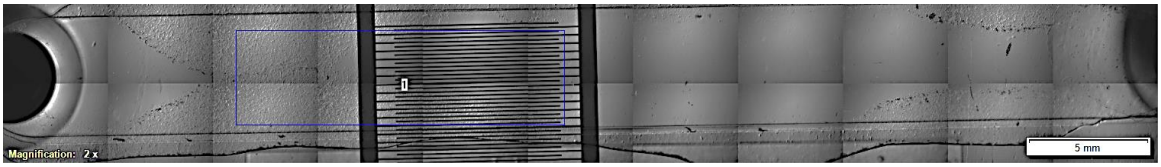

Figure 88: Broad MIA of microfluidic channel showing position of cell monolayer after 208 h of migration and proliferation.

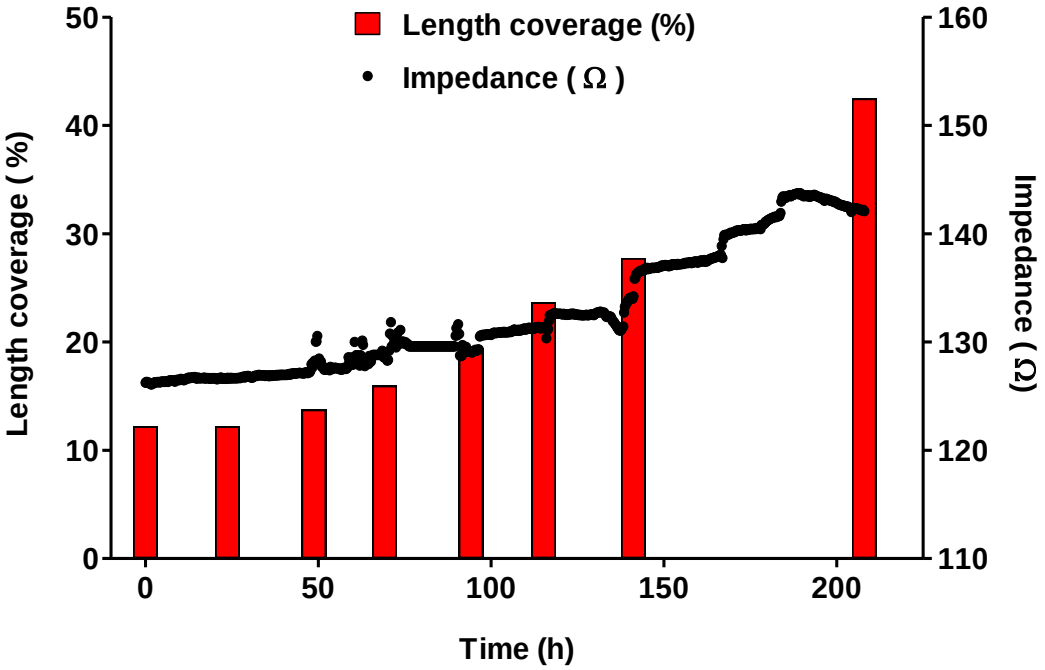

Figure 89: Length coverage of nIDE and impedance changes due to mouse endothelial cell monolayer proliferation and migration 5 mL / min counterflow within microfluidic channel.

The images in Table 9 show the mouse endothelial cell monolayer at 0 h (start of timelapse), 70 h, 116 h, 142 h and 208 h (end of timelapse). The yellow line all the images indicate the boundaries of monolayer. At 0 h, the monolayer was split in 2 parts, with cells towards the top and bottom of the channel. This could be due to a non-uniform collagen coating of the channel, leaving the middle portion of the channel with no or very little collagen. Hence cells in the middle of the channel were easily detached when the flow circuit was connected. The detachment of the cells in the middle of the channel could also be due to higher fluid velocity in the middle of the channel, leading to higher shear stresses in the cells in the middle, compared to cells close the edges.

As the experiment progressed, the cells migrated / proliferated towards the middle of the channel and the gap was completely closed at 208 h. Moreover, the cells migrated / proliferated towards the electrodes as a result of the counterflow of 5 mL / min. The number of fingers covered by the cell monolayer increase with time and this was assessed through the percentage length coverage.

At 0 h, there was length coverage of 12 % and an impedance of 126 Ω. At 94 h, there is a 19 % coverage and an impedance of 129 Ω. At 208 h, there was a 42 % coverage and an impedance of 142 Ω. There seemed to be a positive correlation between the length coverage and the impedance. This correlation was not linear. Further experiments were required to ensure the relation between impedance and percentage coverage.

This experiment attempted to simulate regrowth of an endothelial cell monolayer over one of the sensors of the hypothetical smart stent. The positive correlation between length coverage and impedance indicates that the IDE could be used to track regrowth of endothelium under more physiological conditions. Due to the challenges of culturing cells under flow, the cells could not be kept alive after 208 h and hence full coverage of the electrode could not be achieved. It was thus unclear whether the impedance reached a plateau phase when electrode was fully covered.

6.11 Endothelial cell migration and sensing using ssIDE under culture media flow conditions

6.11.1 Rationale

In the previous experiment (Section 6.10) endothelial cell migration and proliferation under flow conditions was monitored using nIDE. Due to the large surface area of the electrode, 8 days was required to achieve 42 % coverage. In this experiment the ssIDE are used in order to achieve similar or higher percentage coverage in a shorter time period.

6.11.2 Experimental procedure

The experiment was carried out as follows:

- A flow device containing ssIDE was sterilised (Section 2.7.1).
- An endothelial cell suspension (density 500000 cells / mL) was prepared in DMEM and pipetted (Section 2.2.3) into approximately one third of the channel (Figure 84).
- The cells were allowed to settle down and adhere to the bottom of the channel for 3 h in an incubator.
- Then, the channel and the 2 mini-reservoirs were filled with fresh DMEM and the cells were allowed to adhere further for 6 h.
- The flow circuit was connected (Section 2.8).
- The flow device + circuit was transferred to the live cell microscope with warmed enclosure.
- The ssIDE was connected to the LCR meter.
- The peristaltic pump was switched on and set at a flow rate of 5 mL / min.
- MIA timelapse imaging and impedance measurements were started simultaneously and acquired at 15 min intervals up to the 40 h timepoint.

6.11.3 Image analysis

Migration and proliferation of the endothelial cell monolayer was analysed by:

- Measuring the area occupied by the monolayer on the MIA at 0 h.
- Measuring the area occupied by the monolayer on the MIA every 2.5 h up to the 47.5 h timepoint.
- Calculating the increase in area occupied by monolayer.

Coverage of the ssIDE by cells was assessed using 2 methods. In the first method, the total effective length of the ssIDE was calculated. This was the total of the length of the middle part of 40 fingers. In this method, it was assumed that only cells directly adhering to the fingers contribute to the impedance increase. Hence the lengths of the portions of the fingers covered by cells was measured. The total length covered was calculated and expressed as a percentage of the total effective length of the ssIDE.

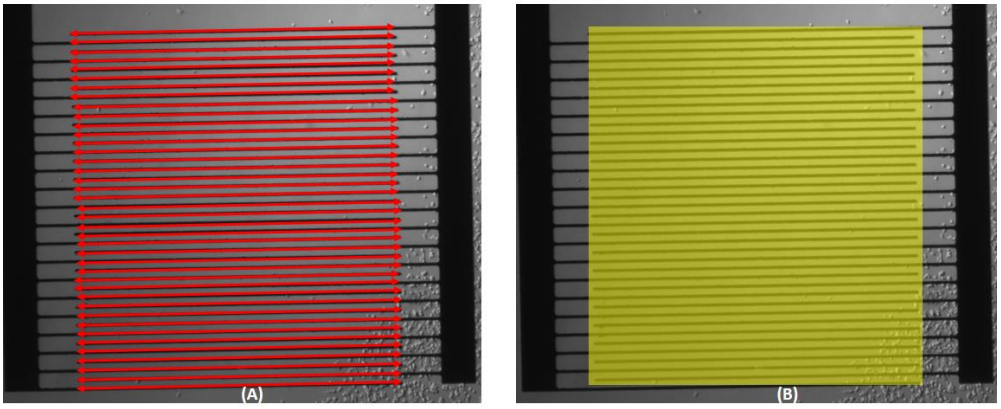

Figure 90: (A) Red arrows represent effective length of each finger of the ssIDE. The total effective length is the total length of all the 40 arrows together. (B) Yellow box represents total effective electrode area.

In the second method, the total effective electrode area was calculated. This was the middle area of the ssIDE. In this method, it was assumed that both cells adhering directly to the fingers and in between the fingers contributed to the impedance increase. The area occupied by the portion of the cell monolayer on the ssIDE were measured at the different timepoints and expressed as a percentage of the total effective electrode area.

6.11.4 Results

Time (h)	Image
0.0	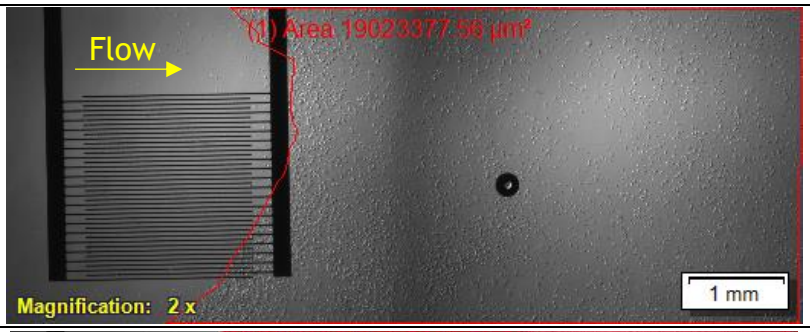
12.5	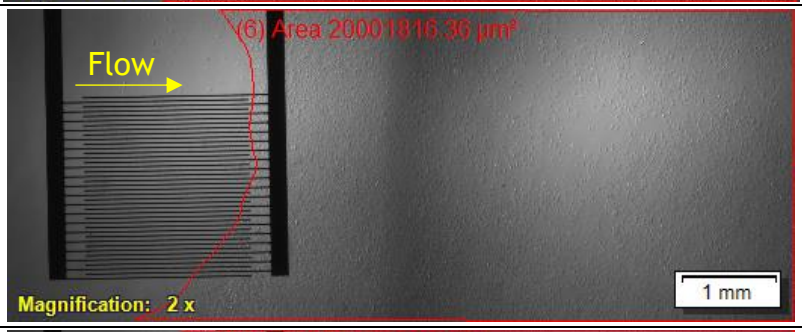
25.0	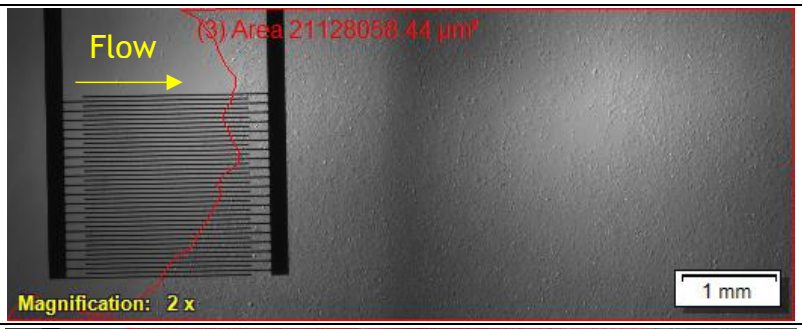
37.5	
50.0	

Table 10: MIA images showing increase in area occupied by monolayer with time.

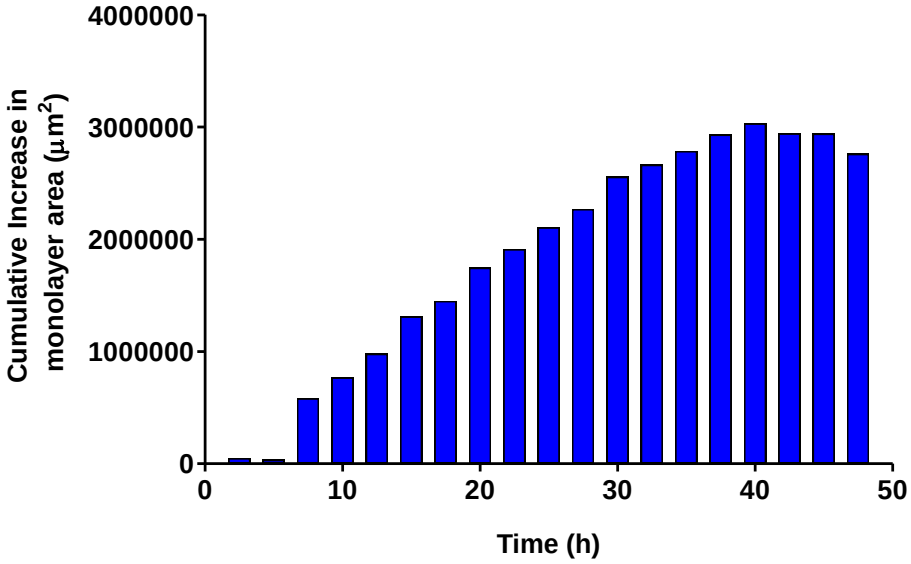

Figure 91: Cumulative increase in area occupied by monolayer with time.

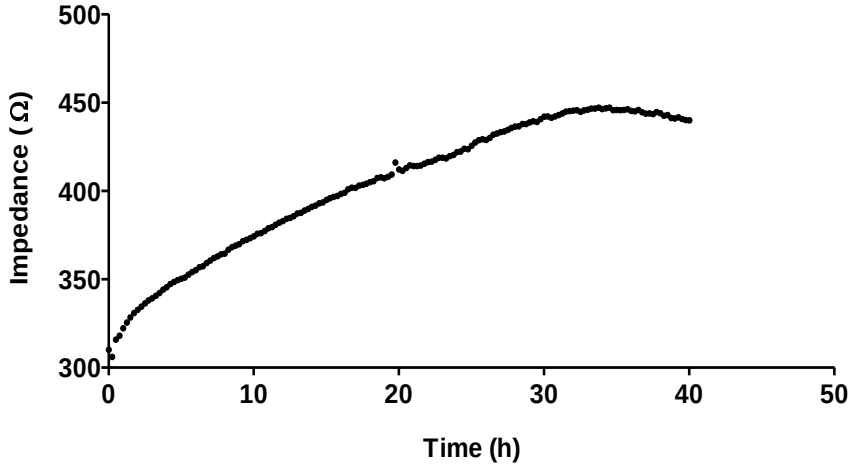

Figure 92: Impedance measurements (at 10 kHz) of endothelial cells migrating and proliferating under flow conditions for 50 h.

Time (h)	Image	Length coverage (%)	Image	Area coverage (%)
12.5	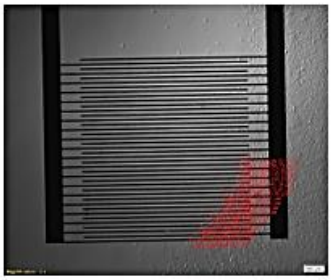	7.98	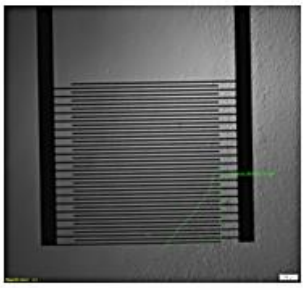	7.69
25.0		21.20	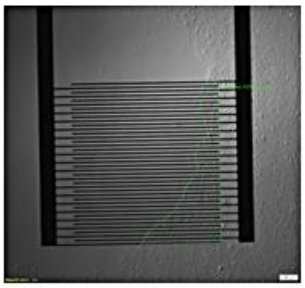	21.28
37.5	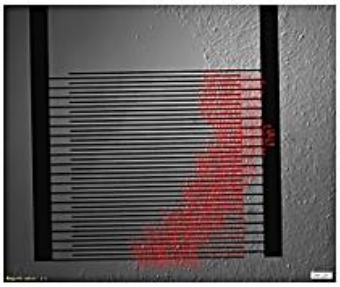	34.32	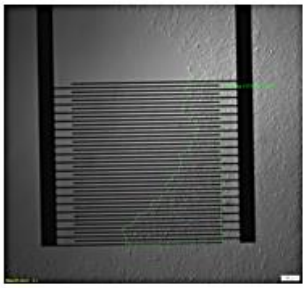	33.73

Table 11: Percentage length and area coverage of the ssIDE by endothelial cells at the different timepoints.

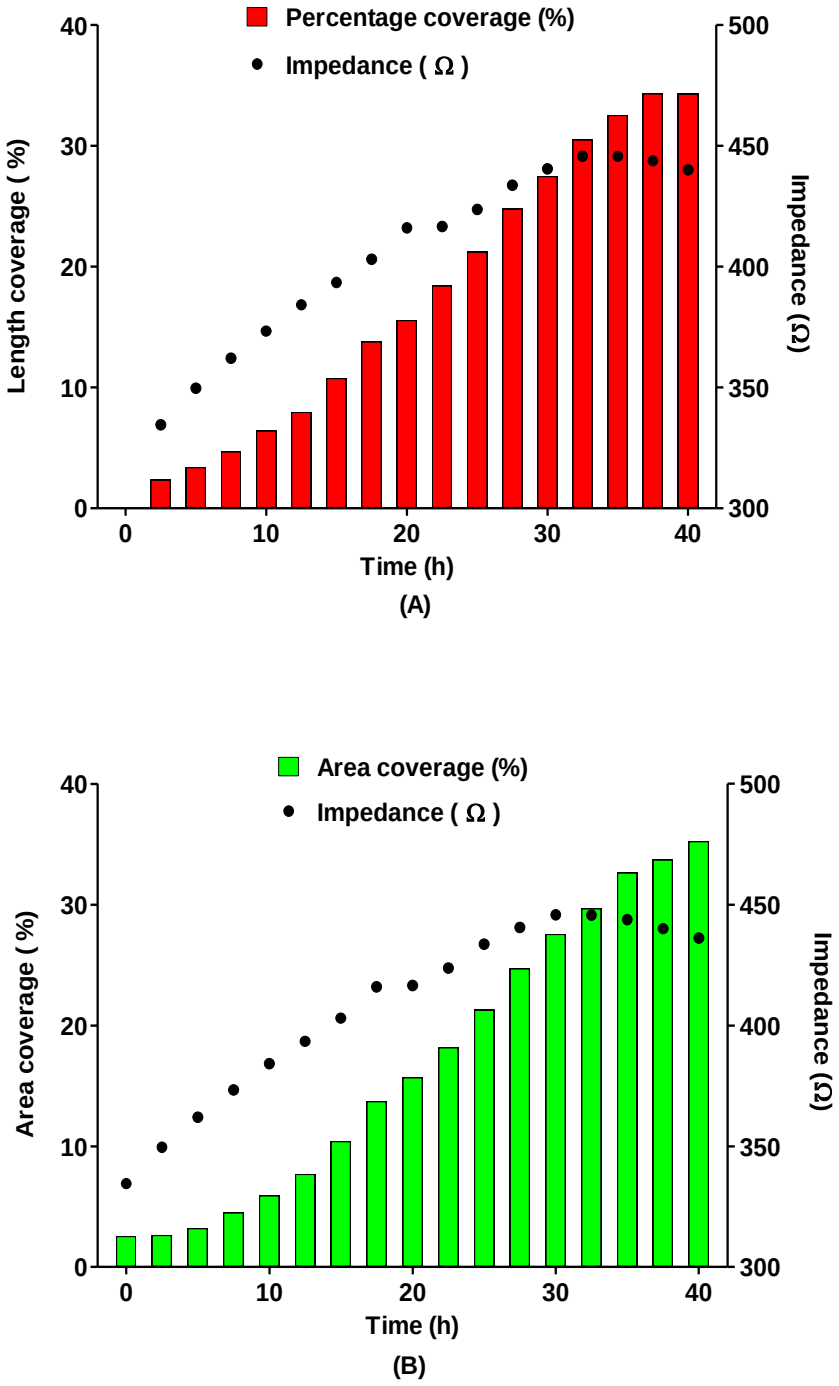

Figure 93: (A) Percentage length coverage of the electrodes and corresponding impedance with time. (B) Percentage area coverage of effective electrode area and corresponding impedance with time.

6.11.5 Discussion

The cumulative increase in the area occupied by the monolayer (Figure 91) showed a gradual increase from 0.0 h to 40.0 h, indicating that the monolayer proliferated and migrated towards the electrode. At 40 h, a peak was reached. From 40.0 h to 47.5 h, there was a decrease indicating that the cell monolayer started to die and recede away from the electrode.

Figure 92 shows that the impedance gradually increased from 310 Ω at 0.0 h and reached a maximum of 447 Ω at 34.0 h. Then, the impedance gradually decreased to 434 Ω at 40.0 h.

Figure 93 shows that both the percentage length coverage and percentage area coverage curves showed good correlation with the impedance. Both methods were suitable for assessing coverage of the electrodes. As endothelial cells covered more of the electrode, a corresponding increase in the impedance occurred. The percentage length coverage reached a plateau at 37.5 h and this caused a small decrease in impedance. This was possibly due to cell death on and in between the electrodes. The experiment could not be continued after 40.0 h because the cells in the channel started to die. Hence only a maximum percentage length coverage and area coverage of 34 % and 35 %, respectively, could be achieved.

It was not clear whether the impedance increased further for higher percentage coverages and whether the impedance reached a plateau once the electrode was fully covered. Hence, further experiments are required to investigate this.

However, these were promising results, as low percentage coverages could also be detected. It also implied that the sensors could be used to monitor regrowth of an endothelial monolayer.

6.12 Summary and discussion

In this Chapter, we tested whether the IDE could detect cells under culture medium flow conditions. The flow devices consisted of a microfluidic chamber with a central channel enclosing the IDE and inlet / outlet ports. Experiments under static conditions showed that the IDE could detect Mouse Endothelial Cell (MEC) adhesion (Figure 79).

When the MEC were subjected to a culture medium flow of 5 mL / min for 18 h, the cells became elongated (Figure 80 and 81). This was consistent with results by Li *et al*. (2013), who demonstrated cell elongation as a result of flow of culture medium.

The results in Figures 82 and 85 show that the MEC migrated / proliferated faster against the flow of culture medium. This could be an innate characteristic of endothelial cells, as demonstrated by other research groups (Franco *et al.*, 2015; Rochon, Menon and Roman, 2016). However, this could also be due to the flow dynamics within the microfluidic channel.

The flow of culture medium was generated by using a peristaltic pump. The rotor assembly compressed the tubing at regular time intervals leading to a pulsatile flow. However, due to the absence of valves within the flow circuit (as it is the case within the cardiovascular system), it is likely that flow reversal occurs. This could affect adhesion, growth and proliferation of endothelial cells within the microfluidic channel. Moreover, the 130 nm thickness of the electrodes within the channel could also disturb the laminar flow and affect endothelial cell proliferation.

CHAPTER 7

FINAL CONCLUSION AND FUTURE PERSPECTIVES

7.1 Final Conclusion

The two main aims of the project were to develop a cell sensing and electrotherapeutic system that could be integrated onto a future smart stent, allowing monitoring of and intervention on in-stent restenosis. This future smart stent could thus be referred to as a theranostic device.

During the course of this project, I was able to show that I could develop biosensors, within the facilities of the James Watt Nanofabrication Centre of the University of Glasgow. Fabricating my own electrodes gave me the flexibility of testing different designs and dimensions. The most promising results were obtained using Interdigitated Electrodes (IDE) and Pendulum Electrodes (PE).

Preliminary tests with culture medium only (without biological cells) showed that the IDEs were less susceptible to changes in volume and conductivity of culture medium, compared to the PEs. Hence, the IDEs were chosen as the ideal configuration for cell sensing experiments. PEs were considered more suitable for electromediated cell death experiments, as they had a similar large-counter-electrode v/s small-working-electrode configuration to the 8W1E electrodes (Figure 18a) used by Stolwijk, Michaelis and Wegener (2012). They applied invasive voltages (AC sinusoidal voltage of 5 V and 40 kHz for 30 s) to Normal Rat Kidney (NRK) cells and successfully induced cell death on the electrodes (Figure 22).The IDEs were also successfully used for electromediated cell death experiments using AC voltages.

Initial tests with Mouse Aortic Smooth Muscle Cells (MASMCs) and Mouse Endothelial Cells (MECs) using a broad impedance sweep showed that the IDEs were sensitive to cells in the 1 kHz to 50 kHz (which was thus chosen as optimum sensing frequency range). Results from Figure 39 showed that the nIDE (electrode area 28.8 mm^2) were sensitive to MASMCs in the 1 kHz to 1 MHz range. Giaever and Keese (1991) used 0.1 mm^2 electrodes to sense fibroblasts. These cells were detected in the 100 Hz to 100 kHz range. Mamouni and Yang (2011) used 7.5 mm^2 electrodes to sense epithelial cells. These cells were detected in the 1 kHz to 100 kHz range. It was not clear whether the differences in sensing frequency range was due to electrode surface area, different cell types or to a combination of the two factors. A single optimum sensing frequency of 10 kHz was also chosen for the IDE.

The effects of changing the dimensions of the IDE on its sensitivity for cell detection were also investigated. Halving the finger width and doubling the number of fingers, while conserving the effective electrode surface area did not change the sensitivity of the detection. Decreasing the finger length and width by a factor of 4 (decreasing effective electrode surface area by a factor of 16) increased the sensitivity by a factor of 4. This is in line with results (Figure 13) obtained by Zhang *et al*. (2017), which showed an inverse relation between electrode size and impedance increase detected with cells. This was an important and significant finding when it comes to the future fabrication of these types of sensors, as the sensor sizes will dictate the clinical application the device can be used for.

A small AC voltage of 10 mV was applied to the IDEs in order to measure impedance of culture medium only or culture medium + cells. Stolwijk, Michaelis and Wegener (2012) used ECIS 8W1E electrodes (Figure 18a) to apply invasive voltages (AC sinusoidal voltage of 5 V and 40 kHz for 30 s) to Normal Rat Kidney (NRK) cells and successfully induced cell death on the electrodes (Figure 21). The PE, which had a similar configuration to the ECIS 8W1E electrodes, were first used to apply invasive voltages to a MASMC monolayer. Applying a DC voltage of 2.5 V to the monolayer caused a reproducible "tearing effect" around the PEs. The type of cell death induced was not clear from the first sets of experiments. Preliminary tests using DC voltages on the IDE showed that this could damage the electrodes and thus further experiments using DC voltages on the IDEs were not carried out.

Instead, AC voltages were routinely applied to MASMCs monolayers using the IDEs. The literature suggested that the voltages had to be applied at a frequency of 40 kHz in order to induce cell death. Application of a sine voltage of 2 $V_{\text{peak to peak}}$ and 40 kHz for 1 min using the nIDE and ssIDE caused a reproducible drop in impedance. The type of cell death induced was investigated using an Apoptosis / Necrosis kit. Results showed that application of the AC voltage caused an increase in rates of apoptosis. This is a critical finding as apoptotic death in the context of restenotic smart stent therapy would be predicted to be significantly less thrombogenic.

As the developed biosensors were intended to be incorporated onto a future smart stent, which would be implanted *in vivo* and would be subjected to blood flow, it was important to test whether they would work under flow conditions. Flow of

culture medium was used to simulate blood flow. Experiments were carried out, simulating the regrowth of a hypothetical endothelium *in vivo* from an undamaged portion of an artery to a damaged portion (mimicking the effects of stent deployment). The electrode coverage with cells thus increased gradually with time at an average migration-proliferation rate of 138054 μm^2 / h. The increase in impedance showed a strong positive correlation with increase in electrode coverage, implying that the biosensors integrated onto the hypothetical smart stent could track regrowth of an endothelial layer.

While the cell sensing system developed in this project has some similarities to the ECIS system, the bespoke system has significant improvements that make it much more amenable to a future integration on an implantable medical device, rather than a purely 2D system. Our system is completely scalable and suitable for mounting on stents across a variety of sizes and hence clinical applications.

The sensor design is also suitable for being used with a variety of conductive materials beyond Gold to include Platinum and inorganics sensor materials. The research group is currently in collaboration with a Bioelectronics group at the University of Glasgow in order to miniaturise the impedance acquisition system and also incorporate a wireless communication module.

Importantly, my results showed the same electrodes could be used both as diagnostic sensors and therapeutic probes. This opens the possibility of intervening on in-stent restenosis without further medication or surgery. Moreover, the success of the “cell apoptosing” intervention could be monitored immediately after treatment and for further long term monitoring, perhaps many months after stent deployment when the risk of instent restenosis still exists.

7.2 Future perspectives

All experiments have been carried out *in vitro* during this PhD project. The fabricated biosensors and cell chambers could complement normal cell culturing techniques by allowing cell adherence, spreading, viability and death to be non-invasively tracked with time.

The electrodes could also be used to apply voltages in order to induce apoptosis or necrosis of different cells types. These results could then be compared against cell death induced by chemical or biological agents. By using a small controlled voltage, the electrode could also be used for reversibly electroporating to insert drugs, plasmids, DNA or RNA. Although these are already largely commercially available, the ability to porate cells in the vicinity of the stent *in vivo* is novel and could yet be useful for the targeted delivery of drug, microparticles and nanocarriers for vascular diseases such as atherosclerosis.

All experiments were also carried out with mouse cells. As the developed biosensors are intended to be integrated onto a smart stent for human implantation, it is important to investigate whether they can detect and induce apoptosis of human cells in a similar way to mouse cells.

Moreover, to integrate such biosensors onto a coronary stent, these will need to be miniaturised to dimensions similar to the stent struts (100 µm wide). Further works will be required to determine the efficiency of these miniaturised biosensors at detecting smooth muscle cells and endothelial cells *in situ*.

Results in Sections 4.5, 4.6 and 4.7 showed that the IDEs had the potential to distinguish a pure smooth muscle cell population from a pure endothelial cell population. However, the number of biological replicates were low and thus further experiments are required to verify whether IDEs can reliably distinguish smooth muscle cells from endothelial cells. Experiments would also need to be carried out with mixed cells populations comprising different ratios of these 2 cell types.

In order to investigate the type of cell death induced by application of an AC voltage, the protocol for a commercial Apoptosis / Necrosis assay had to be modified in order allow multi-timepoint imaging rather than endpoint imaging

only. One of the issues encountered was the dye for live cells (Cytocalcein Violet) leached out of live cells, making it them unobservable after 5 h. The stain had to be applied again at the endpoint of the experiment to observe the live cells. It would be useful to find a way of preventing the leaching or using another live cell dye. This modified assay would thus allow all the changes occurring to cells during adherence, proliferation, apoptosis and necrosis to be imaged and quantified.

The flow system developed for Chapter 6 was a low-cost system allowing flow conditions within an artery to be simulated. However, the actuator system was a peristaltic pump and the flow rates varied largely with calibre of the tubing. Hence, in order to obtain more reliable results under flow conditions, a more sophisticated flow system would have to be developed or purchased. This system would allow cell culturing under more physiological conditions and would also allow cells to be maintained alive for longer durations. Chemical or biological treatments could be applied by pausing the flow for a specific duration, then restarting the flow, without the need for washes.

One of the major limitations of the impedance acquisition system (LCR meter) was that only one device could be connected at a time. It was thus not possible to obtain replicate data during continuous impedance monitoring. Current work is underway to develop a multiplexer board and corresponding software that would allow multi-electrode configuration on a single chip with continuous monitoring, making it possible to generate replicate treatment and negative control data simultaneously on several biological replicates.

The simultaneous use of several biosensors on the future smart stent would allow the possibility of electrical impedance tomography. Using this technique, the whole lumen of the stented portion could be imaged and monitored with time. This would allow surveillance of in-stent restenosis, in case early inhibition of smooth muscle cells proliferation, using irreversible electroporation, failed.

The results generated during this thesis, further works building on these results and industrial collaborations would ultimately generate a smart coronary stent. This would include biosensors (which also work as therapeutic probes) and integrated chips for impedance measurements, wireless powering and wireless communication. In order to relay information to the external world (for example onto a smart phone or other portable device) an intermediate relay device would

be placed on the patient's chest. The relay device would also be the wireless powering unit and would have to be regularly recharged.

Immediately after the implantation of the smart stent, the baseline impedances sweeps for the individual biosensors would be acquired. The changes in impedance would be measured once every day through the smart phone. The biosensors would be capable of identifying whether an endothelial cell, smooth muscle cell or mixed cell population were covering the stent surface.

In case of pure endothelial cell coverage, the thickness of the tissue would be expected to be only one-cell thick. This could be confirmed using electrical impedance tomography by using several biosensors simultaneously. Complete reendothelialisation would be an indication for stopping dual antiplatelet therapy, which would thus decrease the rates of haemorrhagic events.

In case of a pure smooth muscle cell population or mixed population covering the stent, intervention would be possible using electro-mediated apoptosis. The small voltage would be applied to the biosensors, turning them into therapeutic probes. The characteristics of the voltage applied would be optimised so as to induce higher rates of apoptosis in smooth muscle cells compared to endothelial cells. The smooth muscle cells would undergo apoptosis within 24 h of voltage application. This would allow the unaffected and minimally affected endothelial cells to proliferate and cover the stent struts and biosensors.

If the electromediated apoptosis of smooth muscle cells failed after several attempts, electrical impedance tomography could be used to track the extent of the hyperplasia. This would allow further percutaneous coronary interventions or surgical intervention before the patient experienced the symptoms of in-stent restenosis.

References

AAT, B. (2019) *Acridine orange | AAT Bioquest*. Available at: https://www.aatbio.com/products/acridine-orange?gclid=EAIaIQobChMI9vbp6KXz4wIVibbtCh1YrwJYEAAYASAAEgI1xvD_BwE (Accessed: 8 August 2019).

Abcam (2016) 'Apoptosis / Necrosis Detection Kit (blue , green , red) ASSAY SUMMARY PRECAUTIONS STORAGE AND STABILITY LIMITATIONS MATERIALS SUPPLIED TECHNICAL HINTS REAGENT PREPARATION ASSAY PROCEDURE DATA ANALYSIS TYPICAL DATA', (May).

Ablin, R. J. and Jiang, W. G. (2012) *Electric Cell-Substrate Impedance Sensing and Cancer Metastasis*. doi: 10.1007/978-94-007-4927-6.

AimTTI (2019) *TG251xA/501xA Series Function Generators, Pulse Generators, Arbitrary Generators | Aim-TTi International*. Available at: https://www.aimtti.com/product-category/function-generators/aim-tg251xa-501xaseries (Accessed: 8 August 2019).

Alexander, G. C. *et al.* (2018) 'Nanomatrix Coated Stent Enhances Endothelialization but Reduces Platelet, Smooth Muscle Cell, and Monocyte Adhesion under Physiologic Conditions', *ACS Biomaterials Science and Engineering*, 4(1), pp. 107–115. doi: 10.1021/acsbiomaterials.7b00676.

Alexander, J. H. and Smith, P. K. (2016) 'Coronary-Artery Bypass Grafting', *New England Journal of Medicine*. Edited by J. A. Jarcho. Massachusetts Medical Society, 374(20), pp. 1954–1964. doi: 10.1056/NEJMra1406944.

Andukuri, A. *et al.* (2013) 'Enhanced human endothelial progenitor cell adhesion and differentiation by a bioinspired multifunctional nanomatrix.', *Tissue engineering. Part C, Methods*, 19(5), pp. 375–85. doi: 10.1089/ten.TEC.2012.0312.

Anthea Stolwijk, J. (2011) 'Electric Manipulation and Impedance Analysis of Adherent Cells on Gold-Film Electrodes', *Doctoral Thesis*.

AppliedBiophysics (2014) 'Applied Biophysics'. doi: 10.1002/9780470513156.

Asahara, T. *et al.* (1997) 'Isolation of putative progenitor endothelial cells for angiogenesis', *Science*, 275(5302), pp. 964–967. doi: 10.1126/science.275.5302.964.

Berghe, T. Vanden *et al.* (2010) 'Necroptosis, necrosis and secondary necrosis converge on similar cellular disintegration features', *Cell Death & Differentiation*, 17(6), pp. 922–930. doi: 10.1038/cdd.2009.184.

van Beusekom, H. M. M. *et al.* (2012) 'The genous™ endothelial progenitor cell capture stent accelerates stent re-endothelialization but does not affect intimal hyperplasia in porcine coronary arteries', *Catheterization and Cardiovascular Interventions*, 79(2), pp. 231–242. doi: 10.1002/ccd.22928.

Bhatnagar, P. *et al.* (2015) 'The epidemiology of cardiovascular disease in the UK 2014', *Heart*, 101(15), pp. 1182–1189. doi: 10.1136/heartjnl-2015-307516.

Bozsak, F. *et al.* (2017) 'Method for determining at least one type and/or condition of cells and system'. Available at:

https://patentscope.wipo.int/search/en/detail.jsf?docId=WO2017068157&recNum=1&maxRec=&office=&prevFilter=&sortOption=&queryString=&tab=PCT Description (Accessed: 15 June 2017).

Braunwald, E. (2016) 'Treatment of Left Main Coronary Artery Disease', *New England Journal of Medicine*. Massachusetts Medical Society, 375(23), pp. 2284–2285. doi: 10.1056/NEJMe1612570.

Brox, D. *et al.* (2015) 'Wireless Telemetry of Stainless-Steel-Based Smart Antenna Stent using a Transient Resonance Method', *IEEE*. IEEE, pp. 1–1. doi: 10.1109/LAWP.2015.2471955.

Burke, A. P. *et al.* (1997) 'Coronary Risk Factors and Plaque Morphology in Men with Coronary Disease Who Died Suddenly', *New England Journal of Medicine*, 336(18), pp. 1276–1282. doi: 10.1056/NEJM199705013361802.

Byrne, R. A. *et al.* (2013) 'Differential relative efficacy between drug-eluting stents in patients with bare metal and drug-eluting stent restenosis; evidence in support of drug resistance: insights from the ISAR-DESIRE and ISAR-DESIRE 2 trials', *EuroIntervention*, 9(7), pp. 797–802. doi: 10.4244/EIJV9I7A132.

Byrne, R. A. *et al.* (2017) 'Coronary balloon angioplasty, stents, and scaffolds', *The Lancet*. Elsevier Ltd, 390(10096), pp. 781–792. doi: 10.1016/S0140-6736(17)31927-X.

Byrne, R. A., Joner, M. and Kastrati, A. (2015) 'Stent thrombosis and restenosis: what have we learned and where are we going? The Andreas Gruntzig Lecture ESC 2014', *European Heart Journal*, 36, pp. 3320–3331. doi: 10.1093/eurheartj/ehv511.

Campbell, C. E. *et al.* (2007) 'Monitoring viral-induced cell death using electric cell-substrate impedance sensing', *Biosensors and Bioelectronics*, 23(4), pp. 536–542. doi: 10.1016/j.bios.2007.06.015.

Carrozza, J. P. *et al.* (1992) 'Angiographic and clinical outcome of intracoronary stenting: Immediate and long-term results from a large single-center experience', *Journal of the American College of Cardiology*, 20(2), pp. 328–337. doi: 10.1016/0735-1097(92)90098-8.

Chen, X. *et al.* (2016) 'Pyroptosis is driven by non-selective gasdermin-D pore and its morphology is different from MLKL channel-mediated necroptosis', *Cell Research*, 26(9), pp. 1007–1020. doi: 10.1038/cr.2016.100.

Chen, X. *et al.* (2017) 'A pressure-sensing smart stent compatible with angioplasty procedure and its in vivo testing', in *2017 IEEE 30th International Conference on Micro Electro Mechanical Systems (MEMS)*. IEEE, pp. 133–136. doi: 10.1109/MEMSYS.2017.7863358.

Chen, X. *et al.* (2018) 'Enabling Angioplasty-Ready "Smart" Stents to Detect In-Stent Restenosis and Occlusion', *Advanced Science*, 1700560. doi: 10.1002/advs.201700560.

Chen, X., Brox, D. and Assadsangabi, B. (2014) 'Intelligent telemetric stent for wireless monitoring of intravascular pressure and its in vivo testing', pp. 745–759. doi: 10.1007/s10544-014-9879-8.

Coleman, M. L. *et al.* (2001) 'Membrane blebbing during apoptosis results from

caspase-mediated activation of ROCK I', *Nature Cell Biology*, 3(4), pp. 339–345. doi: 10.1038/35070009.

Colleran, R. and Kastrati, A. (2018) 'Percutaneous coronary intervention: balloons, stents and scaffolds', *Clinical Research in Cardiology*. Springer Berlin Heidelberg, 107(2), pp. 55–63. doi: 10.1007/s00392-018-1328-x.

Collet, C. *et al.* (2018) 'Left main coronary artery disease: pathophysiology, diagnosis, and treatment', *Nature Reviews Cardiology*. Nature Publishing Group, 15(6), pp. 321–331. doi: 10.1038/s41569-018-0001-4.

El-Menyar, A. A., Al Suwaidi, J. and Holmes, D. R. (2007) 'Left Main Coronary Artery Stenosis: State-of-the-Art', *Current Problems in Cardiology*, 32(3), pp. 103–193. doi: 10.1016/j.cpcardiol.2006.12.002.

Farkouh, M. E. *et al.* (2012) 'Strategies for Multivessel Revascularization in Patients with Diabetes', *New England Journal of Medicine*, 367(25), pp. 2375–2384. doi: 10.1056/NEJMoa1211585.

Franco, C. A. *et al.* (2015) 'Dynamic Endothelial Cell Rearrangements Drive Developmental Vessel Regression', *PLOS Biology*. Edited by B. L. M. Hogan, 13(4), p. e1002125. doi: 10.1371/journal.pbio.1002125.

Giaever, I. and Keese, C. R. (1984) *Monitoring fibroblast behavior in tissue culture with an applied electric field (cell locomotion/cytochalasin B)*, *Proc. Nadl. Acad. Sci. USA*. Available at: https://www.ncbi.nlm.nih.gov/pmc/articles/PMC345299/pdf/pnas00613-0161.pdf (Accessed: 21 July 2019).

Giaever, I. and Keese, C. R. (1991) 'Micromotion of mammalian cells measured electrically.', *Proceedings of the National Academy of Sciences of the United States of America*, 88(17), pp. 7896–7900. doi: 10.1073/pnas.88.17.7896.

Grüntzig, A. (1978) 'TRANSLUMINAL DILATATION OF CORONARY-ARTERY STENOSIS', *The Lancet*. Elsevier, 311(8058), p. 263. doi: 10.1016/S0140-6736(78)90500-7.

Haider, K. H., Aziz, S. and Al-Reshidi, M. A. (2017) 'Endothelial progenitor cells for cellular angiogenesis and repair: Lessons learned from experimental animal models', *Regenerative Medicine*. Future Medicine Ltd., pp. 969–982. doi: 10.2217/rme-2017-0074.

Harskamp, R. E. *et al.* (2013) 'Saphenous vein graft failure after coronary artery bypass surgery: Pathophysiology, management, and future directions', *Annals of Surgery*, 257(5), pp. 824–833. doi: 10.1097/SLA.0b013e318288c38d.

Van der Heiden, K. *et al.* (2013) 'The effects of stenting on shear stress: relevance to endothelial injury and repair', *Cardiovascular Research*. Narnia, 99(2), pp. 269–275. doi: 10.1093/cvr/cvt090.

Heldman, A. W. *et al.* (2001) 'Paclitaxel stent coating inhibits neointimal hyperplasia at 4 weeks in a porcine model of coronary restenosis.', *Circulation*, 103(18), pp. 2289–95. Available at: http://www.ncbi.nlm.nih.gov/pubmed/11342479 (Accessed: 15 April 2019).

Her, A. Y. and Shin, E. S. (2018) 'Current management of in-stent restenosis', *Korean Circulation Journal*, 48(5), pp. 337–349. doi: 10.4070/kcj.2018.0103.

Herrick, J. B. (1983) 'Clinical Features of Sudden Obstruction of the Coronary Arteries', *JAMA: The Journal of the American Medical Association*. American Medical Association, 250(13), p. 1757. doi: 10.1001/jama.1983.03340130075039.

Hillis, L. D. *et al*. (2011) '2011 ACCF/AHA Guideline for Coronary Artery Bypass Graft Surgery', *Journal of the American College of Cardiology*, 58(24), pp. e123–e210. doi: 10.1016/j.jacc.2011.08.009.

Hioki (2019) *LCR METER IM3536 - Hioki*. Available at: https://www.hioki.com/en/products/detail/?product_key=5824 (Accessed: 8 August 2019).

Holland, I., McCormick, C. and Connolly, P. (2018) 'Towards non-invasive characterisation of coronary stent re-endothelialisation – An in-vitro, electrical impedance study', *PLoS ONE*, 13(11), pp. 1–17. doi: 10.1371/journal.pone.0206758.

Holmes, D. R. *et al*. (2006) 'Sirolimus-Eluting Stents vs Vascular Brachytherapy for In-Stent Restenosis Within Bare-Metal Stents', *JAMA*, 295(11), p. 1264. doi: 10.1001/jama.295.11.1264.

Horiba (2019) *LAQUAtwin EC-22 - LAQUA [Water Quality Analyzer Website] - HORIBA*. Available at: http://www.horiba.com/sg/application/material-property-characterization/water-analysis/water-quality-electrochemistry-instrumentation/compact/details/laquatwin-ec-22-25023/ (Accessed: 8 August 2019).

Ibidi (2015) *Instructions µ-Slide I Luer*. Available at: https://ibidi.com/img/cms/products/labware/channel_slides/S_801XX_Slide_ILuer/IN_801XX_I_Luer.pdf (Accessed: 21 January 2019).

Ibidi (2019) *sticky-Slide I Luer | Self-Adhesive Underside | ibidi*. Available at: https://ibidi.com/sticky-slides/63-sticky-slide-i-luer.html (Accessed: 24 January 2019).

Ibidi GmbH (2016) *Application Note 11 Shear Stress and Shear Rates for ibidi µ-Slides-Based on Numerical Calculations*.

Insull, W. (2009) 'The Pathology of Atherosclerosis: Plaque Development and Plaque Responses to Medical Treatment', *The American Journal of Medicine*. Elsevier Inc. Elsevier Inc., 122(1), pp. S3–S14. doi: 10.1016/j.amjmed.2008.10.013.

Jiménez, J. M. and Davies, P. F. (2009) 'Hemodynamically Driven Stent Strut Design', *Annals of Biomedical Engineering*, 37(8), pp. 1483–1494. doi: 10.1007/s10439-009-9719-9.

Joner, M. *et al*. (2006) 'Pathology of Drug-Eluting Stents in Humans', *Journal of the American College of Cardiology*, 48(1), pp. 193–202. doi: 10.1016/j.jacc.2006.03.042.

Kastrati, A. *et al*. (1993) 'Time course of restenosis during the first year after emergency coronary stenting', *Circulation*, 87(5), pp. 1498–1505. doi: 10.1161/01.CIR.87.5.1498.

Kastrati, A. *et al*. (2005) 'Sirolimus-Eluting Stent or Paclitaxel-Eluting Stent vs

Balloon Angioplasty for Prevention of Recurrences in Patients With Coronary In-Stent Restenosis', *JAMA*, 293(2), pp. 165–71. doi: 10.1001/jama.293.2.165.

Kim, M. S. and Dean, L. S. (2011) 'In-stent Restenosis', *Cardiovascular therapeutics*, 29, pp. 190–198. doi: 10.1016/j.iccl.2015.12.006.

Kobayashi, Y. *et al.* (1999) 'Stented segment length as an independent predictor of restenosis', *Journal of the American College of Cardiology*. Elsevier, 34(3), pp. 651–659. doi: 10.1016/S0735-1097(99)00303-4.

Koskinas, K. C. *et al.* (2012) 'Role of endothelial shear stress in stent restenosis and thrombosis: Pathophysiologic mechanisms and implications for clinical translation', *Journal of the American College of Cardiology*. Elsevier Inc., 59(15), pp. 1337–1349. doi: 10.1016/j.jacc.2011.10.903.

Krysko, O., de Ridder, L. and Cornelissen, M. (2004) 'Phosphatidylserine exposure during early primary necrosis (oncosis) in JB6 cells as evidenced by immunogold labeling technique', *Apoptosis*, 9(4), pp. 495–500. doi: 10.1023/B:APPT.0000031452.75162.75.

Kung, G., Konstantinidis, K. and Kitsis, R. N. (2011) 'Programmed Necrosis, Not Apoptosis, in the Heart', *Circulation Research*. Lippincott Williams & WilkinsHagerstown, MD, 108(8), pp. 1017–1036. doi: 10.1161/CIRCRESAHA.110.225730.

Kurokawa, M. and Kornbluth, S. (2009) 'Caspases and Kinases in a Death Grip', *Cell*, 138(5), pp. 838–854. doi: 10.1016/j.cell.2009.08.021.

Larsen, K. *et al.* (2012) 'Capture of circulatory endothelial progenitor cells and accelerated re-endothelialization of a bio-engineered stent in human ex vivo shunt and rabbit denudation model', *European Heart Journal*, 33(1), pp. 120–128. doi: 10.1093/eurheartj/ehr196.

Laskey, W. K., Kimmel, S. and Krone, R. J. (2000) 'Contemporary trends in coronary intervention: a report from the Registry of the Society for Cardiac Angiography and Interventions.', *Catheterization and cardiovascular interventions : official journal of the Society for Cardiac Angiography & Interventions*, 49(1), pp. 19–22. Available at: http://www.ncbi.nlm.nih.gov/pubmed/10627359 (Accessed: 7 December 2018).

Lee, J. M. *et al.* (2012) 'Comparison of endothelialization and neointimal formation with stents coated with antibodies against CD34 and vascular endothelial-cadherin', *Biomaterials*, 33(35), pp. 8917–8927. doi: 10.1016/j.biomaterials.2012.08.066.

Leiper, J. *et al.* (2002) 'S-nitrosylation of dimethylarginine dimethylaminohydrolase regulates enzyme activity: Further interactions between nitric oxide synthase and dimethylarginine dimethylaminohydrolase', *Proceedings of the National Academy of Sciences*, 99(21), pp. 13527–13532. doi: 10.1073/pnas.212269799.

Leon, M. B. *et al.* (1998) 'A Clinical Trial Comparing Three Antithrombotic-Drug Regimens after Coronary-Artery Stenting', *New England Journal of Medicine*, 339(23), pp. 1665–1671. doi: 10.1056/NEJM199812033392303.

Leon, M. B. *et al.* (2001) 'Localized Intracoronary Gamma-Radiation Therapy to

Inhibit the Recurrence of Restenosis after Stenting', *New England Journal of Medicine*, 344(4), pp. 250–256. doi: 10.1056/NEJM200101253440402.

Levine, G. N. *et al.* (2011) '2011 ACCF/AHA/SCAI Guideline for Percutaneous Coronary Intervention', *Journal of the American College of Cardiology*. Journal of the American College of Cardiology, 58(24), pp. e44–e122. doi: 10.1016/j.jacc.2011.08.007.

Li, M. *et al.* (2013) 'High Pulsatility Flow Induces Acute Endothelial Inflammation through Overpolarizing Cells to Activate NF-κB NIH Public Access', *Cardiovasc Eng Technol*, 4(1), pp. 26–38. doi: 10.1007/s13239-012-0115-5.

Libby, P. (2012) 'History of Discovery : Inflammation in Atherosclerosis', *Arterioscler Thromb Vasc Biol.*, 32(9), pp. 2045–2051. doi: 10.1161/ATVBAHA.108.179705.History.

Luengo-Fernández, R. *et al.* (2006) 'Cost of cardiovascular diseases in the United Kingdom.', *Heart (British Cardiac Society)*, 92(10), pp. 1384–9. doi: 10.1136/hrt.2005.072173.

Lüscher, T. F. *et al.* (2007) 'Drug-Eluting Stent and Coronary Thrombosis', *Circulation*, 115(8), pp. 1051–1058. doi: 10.1161/circulationaha.106.675934.

Lusis, A. J. (2000) 'Insight Review Articles', *Nature*, 407(September), pp. 233–241. doi: 10.1038/35025203.

Macander, P. J. *et al.* (1994) 'Balloon angioplasty for treatment of in-stent restenosis: feasibility, safety, and efficacy.', *Catheterization and cardiovascular diagnosis*, 32(2), pp. 125–31. Available at: http://www.ncbi.nlm.nih.gov/pubmed/8062366 (Accessed: 15 April 2019).

Mäkikallio, T. *et al.* (2016) 'Percutaneous coronary angioplasty versus coronary artery bypass grafting in treatment of unprotected left main stenosis (NOBLE): a prospective, randomised, open-label, non-inferiority trial', *The Lancet*, 388(10061), pp. 2743–2752. doi: 10.1016/S0140-6736(16)32052-9.

Mamouni, J. and Yang, L. (2011) 'Interdigitated microelectrode-based microchip for electrical impedance spectroscopic study of oral cancer cells', *Biomedical Microdevices*, 13(6), pp. 1075–1088.

McCormick, C. (2018) 'Overview of cardiovascular stent designs', in *Functionalised Cardiovascular Stents*. Elsevier, pp. 3–26. doi: 10.1016/b978-0-08-100496-8.00001-9.

McCracken, K. E. *et al.* (2013) 'Shear- vs. nanotopography-guided control of growth of endothelial cells on RGD-nanoparticle-nanowell arrays', *Journal of Biological Engineering*. BioMed Central, 7(1), p. 11. doi: 10.1186/1754-1611-7-11.

Mehran, R. *et al.* (2012) 'Treatment of In-Stent Restenosis With Excimer Laser Coronary Angioplasty Versus Rotational Atherectomy', *Circulation*, 101(21), pp. 2484–2489. doi: 10.1161/01.cir.101.21.2484.

Meijering, E., Dzyubachyk, O. and Smal, I. (2012) 'Methods for Cell and Particle Tracking', *Methods in Enzymology*. Academic Press, 504, pp. 183–200. doi: 10.1016/B978-0-12-391857-4.00009-4.

Mercer, J. *et al.* (2005) 'Endogenous p53 Protects Vascular Smooth Muscle Cells

From Apoptosis and Reduces Atherosclerosis in ApoE Knockout Mice'. doi: 10.1161/01.RES.0000161069.15577.ca.

Mintz, G. S. *et al.* (1998) 'In-stent restenosis: the Washington Hospital Center experience.', *The American journal of cardiology*, 81(7A), pp. 7E-13E. Available at: http://www.ncbi.nlm.nih.gov/pubmed/9551588 (Accessed: 24 April 2019).

Mizumoto, K., Rothman, R. J. and Farber, J. L. (1994) 'Programmed cell death (apoptosis) of mouse fibroblasts is induced by the topoisomerase II inhibitor etoposide.', *Molecular Pharmacology*, 46(5).

Moiseeva, E. P. (2001) 'Adhesion receptors of vascular smooth muscle cells and their functions.', *Cardiovascular research*, 52(3), pp. 372–386.

Morin, J. P. *et al.* (2003) 'Rotating wall vessel as a new in vitro shear stress generation system: Application to rat coronary endothelial cell cultures', *Cell Biology and Toxicology*, 19(4), pp. 227–242. doi: 10.1023/B:CBTO.0000003844.59908.0e.

Mudau, M. *et al.* (2012) 'Endothelial dysfunction: the early predictor of atherosclerosis.', *Cardiovascular journal of Africa*, 23(4), pp. 222–31. doi: 10.5830/CVJA-2011-068.

Nagata, S. and Tanaka, M. (2017) 'Programmed cell death and the immune system', *Nature Reviews Immunology*, 17(5), pp. 333–340. doi: 10.1038/nri.2016.153.

Newby, A. C. (2005) 'Dual Role of Matrix Metalloproteinases (Matrixins) in Intimal Thickening and Atherosclerotic Plaque Rupture', *Physiology Review*, 85, pp. 1–31. doi: 10.1152/physrev.00048.2003.

Olympus (2013) 'cellSens'. Available at: http://www.galenica.cl/wp-content/uploads/2015/01/Catalogo-CellSens.pdf.

Otsuka, F. *et al.* (2012) 'The importance of the endothelium in atherothrombosis and coronary stenting', *Nature Reviews Cardiology*, 9(8), pp. 439–453. doi: 10.1038/nrcardio.2012.64.

Pache, J. ürge. *et al.* (2003) 'Intracoronary stenting and angiographic results: strut thickness effect on restenosis outcome (ISAR-STEREO-2) trial', *Journal of the American College of Cardiology*. Elsevier, 41(8), pp. 1283–1288. doi: 10.1016/S0735-1097(03)00119-0.

Pappano, A. J. and Gil Wier, W. (2013) 'Coronary Circulation', *Cardiovascular Physiology*. Content Repository Only!, pp. 223–236. doi: 10.1016/B978-0-323-08697-4.00011-3.

Park, J. *et al.* (2015) 'Magnesium Corrosion Triggered Spontaneous Generation of H2O2 on Oxidized Titanium for Promoting Angiogenesis.', *Angewandte Chemie (International ed. in English)*, 54(49), pp. 14753–7. doi: 10.1002/anie.201507352.

Park, J. *et al.* (2019) 'Interface Engineering of Fully Metallic Stents Enabling Controllable H 2 O 2 Generation for Antirestenosis', *Langmuir*. American Chemical Society, 35(10), pp. 3634–3642. doi: 10.1021/acs.langmuir.8b03753.

Parnaik, R., Raff, M. C. and Scholes, J. (2000) 'Differences between the clearance

of apoptotic cells by professional and non-professional phagocytes.', *Current biology : CB*, 10(14), pp. 857–60. Available at: http://www.ncbi.nlm.nih.gov/pubmed/10899007 (Accessed: 19 June 2019).

Parng, C. *et al.* (2004) 'Zebrafish Apoptosis Assays for Drug Discovery', *Methods in Cell Biology*. Academic Press, 76, pp. 75–85. doi: 10.1016/S0091-679X(04)76005-7.

Parry, T. J. *et al.* (2005) 'Drug-eluting stents: Sirolimus and paclitaxel differentially affect cultured cells and injured arteries', *European Journal of Pharmacology*, 524(1–3), pp. 19–29. doi: 10.1016/j.ejphar.2005.09.042.

Pasterkamp, G. and Smits, P. C. (2002) *Remodelling of coronary arteries*, *Journal of Cardiovascular Risk*. Lippincott Williams & Wilkins. Available at: https://journals.sagepub.com/doi/pdf/10.1177/174182670200900502 (Accessed: 17 July 2019).

Pé Rez De Prado, A. *et al.* (2011) 'Time Course of Reendothelialization of Stents in a Normal Coronary Swine Model: Characterization and Quantification', *Pharmaceutical Pathobiology*, 48(6), pp. 1109–1117. doi: 10.1177/0300985811400446.

Physics Drawings (2019). Available at: https://physicslearning2.colorado.edu/pira/index.php?option=com_content&view=article&id=15&Itemid=176 (Accessed: 4 July 2019).

Poon, I. K. H. *et al.* (2014) 'Apoptotic cell clearance: basic biology and therapeutic potential', *Nature Reviews Immunology*, 14(3), pp. 166–180. doi: 10.1038/nri3607.

Rochon, E. R., Menon, P. G. and Roman, B. L. (2016) 'Alk1 controls arterial endothelial cell migration in lumenized vessels', *Development*, 143(14), pp. 2593–2602. doi: 10.1242/dev.135392.

Rogers, C. *et al.* (2017) 'Cleavage of DFNA5 by caspase-3 during apoptosis mediates progression to secondary necrotic/pyroptotic cell death', *Nature Communications*, 8(1), p. 14128. doi: 10.1038/ncomms14128.

Sabik, J. F. *et al.* (2005) 'Comparison of Saphenous Vein and Internal Thoracic Artery Graft Patency by Coronary System'. doi: 10.1016/j.athoracsur.2004.07.047.

Savage, P. *et al.* (2004) 'Coronary Stent Strut Size Dependent Stress–Strain Response Investigated Using Micromechanical Finite Element Models', *Annals of Biomedical Engineering*. Kluwer Academic Publishers-Plenum Publishers, 32(2), pp. 202–211. doi: 10.1023/B:ABME.0000012740.47963.9e.

Schömig, A. *et al.* (1994) 'Four-year experience with Palmaz-Schatz stenting in coronary angioplasty complicated by dissection with threatened or present vessel closure.', *Circulation*, 90(6), pp. 2716–24. Available at: http://www.ncbi.nlm.nih.gov/pubmed/7994813 (Accessed: 26 February 2019).

Scott, N. A. *et al.* (1996) 'Identification of a potential role for the adventitia in vascular lesion formation after balloon overstretch injury of porcine coronary arteries.', *Circulation*, 93(12), pp. 2178–87. Available at: http://www.ncbi.nlm.nih.gov/pubmed/8925587 (Accessed: 26 February

2019).

Sedaghat, A. *et al.* (2013) 'First in vitro and in vivo results of an anti-human CD133-antibody coated coronary stent in the porcine model', *Clinical Research in Cardiology*, 102(6), pp. 413–425. doi: 10.1007/s00392-013-0547-4.

Serruys, P. W. *et al.* (1991) 'Angiographic Follow-up after Placement of a Self-Expanding Coronary-Artery Stent', *New England Journal of Medicine*. Massachusetts Medical Society , 324(1), pp. 13–17. doi: 10.1056/NEJM199101033240103.

Serruys, P. W. *et al.* (2009) 'Percutaneous Coronary Intervention versus Coronary-Artery Bypass Grafting for Severe Coronary Artery Disease', *New England Journal of Medicine*. Massachusetts Medical Society , 360(10), pp. 961–972. doi: 10.1056/NEJMoa0804626.

Serruys, P. W. and Onuma, Y. (2017) *Bioresorbable scaffolds : from basic concept to clinical applications*. Available at: https://books.google.co.uk/books?hl=en&lr=&id=kGpQDwAAQBAJ&oi=fnd&pg=PA68&dq=%22wall+shear+stress+definition%22&ots=x9HHWKsMM0&sig=tuyZ5qxfaCkMmR_JdGTwuvF4DPY&redir_esc=y#v=onepage&q&f=false (Accessed: 7 August 2019).

Shedden, L. *et al.* (2010) 'Towards a self-reporting coronary artery stent-Measuring neointimal growth associated with in-stent restenosis using electrical impedance techniques', *Biosensors and Bioelectronics*, 26(2), pp. 661–666. doi: 10.1016/j.bios.2010.06.073.

Shedden, L., Oldroyd, K. and Connolly, P. (2009) 'Current issues in coronary stent technology.', *Proceedings of the Institution of Mechanical Engineers. Part H, Journal of engineering in medicine*, 223, pp. 515–524. doi: 10.1243/09544119JEIM541.

Shlofmitz, E., Iantorno, M. and Waksman, R. (2019) 'Restenosis of Drug-Eluting Stents: A New Classification System Based on Disease Mechanism to Guide Treatment and State-of-The-Art Review', *Circulation: Cardiovascular Interventions*, 12(8), pp. 1–8. doi: 10.1161/CIRCINTERVENTIONS.118.007023.

Siddiquei, H. R. *et al.* (2010) 'Electrical cell-substrate impedance sensing (ECIS) based biosensor for characterization of DF-1 cells', *International Conference on Computer and Communication Engineering, ICCCE'10*, 6(0940111), pp. 11–13. doi: 10.1109/ICCCE.2010.5556772.

Sigwart, U. *et al.* (1987) 'Intravascular Stents to Prevent Occlusion and Re-Stenosis after Transluminal Angioplasty', *New England Journal of Medicine*. Massachusetts Medical Society , 316(12), pp. 701–706. doi: 10.1056/NEJM198703193161201.

Slavin, L., Chhabra, A. and Tobis, J. M. (2007) 'Drug-eluting stents: Preventing restenosis', *Cardiology in Review*, 15(1), pp. 1–12. doi: 10.1097/01.crd.0000200844.16899.fc.

Smolina, K. *et al.* (2012) 'Determinants of the decline in mortality from acute myocardial infarction in England between 2002 and 2010: linked national database study.', *BMJ (Clinical research ed.)*, 344(jan25 2), p. d8059. doi: 10.1136/bmj.d8059.

Son, D. *et al.* (2015) 'Bioresorbable Electronic Stent Integrated with Therapeutic Nanoparticles for Endovascular Diseases.', *ACS nano*, (6), pp. 5937–5946. doi: 10.1021/acsnano.5b00651.

Stefanini, G. G. *et al.* (2012) 'Biodegradable polymer drug-eluting stents reduce the risk of stent thrombosis at 4 years in patients undergoing percutaneous coronary intervention: a pooled analysis of individual patient data from the ISAR-TEST 3, ISAR-TEST 4, and LEADERS randomized tria', *European Heart Journal*, 33(10), pp. 1214–1222. doi: 10.1093/eurheartj/ehs086.

Stolwijk, J. A., Michaelis, S. and Wegener, J. (2012) 'Cell Growth and Cell Death Studied by Electric Cell-Substrate Impedance Sensing', in *Electric Cell-Substrate Impedance Sensing and Cancer Metastasis*. Dordrecht: Springer Netherlands, pp. 85–117. doi: 10.1007/978-94-007-4927-6_6.

Stone, G. W. *et al.* (2016) 'Everolimus-Eluting Stents or Bypass Surgery for Left Main Coronary Artery Disease', *New England Journal of Medicine*. Massachusetts Medical Society, 375(23), pp. 2223–2235. doi: 10.1056/NEJMoa1610227.

Sun, T. *et al.* (2010) 'On-chip electrical impedance tomography for imaging biological cells', *Biosensors & Bioelectronics*, 25(5), pp. 1109–1115. doi: 10.1016/j.bios.2009.09.036.

Takahata, K. *et al.* (2003) 'Stentenna: a micromachined antenna stent for wireless monitoring of implantable microsensors', in *Proceedings of the 25th Annual International Conference of the IEEE Engineering in Medicine and Biology Society (IEEE Cat. No.03CH37439)*. IEEE, pp. 3360–3363. doi: 10.1109/IEMBS.2003.1280865.

Tomasevic, M. *et al.* (2019) 'ENDOTHELIAL CELLS BY CORONARY STENTS - FROM HISTOLOGY TO CLINICAL OUTCOMES'. doi: 10.2478/sjecr-2019-0018.

Tousoulis, D. (2018) *Coronary Artery Disease : From Biology to Clinical Practice*.

Vermes, I. and Haanen, C. (1994) 'Apoptosis and Programmed Cell Death in Health and Disease', *Advances in Clinical Chemistry*. Elsevier, 31, pp. 177–246. doi: 10.1016/S0065-2423(08)60336-4.

Virmani, R. *et al.* (2006) 'Pathology of the Vulnerable Plaque', 47(8), pp. 0–5. doi: 10.1016/j.jacc.2005.10.065.

Walter, D. H. *et al.* (2004) 'Local Gene Transfer of phVEGF-2 Plasmid by Gene-Eluting Stents', *Circulation*, 110(1), pp. 36–45. doi: 10.1161/01.CIR.0000133324.38115.0A.

Wegener, J., Keese, C. R. and Giaever, I. (2000) 'Electric cell-substrate impedance sensing (ECIS) as a noninvasive means to monitor the kinetics of cell spreading to artificial surfaces.', *Experimental cell research*, 259(1), pp. 158–166. doi: 10.1006/excr.2000.4919.

Willerson, J. T. and Holmes, D. R. (2015) *Coronary artery disease*. Springer. Available at: https://books.google.co.uk/books?id=x0IyBwAAQBAJ&printsec=frontcover&dq=coronary+artery+disease&hl=en&sa=X&ved=0ahUKEwj78JX36MTeAhXIiiwKHU81BxwQ6AEILzAB#v=onepage&q=coronary artery disease&f=false (Accessed: 8 November 2018).

Wood, J. A. *et al*. (2010) 'Biophysical Cueing and Vascular Endothelial Cell Behavior', *Materials*. Molecular Diversity Preservation International, 3(3), pp. 1620–1639. doi: 10.3390/ma3031620.

Xiao, C. *et al*. (2002) 'Assessment of Cytotoxicity Using Electric Cell-Substrate Impedance Sensing: Concentration and Time Response Function Approach', *Analytical Chemistry*, 74, pp. 5748–5753. doi: 10.1021/ac025848f.

Yin, S.-H.-L. *et al*. (2019) 'Duration of dual antiplatelet therapy after percutaneous coronary intervention with drug-eluting stent: systematic review and network meta-analysis', *BMJ*. doi: 10.1136/bmj.l2222.

Yusuf, S. *et al*. (1994) 'Effect of coronary artery bypass graft surgery on survival: overview of 10-year results from randomised trials by the Coronary Artery Bypass Graft Surgery Trialists Collaboration.', *Lancet (London, England)*. Elsevier, 344(8922), pp. 563–70. doi: 10.1016/S0140-6736(94)91963-1.

Zhang, X. *et al*. (2017) 'The influence of the electrode dimension on the detection sensitivity of electric cell–substrate impedance sensing (ECIS) and its mathematical modeling', *Sensors and Actuators, B: Chemical*. Elsevier B.V., 247, pp. 780–790. doi: 10.1016/j.snb.2017.03.047.

Zhang, Y. *et al*. (2018) 'Plasma membrane changes during programmed cell deaths', *Cell Research*. Nature Publishing Group, 28(1), pp. 9–21. doi: 10.1038/cr.2017.133.